Copy No. 19

APAE-103
AEC Research and
Development Report
UC-81, Reactors-Power
[Special Distribution]

summary report of analysis of physics measurements performed on SM-1 core I

Contract No. AT[30-1]-2639
with U. S. Atomic Energy Commission
New York Operations Office

ALCO NPED
ALCO PRODUCTS, INC.
NUCLEAR POWER ENGINEERING DEPARTMENT

DISCLAIMER

APAE-103
Copy No.
AEC Research and
Development Report
UC-81, Reactors - Power
(Special Distribution)

SUMMARY REPORT OF ANALYSIS OF PHYSICS MEASUREMENTS PERFORMED ON SM-1 CORE I

Edited by:
L. Lois

Analysis by:
S. Paluszkiewicz
B. E. Fried
R. H. Beam
L. Lois

Approved by:
M. H. Dixon, Project Engineer

Issued: March 30, 1962

Contract No. AT(30-1)-2639
with U. S. Atomic Energy Commission
New York Operations Office

ALCO PRODUCTS, INC.
Nuclear Power Engineering Department
Post Office Box 414
Schenectady 1, N. Y.

AEC LEGAL NOTICE

This report was prepared as an account of Government sponsored work. Neither the United States, nor the Commission, nor any person acting on behalf of the Commission:

A. Makes any warranty or representation, expressed or implied, with respect to the accuracy, completeness, or usefulness of the information contained in this report, or that the use of any information, apparatus, method, or process disclosed in this report may not infringe privately owned rights: or

B. Assumes any liabilities with respect to the use of, or for damages resulting from the use of any information, apparatus, method, or process disclosed in this report.

As used in the above, "person acting on behalf of the Commission" includes any employee or contractor of the Commission, or employee of such contractor, to the extent that such employee or contractor of the Commission, or employee of such contractor prepares, disseminates, or provides access to, any information pursuant to his employment or contract with the Commission, or his employment with such contractor.

ALCO LEGAL NOTICE

This report was prepared by Alco Products, Incorporated in the course of work under, or in connection with, Contract No. AT(30-1)-2639 issued by U. S. Atomic Energy Commission, NYOO; and subject only to the rights of the United States, under the provisions of this contract, Alco Products, Incorporated makes no warranty or representation, express or implied, and shall have no liability with respect to this report or any of its contents or with respect to the use thereof or with respect to whether any such use will infringe the rights of others.

DISTRIBUTION

External Copies

1-2 New York Operations Office
U.S. Atomic Energy Commission
376 Hudson Street
New York 14, New York

Attention: Chief, Army Reactors Staff
Reactor Division

3 New York Operations Office
U.S. Atomic Energy Commission
376 Hudson Street
New York 14, New York

Attention: Library

4-6 U.S. Atomic Energy Commission
Washington 25, D. C.

Attention: Chief, Water Systems Project
Branch (Army Reactors)
Division of Reactor Development
Mail Station F-311

7 U.S. Atomic Energy Commission
Washington 25, D. C.

Attention: Chief, Evaluation and Planning Branch
Civilian Reactors
Div. of Reactor Development
Mail Station F-311

8 U.S. Atomic Energy Commission
Chief, New York Patent Group
Brookhaven National Laboratory
Upton, New York

Attention: Harman Potter

DISTRIBUTION (CONT'D)

External Copies

9 Idaho Operations Office
U.S. Atomic Energy Commission
P.O. Box 2108
Idaho Falls, Idaho

Attention: Director, Divisions of Military Reactors

10 U.S. Atomic Energy Commission
Reports and Statistics Branch
Division of Reactor Development
Washinton 25, D. C.

11-12 Office of the Chief of Engineers
Department of the Army
Building T-7
Washinton 25, D. C.

Attention: Chief, Projects Branch
Nuclear Power Division

13-15 Nuclear Power Field Office
U.S. Army Engineer Reactors Group
Fort Belvoir, Virginia

Attention: Chief, Nuclear Power
Field Office

16 Nuclear Power Field Office
U.S. Army Engineer Reactors Group
Fort Belvoir, Virginia

Attention: O.I.C. S.-1

17 Chief, U.S. Army Reactors Group
Fort Greely, Alaska
APO 733
Seattle, Washington

Attention: O.I.C. SM-1A

DISTRIBUTION (CONT'D)

External Copies

18 Commanding Officer
U.S. Army Polar Research
and Development Center
Fort Belvoir, Virginia

Attention: Nuclear Power Officer

19-21 Office of Technical Information Extension
P.O. Box 62
Oak Ridge, Tennessee

22 Union Carbide Nuclear Corporation
Oak Ridge National Laboratory
Y-12 Building 9704-1
P.O. Box "Y"
Oak Ridge, Tennessee

Attention: L. D. Schaffer

23 Union Carbide Nuclear Corporation
Oak Ridge National Laboratory
Y-12 Building 9704-1
P.O. Box "Y"
Oak Ridge, Tennessee

Attention: E. Gross

24 The Martin Company
P.O. Box 5042
Middle River, Maryland

Attention: AEC Contract Document Custodian

25 The Martin Company
P.O. Box 5042
Middle River, Maryland

Attention: C. Eicheldinger

DISTRIBUTION (CONT'D)

External Copies

26-27 Combustion Engineering, Incorporated
Nuclear Division
Prospect Hill Road
Windsor, Connecticut

Attention: Mr. J. B. Anderson

28 Dr. Raymond L. Murray
North Carolina State College
Raleigh, North Carolina

29 Dr. J. L. Meem
University of Virginia
Charlottesville, Virginia

Internal Copies

30	K. Kasschau	43	J. P. Oggerino
31	J. F. Haines	44	R. H. Beam
32	J. G. Gallagher	45	J. F. Scoles
33	M. H. Dixon	46	J. R. Coombe
34	F. G. Moote	47	T. M. Raby
35	J. M. Ravets	48	J. V. Mageean
36	P. E. Bobe	49	K. D. Sontheimer
37	L. Lois	50	A. Svasek
38	W. T. Williams	51	R. E. Neville
39	B. E. Fried	52 - 53	Critical Facility File
40	E. F. Clancy	54 - 55	Core Analysis File
41	S. Paluszkiewicz	56 - 65	NPED File
42	D. H. Lee		

ABSTRACT

This report contains a comprehensive analysis of the nuclear characteristics of the SM-1 Core I. Comparison of analytical and experimental results for neutron ages and core reactivities of a variety of cases investigated shows that the MUFT III with P-1 slowing down approximation gives the best results.

At startup the core reactivity and rod bank worth under various operating conditions are investigated and compared to experiment. Core lifetime was calculated to be 16.8 MWYR compared to 16.4 MWYR experimental.

The temperature coefficient has been calculated and compared to experiment as function of burnup.

In Appendix A, flux distribution, temperature coefficient, effective delayed neutron fraction and core life are analyzed by Dr. R. L. Murray by one and two group modified theory and series expansion calculations.

ACKNOWLEDGEMENT

The analysis in this report was carried out under the direction of P.E. Bobe, who also prepared Appendix C. Dr. R. L. Murray, consultant, performed the calculations included in Appendix A. The assistance of J. G. Gallagher in editing this report is gratefully acknowledged.

THIS PAGE

WAS INTENTIONALLY

LEFT BLANK

TABLE OF CONTENTS

TABLE OF CONTENTS (CONT'D)

TABLE OF CONTENTS (CONT'D)

TABLE OF CONTENTS (CONT'D)

TABLE OF CONTENTS (CONT'D)

TABLE OF CONTENTS (CONT'D)

LIST OF ILLUSTRATIONS

LIST OF ILLUSTRATIONS (CONT'D)

LIST OF ILLUSTRATIONS (CONT'D)

THIS PAGE

WAS INTENTIONALLY

LEFT BLANK

LIST OF TABLES

LIST OF TABLES (CONT'D)

LIST OF TABLES (CONT'D)

LIST OF TABLES (CONT'D)

SUMMARY

A reference calculational model for analysis of SM-1 Core I was developed by application of P-1 and P-1 S. G. slowing down models and MUFT-III and MUFT-V nuclear data to a wide variety of experiments. The analyses indicate P-1 slowing down model and MUFT-III nuclear data yielded the best agreement between calculated and measured reactivity. Calculations indicated that the P-1 MUFT-III model gave the best agreement with the measured neutron age in water. The thermal constants were calculated by use of cross sections evaluated to the effective temperature for the use of P_3 theory. The reference model gave good agreement with the fraction of thermal fissions below cadmium cut-off and the worth of the central control rod in fully poisoned SM-1 cores.

Calculations performed using the reference model and one-and two- dimensional diffusion theory indicated good agreement between themselves and with experimental reactivity for SM-1 Core I at startup, 68°F and 440°F. Application of one-dimensional Windowshade type calculations indicates that the reference model can predict startup bank positions within 1.4 inches.

The use of the CANDLE-2 depletion code indicated a core lifetime of 16.8 MWYR compared with a measured value of 16.4 MWYR. Reasonable agreement was obtained with the burnup distribution of one element from SM-1 Core I. Good agreement was obtained with xenon steady state and transient reactivity.

A simplified model for calculation of the temperature coefficient was developed and applied to SM-1 Core I. Perturbation theory was utilized to predict core life, steady state, temperature coefficient and flux distribution. Good agreement was found in the case of core life prediction. Perturbation theory was utilized to predict an effective delayed neutron fraction of 0.0078.

THIS PAGE

WAS INTENTIONALLY

LEFT BLANK

INTRODUCTION

The analysis in this report was performed under Task 2 of the Program for Engineering Support and Development of Army PWR Power Plants.* The purpose of the study is to calculate the initial and burnup nuclear behavior of the SM-1 Core I and to compare to measurements. The results will be used to form a basis for improvement in prediction of reactor core performance and as a basis for the analysis of replacement cores.

SM-1 Core I is one of the first power reactor cores and for that reason it has been the subject of a fairly comprehensive set of physics measurements to establish all important core physics characteristics during core burnout.

The results of these measurements are published in a companion report, APAE-96, "Summary of Physics Measurements on SM-1 Core I." Part of this report is devoted to a review of the calculational models employed to predict the reactivity of the SM-1 Core I and various similar types of cores in order to select the most accurate model. The analysis employs modified two group theory. Fast constants are obtained using the MUFT Code and thermal constants obtained using P_3 theory. The core nuclear characteristics are subsequently analyzed and compared to measured data at startup. The CANDLE-2 code was utilized to calculate the burnup behavior of the core. Certain special analytical investigations were performed by Dr. R. L. Murray, using perturbation techniques primarily.

It must be recognized that due to the time schedule much of the analysis presented in this report was performed simultaneously. This was a difficulty which could not have been avoided; however, whenever an analysis was performed using core nuclear parameters different from the "reference set" as given in Appendix C, attempts were made to determine the effects upon the calculated results.

---

* The Program plan was issued as AP Note-286, October 10, 1960.

1.0 DESCRIPTION OF SM-1 CORE I

1.1 REACTOR CHARACTERISTICS

The SM-1 is a pressurized water reactor which generates about 1900 ekw net of electricity from 10 tMW.[1]* SM-1 Core I employed fully enriched uranium as fuel in the form of UO_2 dispersed in 0.030 in. thick stainless steel fuel plates. Boron in the form of B_4C is also incorporated in the fuel plates to act as a burnable poison. These fuel plates were assembled into elements by brazing. The core was composed of 38 fixed elements and 7 control rod fuel elements of the follower type. The core contains 22.5 Kg of U-235 and 1.57 gm of B-10. The core is cooled by approximately 4000 gpm of water at 1200 psi pressure and a mean temperature of $440^{\circ}F$.

Fig. 1.1 shows a photograph of a fixed element with the end box removed. Fig. 1.2 shows a control rod fuel element, absorber section and cap as well as the control rod tube. Thirty-eight fixed fuel elements and 7 control rod assemblies are assembled to form the reactor core as shown in Fig. 1.3. The core is approximately a 22 in. right cylinder. The core is surrounded by an essentially infinite water reflector in the radial direction and an axial reflector which consists of a mixture of stainless steel and water. The control rods are adjusted so that rods 1, 2, 3, 4, and C (see Fig. 1.3) are positioned as a bank while control rods A and B are essentially fully withdrawn. Neutrons were provided for initial startup by a 15 curie Po-Be source. After initial operation, startup neutrons are provided by (γ, n) reactions on a 3 in. x 3 in. x 0.5 in. beryllium block attached to the core skirt.

1.2 SOURCE OF PHYSICS MEASUREMENTS

A report documenting all the physics measurements performed on SM-1 Core I has been issued as APAE-96, "Summary Report of Physics Measurements on SM-1 Core I."[2] This report includes measurements on SM-1 Core I and large number of measurements performed on SM-1 ZPE Core I at the Alco Critical Facility. That core was made to identical specifications as SM-1 Core I and has been proven through measurements to be essentially identical.

1.3 DIMENSIONS AND MATERIAL CONTENT OF SM-1 CORE I

The most important dimensions and material content of SM-1 Core I are given in Table 1.1. A comprehensive list of material and geometrical data for SM-1 Core I is given in Appendix C.

* References are in the last subsection of each main section of the report.

1.4 REFERENCES (1.0)

1. Gallagher, J. G. "Summary of Reactor Design Information From Three-Years Operation of a Small PWR," IAEA, Vienna 1960 (also APAE Memo 273, September 9, 1960.

2. Weiss, S. H., "Summary Report of Physics Measurements on SM-1 Core I," APAE-96, February 6, 1962.

TABLE 1.1
DIMENSIONS AND MATERIAL CONTENT OF CORE

Dimensions of Core		
Active length	in.	21.75
Equivalent diameter	in.	22.2
Cell size	in.	2.9375 x 2.9375
Numberof Cells		45
Configuration		7 x 7 with corners missing
Fixed Element		
Number		38
Number of plates		18
Plate dimension	in.	0.030 x 2.778 x 23
Weight of U^{235}	gm	515.16
Weight of UO_2	gm	630.36
Weight of B^{10}	gm	0.3605
Weight of B_4C	gm	2.626
Control Rod Element		
Number		7
Number of plates		16
Plate dimensions		0.030 x 2.56 x 23
Weight of U^{235}	gm	417.76
Weight of UO_2	gm	512.16
Weight of B^{10}	gm	0.2926
Weight of B_4C	gm	2.132
Control Rod Absorber		
Number of plates (box)		4
Weight of B^{10}	gm	56.4
Material Content of Core		
Weight of U^{235}	kg	22.50
Weight of B^{10}	gm	15.75
Weight of SS	kg	208.9
Weight of Water (68°F)	kg	111.08

THIS PAGE

WAS INTENTIONALLY

LEFT BLANK

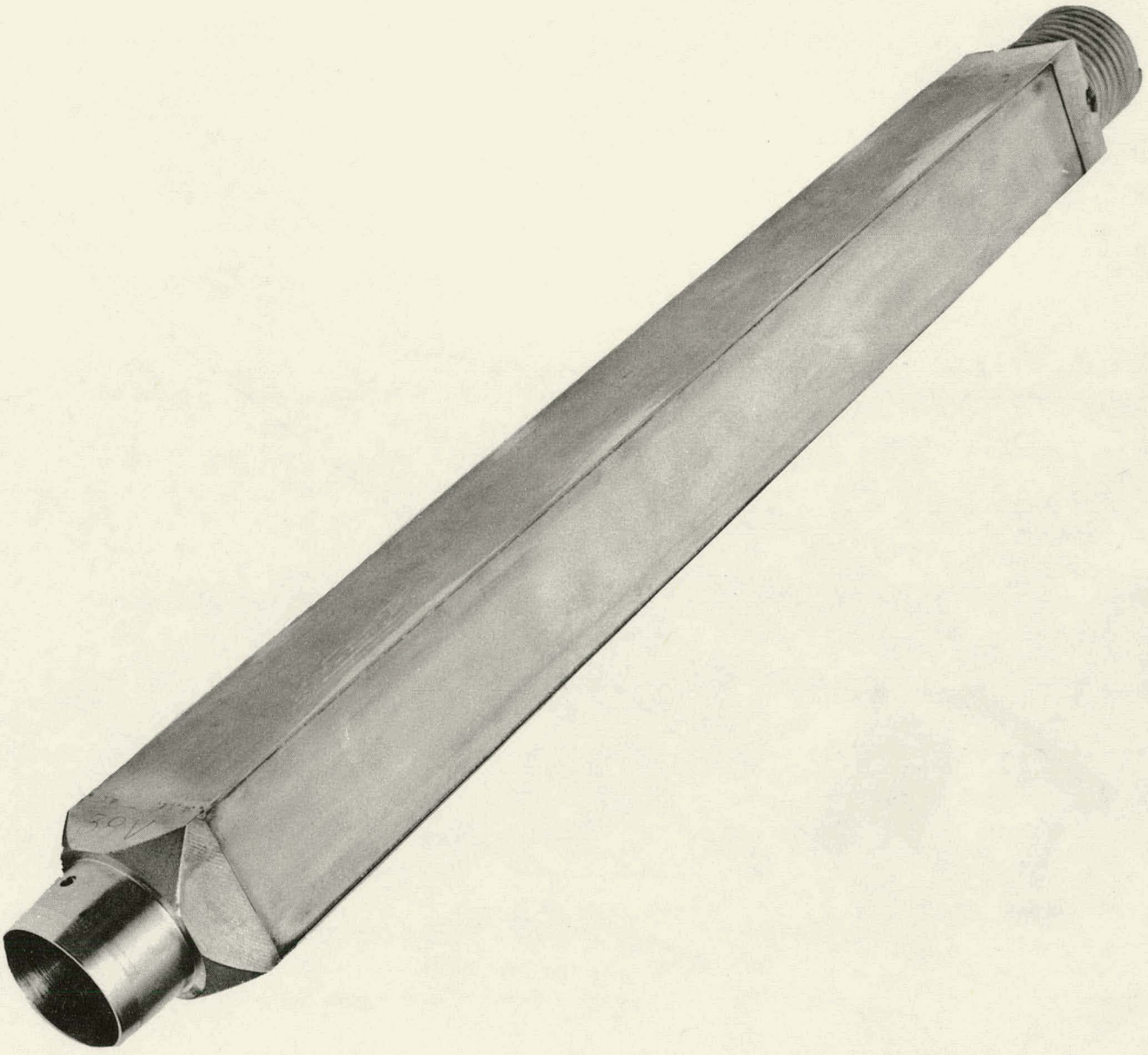

Fig. 1.1 - SM-1 Stationary Fuel Element

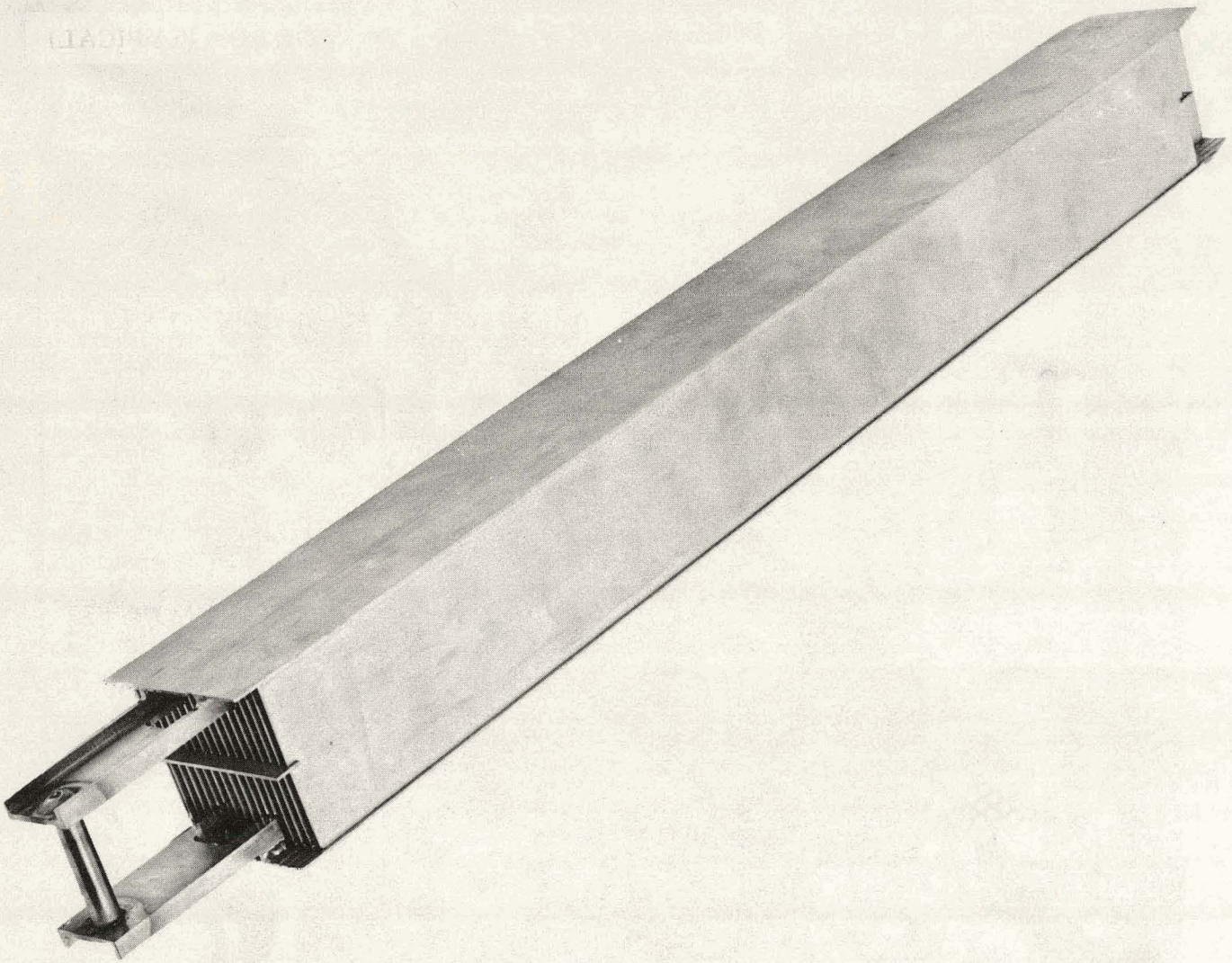

Fig. 1.2 - SM-1 Control Rod Fuel Element

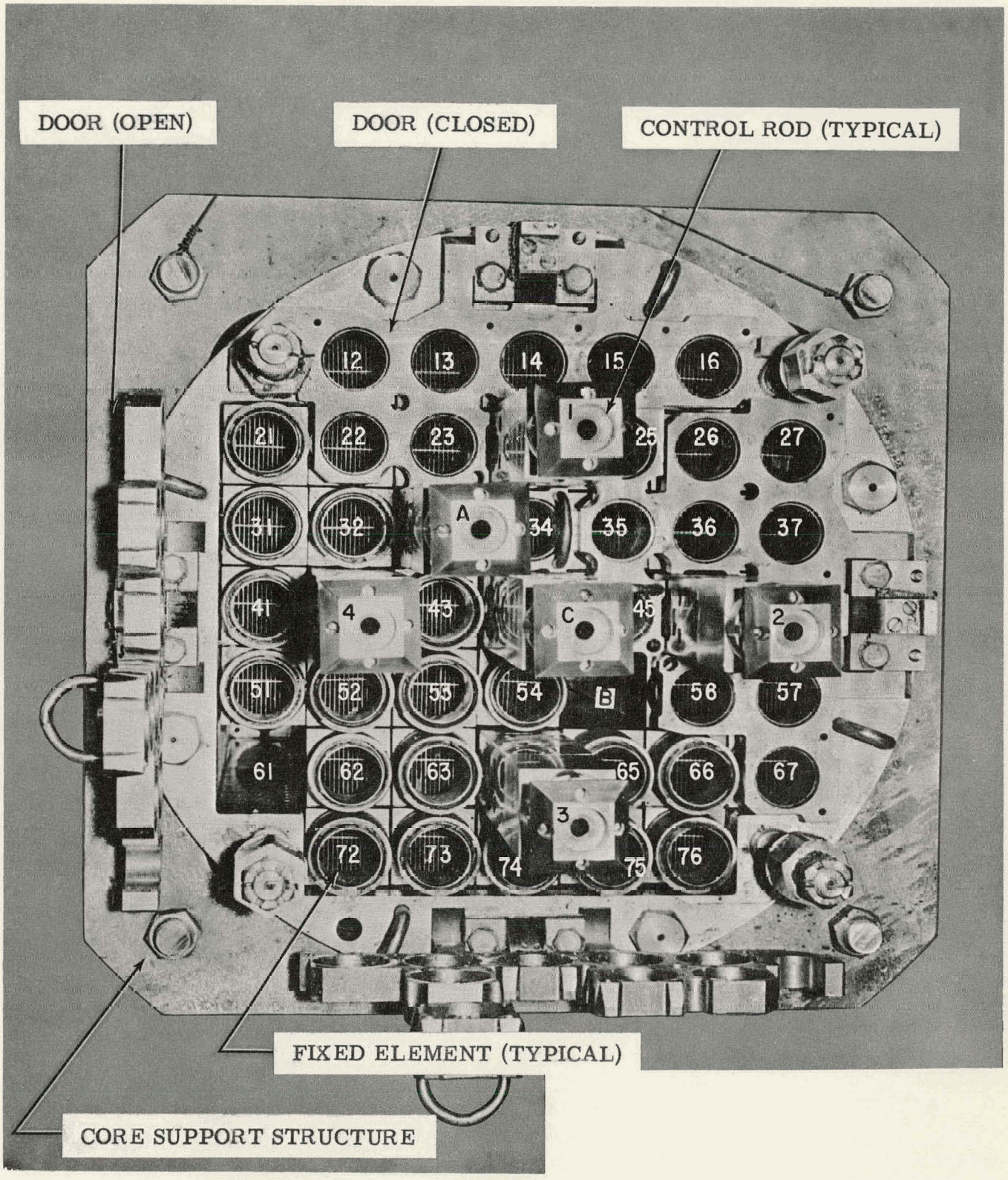

Fig. 1.3 - Top View of Reactor Core and Core Support Structure

2.0 CALCULATIONAL MODELS

The calculational model employed in this report is two-group theory using fundamental nuclear data to determine group constants. The equations and codes used to determine group constants and to solve the diffusion equations are described in this section. The accuracy of the equations and codes is assessed in Section 3.0 by their application to a wide variety of experiments.

2.1 TWO-GROUP THEORY[1]

The SM-1 Core I has an initial loading of 22.5 kg of U-235 in a 22.2 in. diameter cylinder of 21.75 in. height. This results in an average fuel concentration of 4.1×10^{24} atoms/cm^3 of U-235 and H/U-235 ratio of 107 (at 440°F). As a result of this U-235 and H concentration it has an appreciable amount of resonance absorption and fission. The general two-group equations, including resonance fission and absorption are:

$$D_f \nabla^2 \phi_f(\bar{r}) - \sum_R \phi_f(\bar{r}) + S_f(\bar{r}) = 0 \qquad (2.1)$$

$$D \nabla^2 \phi(\bar{r}) - \sum_{a_{th}} \phi(\bar{r}) + S_t(\bar{r}) = 0 \qquad (2.2)$$

where the source terms are defined as,

$$S_f(\bar{r}) = K_{th} \sum_{a_{th}} \phi(\bar{r}) + K_f(1-P) \sum_R \phi_f(\bar{r}) \qquad (2.3)$$

$$S_t(\bar{r}) = P \sum_R \phi_f(\bar{r}) \qquad (2.4)$$

and the effective removal cross section, $\sum_R$, is given by,

$$\sum_R = D_f / \tau \qquad (2.5)$$

The remaining parameters are defined in Appendix E.

With the selection of this model for the treatment of SM-1 Core I it was first necessary to evaluate the effect of various calculational models for the fast and slow coefficients on the agreement of calculation and measurement;

2.1.1 Fast Group Constants

The fast group constants τ, D_f, K_f, and P are calculated employing the MUFT-III, IBM-650 code[2], [3] which solves the Fourier transform of the slowing down distribution from a point source. Two approximations P-1 and P-1 S. G. were investigated.

Microscopic cross section data, atomic concentrations, and the total buckling are the only input required for the calculation. The 59 group cross sections and inelastic scattering matrices used in the MUFT-III calculations are shown in Appendix E.

In this report, the lower limits of the fast group are taken as 0.196 ev at 68°F and 0.248 ev at 440°F. The cutoff energy has been shown to have little effect on k_{eff}.[4]

2.1.2 Thermal Properties

Intercell measurements made in the SM-1 critical experiment[5] and the zero power experiment ZPE-1[6] indicate a significant variation of thermal flux within the fuel element cell. An accurate treatment of these flux variations is necessary if the thermal utilization is to be calculated accurately. The variation of innercell flux, both perpendicular and parallel to the fuel plates in the fixed elements, was calculated using a one velocity P-3 approximation to the Boltzmann equation. The determination of the velocity to be used is discussed in Section 2.1.2.3. The calculational procedure used was basically a superposition of two P-3 solutions to the one-dimensional single velocity transport equation. Murray provides a good description of the one-dimensional problem.[1] This theory has been programmed on the IBM-650 machine for APPR- type fuel elements.[7] For the control rod fuel elements, a one-velocity P-3 calculation in cylindrical geometry was employed. This theory has also been programmed on the IBM-650 for APPR-type control rod fuel elements.[8]

2.1.2.1 Fixed Fuel Elements

Figure 2.1 is a drawing of a typical SM-1 fixed fuel element. The following nomenclature is used for the various regions:

PLATE: This includes the meat and clad, but does not include the dead edges. Properties for this region are calculated as if the clad and meat are homogeneously mixed. The plate width is G.

CHANNEL: This includes material between the fuel plates. The width of this region is G, the same as for the fuel plates. Properties for this region are calculated on a homogenized basis.

ACTIVE: This is a mixed region consisting of the fuel plates and the channel. Its width is G and it is designated as region #2.

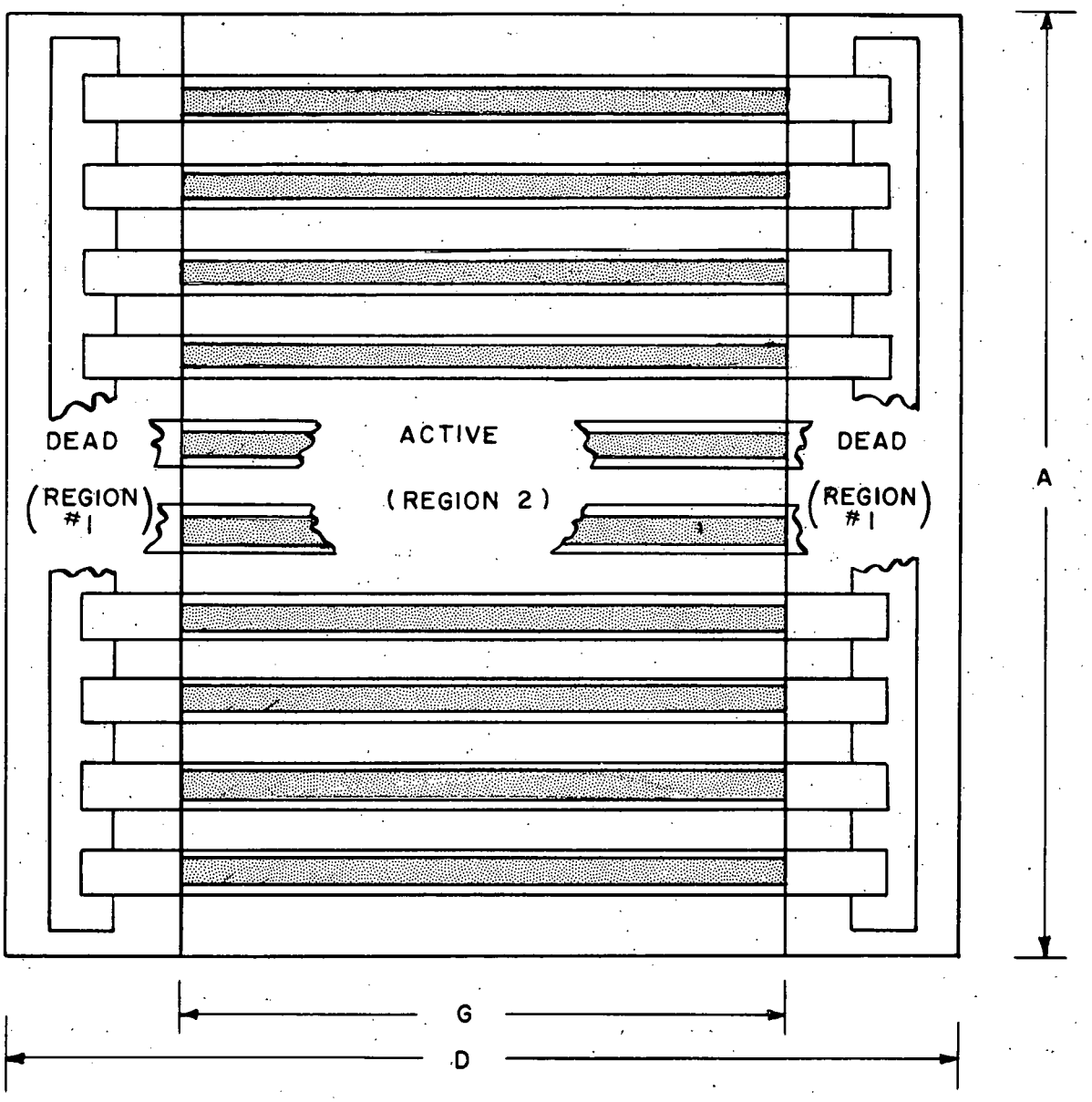

FIGURE 2.1
SUBDIVISION OF A
STATIONARY FUEL ELEMENT

DEAD: This region includes the fuel plate dead edges, side plates, and all of the water in the element that is not in the channels. Its total width is D-G and it is referred to as region #1, its properties are calculated as if all materials in the region are homogeneously distributed.

FUEL ELEMENT CELL: This includes all regions. It is made up of the active plus the dead regions.

The code[7] first calculates the thermal flux distribution normal to the fuel plates. The flux is normalized to one in the active region. Average cross sections are calculated for the active region. Next the thermal flux distribution in the active and dead regions is calculated due to a uniform source of 1 neutron per cm^3 in the dead region. Then the thermal flux distribution in the two regions is calculated due to a uniform source of 1 neutron per cm^3 in the active region. The latter two solutions are weighted and superimposed to obtain the overall flux distribution parallel to the fuel plates. The relative source strength in each region is assumed proportional to the volume fraction of water. The relative flux is normalized to one in the entire cell. From the thermal flux distribution normal and perpendicular to the fuel plates, the nuclear parameters for the whole fuel element cell are calculated.

2.1.2.2 Control Rod Fuel Elements

Figure 2.2 is a drawing of a typical SM-1 control rod fuel element. The nomenclature for the plate, channel, and active region (region #5) is the same as for the fixed elements. Dead region #3 includes the fuel plate dead edges, side plates, portions of the control rod basket, and portions of the water not contained in the channels. Its total width is D-G. Dead region #4 includes portions of the control rod basket and water not contained in the channels. Its total is A-H. The element is cylindricalized into an active region surrounded by a dead region. The relative sources in the active and dead regions were assumed equal to the volume fraction of water in each region.

The code[8] first calculates the thermal flux distribution normal to the fuel plates and normalizes it to one in the active region. Average cross sections are calculated for the active region. The properties of the dead region are calculated on a homogenized basis. The radial flux distribution through the active and dead regions are then calculated and normalized to one in the entire element. The nuclear parameters for the whole element are then calculated by flux weighting from the final thermal flux distribution.

2.1.2.3 Neutron Temperature

The absorption cross section of the SM-1 core is large compared to the scattering cross section.

$$(\overline{\Sigma}_{a_{th}} / \overline{\Sigma}_s = 0.13 \text{ at } 440^{\circ}F).$$

This is known to harden the spectrum, i.e. shift the spectrum to higher energies

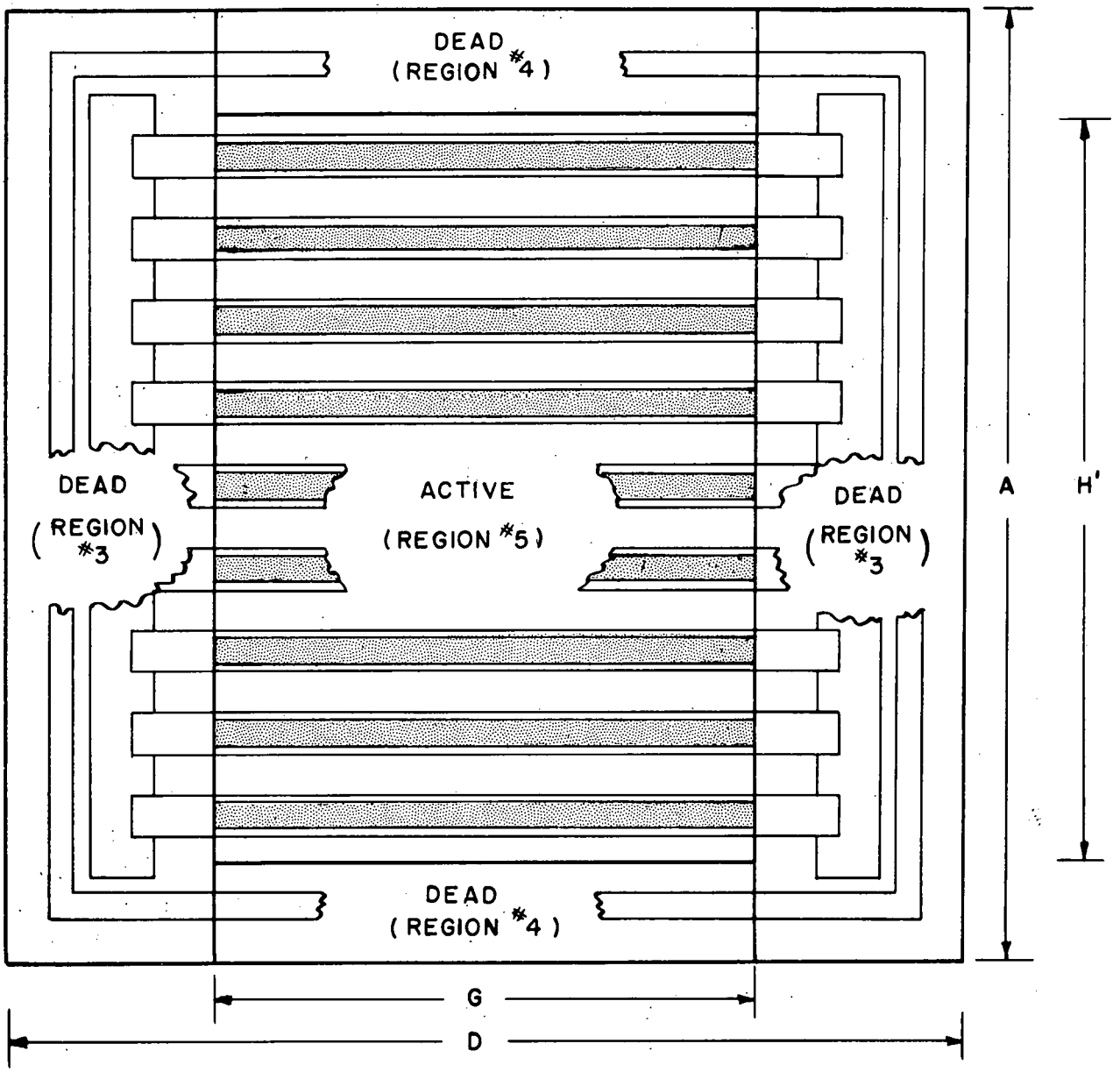

FIGURE 2.2.

SUBDIVISION OF A CONTROL ROD FUEL ELEMENT

as a result of the preferential absorption of low energy neutrons. This problem has been treated by defining an effective neutron temperature which is higher than the physical temperature[9] by an amount which depends on the ratio of absorption to scattering cross section in the assembly. The energy distribution of the thermal neutron flux was assumed to be a Maxwell-Boltzmann distribution about the effective neutron temperature.

The effective neutron temperature was calculated by the following equation,

$$T_n/T_o = 1 + C \sum a_{th}/\xi\Sigma s \qquad (2.6)$$

where the parameters are defined in Appendix E.

2.2 CORE GEOMETRY CONSIDERATIONS

Figure 2.3 presents the fixed and control rod fuel elements assembled in the SM-1 Core I. SM-1 Core I was operated with five of the rods positioned as a bank. A number of different approximations were applied to obtain a solution of the two-group equations.

2.2.1 Equivalent Bare Model

The solutions of the core equations, given in Section 2.1, may be found by proposing that each flux obeys the wave equation, i.e.:

$$\nabla^2 \phi_f(\bar{r}) + B^2 \phi_f(\bar{r}) = 0 \qquad (2.7)$$

$$\nabla^2 \phi(\bar{r}) + B^2 \phi(\bar{r}) = 0$$

where B^2, the buckling, is assumed to be common to both fluxes. These equations may be substituted into (2.1) and (2.2) to yield two homogeneous equations. If these simultaneous equations in ϕ_f and ϕ are to be solved, the determinant formed by the materials dependent coefficients must be zero. This implies that:

$$\frac{K_{th}\ P}{(1 + \tau B^2)(1 + L^2 B^2)} + \frac{K_f\ (1-P)}{(1 + \tau B^2)} = 1 \qquad (2.8)$$

where the square of the diffusion length, L^2, is defined as:

$$L^2 = D/\sum a_{th} \qquad (2.9)$$

This equation has been derived for a critical reactor. For a non-critical reactor, the multiplication factor for the system, k_{eff}, may be expressed in terms of the factors ν and ν_c, the neutrons produced per fission and the

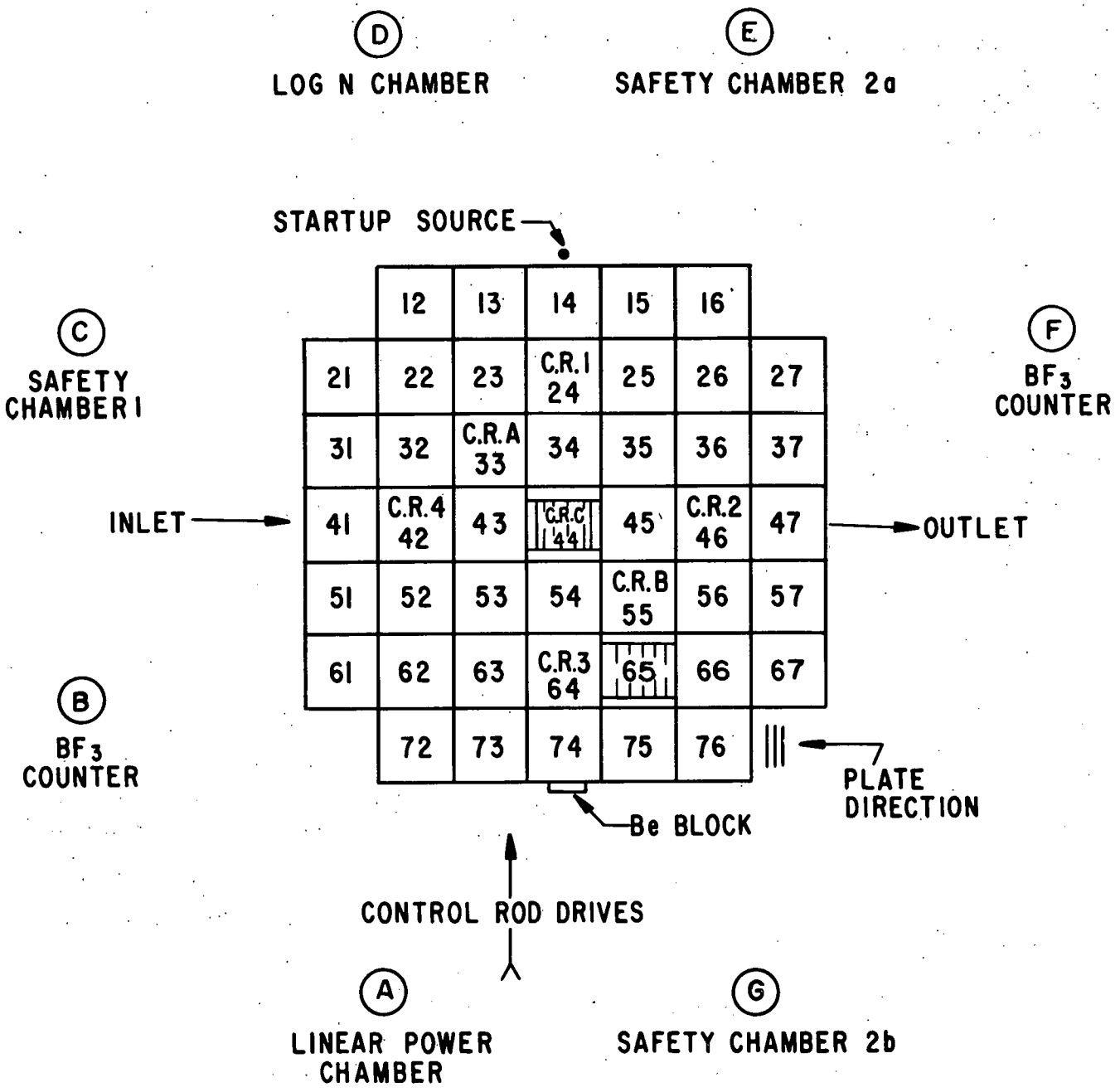

Figure 2.3 SM-1 Core Layout

neutrons produced per fission required for criticality, respectively. Therefore:

$$k_{eff} = \frac{\nu}{\nu_c} = \frac{PK_{th}}{(1 + \tau B^2)(1 + L^2 B^2)} + \frac{K_f (1-P)}{(1 + \tau B^2)} \qquad (2.10)$$

No distinction is made in this report between calculated static multiplication and measured dynamic multiplication.[20] The difference of static and dynamic multiplication has been found to be less than 1% in similar cores.[21] The effect of a reflector may be included in the bare reactor calculation by modifying the definition of the buckling. For a finite cylindrical core:

$$B^2 = \left(\frac{\pi}{H + 2'S_z} \right)^2 + \left(\frac{2.405}{R + S_r} \right)^2 \qquad (2.11)$$

where the parameters are defined in Appendix E. The change in reactivity of a core due to a change in k_{eff} from $(k_{eff})_1$ to $(k_{eff})_2$ is computed by:

$$\Delta \rho = \frac{(k_{eff})_2 - (k_{eff})_1}{(k_{eff})_2 \ (k_{eff})_1} \qquad (2.12)$$

for a critical core $\rho = 0$ and for change from critical

$$\rho = \frac{k_{eff} - 1}{k_{eff}} \qquad (2.13)$$

2.2.2 Multi-Region One-Dimensional Calculations

For one dimensional radial calculations the core is approximated by an equivalent cylinder having a cross-sectional area equal to the cross-sectional area of the actual core array. The modifed two-group equations were employed to obtain the core reactivity and flux and power distributions. These one dimensional calculations were performed by use of VALPROD[10] and WINDOW-SHADE,[11] two IBM-650 programs which are used to treat the radial and axial directions, respectively.

2.2.2.1 VALPROD[10]

The VALPROD code for the IBM-650 is used for the treatment of the radial direction where the height of the cylinder is accounted for by a perpendicular buckling. The code may also be used for axial calculations in which case the width or radius of the core is accounted for by a radial buckling. Input to the code includes group constants in each region, configuration of the core, and number of calculational points in each region. Output includes the flux distribution for each neutron group, the power distribution, and k_{eff} of the core.

2.2.2.2 WINDOWSHADE[11]

The WINDOWSHADE code is a nine-region, two-group finite difference calculation in slab geometry for the IBM-650 used to perform axial calculations. A perpendicular buckling must be specified as well as nuclear properties for each neutron group in each region. Also included is the addition of a uniform thermal poison to one section of the reactor to represent the effect of control rods. The program has two options: the placement of the control rod bank may be adjusted until criticality is obtained (the code may be made to iterate to $k_{eff} \neq 1$) or the location of the bank may be specified and the code will calculate k_{eff}. Output includes the flux distribution for each group, the power distribution, the bank position, and the k_{eff} of the core.

2.2.3 Analytical Two-Region, Two-Group Calculations

An analytical solution of the two-group, two-region equations for a finite cylindrical core has been programmed for the IBM-650. The FINK-1 Code[13] first solves the problem radially with an assumed axial savings and then axially with the computed radial savings. The process is repeated until satisfactory convergence is obtained.

2.2.4 Multiregion, Two-Dimensional Calculations

The PDQ, IBM-704 code,[14],[15],[16] is a few-group, two dimensional, reactor design code. It finds a discrete numerical approximation to the few-group, time independent, neutron diffusion equations for a heterogeneous reactor in a two-dimensional bounded region. It solves for one to four lethargy groups, with variables either x-y, in rectangular co-ordinates, or r-z, in cylindrical coordinates. Input to the code includes nuclear parameters for each neutron group for each region, core configuration, and number of mesh points in each region. Output includes flux and power distributions and the k_{eff} of the core. The code provides a much better estimate of the detailed power distribution within the core than can be obtained with the one-dimensional codes.

2.2.5 Multiregion, One-Dimensional Depletion Calculation

The CANDLE-2, IBM-704 code is a one-dimensional, few-group depletion code for rectangular, cylindrical, and spherical geometry. The following four type searches are provided as options: criticality buckling, criticality poison, criticality boundary, and no criticality search. The output to the code includes geometry (mesh points and regions), isotopic number densities (constant distribution within a region), and number of time steps. The output provides group constants in each region at the initial time step, the eigenvalue and control parameters for each iteration, and the atomic density for each burnable element at each mesh point.

2.3 SPECIAL PREPARATION IBM-650 PROGRAM

To facilitate the calculation of nuclear parameters for use in the various codes, a special routine was devised and programmed on the IBM-650.

2.3.1 Program 50 (PROMPT-I)

Program 50 (PROMPT-I) prepares input for the MUFT-III and Plate-Type P_3 codes for APPR-type fixed fuel elements. Input includes element and core geometry, material, and loading data. Temperature-dependent input data, including microscopic cross sections and densities, are obtained from specially prepared files. Output includes loading as a function of fuel burnup, weight and volume fractions, metal-water ratios, volumes, etc.

2.4 NUCLEAR DATA

2.4.1 MUFT-III Cross Section Files

The MUFT-III microscopic cross section files is listed in Appendix D. The cross sections have been obtained from reference (22). Modifications have been made and the number of groups increased to 59 so that the lowest energy is 0.196 ev.

2.4.2 MUFT-V Cross Section Files

The MUFT-V microscopic cross section files have been obtained from reference (23). These have been modified for use in the MUFT-III.

2.5 REFERENCES (2.0)

1. Murray, R. L., "Nuclear Reactor Physics," Englewood Cliffs, New Jersey, Prentice-Hall, Inc., 1957.

2. Hellens, R. L., "Multigroup Fourier Transform Calculation, Description of the MUFT-III Code," Westinghouse Atomic Power Division, WAPD-TM-4, July, 1956.

3. Rosen, S. S., "Supplement to MUFT-III Code, Multigroup Fourier Transform Calculation," AP Note 90, Alco Products, Inc., December 6, 1957.

4. Byrne, B. J., "Analysis of Extended Zero Power Experiments on the Army Package Power Reactor, ZPE-2," APAE No. 27, May 7, 1958.

5. Williams, D. V. P., "Army Package Power Reactor Critical Experiment," Oak Ridge National Laboratory, ORNL-2128, (1956).

6. Noaks, J. W., and Johnson, W. R., "Army Package Power Reactor Zero Power Experiments, ZPE-1," APAE No. 8, February 8, 1957.

7. Byrne, B. J., and Caton, R. L., "Two-Dimensional P-3 Calculation for APPR-Type Fixed Fuel Elements," AP Note 96, Alco Products, Inc., February 14, 1958.

8. Bobe, P. E., and Oby, P. V., "Calculation of Thermal Properties of APPR-Type Control Fuel Elements, Program 54," AP Note 192, Alco Products, Inc., October 23, 1959.

9. Cohn, E. R., "Survey of Neutron Thermalization Theories," Geneva Conference Paper P/611, Session 23A, August, 1955.

10. Oby, P. V., "Modified Two-Group Multiregion Calculation Using the VALPROD Code for the IBM-650," AP Note 24 (Revised), Alco Products, Inc., August 14, 1957.

11. Fairbanks, F. B., "Two-Group Multiregion Axial Windowshade Calculation on the IBM-650," APAE Memo 88, March 29, 1957.

12. Bohl, H., et al, "P1MG - A One-Dimensional Multigroup P_1 Code for the IBM-704," WAPD-TM-135, July, 1959.

13. McElligott, P. E., "FINK-I: A Two-Group, Two Region Calculation on the IBM-650," APAE Memo 121, January 28, 1958.

14. Bilodeaux, G. G., et al, "PDQ - An IBM-704 Code to Solve the Two-Dimensional, Few-Group Neutron Diffusion Equation," Westinghouse Atomic Power Division, WAPD-TM-70, August, 1957.

15. Cadwell, W. R., "PDQ-2: A Two-Dimensional, Few-Group Diffusion Code," Bettis Technical Review, WAPD-BT-13, May, 1959.

16. Cadwell, W. R., "PDS-3, A Program for the Solution of the Neutron Diffusion Equations in Two-Dimensions on the IBM-704," WAPD-TM-179, May, 1960.

17. Marlowe, O. J., and Ombrellaro, P. A., "CANDLE-A One-Dimensional Few-Group Depletion Code for the IBM-704," WAPD-TM-53, May, 1957.

18. Marlowe, O. J., and Ombrellaro, P. A., "CANDLE-A One-Dimensional Few-Group Depletion Code for the IBM-704, Addendum 1, CANDLE-2," WAPD-TM-53 Addendum 1, October, 1957.

19. Hughes, D. J., Carter, R. S., "Neutron Cross Section Angular Distribution," BNL-400, June, 1956.

20. Gross, E. E., Marable, T. H., "Static and Dynamic Multiplication Factors and their Relation to the Inhour Equation," Nuc. Sc. and Eng., Vol. 7, No. 4, April, 1960.

21. Olsen, T. M., Welshans, L., "ANPP Code Development Program Pressurized Water Task Quarterly Progress Report Number Eight," MND-C-2207, August, 1961.

22. Hellens, R. L., "Multigroup Fourier Transform Calculation Description of the MUFT-III Code," WAPD-TM-4, July 19, 1956.

23. Henry, A. F., "54 Group Library for P-1 Programs," WAPD-TM-224, April, 1960.

3.0 REVIEW OF THE CALCULATIONAL MODELS

3.1 INTRODUCTION

The purpose of this analysis is to determine the accuracy of various calculational models and nuclear data described in Section 2.0 by comparing calculated and measured parameters for a wide range of reactor cores, and thereby select the best calculational model and nuclear data for analysis of SM-1 Core I.

The following core parameters were investigated, using various fast files (containing fast microscopic cross sections and slowing-down parameters) and slowing-down models: core reactivity, fast flux distribution, and fraction of thermal fissions. In order to provide a more fundamental check on the nuclear model and data, the neutron age from Po-Be and a fission source was calculated for both pure water and for iron water mixtures. This latter calculation is presented first.

3.2 EFFECT OF CALCULATIONAL MODEL ON NEUTRON AGE

The effects of the MUFT-III and MUFT-V fast files, and the P-1 and P-1 S.G. slowing-down models, on the calculated ages of fission and polonium-beryllium source neutrons in pure water and iron-water mixtures, were analyzed and compared to experiment.

3.2.1 Systems Investigated

The following two systems were investigated to obtain the effects of the fast calculations on calculated ages:

1. Fission energy neutrons in pure water within a plant-source geometry,[1]
2. Polonium-beryllium energy neutrons in various iron-water mixtures within a plane-source geometry.[2]

In both systems the ages were measured up to the resonance energy of indium (1.46 ev).

Comparison of the calculated ages of fission neutrons in pure water and experimental results provides a test of the slowing-down approximation as applied to pure water. The Po-Be energy neutrons were investigated for metal-to-water ratios of 0.0, 0.5, 1.0, 2.0, and 3.0 in order to test the iron nuclear data.

3.2.2 Calculational Approach

The MUFT-III code, with the MUFT-III and MUFT-V fast files, and P-1 and P-1 S. G. slowing-down models, was used to predict neutron ages and compare to experiment. Since the resonance energy of indium (1.46 ev) was used to measure ages in both systems, the MUFT-III and MUFT-V fast files were used with 51 lethary groups (corresponding to a lower energy cut-off of 1.44 ev). The input total buckling, B^2, used was 10^{-6} cm^{-2}, in order to simulate an infinite system as closely as possible. (This is the smallest buckling accepted by the MUFT-III code.)

The fission energy spectrum[3] used as a source file in the calculations are given in Fig. 3.1. Figure 3.2 presents the Po-Be energy spectrum as used in the calculations. The spectrum was determined by averaging several spectra collected and reported in graphical form in reference.[2] Although there is a lack of similarity in the detailed structure of these curves, their overall shape and average energy compare favorably. It has been found that each particular spectrum provided a negligible effect on the calculated age.[2]

3.2.3 Results

Table 3.1 presents the experimental and calculated ages for fission neutrons in pure water, employing the MUFT-III and MUFT-V fast files, with the P-1 S. G. slowing-down models. The experimental age of 27.68 ± 0.10 cm^2 was obtained at the Argonne National Laboratory,[1] and is reported to be the latest age determination. Previous published measurements have yielded ages of 30.5 ± 1.5 cm^2.[1]

TABLE 3.1
NEUTRON AGES OF FISSION NEUTRONS IN PURE WATER
USING FAST FILES AND SLOWING-DOWN MODEL

Measured Age (cm^2)	MUFT-III, P-1	MUFT-III, P-1 S. G.	MUFT-V, P-1	MUFT-V, P-1 S. G.
27.68 ± 0.10	26.65	34.03	24.77	30.61

As is shown in Table 3.1 the calculated age of 26.65 cm^2 of fission neutrons in pure water, based on the MUFT-III fast files and P-1 slowing-down model, provides the best prediction of the measured age of 27.68 ± 0.10 cm^2.

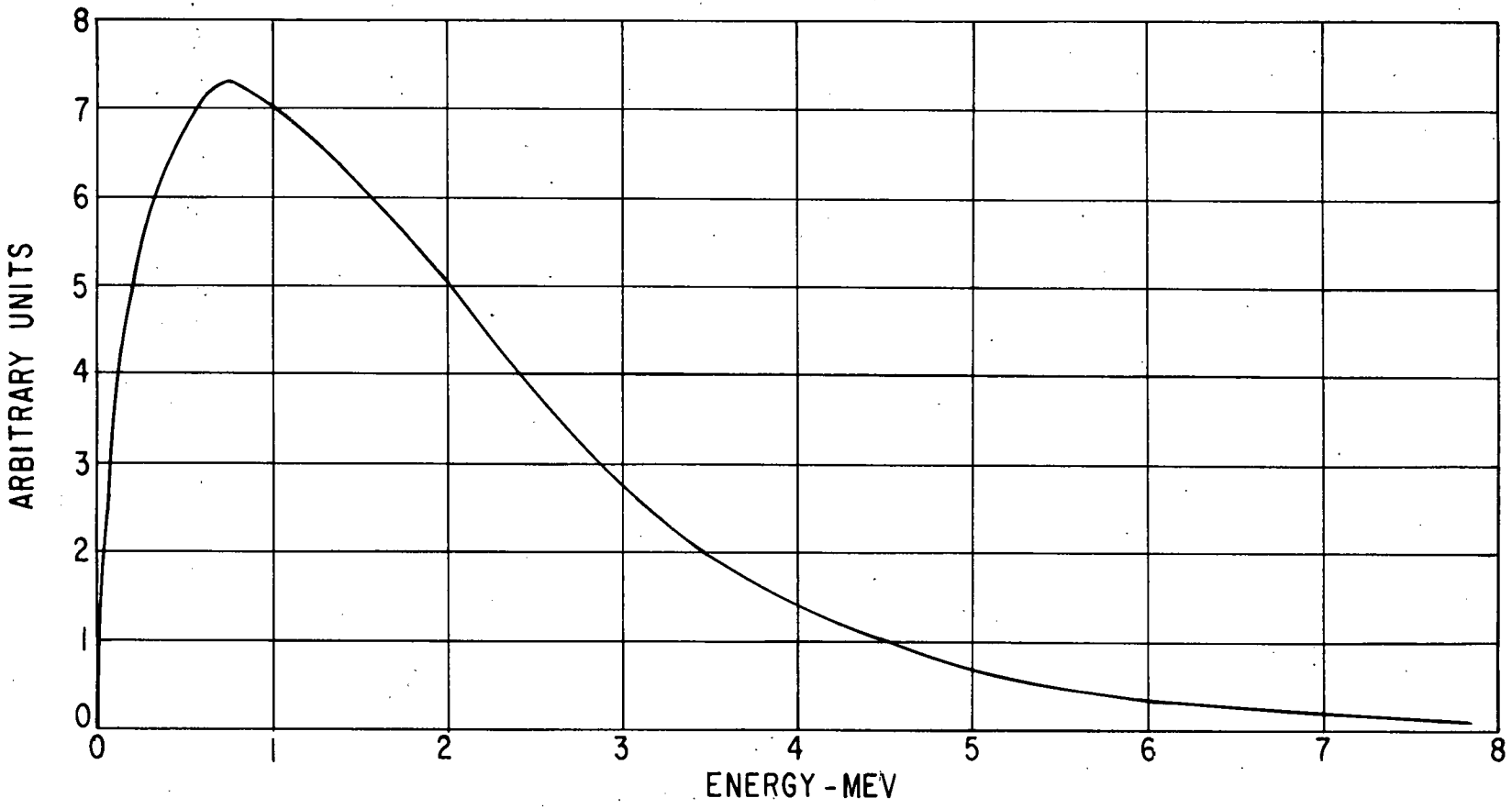

Figure 3.1 Energy Distribution of Fission Neutrons

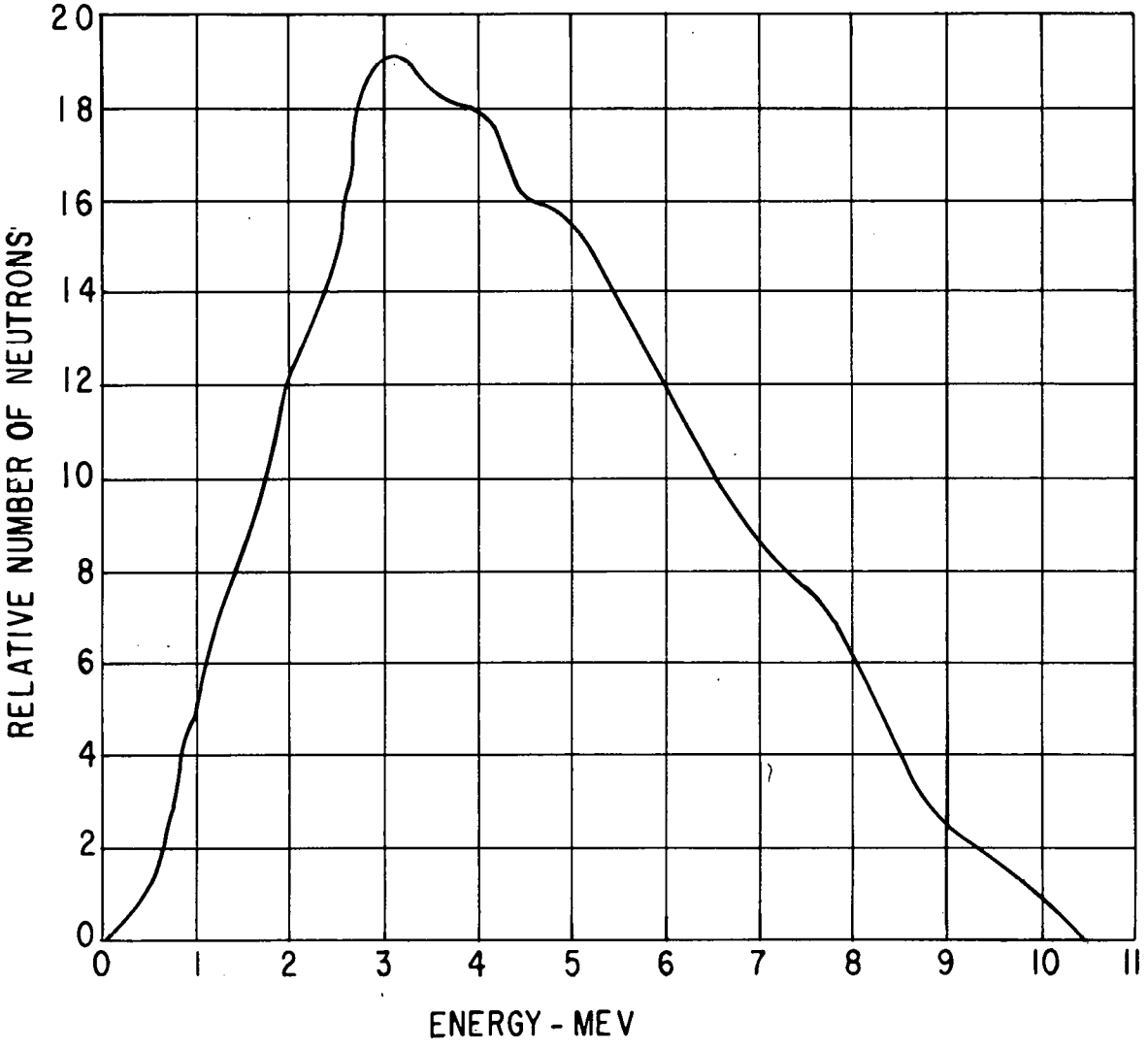

Figure 3.2. Energy Spectrum From Po^{210}-α-Be Neutron Source

Table 3.2 reports the effects of the fast calculations on the fast nuclear parameters for pure water with fission neutrons, using 51 lethargy groups (corresponding to a lower energy cutoff of 1.44 ev).

TABLE 3.2
EFFECTS OF FAST CALCULATIONS ON FAST PROPERTIES OF WATER USING FISSION NEUTRONS (FAST FILES AND SLOWING-DOWN MODEL)

Nuclear Parameter	MUFT-III, P-1	MUFT-III, P1-SG	MUFT-V, P-1	MUFT-V, P1-SG
$\Sigma_{a_f}(cm^{-1})$	0.000517	0.000517	0.000726	0.000726
$\Sigma_{sl}(cm^{-1})$*	0.050717	0.050717	0.050785	0.050785
D_f (cm)	1.365230	1.743313	1.276113	1.576858
P	0.9899914	0.989914	0.985910	0.985910

* Macroscopic slowing-down cross section from fast group, i.e., $\xi \Sigma_s / \Delta U$

Table 3.3 presents the experimental and calculated ages for Pe-Be neutrons in various iron-water mixtures, and their dependence on the fast calculations. The experimental ages were obtained at the Bettis Atomic Power Division.(2)

TABLE 3.3
NEUTRON AGES OF Po-Be NEUTRONS IN IRON-WATER MIXTURES
(USING FAST FILES AND SLOWING-DOWN MODEL)

Metal/Water Volume Ratio	Measured Age (cm^2)	MUFT-III, P-1	MUFT-III, P1-SG	MUFT-V, P-1	MUFT-V, P1-SG
0.0	55.4 ± 1.7 57.9 ± 1.7	62.1	83.9	52.6	66.5
0.5	56.2 ± 2.2	53.0	59.1	53.2	59.0
1.0	58.8 ± 1.8	54.0	57.8	58.1	62.1
2.0	72.1 ± 2.2	60.4	63.0	69.6	72.6
3.0	83.0 ± 2.5	67.4	69.5	81.1	83.7

According to Table 3.3, the MUFT-V fast files with the P-1 slowing-down model affords the best comparison between calculated and measured ages of Po-Be neutrons in iron-water mixtures.

TABLE 3.4
EFFECTS OF FAST CALCULATIONS ON FAST PROPERTIES OF IRON-WATER MIXTURES USING Po-Be NEUTRONS

($M/W = 0.0$)

Nuclear Parameter	MUFT-III, P-1	MUFT-III, P1-SG	MUFT-V, P-1	MUFT-V, P1-SG
$\Sigma_{a_f}(cm^{-1})$	0.001954	0.001954	0.002376	0.002376
$\Sigma_s (cm^{-1})$	0.034698	0.034698	0.035262	0.035262
D_f (cm)	2.276717	3.076325	1.980150	2.500933
P	0.946682	0.946683	0.936868	0.936869

Table 3.4 and 3.5 list the effects of the fast calculations on the fast properties for the metal/water volume ratios of 0.0 and 3.0; i.e., pure water and highly concentrated iron mixture, respectively, using Po-Be source neutrons.

TABLE 3.5
EFFECTS OF FAST CALCULATIONS ON FAST PROPERTIES OF IRON-WATER MIXTURES USING Po-Be NEUTRONS

($^{M}/_{W}$ = 3.0)

FAST FILES AND SLOWING-DOWN MODEL

Nuclear Parameter	MUFT-III, P-1	MUFT-III, P1-SG	MUFT-V, P-1	MUFT-V, P1-SG
$\sum_{a_f}$ (cm^{-1})	0.005900	0.005900	0.001855	0.001855
$\sum_{sl}$* (cm^{-1})	0.011949	0.011949	0.012718	0.012718
D_f (cm)	1.202927	1.240689	1.181425	1.220028
P	0.669467	0.669468	0.872718	0.872717

* Macroscopic slowing-down cross section from fast group, i.e. $\xi\sum_s/\Delta u$

A study has been performed[2] to determine the effect of the rather uncertain capture and inelastic scattering cross sections of oxygen on the calculated age of fission neutrons in pure water. The results[2] are listed in Table 3.6. The results for the Po-Be spectrum are also given.

TABLE 3.6
EFFECT ON AGE OF ELIMINATING CAPTURE AND INELASTIC CROSS SECTIONS OF OXYGEN

Condition of Oxygen	Fission Spectrum	Po-Be Spectrum
All Cross Sections Used	25.9 cm^2	53.5 cm^2
$\sigma_c = 0$	27.0	61.1
$\sigma_{in} = 0$	26.1	55.2
$\sigma_c = \sigma_{in} = 0$	27.3	63.6

It can be seen in Table 3.6 that the effect of suppressing the capture and inelastic cross sections of oxygen on the calculated age of fission neutrons is reasonably small. The MUFT-III fast files do not consider inelastic scattering for oxygen and have a smaller effective oxygen capture cross section than the MUFT-V fast files (as can be seen from Table 3.6).

Table 3.2 indicates that the fast water capture cross section is greater for the MUFT-V fast files than for the MUFT-III files. However, according to Table 3.6 eliminating the oxygen capture cross section considerably alters the calculated age of Po-Be neutrons in pure water. The effect of neglecting oxygen inelastic scattering is relatively small. The strong sensitivity of the oxygen capture cross section on the calculated age of Po-Be neutrons in pure water is due to the rapid fall-off of the hydrogen capture cross section relative to that of oxygen at higher neutron energies. According to Table 3.3, the MUFT-III, P-1 fast model considerably overestimates the experimental age of Po-Be neutrons in pure water, whereas the MUFT-V, P-1 fast model slightly underestimates the experimental results. It is concluded that the oxygen capture cross section as used in the MUFT-III fast files is too low for high neutron energies near 5 Mev (average energy of Po-Be source spectrum). This does not affect the conclusion that the MUFT-III, P-1 fast model is best in predicting the age of fission neutrons in pure water, since for neutrons of 2 Mev (average energy of fission source spectrum), capture and inelastic scattering effects of oxygen were observed to have relatively small effect on the calculated age of fission neutrons in pure water, according to Table 3.6.

As seen in Table 3.5 the iron capture cross section as used in the MUFT-III fast files is considerably greater than that for the MUFT-V fast files, at high energies near 5 Mev. According to Table 3.3 the calculated age of Po-Be neutrons for M/W = 3.0, based on the MUFT-III, P-1 fast model, considerably underestimates the measured result, where as the age based on the MUFT-V, P-1 fast model is in excellent agreement with experiment. Indeed, this comparison is the same for the low metal-to-water volume rates; i.e., 0.5, 1.0, and 2.0 where the concentration of iron in the mixtures is relatively small. Therefore, it is concluded that the iron capture cross section, as used in the MUFT-III fast files, is definitely too large at high energies near 5 Mev. However, this does not imply that the MUFT-III iron fast file is inaccurate at lower energies below 2 Mev, at which it is necessary to properly describe the fast absorption and slowing-down properties for reactors.

3.2.4 Conclusions

From the investigation of the effect of calculational model on neutron age from fission and Po-Be sources the following conclusions can be drawn.

1. The P-1 model employing MUFT-III nuclear data file (Appendix F) gives the best calculated fission age in water.

2. The P-1 model employing MUFT-V nuclear data file gives the best calculated Po-Be ages in water and iron-water mixtures.

3. The MUFT-III iron data need revision at energies greater than 2 Mev to improve agreement with Po-Be ages.

3.3 EFFECT OF FAST GROUP CALCULATIONAL MODEL ON CORE REACTIVITY

The reactivity of a number of cores has been calculated using the P-1 and P1-SG slowing-down models and MUFT-III and MUFT-V nuclear data.

The core types chosen for investigation provide a wide variety of test cores, since they range from cores consisting of only uranium and water, to cores containing uranium, water, stainless steel and boron. The cores calculated vary from those containing little or no reactivity to those containing as much as 30 dollars with the rods out. The critical cores provide the cleanest comparison of calculated to experimental reactivities since there are uncertainties when dealing with cores with large excess reactivity. These uncertainties are the method of measurement, the effective delayed neutron fraction β_{eff} as a function of control rod position, and the equation used to convert experimental reactivities obtained in dollars to reactivities (ρ).

In this report the experimental excess reactivities, expressed in dollars are converted to reactivities (ρ) using the relation,[4]

$$\rho = 1 - e^{-I_{ex}\,\beta_{eff}} \qquad (3.1)$$

where, ρ = reactivity

I_{ex} = excess reactivity (dollars)

β_{eff} = effective delayed neutron fraction

Previous analyses of the SM-1 Core I have been based on a value for the effective delayed neutron fraction, β_{eff}, of 0.0073. Measurements performed upon the SPERT-III[5] and BSR-II[6] cores, indicate a value of 0.0078 for β_{eff}. In addition, β_{eff} has been calculated for SM-1 to be 0.0078 by R. L. Murray (See Appendix A) using modified one-group theory and $\beta = 0.0065$. Therefore, the value of 0.0078 will be adopted for the effective delayed neutron fraction, β_{eff}, throughout this report.

3.3.1 Core Types Investigated

The following core types were analyzed to obtain the reactivity effect of the MUFT-III and MUFT-V fast files, with the P-1 and P1-SG slowing-down models:

1, 2. WAPD homogeneous critical cores with no B-10 or stainless steel, 68°F, ($\%\rho \cong 0$)[7]

3. ORNL critical core ("light loading") with no B-10, 68°F, ($\%\rho \cong 0$)[8]

4. SPERT-III critical water height core ("A") with no B-10, 80°F ($\%\rho \cong 0$)[5]

5. SM-1 Core I (10 fixed plus 7 control fuel elements) with "as fabricated" B-10 loading, 68°F, ($\%\rho \cong 0$)[9]

6. SM-1 Core I (15 fixed plus 1 control fuel element) with "as fabricated" B-10 loading, 68°F, ($\%\rho \cong 0$)[10]

7. SM-1 Core I critical water height core (38 fixed plus 7 control fuel elements) with "as fabricated" B-10 loading, 68°F ($\%\rho \cong 0$)[11]

8. SM-1 Core I (38 fixed plus 7 control fuel elements, poisoned with boron-stainless steel strips) with "as fabricated" B-10 loading, 68°F, ($\%\rho \cong 0$)[11]

9. SM-1 Core I (38 fixed plus 7 control fuel elements, poisoned with stainless steel strips) with "as fabricated" B-10 loading, 68°F, ($\%\rho \cong 0$)[11]

10, 11. SM-1 Core I (38 fixed plus 7 control fuel elements) with "as fabricated" B-10 loadings, 68°F and 440°F, ($\%\rho >= 0$)[12], [13], [14]

12. SM-1 Core I (all 45 fixed fuel elements) with "as fabricated" B-10 loading, 68°F, ($\%\rho >= 0$)[10]

13. SM-2 experimental core (all 45 fixed fuel elements) with no B-10 loading, 68°F, ($\%\rho >= 0$)[15]

The first two cores are aqueous homogeneous solutions employing fully enriched uranium. All the rest of the cores are fully enriched uranium, stainless steel, water-moderated cores, with the SM-1 type cores containing boron as a burnable poison.

Table 3.7 lists the atomic number densities of the various cores investigated. U-238 was included in the MUFT-V files but not in the MUFT-III files. The reactivity effect of U-238 is approximately 0.25%ρ for these cores.

TABLE 3.7

ATOMIC NUMBER DENSITIES (atoms/cm^3) x 10^{24} OF CORE TYPES INVESTIGATED

Core No.	Core Type		U-235	U-238	Hydrogen	Oxygen	Stainless Steel *	B-10	H/U-235 Ratio
1, 2	WAPD Critical	#15	0.0006510	0.0000430	0.0349900	0.0647800	0.034900		99.5
	68°F	#21	0.0005443	0.0000359	0.0647700	0.0345600	-	-	119.0
3	ORNL Critical 68°F		0.0001937	0.0000141	0.0535300	0.0271824	0.0171946	-	276.4
4	SPERT-III Critical Core "A", 80°F		0.0003122	0.0000228	0.0513640	0.0263520	0.0189820	-	164.5
5	SM-1 Core I (10 Fixed + 7 Control Elements "As Fabricated Boron", 68°F		0.0003957	0.00002909	0.05262565	0.0271622	0.0157895	0.0000065	133.0
6	SM-1 Core I (15 Fixed 1 Control Element) "As Fabricated Boron" 68°F		0.0004240	0.000031177	0.0532893	0.0275548	0.0147758	0.00000697	125.7
7, 10	SM-1 Core I 68°F, Clean		0.0004165	0.0000307	0.0531124	0.0274501	.0150465	0.00000684	127.5
8	SM-1 Core I Fixed Fuel Elements, 68°F, with B-SS Strips		0.0004289	0.0000316	0.0518003	0.0268210	0.0164488	0.00002314	120.8
9	SM-1 Core I Fixed Fuel Elements, 68°F, with SS Strips		0.0004289	0.0000316	0.0414968	0.0216692	0.0294340	0.00000706	96.8
11	SM-1 Core I 440°F Clean		0.0004165	0.0000307	0.0443620	0.0230754	0.0150465	0.00000684	106.5
12	SM-1 Core I All Fixed Fuel Elements 68°F Clean		0.0004291	0.0000316	0.053408	0.027624	0.014594	0.00000705	124.5
13	SM-2 Experimental 68°F		0.0006990	0.0000504	0.0491484	0.0250982	0.0177171	-	70.3

* Stainless steel is assumed to be composed only of Fe, Ni, Cr and Mn. The Type 304L has a density of 7.9 gm/cm^3 and 2.0 wt% Mn, 9.0 wt% Cr and balance of Fe. Number densities in this table include all elements.

3.3.2 Results

Cores No. 1 and 2

The reactivity of Cores No. 1 and 2(homogeneous cores No. 15 and 21, respectively) were calculated using an equivalent bare model. The measured reactivity was reported to be 0.0 + 0.6% ρ and 0.0 + 0.2% ρ for the critical cores No. 15 and 21, respectively. Tables 3.8 and 3.9 contain the group constants and reactivity calculated by several different slowing down models and nuclear data files. The results indicate that the P-1 slowing down model employing MUFT-III data file yields the closest agreement to measured reactivities. It is of interest to note that the calculated reactivities for both cores are within experimental error.

Core No. 3

As part of the ORNL critical experiment program for the APPR-1, an experiment was assembled with no reactivity containing fully enriched uranium stainless steel and light water in the SM-1 Core I configuration. The critical experiment employed uranium metal foils stainless steel clad fuel plates. In order to determine the most accurate thermal group constants P-5 theory has previously been applied. The measured reactivity of the critical core was reported to be 0.0 $\pm$ 0.5% ρ. The reactivity was calculated using the equivalent bare model and several slowing down models and nuclear data files. The results are given in Table 3.10. The table shows that the MUFT-III P-1 files give the most accurate reactivity. The calculated reactivity for this slowing down model and nuclear data are within experimental error.

Core No. 4

The SPERT-III core employs fuel elements of stainless steel UO_2 dispersion. As part of the initial experiments on this program several clean cores were assembled. One of these was known as SPERT-III critical water height core "A". No estimate of the experimental uncertainty in measured reactivity was available. The calculated reactivity using the equivalent bare model in several slowing down models and nuclear data files is shown in Table 3.11.

TABLE 3.8

REACTIVITY ANALYSIS OF WAPD HOMOGENEOUS CRITICAL CORE NO. 1 (#15) (NO B-10 OR STAINLESS STEEL), 68°F

FAST FILES AND SLOWING-DOWN MODEL

Nuclear Parameter	MUFT-III, P-1	MUFT-III, P1-SG	MUFT-V, P-1	MUFT-V, P1-SG
P	0.756463	0.759281		
τ (cm^2)	29.356796	32.430402		
$\nu\Sigma_{f_f}$ (cm^{-1})	0.018394	0.019177		
Σ_{a_f} (cm^{-1})	0.010615	0.010984		
$K_f = \nu\Sigma_{f_f} / \Sigma_{a_f}$	1.732802	1.745843		
$K_{th} = \nu\Sigma_{f_{th}} / \Sigma_{a_{th}}$	1.980030	1.980030	Not	Not
L^2 (cm^2)	0.426740	0.426740	Performed	Performed
B^2 (cm^{-2})	0.030320	0.030320		
$\%\rho$ (Equivalent Bare)	0.56	-4.14		
$\%\rho$ (Measured)	0.0 ± 0.6	0.0 ± 0.6		

TABLE 3.9
REACTIVITY ANALYSIS OF WAPD HOMOGENEOUS CRITICAL CORE No. 2 (#21) (NO B-10 OR STAINLESS STEEL), 68°F

FAST FILES AND SLOWING-DOWN MODEL

Nuclear Parameter	MUFT-III, P-1	MUFT-III, P1-SG	MUFT-V, P-1	MUFT-V, P1-SG
P	0.788840	0.791592	0.840514	0.842889
τ (cm^2)	29.820942	33.005086	28.060109	31.187952
$\nu\Sigma_{f_f}$ (cm^{-1})	0.015674	0.016343	0.011131	0.011519
Σ_{a_f} (cm^{-1})	0.009125	0.009429	0.007131	0.007315
$K_f = \nu\Sigma_{f_f}/\Sigma_{a_f}$	1.717651	1.733163	1.560900	1.574690
$K_{th} = \nu\Sigma_{f_{th}}/\Sigma_{a_{th}}$	1.961939	1.961939	1.961939	1.961939
L^2 (cm^2)	0.519135	0.519135	0.519135	0.519135
B^2 (cm^{-2})	0.029799	0.029799	0.029799	0.029799
$\%\rho$ (Equivalent Bare)	-0.10	-4.91	1.96	-2.85
$\%\rho$ (Measured)	0.0 ± 0.2	0.0 ± 0.2	0 ± 0.2	0.0 ± 0.2

TABLE 3.10
REACTIVITY ANALYSIS OF ORNL CRITICAL CORE NO. 3
("LIGHT LOADING") (NO B-10), 68°F

FAST FILES AND SLOWING-DOWN MODEL

Nuclear Parameter	MUFT-III, P-1	MUFT-III, P1-SG	MUFT-V, P-1	MUFT-V, P1-SG
P	0.844098	0.844858	0.905917	0.906291
τ (cm^2)	29.712738	33.492978	27.709370	31.139038
$\nu\Sigma_{f_f}$ (cm^{-1})	0.006327	0.006382	0.004439	0.004470
Σ_{a_f} (cm^{-1})	0.006279	0.006305	0.003868	0.003883
$K_f = \nu\Sigma_{f_f}/\Sigma_{a_f}$	1.007645	1.012213	1.147688	1.150989
$K_{th} = \nu\Sigma_{f_{th}}/\Sigma_{a_{th}}$ *	1.253974	1.253974	1.253974	1.253974
L^2 (cm^2)*	1.102640	1.102640	1.102640	1.102640
B^2 (cm^{-2})	0.007154	0.007154	0.007154	0.007154
$\%\rho$ (Equivalent Bare)	-0.44	2.60	2.88	0.90
$\%\rho$ (Measured)	0.0 ± 0.5%	0.0 ± 0.5%	0.0 ± 0.5%	0.0 ± 0.5%

* Obtained by P_5 theory.[8]

TABLE 3.11

REACTIVITY ANALYSIS OF SPERT-III CRITICAL WATER HEIGHT CORE "A" (CORE NO. 4) (NO B-10), 80°F

FAST FILES AND SLOWING-DOWN MODEL

Nuclear Parameter	MUFT-III, P-1	MUFT-III, P1-SG	MUFT-V, P-1	MUFT-V, P1-SG
P	0.784109	0.785388	0.864791	0.865403
τ (cm^2)	31.478520	34.785106	29.354799	32.426552
$\nu\Sigma_{f_f}$ (cm^{-1})	0.009673	0.009813	0.006927	0.007004
Σ_{a_f} (cm^{-1})	0.008260	0.008336	0.005266	0.005312
$K_f = \nu\Sigma_{f_f}/\Sigma_{a_f}$	1.171059	1.177090	1.315241	1.318649
$K_{th} = \nu\Sigma_{f_{th}}/\Sigma_{a_{th}}$	1.494952	1.494952	1.494952	1.494952
L^2 (cm^2)	0.739830	0.739830	0.739830	0.739830
B^2 (cm^{-2})	0.012766	0.012766	0.012766	0.012766
$\%\rho$(Equivalent Bare)	0.86	-2.00	5.75	3.10
$\%\rho$(Measured	~0	~0	~0	~0

Core No. 5

The initial critical configuration of SM-1 ZPE Core I consisted of 10 fixed elements plus 7 control rod elements. The core which obtained criticality was 6 control rod fuel elements fully inserted into the core in the central control rod fuel element inserted 17 in. Measured calibrations of the central control rod in the 45 and 21 element core (see Fig. 2.3) were used to estimate the worth of the central rod in a 17 element core by extrapolation. The worth of the central rod in the 17 element core from 17 to 22 in. withdrawal was estimated to be 113 cents or 0.93%ρ. The experimental uncertainty is probably large due to the method used for obtaining the rod worth. The reactivity was calculated using the PDQ code in x, y geometry. The control rod elements were represented explicitly in the calculation. Table 3.12 lists the reactivity for this core. The MUFT-III P-1 S. G. nuclear data and model yield the closest agreement to experiment.

Core No. 6

In a special experiment using SM-1 ZPE Core I fuel elements, the critical core was assembled employing 16 fixed elements plus one control rod fuel element. Criticality was obtained with the control rod withdrawal of 7.92 in. Boron stainless steel strips were added uniformly and the control rod was calibrated. The measured excess reactivity was 317 cents $\pm$ 15 cents or approximately 2.42 $\pm$ 0.1%. The results of PDQ (x, y) calculations are given in Table 3.13. In this configuration the P-1 S. G. model using MUFT-III data yielded closest agreement to experiment. In this as well as in the previous case the smallness of the core may be the cause of the discrepancies between experimental and calculated results.

Core No. 7

In the course of the SM-1 zero power experiments the full 45 element core consisting of 38 fixed elements plus 7 control rod fuel elements was brought critical on water height. The axial buckling determined from previous analysis was utilized. A PDQ (x, y) calculation was employed to determine core reactivity. The results are shown in Table 3.13. It is of interest to note that in this case, the P-1 slowing down model employing the MUFT-III nuclear data yielded best agreement with experiment.

TABLE 3.12
EXCESS REACTIVITY (%ρ) OF CRITICAL SM-1 CORE I (CORE 5) 68°F
(10 FIXED PLUS 7 CONTROL ROD FUEL ELEMENTS)

	FAST FILES AND SLOWING DOWN MODEL			
Measured Reactivity (%ρ)	MUFT-III, P-1	MUFT-III, P-1 S. G.	MUFT-V, P-1	MUFT-V, P-1 S. G.
.93	3.00	-.09	Not Performed	

TABLE 3.13
EXCESS REACTIVITY (%ρ) OF SM-1 CORE I

	Core Conditions				Reactivity				
						Fast Files and Slowing Down Approximation			
Core No.	Fixed Elements	Control Elements	Total No. of Elements	Core Temp. °F	Measured	MUFT-III, P-1	MUFT-III, P-1 S. G.	MUFT-V, P-1	MUFT-V, P-1 S. G.
5	10	7	17	68	.93	3.00	-.09	-	-
6	15	1	16	68	2.42	5.76	2.76	-	-
7 +	38	7	45	68	0	.01	-3.22	-	-
8	38**	7**	45	68	.18	1.53	-.56	-	-
9	38**	7**	45	68	.17	1.37	-.25	-	-
10	38	7	45	68	16.95	16.67	15.00	19.13	17.69
11	38	7	45	440	12.10	12.87*	10.87*	16.00	14.00

* Based on 58 fast Lethargy groups (corresponding to a lower energy cut-off of .248 ev).

** Poisoned with Boron-Stainless Steel strips.

\+ Critical water height core.

Core No. 8

In the zero power experiments the SM-1 ZPE Core I was fully poisoned with boron stainless steel strips inserted in the water channels in order to completely remove the control rod bank. Six of the control rods were withdrawn 20.5 in. while the central rod was withdrawn 17.7 inches. The excess reactivity of the core was estimated to be 25 cents or 0.18% ρ. Table 3.13 indicates that the calculated reactivity using the P-1 S.G. slowing down model and MUFT-III nuclear data resulted in the best agreement with experiment. However it must be pointed out that the boron content of the stainless steel strips is not accurately known.

Core No. 9

In the zero power experiment the SM-1 ZPE Core I was completely poisoned with stainless steel strips inserted in the water channels. Six of the control rods were withdrawn 20.5 in. while the central rod was withdrawn 18.3 inches. The excess reactivity of the core was determined as 21 cents or 0.17% ρ. Table 3.13 indicates that P-1 S.G. slowing down model using the MUFT-III nuclear data yielded the best agreement with experiment. From Table 3.7 one can see that this case is an extreme as far as the stainless steel content is concerned.

Cores No. 10 and 11

The reactivity of SM-1 Core I at both 68^{o} (Core No. 10) and 440^{o} (Core No. 11) was estimated using the 5 rod calibration as reported in reference (16). This calibration curve is a result of many different measurements under a variety of conditions and is believed to be the best estimate of 5 rod bank calibration. The measured reactivity in dollars was converted to reactivity in percent using the formula beta effective discussed in the previous section. The uncertainty in the integral bank worth is estimated to be one dollar or 0.7% ρ. Table 3.13 indicates that the P-1 slowing down model using the MUFT-III nuclear data gives calculated reactivities within experimental error.

Core No. 12

The reactivity of SM-1 Core I in the rods out condition with the control rod fuel elements replaced by 7 fixed elements was estimated based on limited experimental data. As reported in reference (16) the substitution of fixed fuel elements for all 7 of the control rod fuel elements results in an increase in core reactivity of 3.15 dollars. The measured substitution effect (3.15 dollars) plus the measured excess reactivity from rod calibrations (23.8 dollars) yields an estimated excess reactivity of the SM-1 Core I with 45 fixed elements of 26.95 dollars or 18.93% ρ. The reactivity of this configuration was calculated using the PDQ code in x, y geometry. The results are shown in Table 3.14 and indicate that the P-1 slowing down model using MUFT-III nuclear data yields the best agreement with the experimental reactivity determined by the recipe previously described.

Core No. 13

In the SM-2 critical experiments a core was assembled with no burnable poison and the reactivity of the core in the rods out conditions estimated from control rod bank calibrations. The effect of replacing the 7 control rod fuel elements by fixed elements was also estimated. The experimental reactivity for this core (45 fixed elements) was estimated to be 30.6 $\pm$ 0.43 dollars or 26% ρ. Table 3.15 gives the results of calculated reactivities using the equivalent bare model. The comparison with experiment indicated the P-1 slowing down model using MUFT-III nuclear data yield the best agreement with experiments.

3.3.3 Conclusions

Based on the results presented in the previous section the following conclusions are drawn relative to the accuracy of various nuclear models and nuclear data for calculation of fast loop constants for use in two group theory.

1. In 13 cores calculated the P-1 slowing down model using MUFT-III nuclear data yielded standard deviation of measured and calculated reactivities of 0.91% ρ.

2. In 13 cores the P-1 S.G. slowing down model using MUFT-III nuclear data yielded standard deviation of measured and calculated reactivities of 1.31% ρ.

3. For 6 experiments calculated using P-1 slowing down model and MUFT-V nuclear data, the calculated reactivities were on the average 3.3% ρ higher than measured.

TABLE 3.14
REACTIVITY ANALYSIS OF SM-1 CORE I, 68°F
(ALL 45 FIXED FUEL ELEMENTS)

FAST FILES AND SLOWING-DOWN MODEL

Nuclear Parameter	MUFT-III, P-1	MUFT-III, P1-SG	MUFT-V, P-1	MUFT-V, P1-SG
P	0.74905822	0.7498659		
τ (cm^2)	30.446965	34.372023		
$\nu\Sigma_{f_f}$ (cm^{-1})	0.01319894	0.0133257		
Σ_{a_f} (cm^{-1})	0.01018787	0.0102585		
$K_f = \nu\Sigma_{f_f}/\Sigma_{a_f}$	1.295554	1.2989911	Not	Not
$K_{th} = \nu\Sigma_{f_{th}}/\Sigma_{a_{th}}$	1.56093	1.56093	Performed	Performed
L^2 (cm^2)	0.6375275	0.6375275		
B^2 (cm^{-2})	0.007154	0.007154		
$\%\rho$(Equivalent Bare)	18.21	16.39		
$\%\rho$(PDQ)	18.26			
$\%\rho$(measured)*	18.93	18.93		

* Overall measured substitution reactivity effect for 7 elements was obtained by individual element measurements.

TABLE 3.15
REACTIVITY ANALYSIS OF SM-2 EXPERIMENTAL CORE
(ALL 45 FIXED ELEMENTS WITH NO B-10), 68°F

FAST FILES AND SLOWING-DOWN MODEL

Nuclear Parameter	MUFT-III, P-1	MUFT-III, P1-SG	MUFT-V, P-1	MUFT-V, P1-SG
P	0.646630	0.647411	0.750529	0.750986
τ (cm^2)	32.176362	35.886659	30.232861	33.683175
$\nu\Sigma_f$ (cm^{-1})	0.020218	0.013872	0.014935	0.015038
Σ_{a_f} (cm^{-1})	0.013773	0.013872	0.009849	0.009911
$K_f = \nu\Sigma_{f_f}/\Sigma_{a_f}$	1.467913	1.470408	1.516400	1.517380
$K_{th} = \nu\Sigma_{f_{th}}/\Sigma_{a_{th}}$	1.775900	1.775900	1.775900	1.775900
L^2 (cm^2)	0.472351	0.472351	0.472351	0.472351
B^2 (cm^{-2})	0.006956	0.006956	0.006956	0.006956
%ρ(Equivalent Bare)	26.42	24.92	29.09	27.70
%ρ(Measured)	~26.00	~26.00	~26.00	~26.00

4. There are some inconsistencies in comparison of various nuclear models and data with certain of the experiments; in particular, the minimum size SM-1 ZPE Core I experiments, and the fully poisoned ZPE experiments. The cause of this may be due to the very small size of the cores in the first case and the possible inaccuracies of material content of the fully poisoned cores.

3.4 EFFECT OF FAST GROUP CALCULATIONAL MODEL ON FRACTION OF THERMAL FISSIONS

The effect of the fast calculation model on the fraction of thermal fissions was calculated and compared to experiment. The analysis was performed for the SM-1 Core I at 68°F.

3.4.1 Experimental Data

The experimental determination of the fraction of thermal fissions, Ψ, was based upon the irradiation of bare and cadmium covered uranium foils. The measurements were performed in the SM-1 ZPE Core I[17] which employs a core which is a duplicate of SM-1 Core I. The initial 5 rod actual bank position was 3.7 in. withdrawn from the bottom of the active core which indicates 18.3 in. of the core was rodded. The experimental method is described in reference (9). The effective cutoff energy for the 0.020 in. cadmium covers used in the measurements is 0.414 ev.[18] Bare and cadmium covered uranium foils were irradiated in several fuel element cells at 9 in. elevation. The results are shown in Table 3.16.

TABLE 3.16
FRACTION OF THERMAL FISSIONS FOR THE SM-1 ZPE CORE I FOR VARIOUS AXIAL AND RADIAL POSITIONS

Radial Position from Center of Core (Inches)	Axial Position from Bottom of Core (Inches)	Fraction of Thermal Fission
0	9.0	.801
5.9	9.0	.840
4.2	11.0	.802
4.2	5.0	.825

Table 3.16 indicates that the average fraction of thermal fissions below 0.414 ev is 0.82 ± 0.02 for SM-1 ZPE Core I at 68°F.

3.4.2 Calculational Approach

The following definition of Ψ was used

$$\Psi = \frac{1}{k_{eff}} \frac{K_{th}\, P}{(1 + \tau B^2)(1 + L^2 B^2)}$$

Where k_{eff} is given by equation (2.10), and the remaining parameters are defined in Appendix E.

The effective cutoff energy of 0.414 ev corresponds to the use of 56 fast groups with a lower cutoff of 0.400 ev.

3.4.3 Results

Table 3.17 presents the measured and calculated values of the fraction of thermal fission, Ψ, for the clean SM-1 Core I ZPE-2, at 68°F, using various fast files and number of fast groups, with the P-1 slowing-down model.

TABLE 3.17
COMPARISON OF FRACTION OF THERMAL FISSION, SM-1 CORE I ZPE-2 (CLEAN), 68°F

Calculational Method	Number of Fast Groups	Lower Cutoff Energy (ev)	Calculated	Measured
MUFT-V, P-1	54	0.625	0.85	0.82 ± 0.02
MUFT-III, P-1	54	0.625	0.85	0.82 ± 0.02
MUFT-III, P-1	56	0.400	0.83	0.82 ± 0.02
MUFT-III, P-1	59	0.196	0.78	0.82 ± 0.02

According to Table 3.17, the calculated fraction of thermal fission, Ψ as obtained by the 56 fast group, MUFT-III fast files (approximately corresponding to the effective cadmium cutoff energy of 0.414 ev), using the P-1 slowing-down model, agrees well with the measured value. The calculated values for Ψ, as obtained by the MUFT-III and MUFT-V fast files, using 54 fast groups (corresponding to a lower cutoff energy of 0.625 ev), are identical. It is not possible to decide whether the MUFT-III or MUFT-V fast files are more accurate in predicting Ψ for an arbitrary lower cutoff energy.

3.4.3 Conclusions

Using MUFT-III nuclear data and the P-1 slowing down model the predicted fraction of thermal fission was found to be in very good agreement with experiment. At the center of the fuel elements, the calculated and measured values are within experimental error.

3.5 EFFECT OF FAST CALCULATIONS ON FAST FLUX DISTRIBUTIONS

An analysis was performed to obtain the effect of the fast group constants on the fast flux distributions for the reference SM-1 Core I (38 fixed plus 7 control rod fuel elements), at 68°F. The measurements were performed for the clean SM-1 ZPE Core.[9] The measurements were limited to the center positions of one row of elements in the unrodded region of the core. The analytical flux distributions were compared to experiment.

3.5.1 Experimental Data

The experimental determination of the fast flux distributions was based upon the irradiation of bare and cadmium covered gold foils in the clean SM-1 ZPE Core[9] at 68°F. The initial five rod bank position was 3.7 in. withdrawn from the bottom of the active core. The bare gold foils provided an indication of the total flux, whereas the cadmium covered gold foil readings yielded the fast flux above 0.414 ev (effective cutoff energy of 0.020 in. cadmium).

A radial traverse through the center of elements 44, 45, 46 and 47 at 2.5 in. axially was made with bare and cadmium covered gold foils.

3.5.2 Results

Figure 3.3 presents measured and calculated fast radial flux distributions, for SM-1 Core I ZPE-1, at 68°F. The calculated fluxes as based on the MUFT-III and MUFT-V fast files, with the P-1 slowing-down model, were found to be undistinguishable. A one-dimensional two region calculation was performed with VALPROD.

3.5.3 Conclusions

1. The difference in calculated radial fast flux distribution using P-1 MUFT-III and MUFT-V was undistinguishable for SM-1 Core I.

2. The calculated radial fast flux distribution is in good agreement with the fast flux as measured with cadmium covered gold foils.

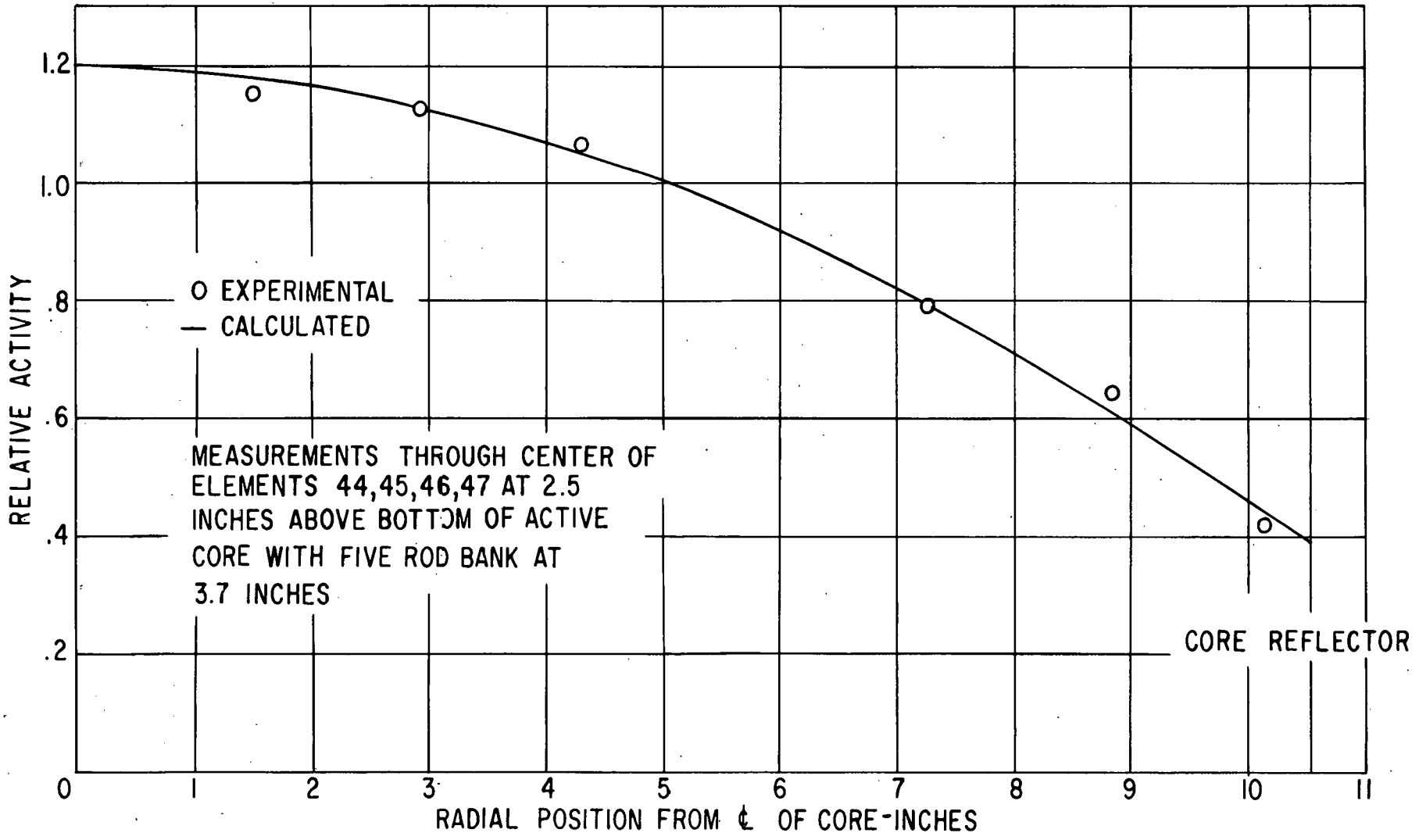

Figure 3.3 Fast Flux vs. Radial Position - SM-1 Core I, 68°F

3.6 EFFECT OF THERMAL MODEL ON REACTIVITY OF SM-1 CORE I

3.6.1 Introduction

The thermal model currently employed by Alco to calculate thermal flux distribution is based on the one velocity, P_3 spherical harmonics approximation to the transport equation. Hardened, Maxwellian averaged cross sections are employed. The thermal neutron energy spectrum is assumed independent of position and is taken to be that for an infinite homogeneous mixture of the materials comprising the core.

Flux disadvantage factors are obtained from the calculated thermal flux distribution and are used to obtain effective nuclear constants for an infinite array of fuel element cells. K_{th}*, D and L^2 for the cell are computed in this manner.[19]

Only one direct comparison between measured and calculated (i.e., by the hardened Maxwellian, P_3 scheme) microscopic intraplate flux distribution has been performed. This comparison was made with data obtained during zero power experiments on the SM-1 Core I mockup (core spectral hardening index, $\beta\gamma$**, equal to 0.35 at room temperature) and yielded reasonable agreement between the calculated and experimental flux distributions.[20]

Measured and calculated gross intracell power distributions for the SM-1 have been compared. However, the results of this comparison are not a direct measure of the validity of the thermal model since the thermal constants used in the calculation (as computed by the hardened Maxwellian, P_3 scheme) are subsequently used in a diffusion theory calculation which determined the gross intracell power distribution.

The rods-out excess reactivity of the SM-1 Core I is computed for an all fixed element core based on Wigner-Wilkins averaged thermal cross sections and compared to the excess reactivity computed using hardened Maxwellian averaged cross sections. The same fast model (MUFT-III, P-1) is used for both cases.

---

* $K_{th} = \frac{\nu\Sigma_{f_{th}}}{\Sigma_{a_{th}}}$ where ν, $\Sigma_{f_{th}}$, $\Sigma_{a_{th}}$ are defined in Appendix E.

** $\beta\gamma$ is defined as $\Sigma_a (KT_m) / \xi\Sigma_s$. $\Sigma_{a_{th}}$ and Σ_s are defined in Appendix E.

3.6.2 Results

The thermal multiplication constant, K_{th}, for the rods-out SM-1 Core I was computed with Wigner-Wilkins averaged thermal cross sections and compared to K_{th} calculated with Maxwellian averaged thermal cross sections. The cutoff energy of the Wigner-Wilkins distribution was 10 KT_m while the Maxwellian distribution was assumed to extend to infinity. The values of the fast and thermal constants used in the calculation are given in Table 3.18. The equivalent bare model was used.

TABLE 3.18
FAST AND THERMAL CONSTANTS AND REACTIVITY ρ FOR THE SM-1

Method of Obtaining Thermal Constants	K_{th}	L^2	B^2	τ	K_f	P*	$\%\rho$
Hardened Maxwellian	1.56093	.6375	.007154	30.45	1.29555	.74906	18.21
Wigner-Wilkins Averaged	1.55777	.6796	.007154	30.45	1.29555	.74906	18.06

* The fast constants were obtained from MUFT-III using the P-1 slowing down approximation.

3.6.3 Conclusions

1. Use of Wigner-Wilkins averaging of thermal constants for calculation of thermal group constants lowers reactivity of SM-1 Core I by about 0.2%.

2. Core reactivities are not known for SM-1 Core I to sufficient accuracy to be used as a criteria for thermal selection.

3. Insufficient thermal flux distributions and no thermal spectra are available to serve as a test of calculational model.

3.6.4 Summary

In this section we have investigated the accuracy of various models and files in predicting nuclear constants and reactivity of various assemblies. MUFT-III files and P-1 slowing down model gave the best results for reactivity, thermal fission fraction and fast flux.

In the following section this will be applied in the investigation of the characteristics of SM-1 Core I at startup.

3.7 REFERENCES (3.0)

1. Doerner, R. C., et al, "Age of Fission Energy Neutrons to Indium Resonance in Water," Nuclear Sc. & Engr., Vol. 9 No. 2, P. 221, February 1961.

2. Reier, M., "The Age of Polonium-Beryllium and Polonium-Boron Neutrons in Various Metal-Water Mixtures; A Comparison Between Theory and Experiment," A/CONF. 15/P/635, June 1958.

3. Mills, C. B., "The General Methods of Reactor Analysis used by the ANP Physics Group," ORNL-1493, September 22, 1953. (Secret)

4. MacKay, S. D., et al, "SM-1 (APPR-1), Research and Development Program, Interim Report on Core Measurements, Task No. VII, APAE Memo No. 178, March 1, 1959.

5. Forbes, S. G., et al, "Quarterly Technical Report, SPERT Project," IDO-16584, April 12, 1960.

6. Blizard, E. P., "Neutron Physics Division Annual Progress Report for Period ending September 1, 1960," ORNL-3016, December 17, 1960.

7. Rutledge, G. P. and Kantorczyk, P. A., "Nuclear Analysis of Thermal Reflected Cylindrical Homogeneous Critical Assemblies," WAPD-TM-244, November, 1960.

8. Williamson, T. G., "Analysis of the ORNL Experiments for APPR-1 Using Improved Techniques," AP Note 118 Alco Products, Inc., November 14, 1958.

9. Noaks, J. W. and Johnson, W. R., "Army Package Power Reactor Zero Power Experiments (ZPE-1)," APAE-8, February 8, 1957.

10. Giesler, H. W., "Additional Measurements on the Army Package Power Reactor Zero Power Experiments, ZPE-1 and ZPE-2," APAE Memo 115, November 15, 1957.

11. MacKay, S. D., et al, "Extended Zero Power Experiments on the Army Package Power Reactor, ZPE-2," APAE No. 21, November 15, 1957.

12. Paluszkiewicz, S., "Analysis of Zero Power Experiments on SM-1 Core II and SM-1A Core I," APAE No. 71, October 5, 1960.

13. Rosen, S. S., "Hazards Summary Report for the Army Package Power Reactor SM-1, Task XVII," APAE No. 2, Revision 1, May, 1960.

14. O'Brien, J. F., et al, "A Boron Determination for the APPR-1," MND-E-1718-1, May 25, 1959.

15. Bobe, P. E., et al, "Interim Report of Nuclear Analysis Performed on SM-2 Core and Vessel, September 1, 1958 to December 31, 1959," APAE No. 65, May 27, 1960.

16. Weiss, S. H., "Summary Report of Physics Measurements on SM-1 Core I," APAE-96, February 6, 1962.

17. Mackay, J. D., et al, "Extended Zero Power Experiments on the APPR-ZPE-2," APAE-21, November 15, 1957.

18. Dayton, T. E. and Pettus, W. J., "Effective Cadium Cut Off Energy," Nucleonics, Vol. 15 No. 12 p. 86, December 1957.

19. Byrne, B. J., Caton, R. L., "Two-Dimensional P-3 Calculation for APPR-Type Fixed Fuel Elements," AP Note 96, Alco Products, Inc., February 14, 1958.

20. Caton, R. L., Byrne, B. J., "Two Dimensional P_3 Calculation for APPR-Type Fixed Fuel Elements," AP Note 96, Alco Products, Inc., February 14, 1958.

21. Hellens, R. H., et al, "Multigroup Fourier Transform Calculation Description of MUFT-III Code," WAPD-TM-4, July 1956.

22. Rosen, S. S., "Supplement to MUFT-III Code Multigroup Fourier Transform Calculations," AP Note-90, Alco Products, Inc., December 6, 1957.

23. Paluszkiewicz, S., "Nuclear Analysis of Various SPERT-III Critical Experiments," APAE Memo No. 279, April 27, 1961.

24. Henry, A. F., "54 Group Library for P-1 Programs," WAPD-TM-224, April, 1960.

25. Byrne, B. J., and Oby, P. V., "Analysis of Extended Zero Power Experiments on the Army Package Power Reactor, ZPE-2," APAE No. 27, May 7, 1958.

26. Noaks, J. W., "SM-2 Critical Experiments, CE-1," APAE No. 54, November 30, 1959.

27. Williams, D., "Army Package Power Reactor Critical Experiment," ORNL-2128, August 8, 1956.

28. Spano, A. H., "Experimental and Analytical Studies of Clean Critical Stainless Steel Cores," IDO-16691, June 16, 1961.

4.0 CORE CHARACTERISTICS AT STARTUP

4.1 INTRODUCTION

Using the nuclear model (P-1) and nuclear data (MUFT-III) selected in Section 3.0, a number of important SM-1 Core I characteristics were calculated and compared to experiment. These are as follows:

Core Reactivity at 68°F

Core Reactivity at 440°F

Core Reactivity at 440°F equilibrium Xe

Bank Position at 68°F

Bank Position at 440°F

Bank Position at 440°F equilibrium Xe

Central control rod worth in poisoned core, 68°F

4.2 CORE REACTIVITY

The reactivity of SM-1 Core I at 68°F, 440°F and 440°F equilibrium Xe was obtained from 5 rod critical positions and a 5 rod bank calibration curve. The positions and curves are given in reference (1) for SM-1 Core I at startup.

Table 4.1 presents this experimental data.

TABLE 4.1
EXPERIMENTAL INITIAL FIVE ROD BANK POSITIONS AND EXCESS CORE REACTIVITIES OF THE SM-1 CORE I, 0 MWYR

Operating Condition	Initial 5 Rod Bank Position (in.)	Excess Core Reactivity ($)	Excess Core Reactivity (% ρ)
68°F (no xenon)	3.7	23.80	16.95
440°F (no xenon)	6.7	16.50	12.10
440°F (eq. xenon)	8.3	12.90	9.55

4.2.1. Geometrical Models

The reactivity of the SM-1 Core I for the various core operating conditions was calculated by both one-and two-dimensional models.

4.2.1.1 Two-Dimensional Model PDQ (x, y)

The reactivity of the SM-1 Core I at 68°F (clean) and 440°F (clean) were calculated using the PDQ (x, y) code. The fixed and control rod fuel elements were broken down into active and dead regions according to Fig. 2.1 and 2.2 respectively. Tables 4.2 and 4.3 present the region isotopic number densities of the SM-1 Core I at 68°F and 440°F (clean) respectively.

Fast nuclear constants, required as input to the PDQ code, were calculated by the MUFT-III code, employing MUFT-III fast files with the P-1 slowing-down model. The MUFT-III code requires the total core buckling, B^2, as an input parameter. The buckling was calculated employing Eq. (2.11). Reflector savings was calculated from the fast flux distributions obtained from cadmium covered gold foil measurements at 68°F. The savings was also determined by the FINK-I, IBM-650 machine code, which employs the equivalent bare model at 68°F and 440°F. The difference between the calculated and measured savings at 68°F was used as a correction to the hot, calculated savings to obtain the "measured" savings at 440°F. Table 4.4 presents the reflector savings and bucklings for the SM-1 Core I at 68°F and 440°F. The axial bucklings, B_z^2, that are listed, were used as input parameters to the PDQ (x, y) calculations.

Tables 4.5 and 4.6 present the fast macroscopic cross sections for the various regions as used in the PDQ (x, y) code, at 68°F and 440°F (clean), respectively. The cold (68°F) calculations were based on 59 fast lethargy groups (lower energy cutoff of 0.196 ev), whereas the hot (440°F) calculations were based on 58 fast groups (0.248 ev).

The thermal macroscopic cross sections were calculated using an IBM-650, two-dimensional P-3 superposition code written for the APPR type fuel cell geometry. Input parameters to the code were based upon Maxwell-Boltzmann averaged microscopic cross sections evaluated at hardened neutron temperatures according to Eq. (2.6). Effective neutron temperatures of 0.0331 ev and 0.0549 ev, corresponding to coolant temperatures at 68°F and 440°F respectively, were determined by this relation. Microscopic thermal neutron cross section were evaluated [2] at these effective temperatures and are tabulated in Tables 4.7 and 4.8 for coolant temperatures of 68°F and 440°F respectively.

Tables 4.9 and 4.10 present the thermal macroscopic cross sections as obtained by the P-3 code for the various regions as seen by the PDQ (x, y) code, at 68°F and 440°F, respectively. Slowing-down sources, required as input to the P-3 code, were taken to be the volume fractions of water in any region.

TABLE 4.2
NUMBER DENSITIES (ATOMS/CC x 10^{-24}) FOR SM-1 CORE I
($T = 68^{o}F$)

REGIONS

Atom	Fixed (Active #2)	Fixed (Dead #1)	Control (Active #5)	Control (Dead #4)	Control (Dead #3)	Skirt	Reflector
H	0.05466747	0.0433887	0.05466747	0.0462858	0.04079855	-	0.06672998
0	0.02839861	0.0216944	0.02839861	0.0231429	0.02039928	-	0.03336499
SS	0.01248895	0.0297711	0.01248895	0.0260761	0.03307484	0.0851123	-
B-10	0.00000816	-	0.00000816	-	-	-	-
U-235	0.00049598	-	0.00049598	-	-	-	-

TABLE 4.3
NUMBER DENSITIES (ATOMS/CC x 10^{-24}) FOR SM-1 CORE I
($T = 440^{o}F$)

REGIONS

Atom	Fixed (Active #2)	Fixed (Dead #1)	Control (Active #5)	Control (Dead #4)	Control (Dead #4)	Skirt	Reflector
H	0.04571872	0.0362862	0.04571872	0.03870904	0.0341201	-	0.05580667
0	0.02392424	0.0181431	0.02392424	0.01935451	0.0170600	-	0.02790334
SS	0.01248895	0.0297711	0.01248895	0.0260761	0.03307484	0.0851123	-
B-10	0.00000816	-	0.00000816	-	-	-	-
U-235	0.00049598	-	0.00049598	-	-	-	-

TABLE 4.4
REFLECTOR SAVINGS AND BUCKLINGS FOR SM-1 CORE I

Temperature	Axial Reflector Savings, S_z(cm)	Radial Reflector Savings, S r(cm)	Axial Buckling $B z^2$ (cm^{-2})	Axial Buckling $B r^2$(cm^{-2})	Total Buckling, B^2(cm^{-2})
Cold (68°F)	5.11	6.18	0.002259	0.004895	0.007154
Hot (440°F)	6.10	7.80	0.002129	0.004465	0.006594

TABLE 4.5
FAST MACROSCOPIC CROSS SECTIONS FOR SM-1 CORE I
(T = 68°F, E_n = 0.0331 ev)

Region	D_f (cm)	Σ_{af}(cm^{-1})	Σ_{sl}(cm^{-1})	$\nu\Sigma_{ff}$(cm^{-1})
Fixed (Active #2)	1.249010	0.010989	0.030652	0.015080
Fixed (Dead #1)	1.161803	0.004505	0.029212	0
Control (Active #5)	1.249010	0.010989	0.030652	0.015080
Control (Dead #4)	1.174127	0.004029	0.031347	0
Control (Dead #3)	1.151920	0.004927	0.027290	0
Stainless Stl. Skirt				
Water Reflector				

TABLE 4.6
FAST MACROSCOPIC CROSS SECTIONS FOR SM-1 CORE I
(T = 440°F, E_n = 0.0549 ev)

Region	D_f (cm)	Σ_{af}(cm^{-1})	Σ_{sl}(cm^{-1})	$\nu\Sigma_{ff}$(cm^{-1})
Fixed (Active #2)	1.441284	0.010016	0.025256	0.013702
Fixed (Dead #1)	1.296577	0.004233	0.024447	0
Control (Active #5)	1.441284	0.010016	0.025256	0.013702
Control (Dead #4)	1.320149	0.003773	0.026239	0
Control (Dead #3)	1.277278	0.004643	0.022832	0
Stain. Stl. Skirt	1.513043	0.008133	0	0
Water Reflector	1.561416	0.000499	0.038424	0

TABLE 4.7
THERMAL MICROSCOPIC CROSS SECTIONS FOR COOLANT TEMPERATURE, 68°F
(EFFECTIVE NEUTRON TEMPERATURE, 0.0331 ev)

Nuclide	$\overline{\sigma}_s$	$\overline{\sigma}_a$	$\overline{\sigma}_{tr}$	$\nu\overline{\sigma}_f$
U-235	9.0	512.6564	521.630	1065.1394
U-238	9.0	2.118036	11.093	-
H	34.32	0.254164	27.170	-
0	3.9	0	3.7375	
B-10*	4.4	2932.4980	2936.6051	-
SS	10.44	2.270275	12.586	-

TABLE 4.8
THERMAL MICROSCOPIC CROSS SECTIONS FOR COOLANT TEMPERATURE, 440°F
(EFFECTIVE NEUTRON TEMPERATURE, 0.0549 ev)

Nuclide	$\overline{\sigma}_s$	$\overline{\sigma}_a$	$\overline{\sigma}_{tr}$	$\nu\overline{\sigma}_f$
U-235	9.0	385.5384	394.512	801.0342
U-238	9.0	1.644605	10.620	-
H	28.97	0.197353	20.65	-
0	3.9	0	3.7375	-
B-10*	4.4	2277.0146	2281.1217	-
SS	10.44	1.762814	12.078	-

* Based upon 19.8 a/o of B-10 in natural boron.

TABLE 4.9
THERMAL MACROSCOPIC CROSS SECTIONS FOR SM-1 CORE I
($T = 68^{o}F$, $E_n = 0.0331$ ev)

Region	D_{th} (cm)	$\Sigma_{ath}(cm^{-1})$	$\nu\Sigma_{fth}$ (cm^{-1})
Fixed (Active #2)	0.164460	0.305872	0.502897
Fixed (Dead #1)	0.203917	0.078616	0
Control (Active #5)	0.164460	0.305872	0.502897
Control (Dead #4)	0.199329	0.070964	0
Control (Dead #3)	0.208201	0.085458	0
Stainless Steel Skirt	0.311171	0.193228	0
Water Reflector	0.172020	0.016960	0

TABLE 4.10
THERMAL MACROSCOPIC CROSS SECTIONS FOR SM-1 CORE I
($T = 440^{o}F$, $E_n = 0.0549$ ev)

Region	D_{th}(cm)	$\Sigma_{a_{th}}(cm^{-1})$	$\nu\Sigma_{f_{th}}(cm^{-1})$
Fixed (Active #2)	0.240550	0.234431	0.386374
Fixed (Dead #1)	0.283279	0.059642	0
Control (Active #5)	0.240550	0.234431	0.386374
Control (Dead #4)	0.280908	0.053607	0
Control (Dead #3)	0.285432	0.065038	0
Stainless Steel Skirt	0.324259	0.150037	0
Water Reflector	0.265246	0.011014	0

4.2.1.2 One Dimensional Models (VALPROD and WINDOWSHADE)

The reactivity of the SM-1 Core I was calculated by two one-dimensional models. The VALPROD code was used to calculate a slab configuration in which the fixed elements were homogenized. The transverse buckling in the VALPROD code was taken as

$$B_L^2 = B_z^2 + B_y^2 = B_z^2 + \frac{B_y^2}{2} = .004707$$

4.2.1.3 VALPROD and WINDOWSHADE

In addition to the detailed reactivity analysis afforded by the two-dimensional PDQ (x, y) code, the excess reactivity of the SM-1 Core I, at 68°F, clean, was calculated by the one-dimensional VALPROD and WINDOWSHADE, IBM-650 codes. A slab VALPROD case was run for a completely homogenized core. The effect of the control rod elements has been accounted for by the addition of a thermal absorption cross section $\sum_a^{sub}$ derived as it is described in Section 5.2.1 of this report. For a 2.4% ρ measured reactivity change for the substitution of seven control rod elements with fixed elements, $\sum_a^{sub}$ was found to be 0.008416 cm^{-1} and added to $\sum a$ of the core. The 68°F homogenized and fast constants for the fixed element can be found in Appendix C. The WINDOWSHADE code was used to calculate the reactivity of the core, using bucklings to account for the x and y dimensions.

4.2.2 Results

The results of the two-dimensional and one-dimensional reactivity calculations for SM-1 Core I rods out is given in Table 4.11.

TABLE 4.11
MEASURED AND CALCULATED REACTIVITY OF SM-1 CORE I
(0 MWYR)

Condition	Measured	Two-Dimensional	One-Dimensional	
			VALPROD	WINDOWSHADE
68°F	16.35	16.67	16.80	17.04
440°F	12.10	12.87	-	12.88
440°F Eq. Xenon	9.55	-	-	10.56

It is seen that there is very good agreement between the one-dimensional and two-dimensional reactivity calculations. It is not known how much of this agreement may be due to an error in the treatment of the control rod substitution effect.

It is noted that the hot to cold reactivity is 3.8% ρ calculated (two- dimensional) and 4.85 % ρ measured.

4.2.3 Conclusions

1. The two-dimensional calculations, using the model from Section 3.0, yield hot and cold reactivities within 0.8% ρ .

2. The cold to hot reactivity is underestimated by 1% ρ using two dimensional calculation.

3. There is little difference between one-and two-dimensional calculations of reactivity provided the control rod element substitution effect is properly chosen.

4.3 BANK POSITIONS

A comparison of calculated and measured initial bank positions (five and seven rods) was performed for several core operating conditions at the start of life.

The analytical results were determined by the WINDOWSHADE code.

4.3.1 Analytical Results

Axial WINDOWSHADE calculations were performed to predict critical bank conditions for the SM-1 Core I at various initial operating conditions. The reference analytical model was used, employing modified two-group theory.

The equivalent bare model, as given by Eq. (2.7), was used to calculate $\sum_a^{sub}$ and $\sum_p$, thermal absorption cross sections used to represent the effects of the control rod fuel elements and control rods respectively. The substitution cross section, $\sum_a^{sub}$, was added to $\sum_{ath}$, the thermal absorption cross section, uniformly throughout the core. The thermal poison cross section, $\sum \hat{p}$, was added to $\sum_{a_{th}}$ uniformly throughout the rodded region located at the top of the core.

The calculated bank positions were obtained by forcing the WINDOWSHADE code to iterate to a bank position corresponding to $k_{eff} = 1 \pm \Delta k'_{eff}$, where $\Delta k'_{eff}$, is the difference between the excess core reactivities in terms of k_{eff}, as obtained by experiment and the WINDOWSHADE code (rod bank fully withdrawn), called a "model" correction. Table 4.12 presents the excess reactivity, in terms of K_{eff}, of the SM-1 core under various operating conditions, as obtained by measurement and the WINDOWSHADE code, with the corresponding values of $\Delta k'_{eff}$.

TABLE 4.12
CORE REACTIVITY OF SM-1 CORE I, 0 MWYR

Core Condition	Measured Reactivity (k_{eff})	Calculated Reactivity (k'_{eff})	$\Delta k'_{eff}$ (Calc. -Exp.)
68°F, clean	1.2034	1.2054	+0.0020
440°F, clean	1.1377	1.1478	+0.0101
440°F, eq. xe.	1.1056	1.1181	+0.0125

Table 4.13 presents the comparison of initial bank positions between measurements and analysis for the SM-1 Core I under various operating conditions at the start of life.

Table 4.13a presents the values of $\sum_p$ and $\sum_a^{sub}$ for a five and a seven rod bank for various core conditions.

TABLE 4.13
SM-1 CORE I FIVE AND SEVEN ROD BANK POSITION
FOR VARIOUS CORE CONDITIONS

Rod Bank Position (Inches From Bottom Of Core)

		Calculated		Difference between Measured and Calculated	
Core Conditions	Measured	No Model Correction	With Model Correction	No Model Correction	With Model Correction
Five Rods 68°F, clean	3.7	3.0	3.6	.7	.1
Seven Rod 68°F, clean	5.3	4.6	4.9	.7	.4
Five Rods 440°F, clean	6.7	5.2	6.8	1.5	-.1
Five Rods 440°F, Eq. Xe.	8.3	6.9	8.0	1.4	.3

TABLE 4.13a

SM-1 CORE I Σ_p AND Σ_a^{sub} FOR VARIOUS CONDITIONS

Bank Type, Core Conditions	Σ_p (cm^{-1})	Σ_a^{sub} (cm^{-1})
Five Rods 68°F	.088969	.008416 ~~.088969~~
Five Rods 440°F	.078180	.006329 ~~.078180~~
Seven Rods 68°F	.111716	.008416

As seen in Table 4.13, the calculated bank positions are observed to be in good agreement with the measured positions, on the basis that the excess core reactivities as calculated by the WINDOWSHADE code were corrected to the measured reactivities.

4.3.2 Conclusions

1. The five rod bank position can be predicted within 1.4 in. without any model correction and 0.3 in. using a model correction on core reactivity.
2. The use of a homogeneous Σ_p for rods and Σ_a^{sub} in a one-dimensional axial calculation can give reasonable agreement with experiment.

4.4 CENTRAL ROD WORTH IN POISONED CORES

The integral worth of the central control rod alone was determied experimentally in two ways [3]: one, by poisoning the core, using boron stainless steel strips, and the other, employing pure stainless steel strips. The worth of the central rod was determined analytically by use of the VALPROD, IBM-650 machine code, and compared to measurement.

4.4.1 Experimental Results

The calibration of the central control rod, using boron-stainless steel and pure stainless steel strips to poison the core, was measured during the SM-1 ZPE-2 critical experiments [3] at the Alco Products Critical Facility. Fig. 4.1 presents the results of the calibration. All control rods, except for the central rod, were fully withdrawn while the calibration was performed.

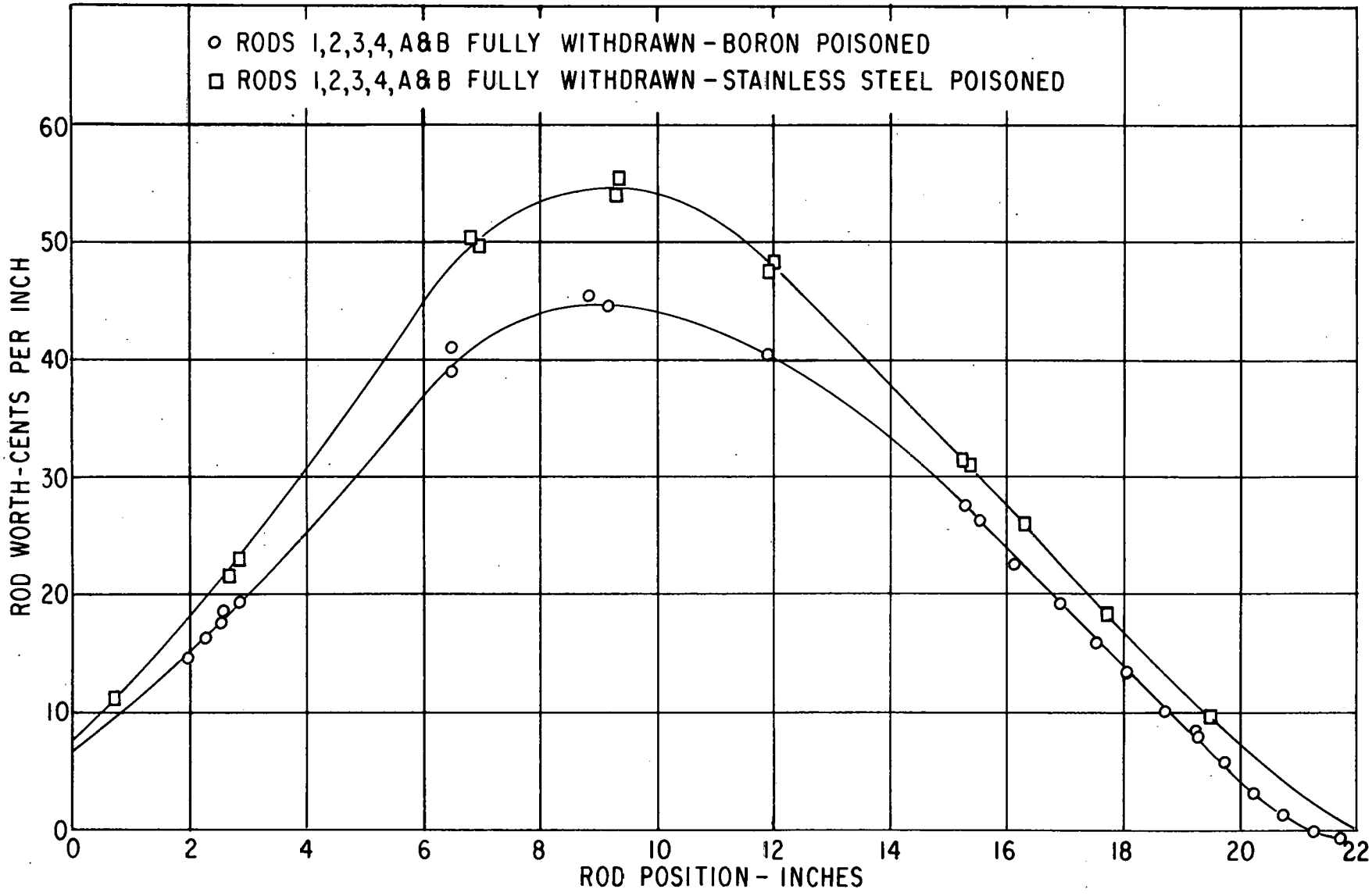

Figure 4.1 Rod C Calibration Curves - SM-1 ZPE-2

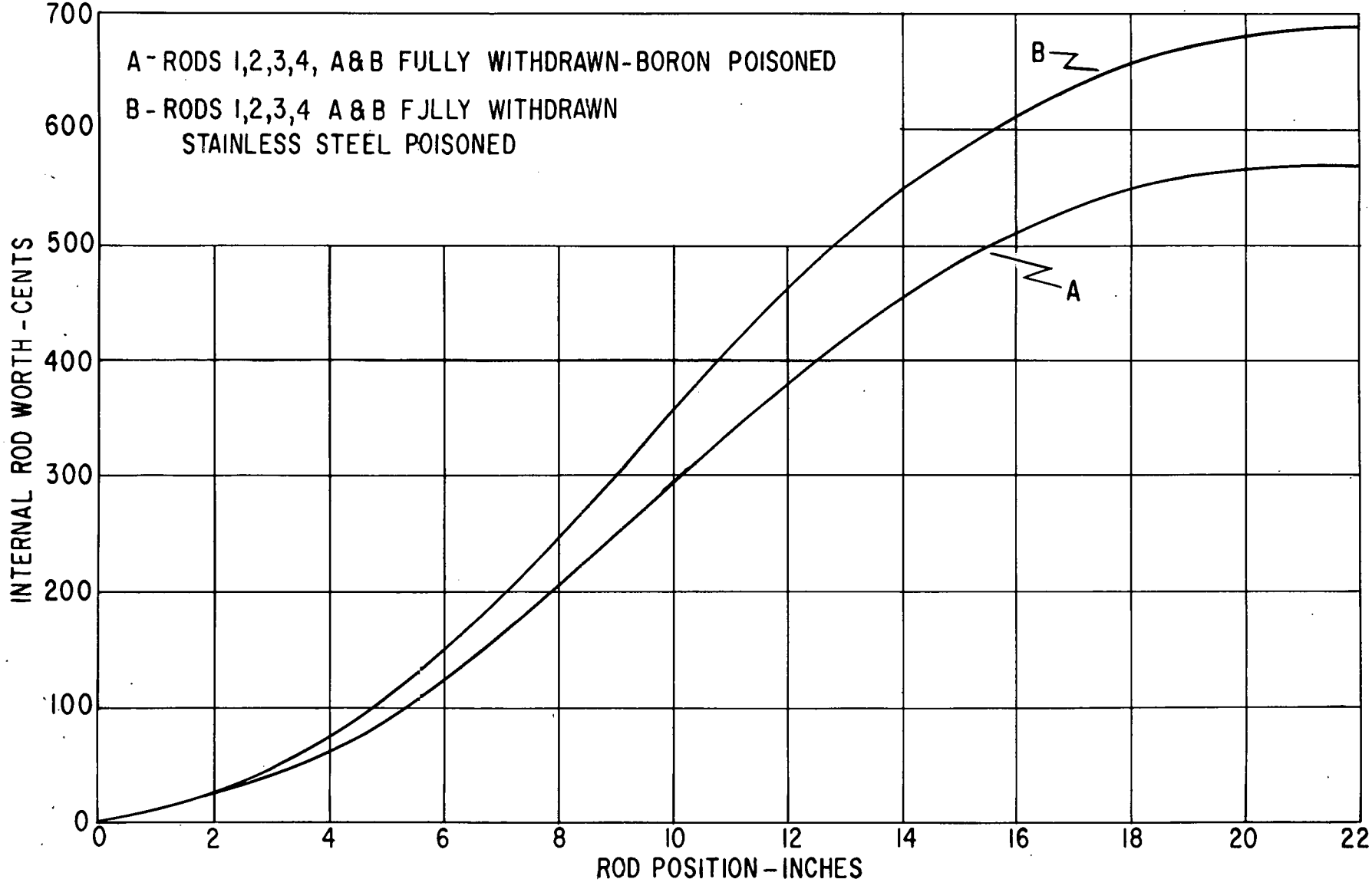

Figure 4.2 Rod C Integral Worth - SM-1 ZPE-2

The integral worth of the central rod obtained from the calibration curves in Fig. 4.2 indicates that the control rod is worth approximately one dollar greater for the stainless steel poisoned core than for the boron-stainless steel poisoned core.

4.4.2 Analytical Results

VALPROD calculations were performed for the following two configurations: one containing all poisoned fixed fuel elements, and the other with a control rod substituted for the central poisoned fuel element. The reactivity results of these calculations yield the worth of the central rod relative to a poisoned fixed fuel element. The measurements yielded the worth of the central rod relative to a clean control rod fuel element. Therefore, the worths of the central rod, as obtained by experiment and analytically, are not directly comparable. However, the analysis will indicate the dependence of rod worth on the type of poisoning employed, which can be directly compared to experiment.

Fig. 4.3 presents the cylindrical representation of the core containing a central control rod, as seen by the VALPROD code.

FIGURE 4.3
SM-1 CORE I AS SEEN BY VALPROD CODE

(CENTRAL CONTROL ROD PLUS 44 FIXED FUEL ELEMENTS)

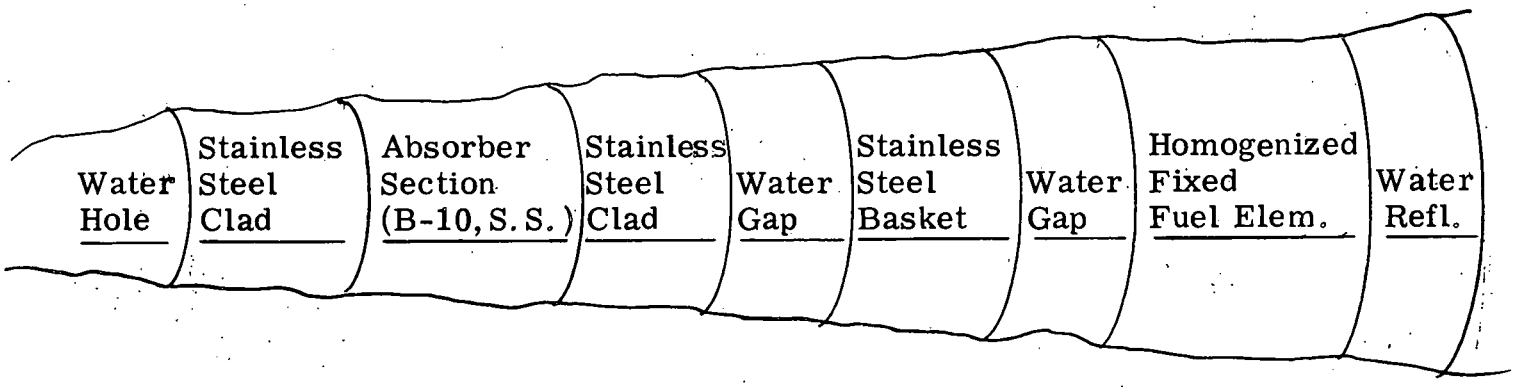

The area was conserved in all regions except for the absorber section where, instead, the thickness was conserved in order to maintain the thermally black absorption properties of the region.

The absorber section, consisting of a homogeneous mixture of Boron-10 and stainless steel, was treated as a thermally black region with resonance absorption included. The thermal properties were represented by "effective" diffusion theory constants obtained from blackness theory.[4],[5] Resonance absorption was calculated, using the same basic theory,[4] except that the absorption was treated as gray in this case. Table 4.14 presents the fast and thermal constants of the absorber section, as used for the VALPROD code.

TABLE 4.14
FAST AND THERMAL CONSTANTS OF ABSORBER SECTION

Constant	Fast	Thermal
D (cm)	1.520834*	0.000651
$\sum_a (cm^{-1})$	0.33	8.572055

* Diffusion constant for pure stainless steel.

Table 4.15 presents the results of the worth of the central control rod, as obtained by measurement and the VALPROD calculations. The calculated worths were obtained from the difference in reactivities (% ρ) of the rodded and unrodded cores.

TABLE 4.15
INTEGRAL WORTH OF CENTRAL CONTROL ROD

Poison	Measured (% ρ)	Calculated (% ρ)
Boron-Stainless Steel	4.32	4.80
Stainless Steel	5.07	5.34

4.4.3 Conclusion

1. The worth of a central control rod can be accurately calculated, using P-1 slowing down model, MUFT-III nuclear data and absorber properties from blackness theory.

4.5 SUMMARY

In the present section the application of one and two-dimensional calculations at startup has predicted reactivity of SM-1 Core I within 0.8% ρ. The cold to hot change in reactivity is underestimated by 1% ρ.

Use has been made of substitution poison cross section to represent the control rod bank and it has been found that the control rod bank position can be predicted within 0.4 in. at 68°F and 440°F.

In the following section reactivity and control rod bank will be investigated as a function of core burnup. In addition the spatial dependence of power, material concentration and the effect of xenon, samarium and fission products in reactivity will be sought.

4.6 REFERENCES (4.0)

1. Weiss, S. H., "Summary Report of Physics Measurements on SM-1 Core I," APAE-96, February 6, 1962.

2. Hughes, D.J., et al, "Neutron Cross Sections," Brookhaven National Laboratory, BNL-325, second edition, July 1, 1953.

3. Mackay, S. D., et al, "Extended Zero Power Experiments on the APPR-ZPE-2," APAE No. 21, November 15, 1957.

4. Henry, A. F., "Theoretical Method for Determining the Worth of Control Rods," WAPD-218, August 1959.

5. Fried, B.E., Alford, M.R., and Oggerino, J.P., "Flux and Power Distributions for the SM-2 References and Critical Experimental Cores," APAE Memo No. 286, June 30, 1961.

6. Noaks, J.W., and Johnson, W.R., "Army Package Power Reactor Zero Power Experiments (ZPE-1)," APAE-8, February 8, 1957.

7. Noaks, J.W., et al, "SM-2 Critical Experiments, CE-1", APAE No. 54, November 30, 1959.

8. McCool, W.J. et al, "Extended SM-2 Critical Experiments, CE-2", APAE No. 54, Supplement 1, June 30, 1961.

9. Raby, T.M., et al, "PM-2A Core I Zero Power Experiment," APAE No. 75, October 21, 1960.

5.0 SM-1 CORE I BURNUP CALCULATIONS

This section presents the results of the SM-1 Core I burnup analysis. A review of previous calculations of SM-1 Core I lifetime is also presented. The new calculations were performed by the use of the CANDLE-2 IBM-704 code, described in Section 2.0, Reference (1), and the results were compared with measured data in order to determine the accuracy of the calculational model.

5.1 REVIEW OF PREVIOUS CALCULATIONS

The review of previous burnup calculations for SM-1 can be divided into four distinct periods. These are: (1) calculations performed in the conceptual design stage by Oak Ridge National Laboratory; (2) calculations performed by Alco Products during and following the flexible critical experiments performed at Oak Ridge National Laboratory; (3) calculations performed by Alco Products following the zero power experiment on SM-1 Core I and initial startup of the SM-1 at Fort Belvoir; (4) calculations performed after burnout of the SM-1 Core I at Fort Belvoir.

The calculations reported in this work fall into the latter category. Included in the second category of calculations must be those performed by the Walter Kidde Nuclear Laboratories as a subcontractor to Alco Products. These calculations were performed independent of those at Alco but did make use of the results of the ORNL flexible critical experiments. Most of the calculations performed have employed two-group theory with provisions for resonance absorption and fission of U-235. In the conceptual design stage, ORNL performed certain check calculations using multigroup theory. It is realized that in the course of the transition from the conceptual design to the final design of SM-1, there were certain structural changes to the core. However, these did not account for a significant change in metal-to-water ratio.

TABLE 5.1
REVIEW OF BURNUP CALCULATIONS FOR SM-1 CORE I

Period	Reference	Date of Issue	Kg U-235	Grams B-10	Core Life, MWYR	Predicted ΔK Increase In Core Life
(1)	ORNL-1613	June 1955	17.7	34.0	15	0.07
(2)	APAE-7	May 1956	22.5	21.1	15	0.02
(2)	WKNL-57	March 1956	22.5	(24.9 (31.0	9.4	0.03
(3)	APAE-32	July 1958	22.5	19.5	16.4	0

Flexible critical experiments were performed from September 1955 to February 1956. Once flexible critical experiments information was available (Fall 1955) the predictions of APAE-7[2] of the loadings of fuel and boron were markedly improved over those of the conceptual design. The calculations performed in ORNL-1613[3] and APAE-7 were limited to uniform burnout. All other calculations included the effect of non-uniform fuel and burnable poison burnout with core life. It is noted that the initial design reactivity of the SM-1 was increased during the course of the core development. This was due to a concern of overpoisoning the core with boron. This eliminated to a large extent the expected increase in core reactivity with core burnout. It is of particular interest that the calculations of core burnout performed after initial startup of SM-1 predicted the core life to be 16.2 MWYR. These calculations were performed using the NUB-1 code [4] which employs group constants obtained from MUFT-III (P1-SG) and from plate P-3 theory.

5.2 CANDLE-2 CALCULATIONS

The calculations of SM-1 Core I burnout reported herein involved the use of the CANDLE-2 IBM-704 code. This code is a one-dimensional few group depletion code as described in Section 2.0. Some of the advantages and disadvantages of CANDLE-2 code compared with NUB-1 code used in Reference (4) are given in Table 5.2.

TABLE 5.2
ADVANTAGES AND DISADVANTAGES OF CANDLE-2
COMPARED WITH NUB-1

ADVANTAGES

1. Computing time reduced by a factor varying from 10 to 100.
2. Option of using 2 or 4 energy groups.
3. Calculation of new flux and power distributions at each time step.
4. Pointwise variation of flux, power and material composition in core.
5. Automatic calculation of transient xenon.

DISADVANTAGES

1. Fast and thermal microscopic cross sections cannot vary with burnup.
2. The self-shielding factor for the thermal group does not vary accurately with burnup.
3. The coalescing scheme for three groups to one fast group is not directly equivalent to the results of the MUFT-III code.
4. The Σ_{α}^{sub} for control rod fuel elements cannot vary with burnup.

A review of the advantages and disadvantages of the CANDLE-2 code compared with the NUB code indicates it is superior in treating spatial variations but inferior in calculating group constants. Since the CANDLE-2 code is faster and performs a multistep burnup automatically with the detailed spatial treatment, it was chosen as the basis for the SM-1 Core I burnout calculations reported in the following section.

5.2.1 Geometrical Model

CANDLE-2 is a one-dimensional code which leads to a number of severe problems when applied to SM-1 Core I. A review of Fig. 1.3 in Section 1.0 indicates that SM-1 Core I is highly heterogeneous. The rodded region of the core consists of 5 massive hollow absorbers in a region of 38 fixed fuel elements and 2 control rod fuel elements. In the unrodded region of the core the composition is 38 fixed elements and 7 control rod elements. In addition to the normal complications of the moving control rod bank, the control rods employed in SM-1 introduce the added complication of moving fuel into the unrodded region as the bank is withdrawn.

The core in the unrodded region is represented by fixed element properties on which is superimposed a uniform thermal absorption cross section to account for the control rod fuel elements.

The magnitude of this cross section, referred to as the control rod substitution cross section, $\sum_a^{sub}$, is found using an estimated reactivity effect of replacing seven fixed elements by seven control rod fuel elements and the equivalent bare reactivity equation in the following manner:

K_{eff} can be expressed as $k_{eff} = \dfrac{p\,K_{th}}{(1 + L^2B^2)(1 + \tau B^2)} + \dfrac{(1-p)\,K_f}{(1 + \tau B^2)}$

and, since only the K_{th} term will change, we put $k_{eff} = K_{th}\,H + J$, where:

$$K_{th} = \frac{\nu \sum_{f_{th}}^{F.E.*}}{\sum_{a_{th}}^{F.E.}} \quad , \quad H = \frac{p}{(1 + L^2B^2)(1 + \tau B^2)} \quad , \quad J = \frac{(1-p)\,K_f}{(1 + \tau B^2}$$

Then the measured reactivity difference between 7 fixed and 7 control rod fuel elements is subtracted from the cold clean reactivity giving:

$k'_{eff} = k'_{th}\,H + J$ but now $K'_{th} = \dfrac{\nu \sum_{f_{th}}^{F.E.}}{\sum_{a_{th}}^{F.E.} + \sum_a^{sub}}$ which yields $\sum_a^{sub}$

* The superscript F. E. stands for fixed elements.

the only unknown parameter. To obtain $\sum_a^{sub}$ at operating temperature, i.e. 440°F, it was assumed that $\sum_a^{sub}$ varies with temperature in the same manner as the U-235 microscopic absorption cross section does, since $\sum_a^{25}$ accounts for most of the thermal absorptions.

TABLE 5.3
EQUIVALENT UNIFORM CROSS-SECTION FOR CONTROL ROD FUEL ELEMENTS AND CONTROL ROD ABSORBERS

Cross-Section	68°F	440°F
$\sum_a^{sub}$	.007846	.006131
$\sum_p^{rods}$	.088239	.07754

The core in the rodded region is represented by fixed element properties on which is superimposed a thermal absorption cross section $\sum_p^{rods}$ to account for the 5 absorbers and the $\sum_a^{sub}$ to account for the presence of the control rod elements. This thermal absorption cross section is known as the control rod absorption cross section and is calculated in a similar fashion as $\sum_a^{sub}$ above:

$$k_{eff}\ (\text{rods out}) = \frac{1}{1-\rho'_{F.E.}} = K'_{th}\ H+J \qquad k_{eff}\ (\text{rods in}) = \frac{1}{1-\rho''} = K''_{th}\ H+J$$

$$K''_{th} = \frac{\nu\sum_{f_{th}}}{\sum_a^{F.E.} + \sum_a^{sub} + \sum_p^{rods}}$$ at 68°F it was found that

$$k_{eff}\ (\text{rods out}) = 1.1566 \quad k_{eff}\ (\text{rods in}) = .93950 \quad \sum_p^{rods} = .088239\ cm^{-1}$$

The cold to hot change in bank worth was calculated by solving the multigroup diffusion problem (VALPROD) for a core with a central rod (water, absorber shell, core and water regions). The VALPROD's were run hot and cold with and without the centerline rod inserted. An equivalent $\sum_p^{rod}$ was calculated for the center rod at the two temperatures. The ratio of $\sum_p^{rod}$ at 68°F to that at 440°F was 1.138 and assumed to be the same for the 5 rod bank. The equivalent thermal cross sections used to approximate control rod fuel elements are summarized in Table 5.3. Due to code limitations the uniform cross sections given in Table 5.3 were taken to be invariant with core burnup.

The core is then reduced to a four region configuration as shown in Fig. 5.1.

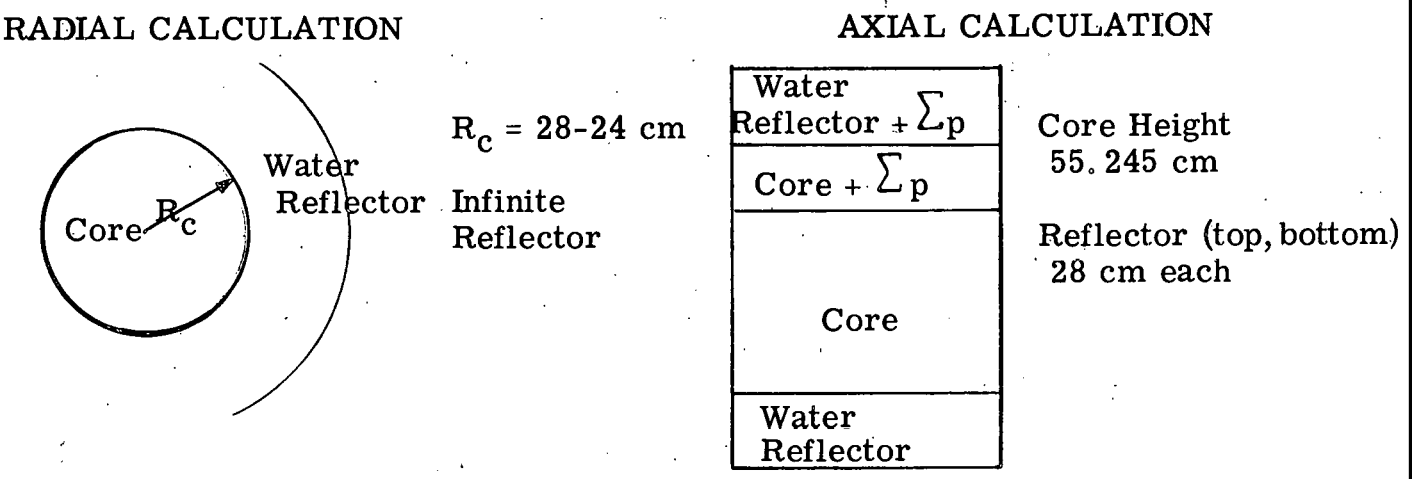

Figure 5.1. Geometrical Models for CANDLE-2 Calculations

5.2.2 Nuclear Constants

The nuclear data required to perform CANDLE-2 calculations are the concentrations of various isotopes in the core and few-group microscopic cross sections. As discussed in Section 2.0 CANDLE-2 calculates group constants from stored microscopic data. Table 5.4 lists the number densities of the elements in the various regions of the SM-1 Core I. The water number densities are employed in the reflector regions. The number densities reported in Table 5.4 vary very slightly from the reference set as given in Appendix C. This latter set is based on slightly better estimates of the material content of the SM-1 Core I. Check calculations indicated that the difference in number densities yielded a negligible effect on core reactivity.

Table 5.5 lists the three group fast cross section library used in the CANDLE-2 code. Table 5.6 lists the thermal microscopic cross section used in CANDLE-2. Table 5.7 shows the results of a comparison of the coalescing schemes of CANDLE-2 with MUFT-III P1-SG and P-1 calculations and equivalent bare core k_{eff} for CANDLE-2, MUFT-III P1-SG and MUFT-III P-1 with P_3 thermal model.

Table 5.8 shows the results of comparison of coalescing schemes for CANDLE-2, MUFT-III P1 - SG, and MUFT-III P-1 for the water reflector region.

TABLE 5.4
NUMBER DENSITIES FOR REGIONS OF SM-1 CORE I AT 440°F

(Atoms/cm^3)

Element	Homogenized Fixed Element Region	Water Region
Hydrogen	0.0443984	0.0559414
Oxygen	0.0231195	0.0279707
Stainless Steel	0.0148188	-
Natural Boron	0.000035602	-
Uranium-235	0.00042863	-

Note: To convert B_{NAT} to B-10, multiply former by 0.198. The number density of boron in the SM-1 Core I reflects a 22.4% fabrication loss.

5.2.3 Results of CANDLE-2 Calculations on SM-1 Core I

CANDLE-2 code calculates a detailed point by point variation in flux, power and material composition, which provides information for comparison with experiment.

5.2.4 Core Life

The SM-1 Core I was first burned up using radial geometry. The calculated variation in ρ from CANDLE-2 with equilibrium xenon at 440°F is shown in Fig. 5.3 along with the results of a uniform burnup calculation normalized to the CANDLE-2 reactivity at the start of life. The normalization was necessary due to different reactivities at the start of life which resulted from differences in constants between CANDLE-2 and MUFT-III P1-SG. as shown in Table 5.7. MUFT-III P1-SG. was used for the uniform burnup calculation. It is noted that CANDLE-2 calculations yield core reactivity at 1.4 MWYR with equilibrium xenon of 8.9 percent. This compares with the measured reactivity of 9.2 percent. The CANDLE-2 radial burnout has been adjusted to a reactivity of 9.2 percent at 1.4 MWYR to correspond to experiment. The results are shown in Fig. 5.4. The indicated core life is 18.4 MWYR for the non-uniform radial burnup.

TABLE 5.5

THREE FAST GROUP DATA FOR CANDLE-2 CODE, SM-1 CORE I AT 440°F

Element No.		Element	Group	Cross Section (barns)				
				σ_{tr}	σ_R	σ_a	σ_f	$\nu\sigma_f$
WAPD 1	(Alco) (1)	H	1	0.992507	1.641435	0	0	0
			2	3.730513	2.192517	0	0	0
			3	6.877471	1.740096	0.005576	0	0
2	(7)	0	1	1.831801	0.127577	0.035240	0	0
			2	3.730184	0.049623	0	0	0
			3	3.800007	0.030890	0	0	0
6	(4)	SS	1	1.315149	0.025227	0.095500	0	0
			2	3.484434	0.013089	0.095500	0	0
			3	8.933687	0.020964	0.197898	0	0
18	(18)	U-235	1	5.960299	0.021852	1.436740	1.299422	3.597993
			2	12.500013	0.009273	2.426571	1.934721	4.724266
			3	52.016437	0.004738	43.797590	31.938991	78.506064
29	(9)	B-10	1	0.435892	0	0.435892	0	0
			2	2.161444	0	2.161444	0	0
			3	206.803657	0	206.803657	0	0

TABLE 5.6
THERMAL MICROSCOPIC CROSS SECTIONS

($T = 440^{o}F$; $E_N = 0.0549$ ev)

Atom	$\overline{\sigma}_s$	$(1-\overline{\mu})$	$\overline{\sigma}_a$	$\overline{\sigma}_{tr}$	$\overline{\nu\sigma}_f$
U-235	9.0	0.997165	385.5384	394.512	801.0342
U-238	9.0	0.997201	1.644605	10.620	-
H	28.97	0.7059	0.197353	20.65	-
O	3.9	0.958334	0	3.7375	-
B-10*	4.4	0.933441	2277.0146	2281.1217	-
S.S.	10.44	0.988	1.762814	12.078	-

* Based upon 19.8 a/o of B-10 in natural boron.

The effect of using the P-1 slowing down model rather than P1-SG [illegible] on core reactivity, and hence on core life, has been investigated. The core reactivity was calculated on a uniform basis using MUFT-III P-1 and P1-SG [illegible] group constants. The reactivity difference is shown in Table 5.7 along with the experimental value. As shown in Table 5.7, MUFT-III, P-1 gives better results.

Fission product absorption excluding Xe was also expressed simply as a thermal absorption cross-section. Data on the variation of the fission product absorption was found in ANL-5800[5] and KAPL-2000-12.[6] This data is reproduced in this report in Fig. 5.2. The curve from ANL-5800 was used to determine the average fission product microscopic absorption cross-section with core burnup. As shown in Fig. 5.2, the curve rises very sharply at 5% fuel burnup due to the accumulation of Sm-149. The slope is then fairly constant for the rest of core burnup. This slope corresponds to a fission product microscopic thermal absorption cross-section of 11 barns per fraction U-235 depletion, this was calculated as follows:

$$\Sigma_{a_{fp}} = \overline{B}\, N^{o}_{U\text{-}235}\, \sigma_{a_{fp}}$$

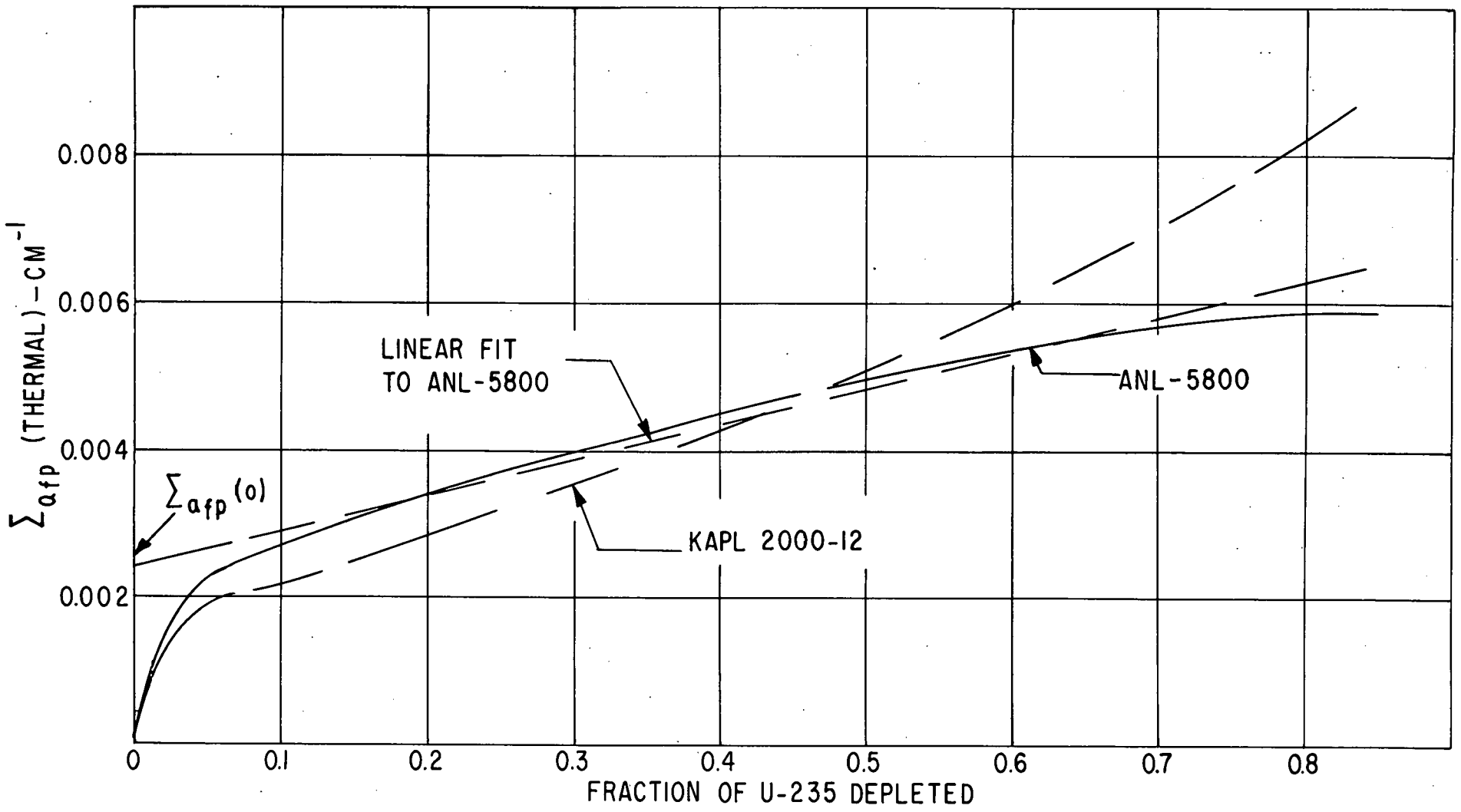

Figure 5.2 Thermal Absorption Cross-Section of Fission Products in SM-1 at 440°F vs. Fuel Burnup

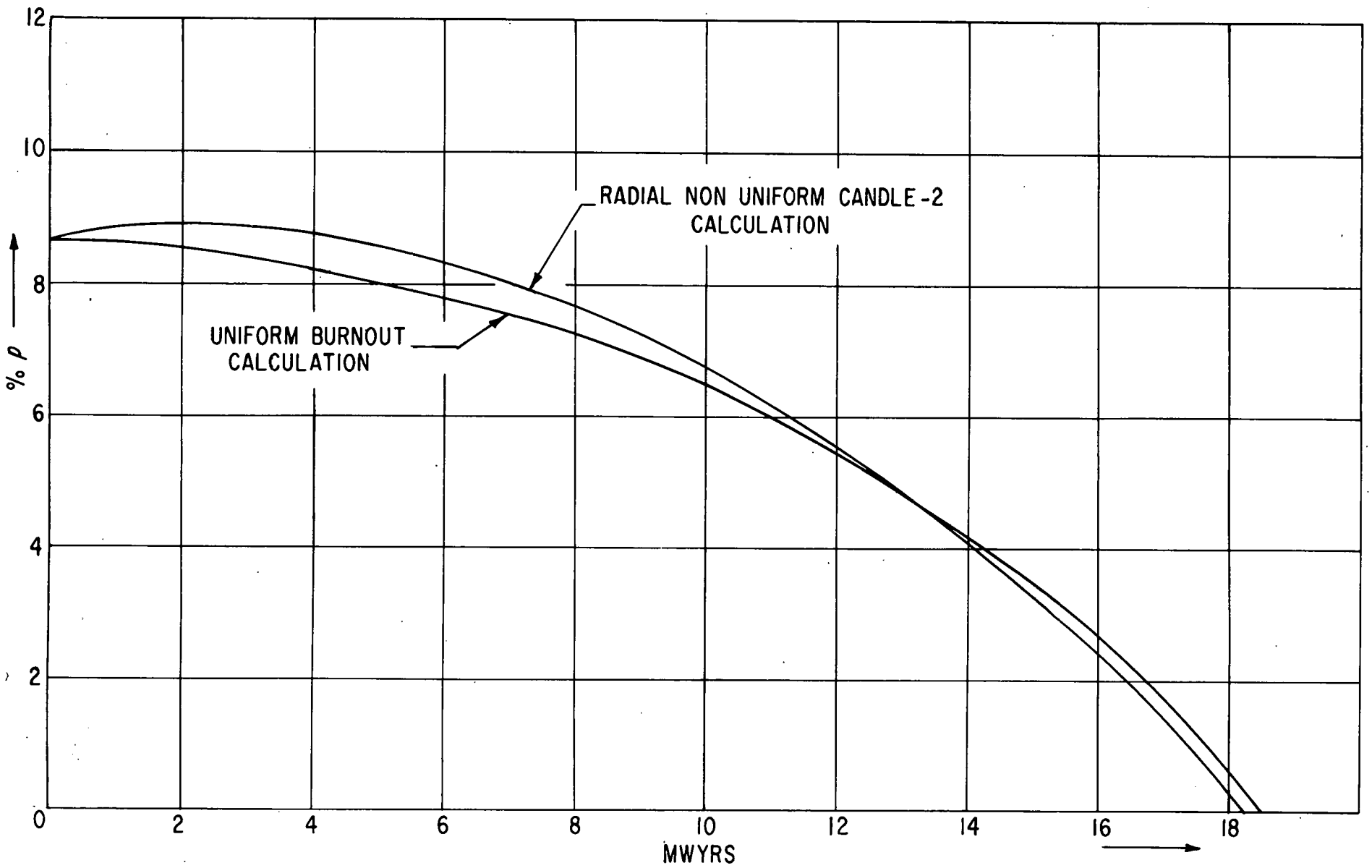

Figure 5.3 SM-1 Core I Radial Burnup, 440°F, Equilibrium Xenon

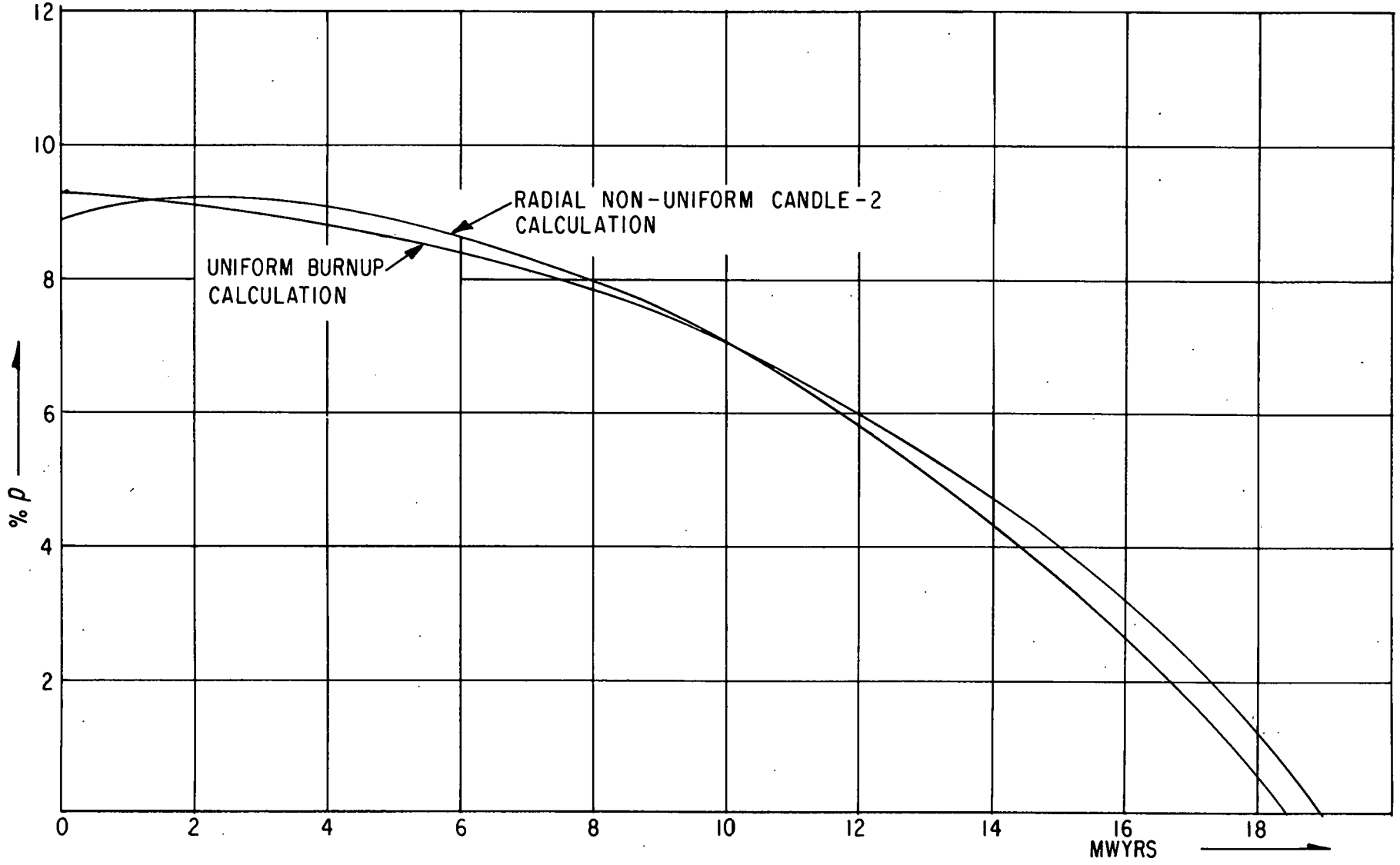

Figure 5.4 Radial Burnup SM-1 Core I, 440°F, Equilibrium Xenon - Normalized to Experimental Reactivity at 1.4 MWYR

TABLE 5.7
COMPARISONS OF COALESCING SCHEMES OF CANDLE-2, MUFT-III P1-SG, AND MUFT-III P-1 CODES
SM-1 Core I At 440°F

Parameter*	Units	Homogenized Fixed Element Cell		
		CANDLE-2	MUFT-III, P1-SG	MUFT-III, P-1
D_f	cm	1.605247	1.611982	1.334972
τ	cm^2	46.867157	46.278158	38.826884
Σ_{Tf}	cm^{-1}	0.034251	0.0348325	0.034383
Σ_{af}	cm^{-1}	0.009279	0.009398	0.009303
Σ_{sl}	cm^{-1}	0.024972	0.025434	0.025080
$\nu\Sigma_{ff}$	cm^{-1}	0.011949	0.012142	0.011992
K_f		1.287746	1.292004	1.289046
p		0.729089	0.730201	0.729426
D_{th}	cm	0.245496	0.247063	
$\Sigma_{a_{th}}$	cm^{-1}	0.206539	0.206452	
$\nu\Sigma_{f_{th}}$	cm^{-1}	0.320447	0.324239	
K_{th}	-	1.551508	1.570528	
ρ% (calculated)		8.63	9.79	13.04
ρ% (measured)		12.10	12.10	12.10

* See Appendix E for definition of parameters.

TABLE 5.8
RESULTS OF COMPARISON OF COALESCING SCHEMES
FOR PURE WATER REFLECTOR REGION- 440°F

Parameter*	Units	CANDLE-2	MUFT-III, P1-SG	MUFT-III, P-1
D_f	cm	1.554893	1.899871	1.56416
τ	cm^2	41.472660	47.830185	40.115196
Σ_{T_f}	cm^{-1}	0.0004200	0.000457	0.000499
Σ_{a_f}	cm^{-1}	0.0004200	0.000457	0.000499
Σ_{s_l}	cm^{-1}	0.0370716	0.039264	0.038424
$\nu\Sigma_{f_f}$	cm^{-1}	0	0	0
K_f	-	0	0	0
p	-	0.988798	0.988490	0.987177
D_{th}	cm	0.265809	0.265809	0.265809
$\Sigma_{a_{th}}$	cm^{-1}	0.011014	0.011014	0.011014
$\nu\Sigma_{f_{th}}$	cm^{-1}	0	0	0
K_{th}	-	0	0	0

* See Appendix E for definition of parameters.

The equation of the linear portion of the curve is:

$$\Sigma_{a_{fp}} = m\,\overline{B} + \Sigma_{a_{fp}}{}^{(o)}$$

$\Sigma_{a_{fp}}{}^{(o)}$ was used as a contant term which was added to the core thermal macroscopic absorption cross-section. By moving the origin up to $\Sigma_{a_{fp}}{}^{(o)}$, the linear equation then reduced to:

$$\Sigma_{a_{fp}} = m\,\overline{B} = \overline{B}\,N^{o}_{U\text{-}235}\,\sigma_{a_{fp}} \quad \text{or} \quad \sigma_{a_{fp}} = \frac{m}{N^{o}_{U\text{-}235}}$$

For the SM-1 core at 440°F,

$$\Sigma_{a_{fp}}^{(o)} = .002442 \text{ cm}^{-1}$$

$$\sigma_{a_{fp}} = \frac{.0047}{.0004286 \times 10^{24}} = 11 \text{ barns per fraction U-235 depletion.}$$

The thermal absorption cross section Σ_a^{Xe} which accounts for the reactivity effect of xenon, is calculated as follows:

$$\Sigma_a^{Xe} = \frac{\alpha x (Y_I + Y_{Xe}) \sigma_a^{-Xe} \left(\frac{\sigma P_{Mw}}{V}\right)}{\lambda_{Xe} + \sigma_a^{-Xe} \left(\frac{\beta \sigma P_{Mw}}{V}\right)\left[\frac{1}{(1-\beta)\Sigma_{f_{th}}}\right]}$$

where $x = (1-\beta) + \beta g'(B)$ and the remaining parameters are given in Appendix E. At start of life and 440°F, Σ_a^{Xe} was found to be 0.006975 cm^{-1}. The values of the parameters used are listed in Appendix C.

Figure 5.5 shows the calculated variation of control rod bank position as obtained from the axial CANDLE-2 calculation. With the effect of the non-uniform radial burnout included. Also shown are the experimental measurements of bank withdrawal versus energy release. Figure 5.6 shows the results of CANDLE-2 including the radial non-uniform burnup correlation normalized to the measured reactivity at 1.4 MWYR. It is seen that the CANDLE-2 axial burnout calculation gives very good prediction of bank position variation with energy release but overestimates the core life by approximately 0.5 MWYR*.

5.2.5 Fuel and Boron Distribution as Function of Core Life

Pointwise distribution of uranium and boron were obtained from the axial and radial CANDLE-2 calculations. Figure 5.7 indicates the radial variation of U-235 and B-10 burnups at two different megawatt years. At 16.8 MWYR, the average U-235 burnup is 37.4% compared to an average B-10 burnup of 93%.

Figure 5.8 shows the axial distribution of U-235 and B-10 burnup at two different energy releases. Only preliminary results of hot cell examinations of SM-1 Core I elements are available for comparison with these calculated U-235 burnups. At the end of SM-1 Core I life, 16.4 MWYR, two elements were sent for hot cell examination. Figure 5.9 shows a comparison of the axial burnout distribution of U-235 in element 79 with that obtained by ORNL. This element was located in position 45 of SM-1 Core I for 16.4 MWYR. The measured burnout corresponds to the average burnout across the width of the fuel plate

*At 10.5 MWYR two new elements were added; it has been calculated that the lifetime is increased by 0.3 MWYR. This correction is shown in Fig. 5.6.

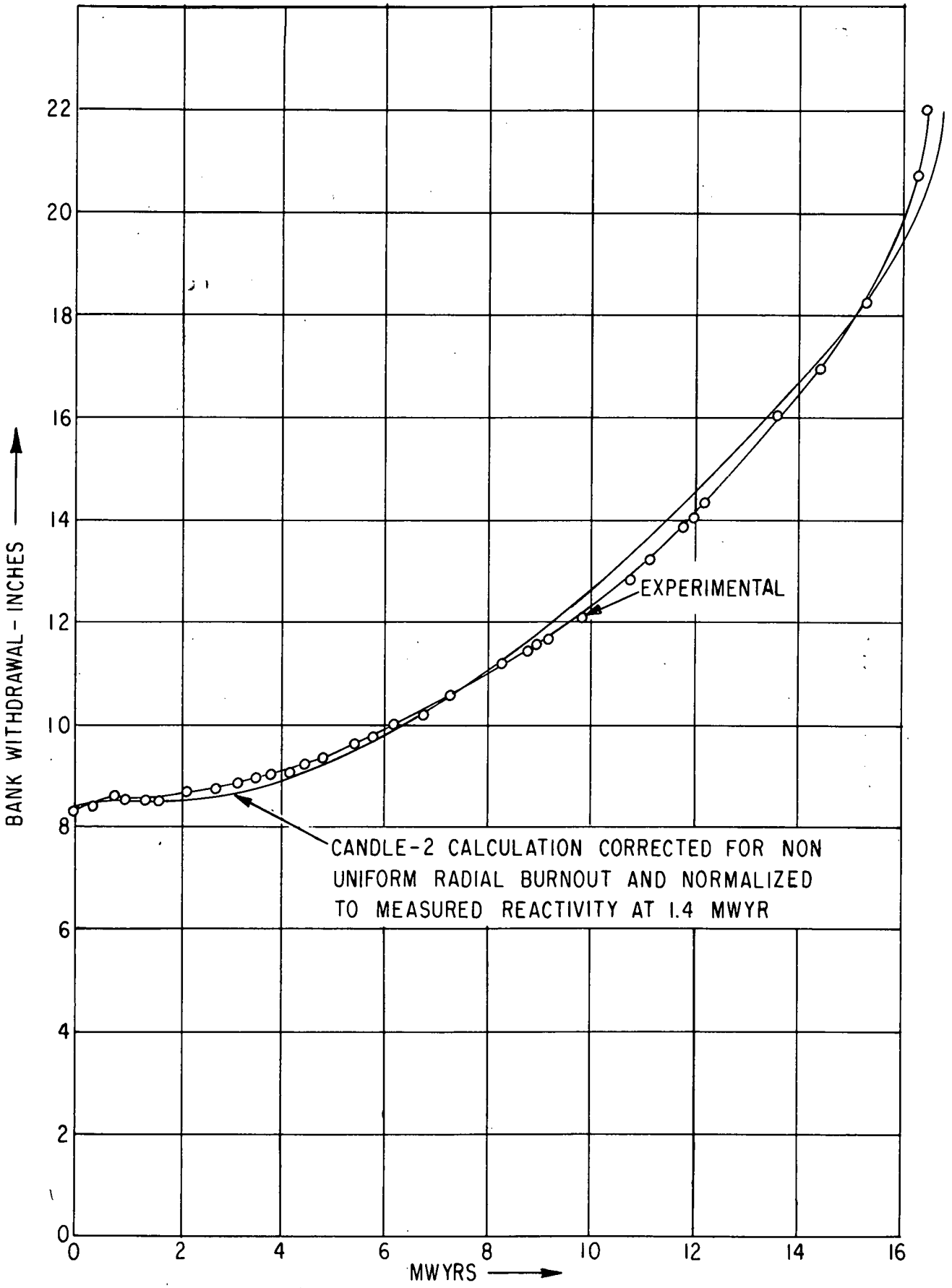

Figure 5.5 SM-1 Core I Control Rod Bank vs. MWYR - 440°F, Equilibrium Xenon

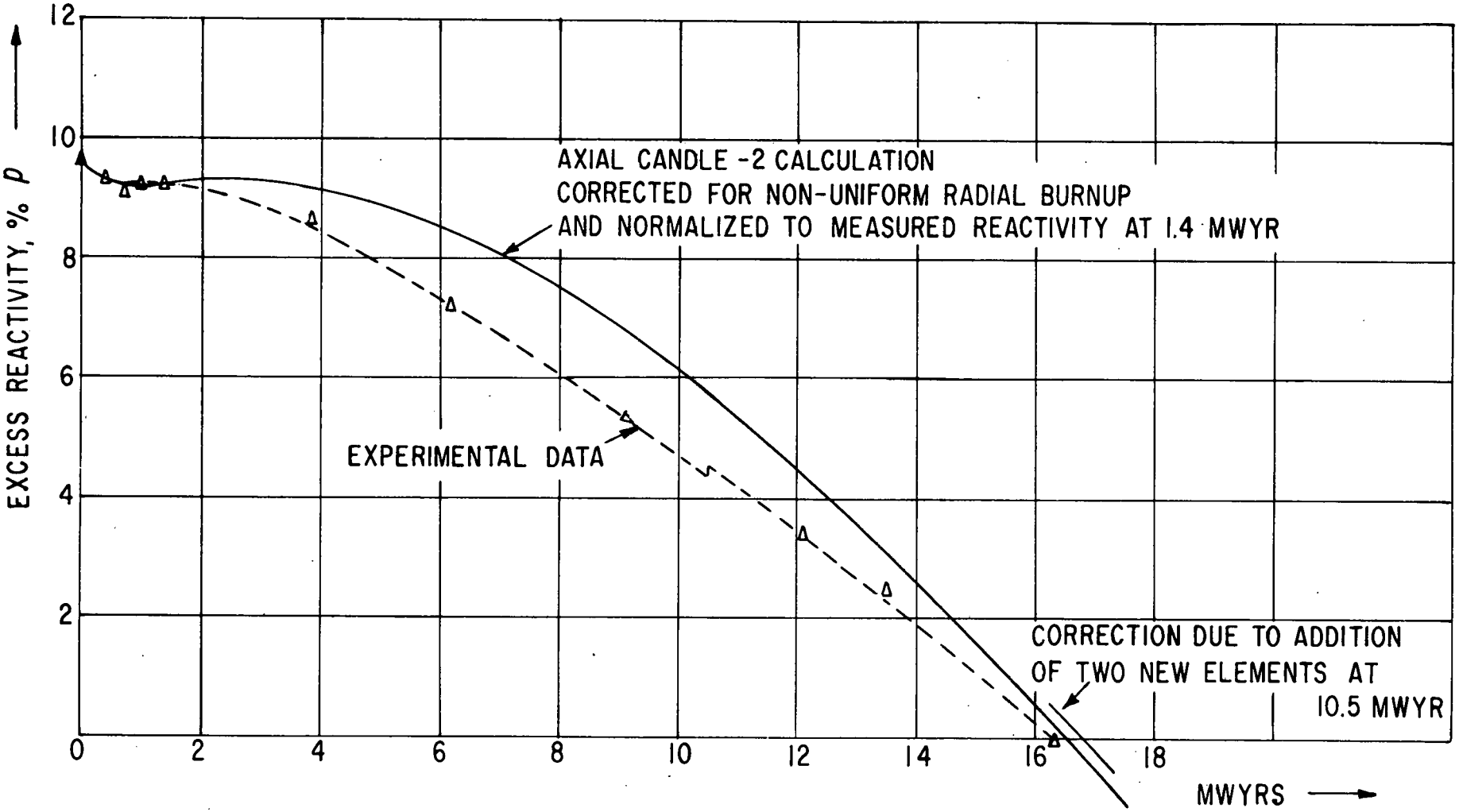

Figure 5.6 Excess Reactivity as a Function of Energy Release - SM-1 Core I, 440°F, Equilibrium Xenon

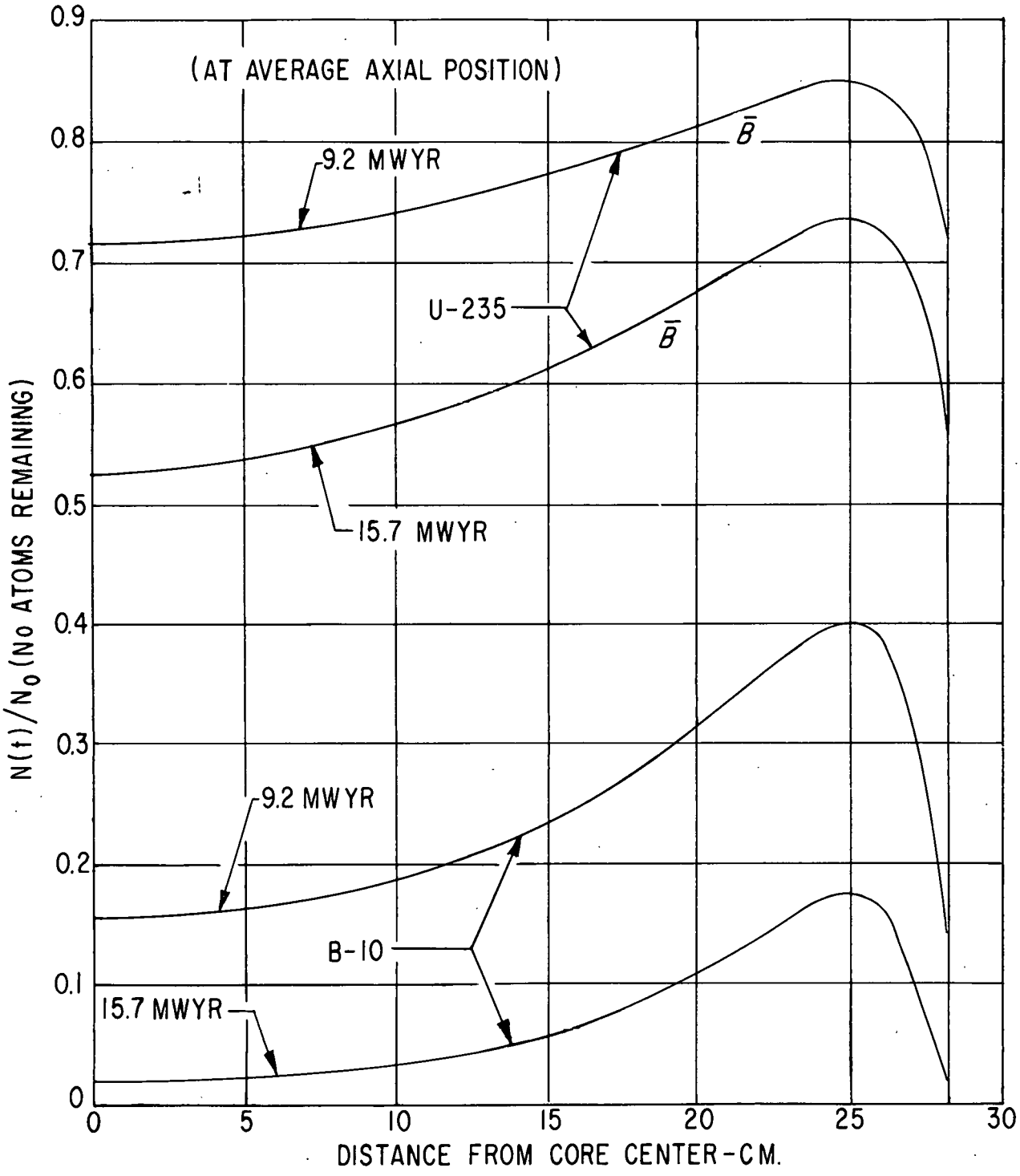

Figure 5.7 SM-1 U-235 and B-10 Radial Burnup at 9.2 MWYR and 15.7 MWYR - All Fixed Elements with $\sum_a$

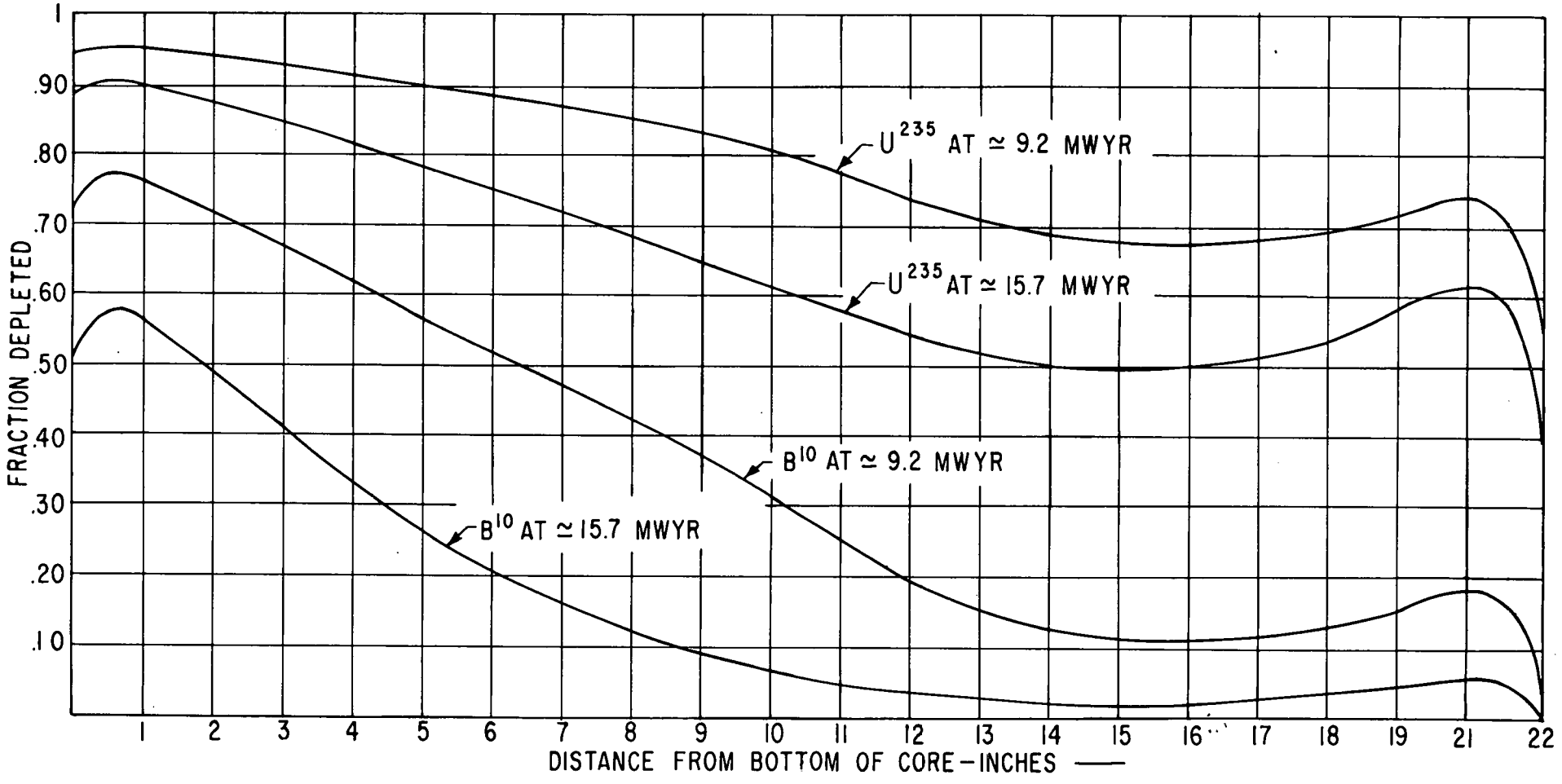

Figure 5.8 SM-1 Core I Axial Variation of Burnup Fraction of B-10 and U-235 at 9.2 and 15.7 MWYR

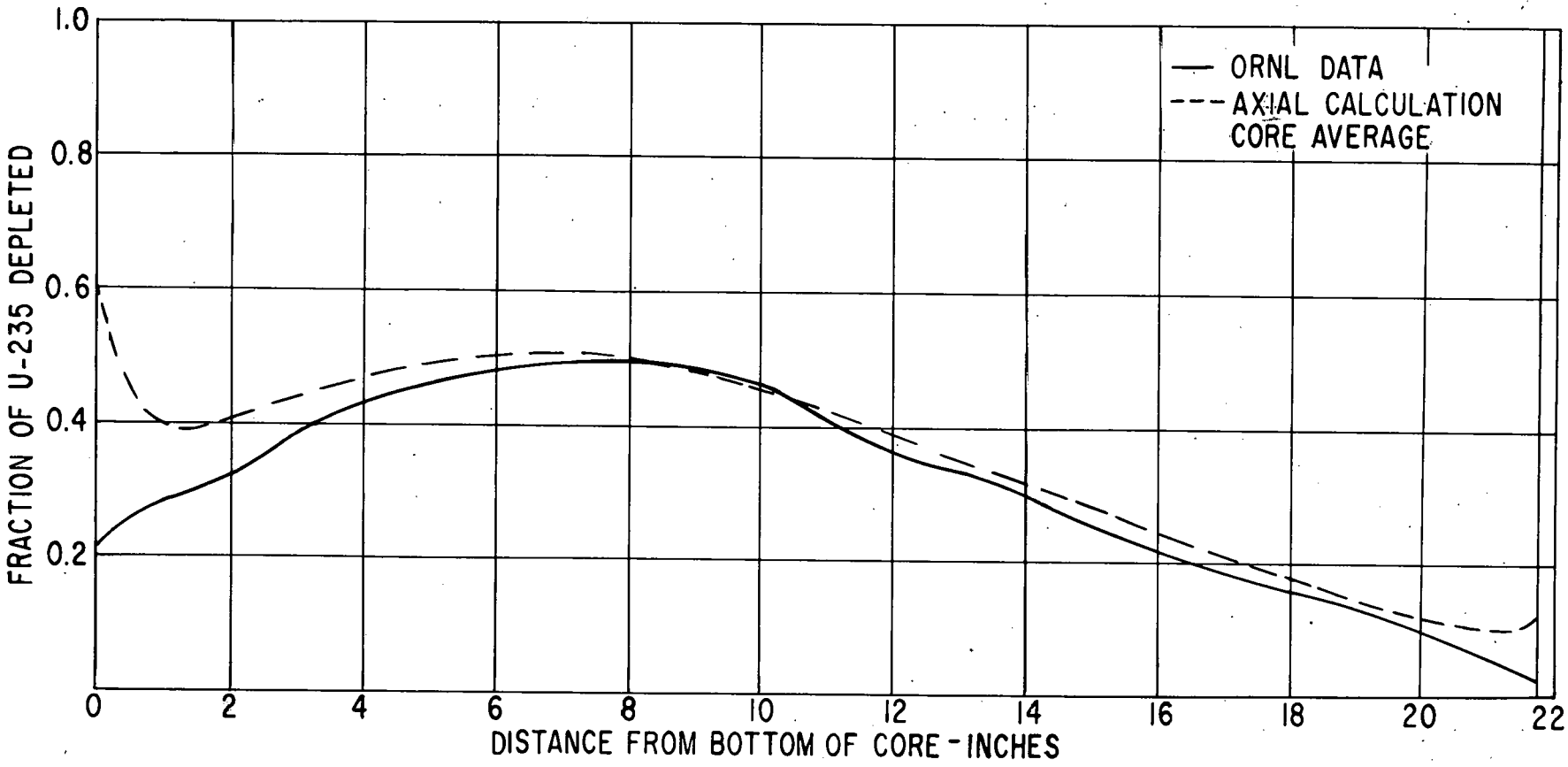

Figure 5.9 Measured Fuel Burnup in Element 45 of SM-1 Core I After 16.4 MWYR of Energy Release

and therefore affords a comparison with the CANDLE-2 one-dimensional results. It is noted that element 45 was located only 3 in. from the core centerline and hence it should have a burnup 24 percent higher than the average radial burnup which is that calculated in the axial CANDLE-2 results presented in Fig. 5.9.

5.2.6 Power Distribution

Results of CANDLE-2 analysis can be used to gain an insight to the variation of gross power distribution with core burnout. Figure 5.12 shows the variation in radial power distribution. This figure indicates that the radial max-to-average is reduced by about 12 percent during core burnout. The variation in axial power distribution with core burnout is illustrated in Fig. 5.11.

A detailed CANDLE-2 calculation was made to determine the decrease in local power peaking with lifetime. The first two rings of elements (central control rod fuel element and a ring of fixed elements) were broken up into active and dead regions (Fig. 5.10A). This two-cell core was then burned out using CANDLE-2. The results are shown in Fig. 5.10. This figure clearly illustrates how the intercell peaking due to the absence of fuel in the side plate region rapidly decreases with core burnout.

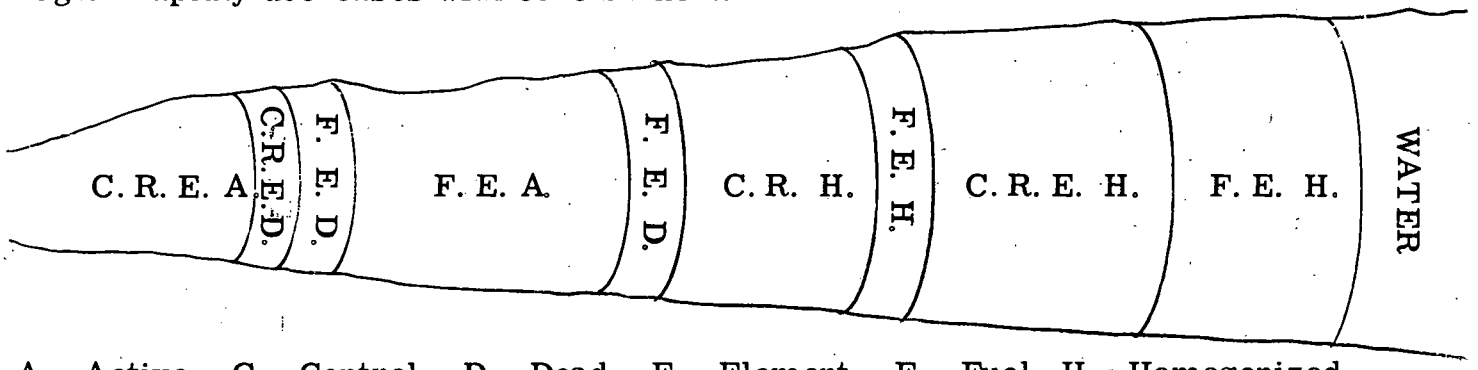

A = Active, C = Control, D = Dead, E = Element, F = Fuel, H = Homogenized

Element	Number Densities x 10^{24}		
	F. E. A.& C. R. E. A.	C. R. E. D.	F. E. D.
Hydrogen	.045719	.035489	.036286
Oxygen	.023924	.017744	.018143
S. S.	.012487	.030986	.029771
U-235	.00049597	0	0
B-10	.00000827	0	0

Figure 5.10A.

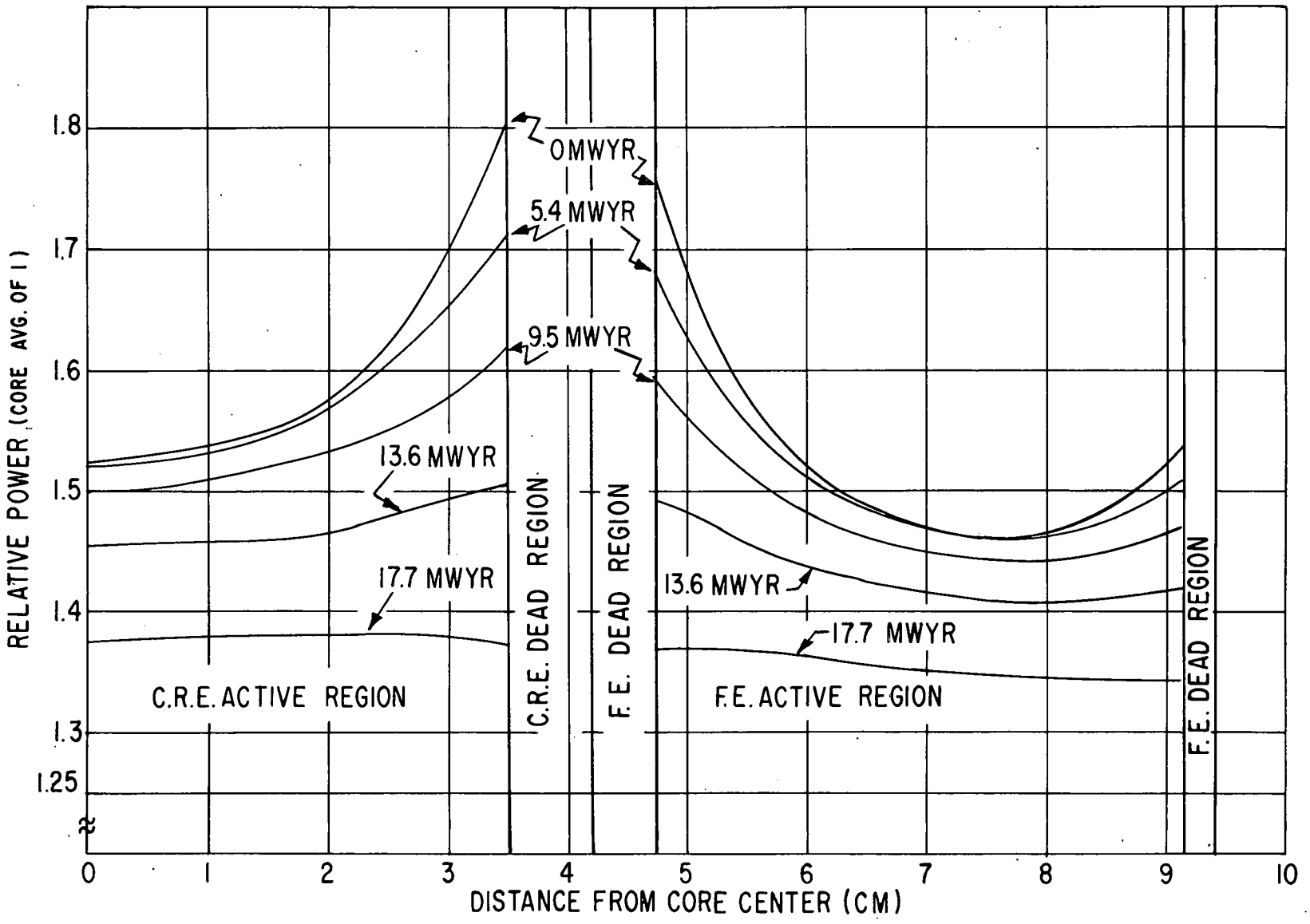

Figure 5.10 Radial Power Distribution of Various Periods of Core Burnup in SM-1 Core I - 440°F

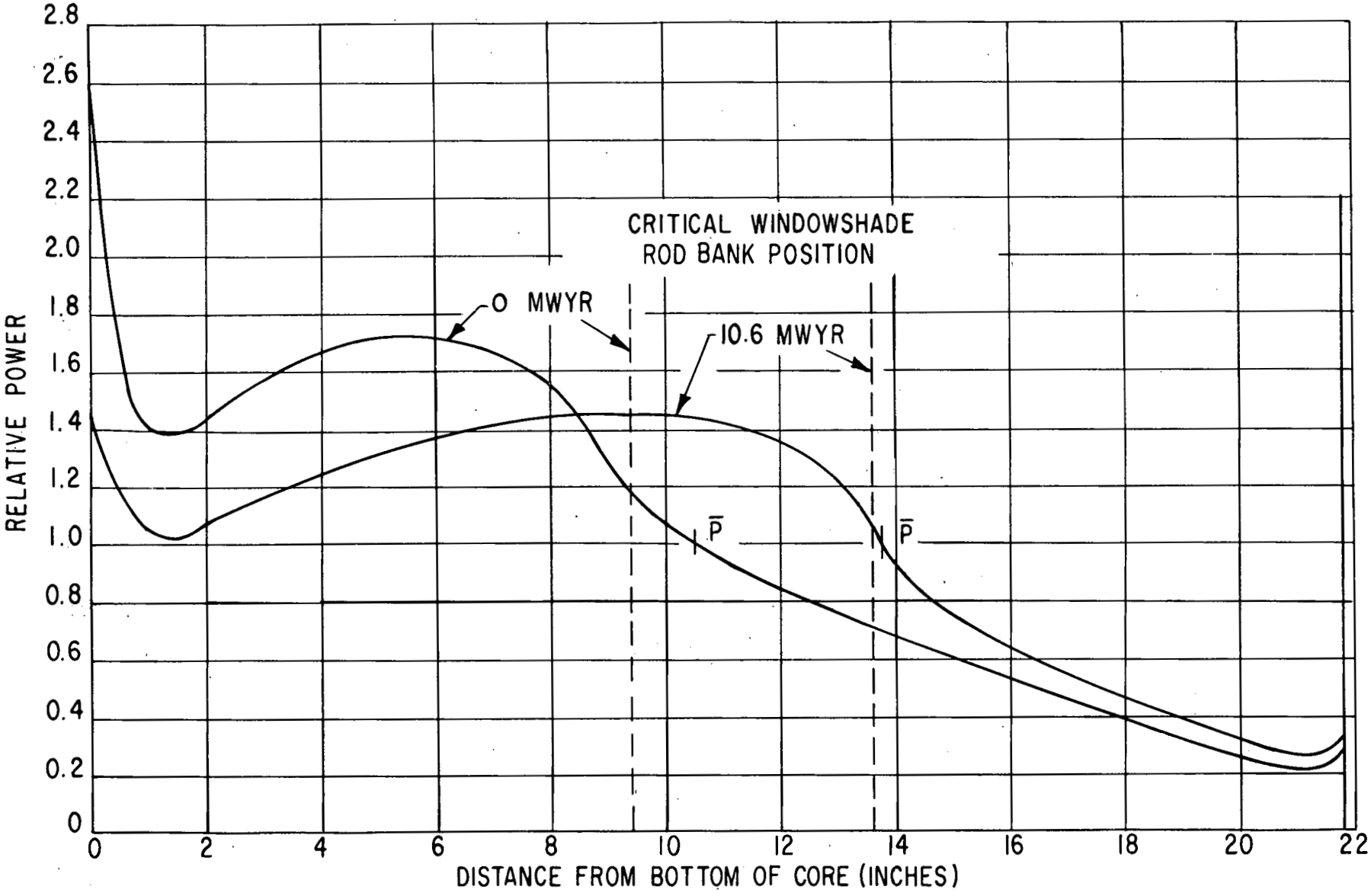

Figure 5.11 SM-1 Axial Power Distribution - 440°F Equilibrium Xenon

Figure 5.12 illustrates the overall radial power distribution for 0 MWYR. It is seen that power interface and center peaks are reduced.

5.2.7 Change in 5 Rod Bank Worth

The measurements[1] made on the SM-1 Core I 5 rod bank worth indicated an increase in worth with core life. In order to determine if CANDLE-2 would predict this increase in rod worth, an analytical calculation of rod worth was carried out for the core at 12 MWYR energy release. In order to obtain a complete rod bank worth curve, material compositions of various regions of axial CANDLE-2 calculations at 12 MWYR were used. These compositions were averaged over six axial core regions. The rod poison $\sum_p^{rods}$ cross section (Table 5.3) was assumed to remain constant with core burnout. A series of axial VALPROD calculations were run with the $\sum_p^{rods}$ moved into the core on 2-in. intervals. The resulting reactivity was converted into rod bank worths and plotted in Fig. 5.13. Also shown in Fig. 5.13 is the calculated rod worth curve for 0 MWYR. The experimental curves for 0 and 12 MWYR are also shown.

5.2.8 Xenon Reactivity

The reactivity associated with equilibrium and maximum xenon was calculated using CANDLE-2 over the lifetime of SM-1 Core I. In addition, a detailed study of a xenon transient of 12 MWYR was performed. In these calculations, a xenon thermal microscopic absorption cross section of 2.0 - 2.6 x 10^6 barns was used. In addition, a non-uniform special distribution factor, $\alpha = 1.134$, for xenon was used. Figure 5.14 shows the calculated and measured variation in reactivity of transient xenon with time after reactor shoutdown. The calculations are presented for two values of average xenon microscopic cross section. The sensitivity of the reactivity on Xe cross section is illustrated in this figure. The analysis of this problem in Appendix D indicates that a cross section in the range of 2.34 to 2.60 x 10^6 barns is the best value.

The CANDLE-2 code was used to compute the equilibrium and maximum Xe reactivity as a function of core energy release. A xe-135 cross section of 2.6 x 10^6 barns and a distribution factor of $\alpha = 1$ was used in this calculation. Figure 5.15 shows the calculated and measured xenon reactivities as a function of core energy release.

5.2.9 Conclusions

1. The application of CANDLE-2 in the radial and axial directions in the SM-1 Core I gave a core life of 16.8 MWYR compared to 16.4 MWYR experimental.
2. The spatial change of fuel due to burnup can be predicted with reasonable accuracy.
3. Equilibrium and maximum xenon reactivity were found to have been predicted very accurately using CANDLE-2 code.

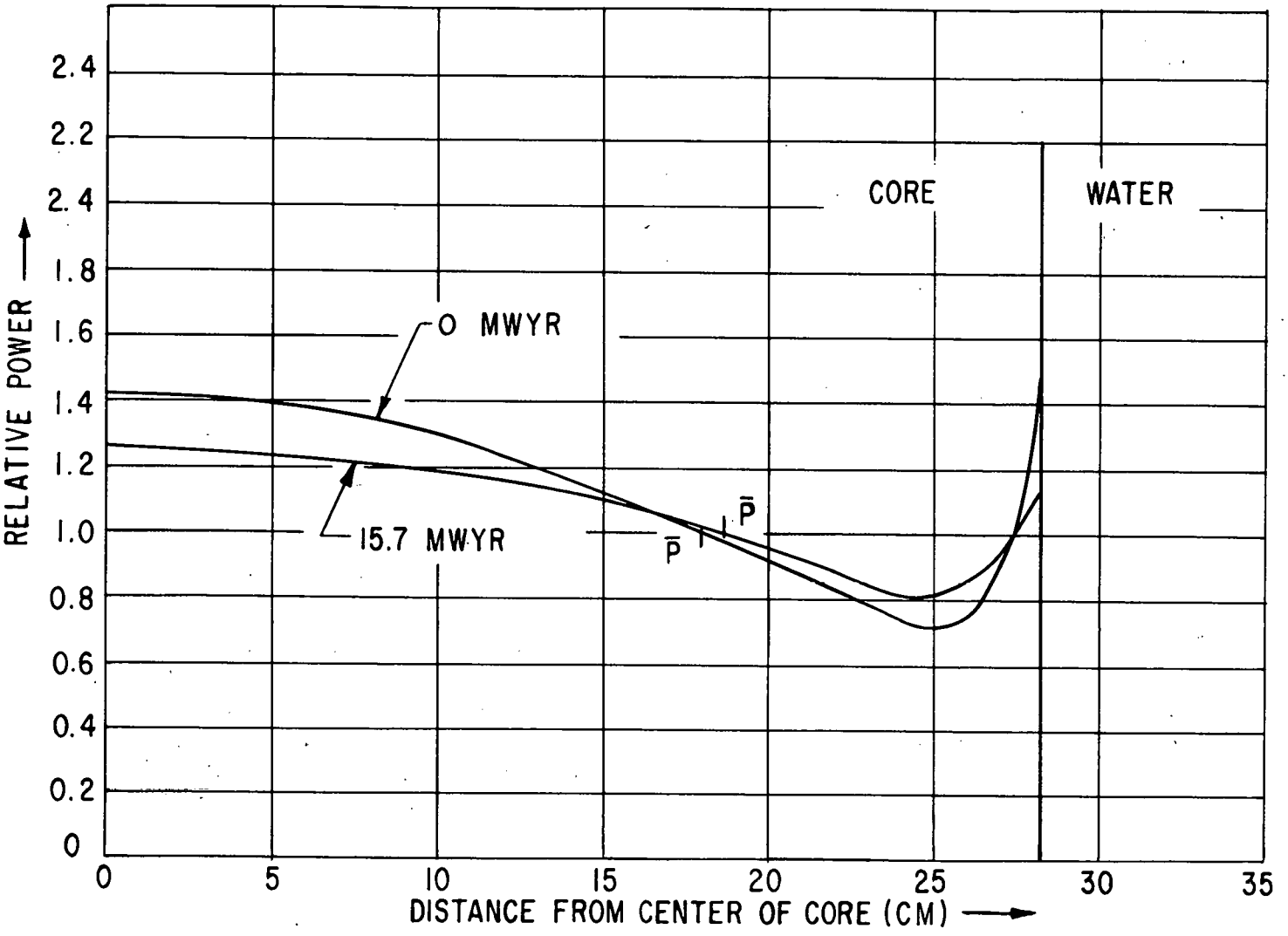

Figure 5.12 SM-1 Radial Power Distribution - 440°F, Equilibrium Xenon - All Fixed Elements - $\sum_a$

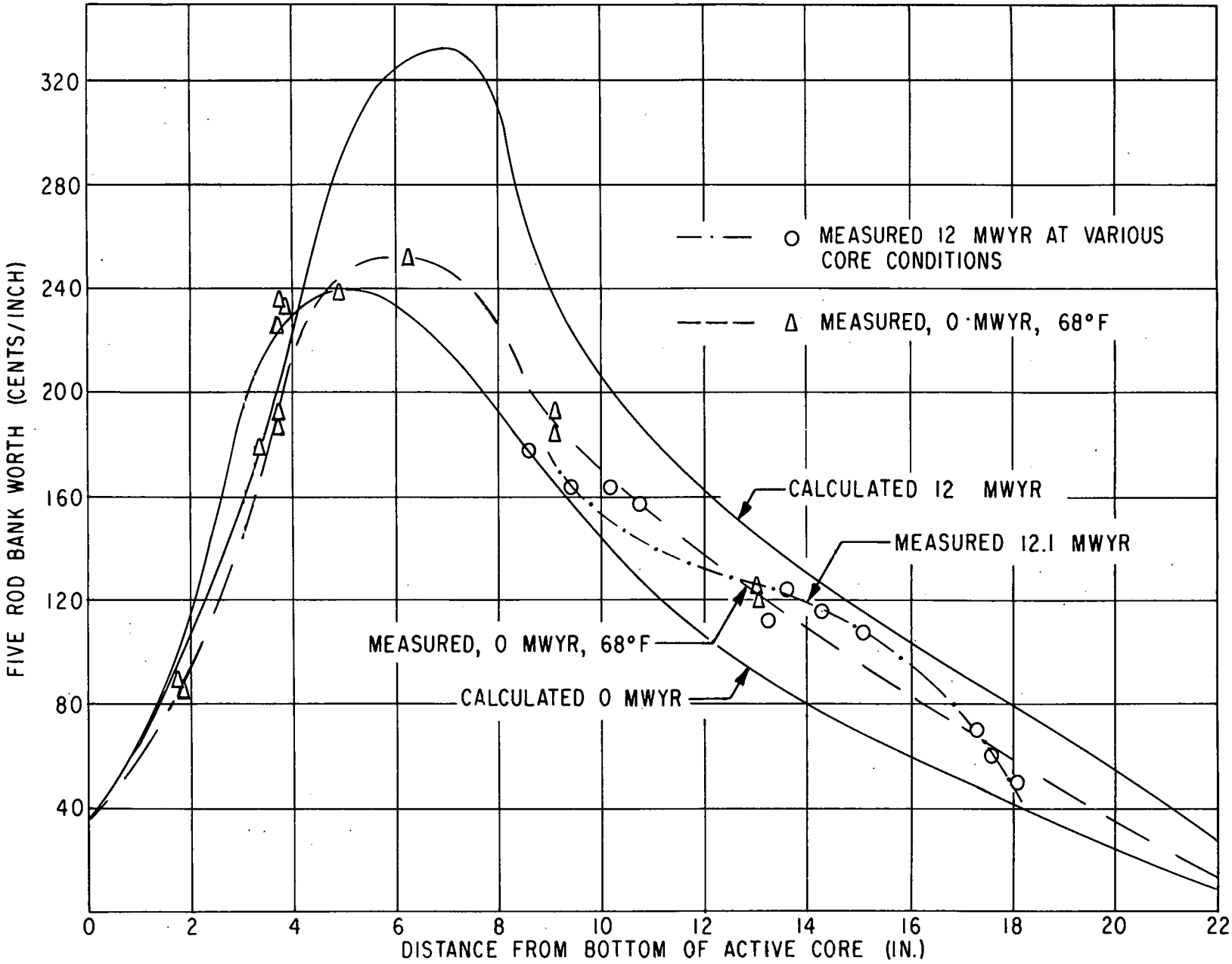

Figure 5.13 SM-1 Five Rod Bank Calibration

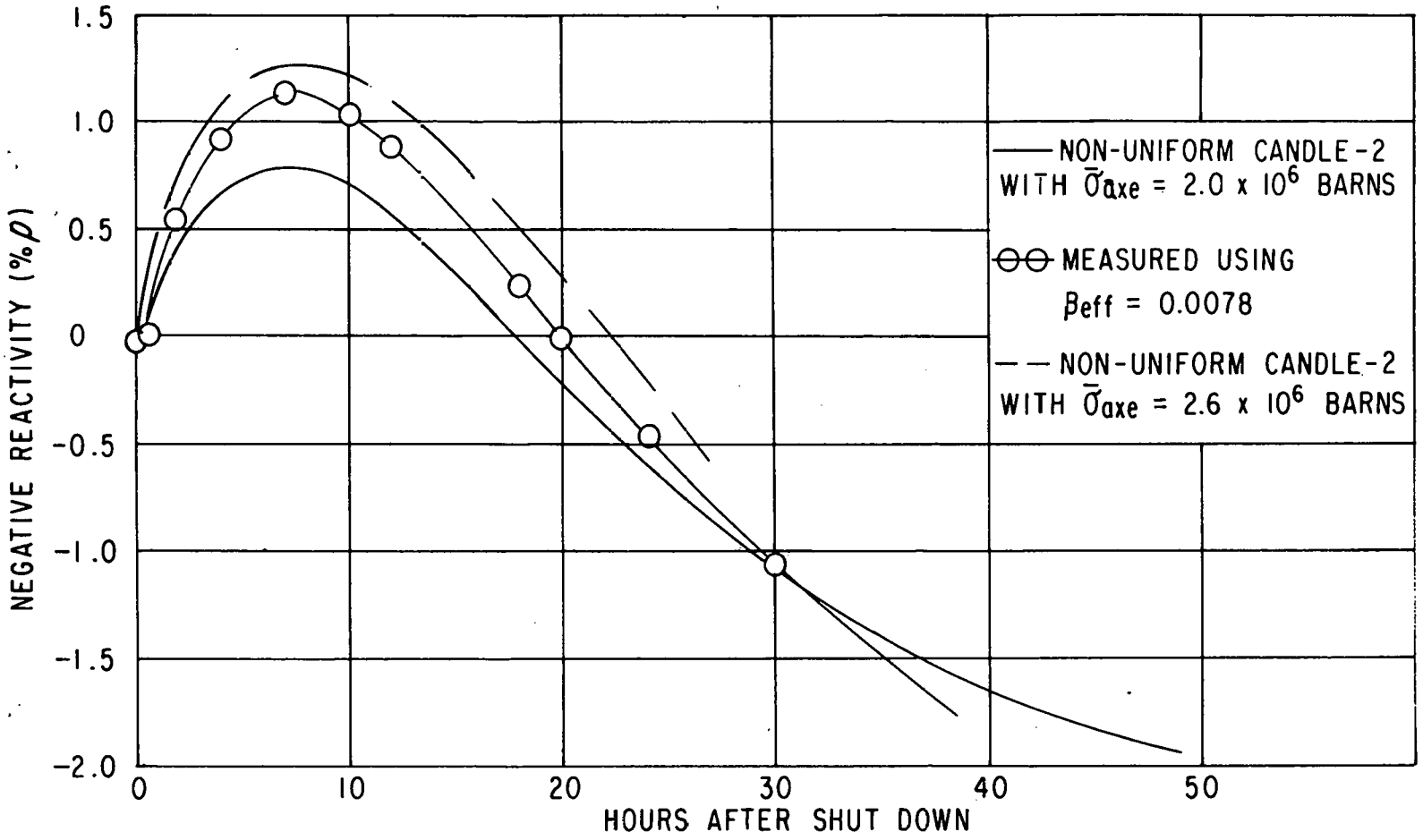

Figure 5.14 Transient Xenon Reactivity in SM-1 Core I at 12 MWYR

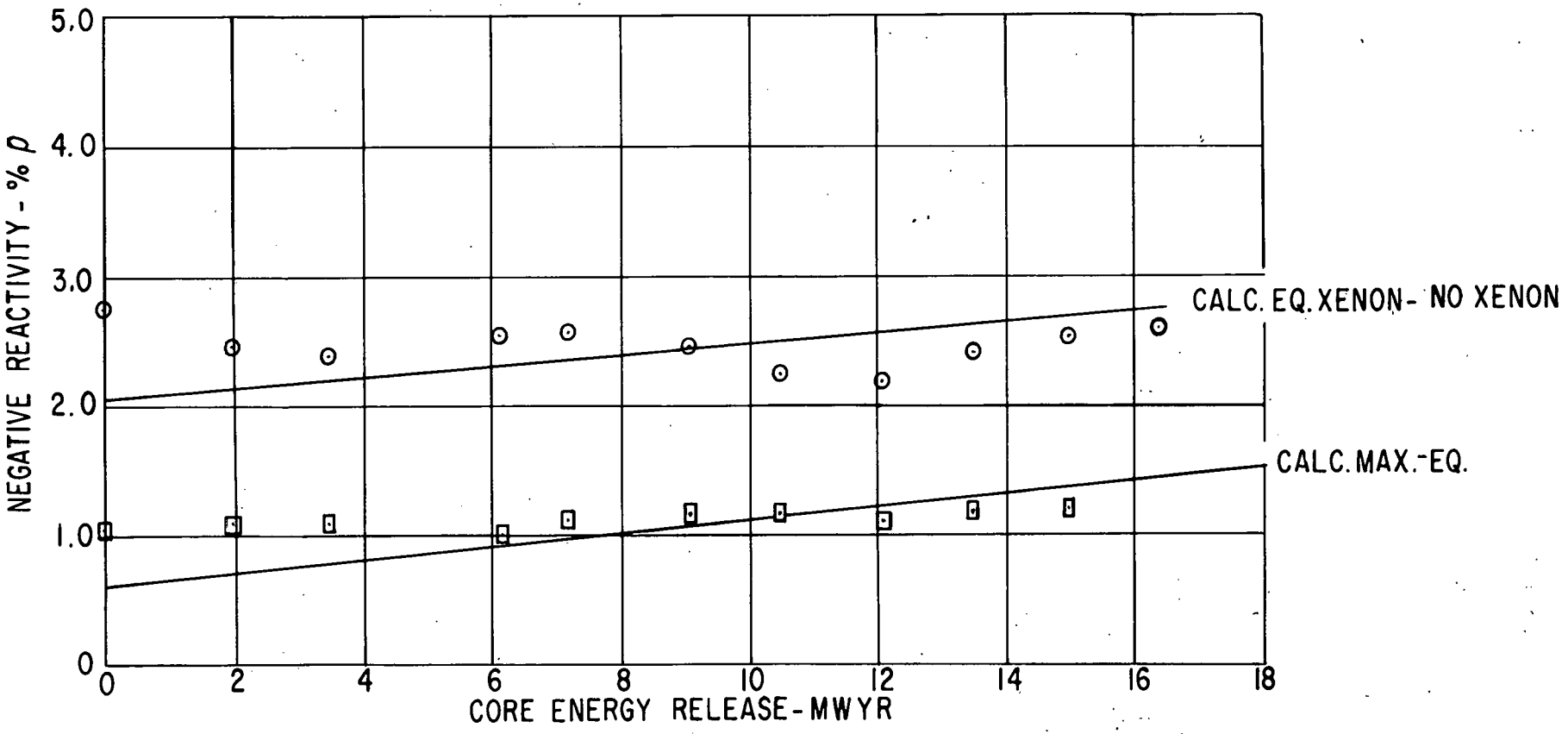

Figure 5.15 SM-1 Core I Xenon Reactivity vs. Lifetime

5.3 ESTIMATE OF CORE CHANGES AT 10.5 MWYR OF CORE LIFE

At 10.5 MWYR energy release of SM-1 two fuel elements were removed and replaced by two new fuel elements.[7] In addition the original absorber sections employing boron enriched in the B-10 isotope were replaced by absorbers containing Eu_2O_3. This latter change had a negligible effect on bank positions and therefore no change in core life. The element in position 64 is a control rod fuel element. The extension of SM-1 Core I life due to substitution of a new element into positions 64 and 56 was estimated using the CANDLE-2 code.

A geometrical model consisting of a control fuel element surrounded by an annulus of fixed elements reflected by water was employed. A CANDLE-2 burnout calculation was performed in this geometry. The core for an energy release of 10.5 MWYR was then modified by the adjustment of atomic concentrations of fuel and burnable poison to initial values in the control region, and the core burnout repeated. The reactivity variations were then compared yielding a 0.5% ρ increase and a core lifetime increase of 0.45 MWYR. Since the two elements substituted were not in the central positions, the reactivity effect was estimated by $J_0^2(\mu r)$ weighing of the value obtained for the central element. The difference between fixed and control rod substitution were neglected. The result for new elements in positions 64 and 56 at 10.5 MWYR is 0.4% increase in core reactivity and a 0.35 MWYR increase in core life. The best estimate of the core life of an unperturbed SM-1 Core I is then 16.4 - 0.35 or 16.05 MWYR energy release.

At the time of the 10.5 MWYR change a reactivity increase of 0.13 percent was estimated and a lifetime increase estimated of 0.35 MWYR.[7]

5.3.1 Buildup of U-236 in SM-1 Core I

Measurements of U-236 buildup in SM-1 Core I are now underway at ORNL on four elements removed from SM-1 Core I, two at 10.5 MWYR and two at end of life (16.4 MWYR). Using CANDLE-2, the buildup of U-236 in SM-1 Core I has been calculated as a function of core life. A value of 4 barns was used for the thermal absorption cross section of U-236 at 440°F.

Similar calculations of U-236 buildup are given for pile irradiated U-235 in Reference (8). From Fig. 8.1 of Reference (8) and a thermal nvt of 5.2×10^{20} neutrons/cm^2 (for 10.5 MWYR operation of SM-1) the U-235 remaining per initial atom of U-235 is 76 percent. This compares with a CANDLE-2 value of 76.6 percent. The number of U-236 atoms per initial U-235 atoms is 4.2 percent from Reference (8) and 4.4 percent from CANDLE-2 at 10.5 MWYR.

5.3.2 Conclusions

1. The substitution of two elements of SM-1 Core I at 10.5 MWYR produced an estimated core life increase of 0.35 MWYR. Therefore the core life of an unperturbed SM-1 Core I would have been 16.05 MWYR.

2. A CANDLE-2 calculation has been performed to estimate the U-236 built up. However lack of experimental measurements prevents evaluation of the results.

5.4 SUMMARY

In the present section CANDLE-2 has been used as the basic tool in predicting the core lifetime of SM-1 Core I.

With a reactivity adjustment at 1.4 MWYR, to the measured value, the core life was found to be 16.8 MWYR compared to 16.4 MWYR measured. U-235 and B-10 axial depletion and power distribution at various burnup levels have been calculated. The reactivity associated with equilibrium xenon was calculated and found in good agreement with experiment.

5.5 REFERENCES

1. Weiss, S. H., "Summary Report of Physics Measurements on SM-1 Core I," APAE-96, February 6, 1962.

2. Gallagher, J. G., "Reactor Analysis for APPR-1," APAE No. 7, May 29, 1956.

3. ORNL-1613, "A Conceptual Design of a Pressurized Water Package Power Reactor." (classified)

4. Williamson, T. G., et al, "NUB-1: A Non-Uniform Burnout Code for the IBM-650," AP Note 116, Alco Products, Inc., October 23, 1958.

5. ANL-5800, Reactor Physics Constants, 1958.

6. KAPL-2000-12, Reactor Technology Report No. 15, December 1960.

7. Obrist, C. M., "SM-1 Reactor Core Inspection at 2/3 Core Life," APAE-55, January 13, 1960.

8. Schuman, R. P., Tromp, R. L., "Calculation of the Composition of Reactor Irradiated Heavy Nuclides," IDO-16571, December 17, 1959.

9. Marlowe, O. J. and Ombrellaro, P. A., "CANDLE-A One-Dimensional Few-Group Depletion Code for the IBM-704, Addendum 1 - CANDLE-2," WAPD-TM-53, Addendum 1, October 1957.

10. Oby, P. V., "Modified Two Group Calculations on the IBM-650," APAE-11, August 21, 1956.

11. Rosen, S. S., "Supplement to MUFT-III Code Multigroup Fourier Transform Calculations," AP Note 90, Alco Products, Inc., December 6, 1957.

12. Williamson, T. G., Leibson, M. J., Byrne, B. J., "Reactor Analysis APPR-1 Core II," APAE No. 32, July 15, 1958.

13. Bobe, P. E., editor "Interim Report of Nuclear Analysis Performed on SM-2 Core and Vessel, September 1, 1958 to December 31, 1959," APAE-65, May 27, 1960.

14. Oby, P. V., "Modified Two Group Multiregion Calculation Using the VALPROD Code for the IBM-650," AP Note 24, August 14, 1957.

15. Fried, B. E., et al, "Flux and Power Distributions for the SM-2 Reference and Critical Experiment Cores," APAE Memo No. 286, June 30, 1961.

16. McElligott, P. E., "Burnout Distribution in SM-1 (APPR-1) Control Rod Elements Fixed Element No. 57 and Absorber Section at 10.5 MWYR," APAE Memo No. 199, June 5, 1959.

17. ORNL-2907, "Army Package Power Reactor Project, Annual Progress Report for Period Ending January 31, 1960."

18. Kemp, S. N., Moote, F. G., McCool, W. J., "PWR Research and Development Program Test Report - Gamma Scanning Spent SM-1 Core I Elements, Test 318," APAE Memo No. 281, April 6, 1961.

6.0 TEMPERATURE COEFFICIENT

6.1 BACKGROUND

An analytical expression for the temperature coefficient of reactivity has been obtained by differentiating the modified two group critical equation with respect to temperature, assuming that all variables except the number density of the moderator are independent of temperature. The justification for this assumption is based on the results of the analysis of SPERT III experimental data as reported in IDO-16586.[1] Although this assumption represents a gross simplification of the physical processes which contribute to the temperature coefficient of a water moderated reactor, the values of temperature coefficient calculated from the equations derived under this assumption agree well with measured values.

6.2 DERIVATION OF THE ANALYTICAL EXPRESSION FOR TEMPERATURE COEFFICIENT

The modified two group critical equation is:

$$k_{eff} = k_{th} L_{th} L_f + k_f L_f \qquad (1)$$

$$k_{th} = PK_{th}$$

$$k_f = (1-P)K_f$$

where the symbols are defined in Appendix E.

Defining the temperature coefficient as:

$$\alpha_T = \frac{1}{k_{eff}} \cdot \frac{dk_{eff}}{dT}$$

and using Equation (1),

$$\alpha_T = \frac{1}{L_f} \frac{dL_f}{dT} + \left(\frac{1}{1 + \frac{K_f}{K_{th} L_{th}}} \right) \frac{1}{L_{th}} \cdot \frac{dL_{th}}{dT} . \qquad (2)$$

where

L_f is:

$$L_f = \frac{1}{1 + \tau B^2} ,$$

and

$$\frac{1}{L_f}\frac{dL_f}{dT} = -\frac{B^2}{1+\tau B^2}\frac{d\tau}{DT} \tag{3}$$

L_t is: $\quad L_{th} = \dfrac{1}{1+B^2L^2}$

and $$\frac{1}{L_{th}}\frac{dL_{th}}{dT} = -\frac{B^2}{1+B^2L^2}\frac{dL^2}{DT} \tag{4}$$

L^2 is: $$L^2 = \frac{D}{\Sigma a_{th}} = \frac{1}{3\Sigma_{tr}\Sigma a_{th}} \simeq \frac{1}{3N^w\sigma_{th}{}^w\Sigma a_{th}}$$

where the superscript, w, denotes water and Σa_{th} is assumed independent of $\Sigma^w a_{th}$

$$\frac{dL^2}{dT} \text{ is: } \frac{dL^2}{dT} = -L^2\frac{1}{N^w}\frac{dN^w}{dT} = L^2\frac{1}{\rho^w}\frac{d\rho w}{dT} \tag{5}$$

where ρ^w is the density of water as a function of temperature (at constant pressure).

Assuming that the neutron age in a heterogeneous medium is given by:[3]

$$\frac{1}{\sqrt{\tau}} \simeq \frac{Vw}{\sqrt{\tau_w}} + \frac{Vm}{\sqrt{\tau_m}} \tag{6}$$

$\dfrac{d\tau}{dT}$ becomes $$\frac{d\tau}{dT} = \tau Vw\sqrt{\frac{\tau}{\tau_w}}\frac{1}{\tau_w}\frac{d\tau w}{dT} \tag{7}$$

where Vw is the volume fraction of water in the core, τw is the neutron age in pure water, τm is the neutron age in metal, and Vm is volume fraction of metal in the core. In obtaining Eq. (7) from Eq. (6), it is further assumed that τm is independent of temperature. τw is given by:

$$\tau_w = \int_{E_{th}}^{E_o} \frac{dE}{3\xi\Sigma_s \Sigma_{tr} E} \approx \frac{1}{(N^w)^2} \int_{E_{th}}^{E_o} \frac{dE}{3\sigma_{tr} \xi\sigma_s^w E} \quad (8)$$

and

$$\frac{1}{\tau_w} \frac{d\tau_w}{dT} = -2 \frac{1}{N^w} \frac{dN^w}{dT} = -2\alpha$$

where

$$\alpha \equiv \frac{1}{\rho^w} \frac{d\rho^w}{dT} \quad (9)$$

Substituting (9) and (7) into (3) yields:

$$\frac{1}{L_f} \frac{dL_f}{dT} = \frac{2 B^2 V_w \tau}{1 + B^2} \sqrt{\frac{\tau}{\tau_w}} \alpha \quad (10)$$

Substituting (4), (5) and (10) into (2) gives:

$$\alpha_T \approx B^2\alpha \left[\frac{2 V_w \tau}{1 + \tau B^2} \sqrt{\frac{\tau}{\tau_w}} + \left(\frac{1}{1 + \frac{K_f}{K_{th} L_{th}}}\right) \left[\frac{L^2}{1 + B^2L^2}\right]\right] \quad (11)$$

The numerical value of the first term in brackets is approximately 80 times the second for the SM-1: therefore, the second term is neglected and the formula for the temperature coefficient becomes:

$$\alpha_T \approx \frac{2V_w \tau B^2}{1 + \tau B^2} \sqrt{\frac{\tau}{\tau_w}} \alpha \quad (12)$$

6.3 COMPARISON OF CALCULATED AND EXPERIMENTAL TEMPERATURE COEFFICIENTS

The 0 MWYR temperature coefficients of the SM-1 and PM-2A as calculated by Eq. (12) are compared to the experimental values in Table 6.1.

TABLE 6.1
COMPARISON OF CALCULATED AND EXPERIMENTAL TEMPERATURE COEFFICIENTS

Core	α_T at 68°F Calculated from Eq. 12 in ¢/°F	α_T at Oper. Temp.* Calc. from Eq. 12 in ¢/°F	Exp. Temp. Coef. ¢/°F	% Error, Calc. to Experimental
SM-1	0.413	——	0.448	-7.80%
		3.86	3.25	+18.8%
PM-2A	0.526	——	0.550	-4.36%
		5.65	4.85	+16.5%

* The operating temperature for the SM-1 is 440°F and 510°F for the PM-2A.

It should be noted that the experimental values recorded in Table 6.1 were obtained from the curve resulting from fitting the curve of the bulk coefficient of expansion of water at the appropriate pressure (1000 psi for the SM-1 and 2000 psi for the PM-2A) to the experimental data.[4],[5] These are the solid curves of Fig. 6.1 and 6.2 which are plots of $\frac{\partial \rho}{\partial T} = C\left[\frac{1}{D}\frac{\partial D}{\partial}\right]_p$ where D is the density of water at constant pressure.

Since the values of α_T at the low temperature are lower than the experimental values (the converse is true at the high temperature) and since SPERT III data indicates that α_T is directly proportional to α, the value of

$$C \equiv \frac{2V_w \tau_B^2}{1+\tau_B^2}\sqrt{\frac{\tau}{\tau_w}}$$

at 68°F was used to calculate α_T at all temperatures of interest. The results of this choice are presented in Fig. 6.1 for the SM-1 and Fig. 6.2 for the PM-2A. The agreement is seen to be good except for PM-2A at high temperature.

B^2 for the 68°F calculation of Table 6.1 for the SM-1 was obtained from experiment[6] and τ and τ_w were calculated by MUFT-III, P1-SG. values obtained with the MUFT-III stainless steel file as given in APAE-27.[6]

B^2 for the 68°F and 510°F calculation of Table 6.1 for the PM-2A was obtained from the IBM-650 Code, FINK-I[21], and τ and τ_w were calculated by MUFT-III, P1-SG. values obtained with the MUFT-III stainless steel files as given in APAE-27.

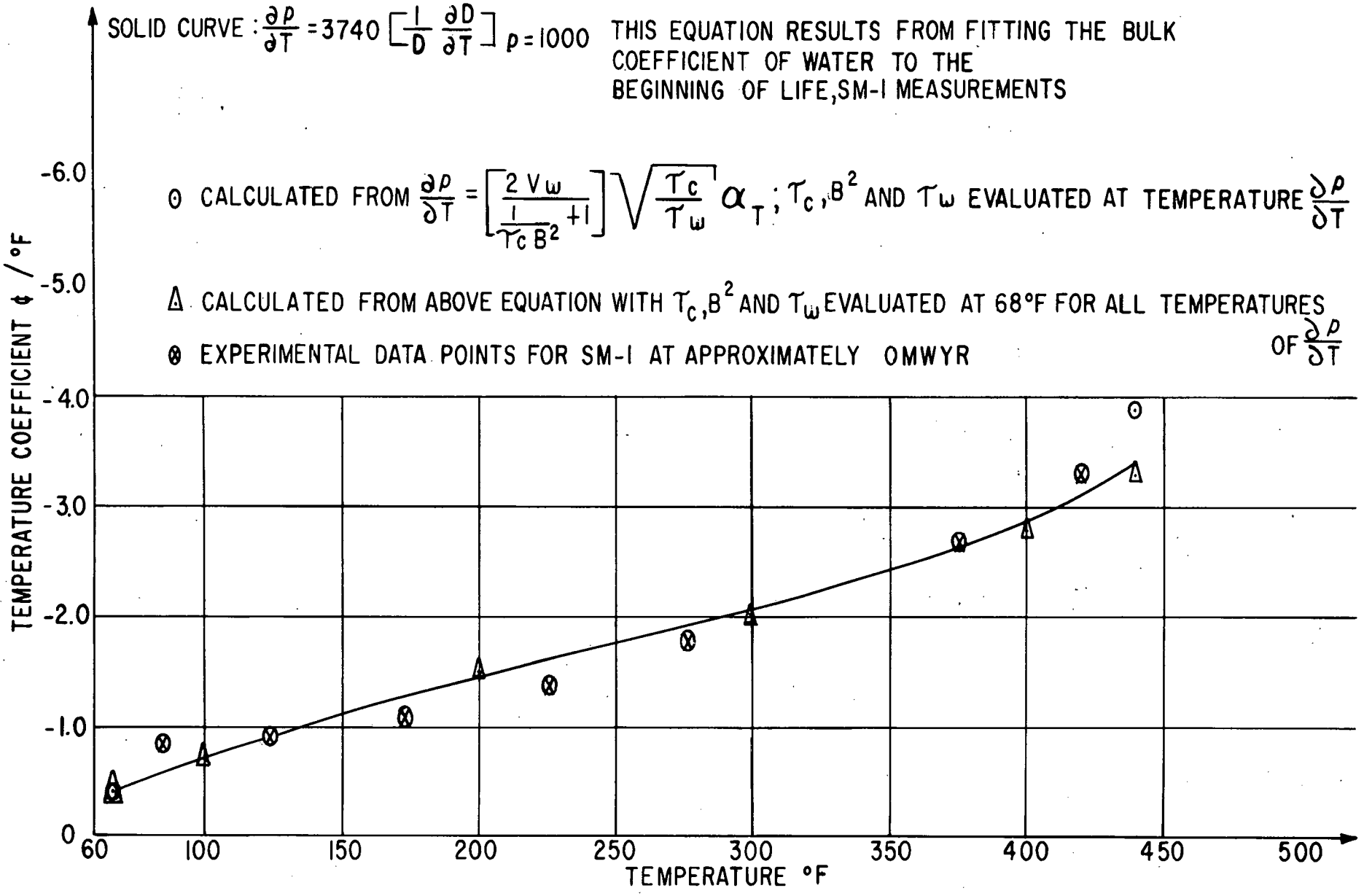

Figure 6.1 SM-1 Temperature Coefficient vs. Temperature

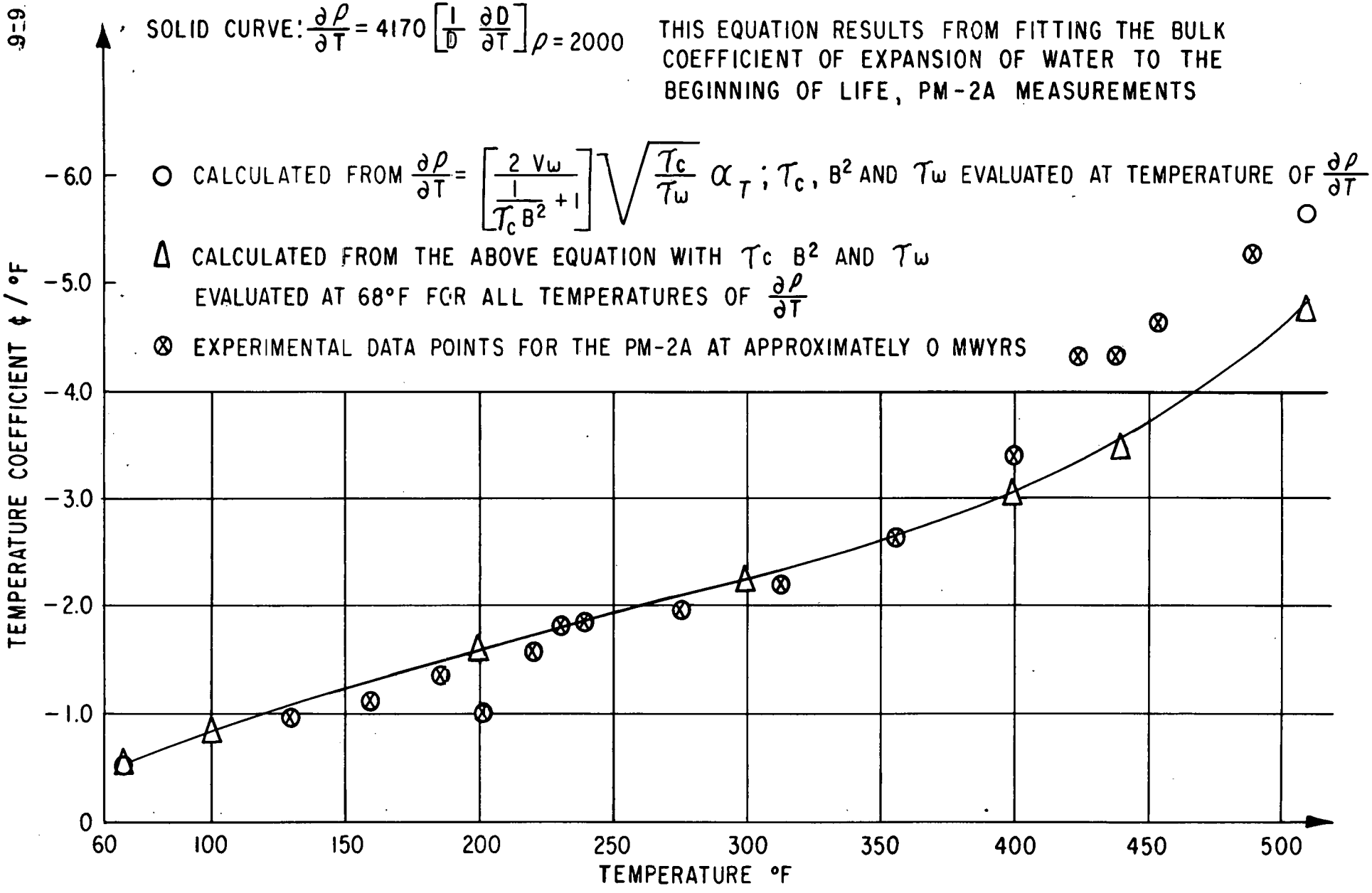

Figure 6.2 PM-2A Temperature Coefficient vs. Temperature

As a further test of this model, τ for the SM-1 was recalculated by MUFT-III using the P-1 slowing down approximation and the revised stainless steel files presented in Appendix F of this report.* B^2 was calculated at 68°F by FINK-I using the fast core and reflector constants obtained from MUFT-III, P-1, revised stainless steel file. The calculated temperature coefficients based on these values (with the value of C assumed constant at its value at 68°F) are compared with experimental results in Table 6.2. The agreement between calculated and experimental values is seen to be even better than the results based on the P1-SG slowing down approximation and the previously used stainless steel files.

TABLE 6.2
EXPERIMENTAL AND CALCULATED TEMPERATURE COEFFICIENTS FOR SM-1 CORE I

Temp. °F	α_T Calculated from Eq. 12 in ¢/°F*	α_T from Experiment in ¢/°F	% Error, Calculated to Experiment
68	0.428	0.448	-4.5%
440	3.21	3.25	-1.23%

* β_{eff} was assumed to be .0078.

6.4 TEMPERATURE COEFFICIENT AS A FUNCTION OF ENERGY RELEASE

Using values of τ calculated as a function of energy release, α_T for the SM-1 Core I was calculated from Eq. (12) of Section 6.1.2. The results are plotted in Fig. 6.3 along with experimental values. The calculated age (from MUFT-III, P-1) is a linear function of energy release. The reflector savings were assumed constant in this calculation.

6.5 CONCLUSIONS

1. A reasonable fit of the measured temperature coefficient data vs. temperature can be obtained with the equation $\partial\rho/\partial T = C\left[\frac{1}{D}\frac{\partial D}{\partial T}\right]\rho$ where D is the density of water.

* This method of calculating τ is currently considered best since reactivities based on this value of τ agree more closely with experiment. For a discussion of this point, refer to Section 3.0.

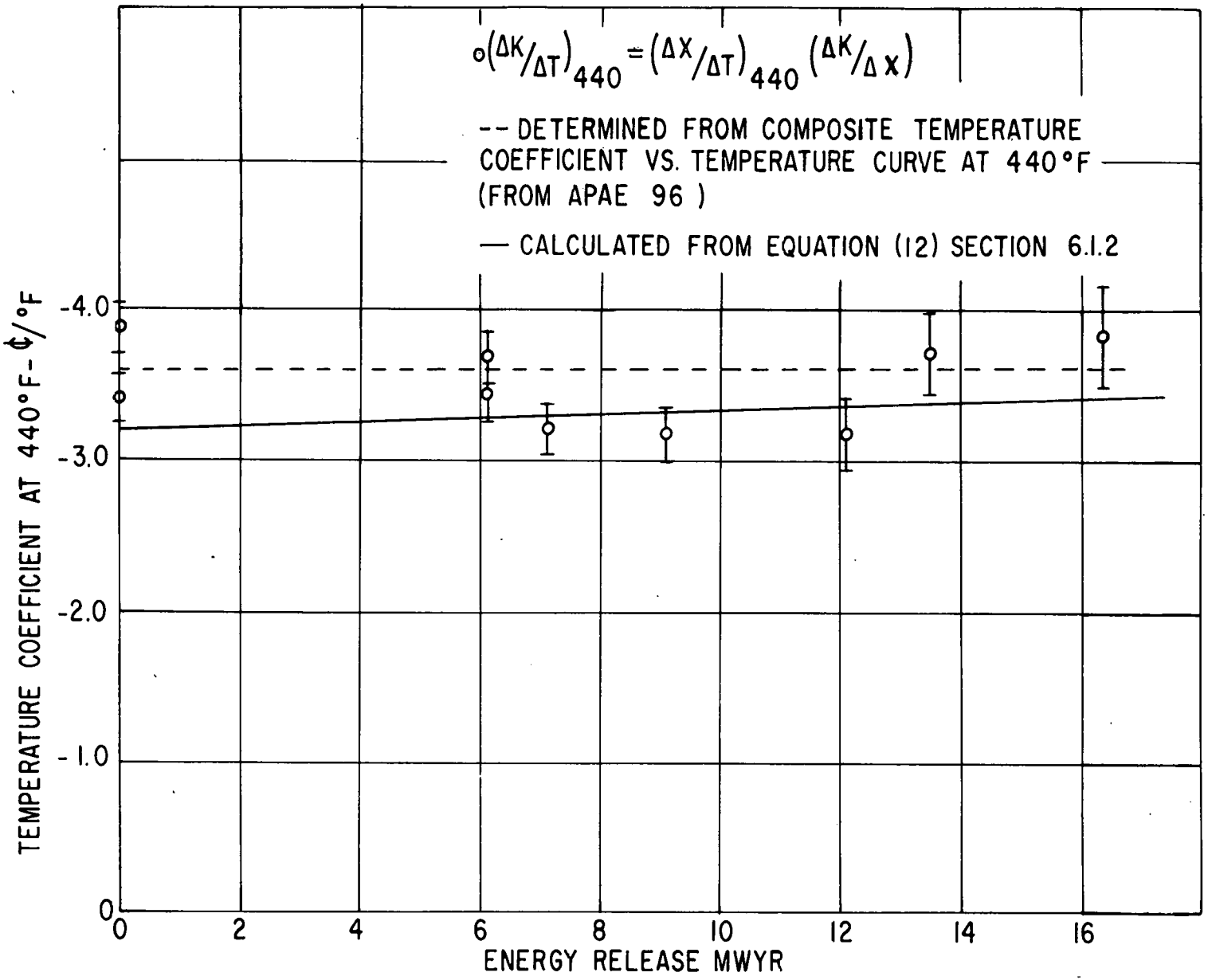

Figure 6.3 Temperature Coefficient at 440°F as a Function of Energy Release for the SM-1

2. A simple equation has been developed for calculation of temperature coefficient that agrees well with experiment.

3. This equation indicates only slight variations of temperature coefficient with burnup.

6.6 SUMMARY

A reasonable fit of experimental and calculated temperature coefficient vs. energy release has been obtained. A slight increase of temperature coefficient vs. lifetime is indicated.

6.7 REFERENCES (6.0)

1. Schroeder, E. T., et al, "The SPERT III Reactor Nuclear Startup," IDO-16586, 1960.

2. Murray, R. L., "Nuclear Reactor Physics," Prentice Hall, Inc., Englewood Cliffs, N. J., 1957.

3. Kaplan and Chernick, "Uranium Graphite Lattices - Brookhaven Reactors," in Peaceful Use of Atomic Energy, Volume 5, "Physics of Reactor Design," Columbia University Press, 1956.

4. Weiss, S. H., "Summary Report of Physics Measurements on SM-1 Core I," APAE-96, February 6, 1962.

5. McCool, W.J., "Startup and Initial Testing of the PM-2A Plant," APAE-92, to be issued March 1962.

6. Byrne, B. J., and Oby, P. V., "Analysis of Extended Zero Power Experiments on the Army Package Power Reactor, ZPE-2," APAE No. 27, May 7, 1958.

7. McElligott, P. E., "FINK I; A Two Group, Two Region Calculation on the IBM-650," APAE Memo 121, January 28, 1958.

7.0 CONCLUSIONS AND RECOMMENDATIONS

7.1 CONCLUSIONS

1. P-1 slowing down theory utilizing MUFT-III nuclear data as given in Appendix F yielded the best agreement between calculated and measured reactivity for a wide range of cores. The calculated reactivities were within a standard deviation of 0.91% ρ.

2. There are inconsistencies in the agreement of P-1, MUFT-III calculations of reactivity and measurements on minimum size and fully poisoned SM-1 ZPE Core I experiments.

3. The agreement of P-1 and P1-SG slowing down models with both MUFT-III and MUFT-V files with neutron ages of Po-Be neutrons in iron water mixtures is not good.

4. The use of Wigner-Wilkins averaged thermal cross sections rather than hardened Maxwellian cross sections results in a reactivity increase for SM-1 Core I of about 0.2% ρ.

5. There is little difference between reactivity calculated using one-and two-dimensional diffusion theory, provided the substitution effects are properly treated.

6. The calculation ofcritical bank positions at room and operating temperatures can be made utilizing a one-dimensional axial model and homogenized rod cross section and give agreement within 1.4 in. of measurement.

7. A calculation of the central control rod worth in both a boron stainless steel and a stainless steel poisoned SM-1 Core I indicate good agreement with experiments when utilizing the P-1 MUFT-III fast constants and absorber properties from blackness theory.

8. One-dimensional depletion calculations are applied to SM-1 with difficulty because of the presence of the control rod fuel elements and the problems of selecting an equivalent uniform cross section for the control rod absorbers. The results of the application of CANDLE III to the SM-1 is a core life of 16.8 MWYR compared with a measured value of 16.4 MWYR.

9. Calculations indicate that the substitution of two new fuel elements in SM-1 Core I at 2/3 life increased the core life by 0.3 MWYR. The best estimate of SM-1 Core I life unmodified is 16.1 MWYR.

10. A simplified model for calculation of temperature coefficient has been developed and applied to SM-1 with good agreement with the measurements.

11. An anlytical model based on perturbation theory was applied to SM-1 Core I and yielded a good estimate of core life. These parameters such as xenon which are highly dependent on flux distribution were not accurately treated.

12. A calculation of effective delayed neutron fraction for SM-1 Core I indicated a value of 0.0078 based on a value of delayed neutron fraction of 0.0065. Calculation indicated the effective delay in neutron fraction was not a sensitive function of bank position.

13. Calculations indicated that the xenon cross section for SM-1 Core I is a sensitive function of effective neutron temperature.

7.2 RECOMMENDATIONS

1. A concentrated effort should be made to obtain an improved set of basic nuclear cross section data for stainless steel in the energy region from 10 Mev to a few kev. The validity of this set of improved data should be checked against available experimental ages from Po-Be sources and clean critical experiments with high steel-to-water rations.

2. Measurements of the age of fission neutrons in steel-water mixtures are needed to provide a check on slowing down models and nuclear data.

3. Experimental information is needed on the variation of thermal flux and neutron spectrum in the SM type cells. This information can then be used as a basis for determining the validity of various models for calculations of thermal group properties.

4. The inherent difficulties in the application of one-dimensional burnout codes to cores as heterogeneous as the SM-1 Core I indicate the desirability of investigating the application of at least two-dimensional codes such as TURBO to the burnout of SM-1 type cores. The most preferable calculational model would be a three-dimensional model such as DRACO, modified to account explicitly for the presence of moving control rod fuel elements. A computer of the capacity of the Philco-2000 is needed to accurately treat the geometry.

5. Consideration should be given to programming the series burnup method [1] calculation of core lifetime accounting for non-uniform burnup. The availability of such a code would facilitate parameter studies on core life.

6. A series of clean critical experiments should be performed utilizing actual SM-2 mockup fuel plates in order to have available configurations for checking analytical models.

7. The development of longer-lived replacement cores with higher metal/water ratios will require an improved treatment of the epithermal effects of fission products.

8. An effort should be made to obtain good agreement between the constants resulting from the fast group coalescing schemes as used in the MUFT codes and coalescing schemes as used in the burnup codes CANDLE and TURBO.

9. More accurate measurements of the fuel (and poison) burnup in the fuel element SM-1 Core I is needed to provide a check of analytical predictions.

---

(1) Murray, R. L. et al., "Reactor Fuel Cycle Analysis by Series Method," Nuclear Science and Engineering, July 1959.

APPENDIX A
PREDICTION OF SM-1 CORE I BURNUP CHARACTERISTICS USING SERIES TECHNIQUE

INTRODUCTION

Appendix A consists of analytic studies of the behavior of the SM-1 Core I. The reactor physics employed is intended to be of such nature that the maximum physical content is included, compatible with a model that admits hand calculations. The procedure consists of the following steps: (a) to adapt burnup theory to a reactor with control rod bank and to determine the variation of reactivity with time, (b) to employ data on successive "states" of the reactor during its operating life to predict its flux pattern, the xenon poisoning and the temperature coefficient, (c) to develop a theory of the effective delayed neutron fraction that is consistent with the burnup model to permit interpretation of experimental rod calibration. However the burnup theory, while adaptable to hand calculation is quite approximate for higher burnup as the fuel and poison distributions constantly depart from the initial and are constantly substituted with equivalent states. Although the numbers may not be as accurate as in more sophisticated techniques, the physical trends of the core are present.

THIS PAGE

WAS INTENTIONALLY

LEFT BLANK

A.1 PREDICTION OF CORE LIFE BY BURNUP THEORY

A.1.1 Introduction

Analytic approximate methods are used to predict the SM-1 core life. The approach is an adaptation of that developed for a reactor controlled by a uniform adjustable poison. * The generalizations effected are as follows.

a. Inclusion of effect of epithermal processes on criticality and on fuel consumption.

b. Account of the reactivity variation due to discrete control bank motion.

c. Distinction between fixed and control fuel elements.

Several necessary simplifying assumptions are made:

a. For purposes of computation the core fluxes are as in a two-region bare equivalent core. Burnup is taken to occur however, only in the actual physical dimensions of the core and rod region.

b. Although the flux amplitude is allowed to change with time as burnup ensues, the initial shape is retained. The total core power is maintained constant in time and the reactor is always critical.

c. Effects of xenon poisoning and long-lived fission product poisoning are superimposed on the basic dynamic response.

d. A modified one-group diffusion theory that is dominated by fast leakage effects is employed.

A.1.2 Initial Criticality and Flux Distributions

Physical arrangement. The essential features of the actual core and the equivalent model for analysis are sketched in Figs. 1a and 1b.

The bare equivalent core has dimension $H' - H + 2S_a$ and $R' - R + S_r$, where axial and radial reflector savings are employed. The radial flux distribution is automatically a zero order Bessel function $J_0(j_0 r/R')$. The axial distribution has two parts $\phi(z)$ and $\phi_r(z)$ for the core and rod region respectively.

---

* Murray, Raymond L., S. A. Hasnain and A. L. Mowery, Jr. "Reactor Fuel Cycle Analysis by Series Methods," Nuclear Science and Engineering, 6, 18 (1959)

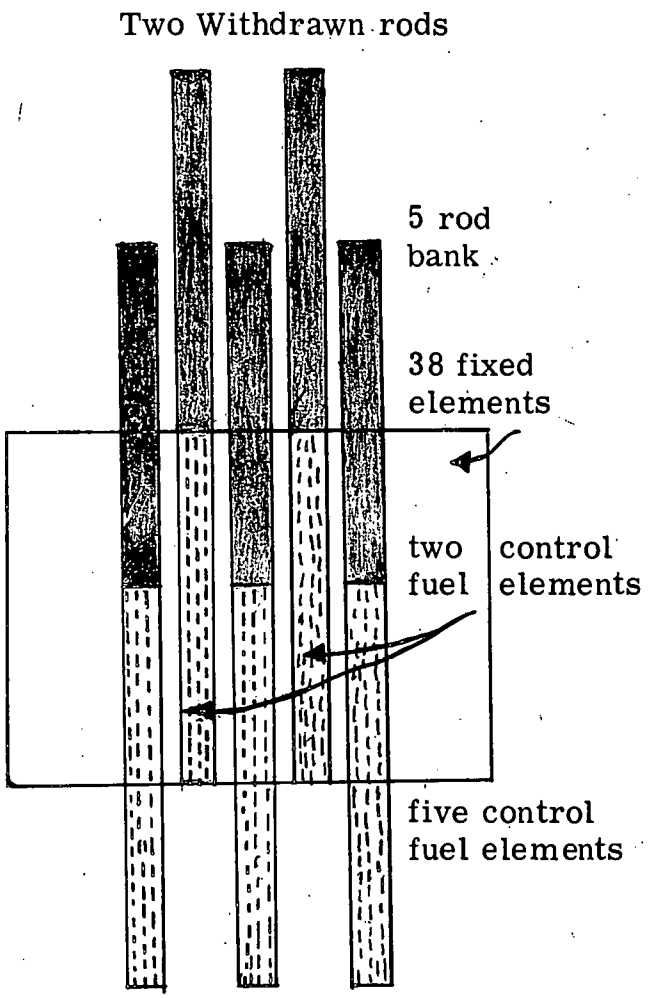

Fig. A.1a Physical Core

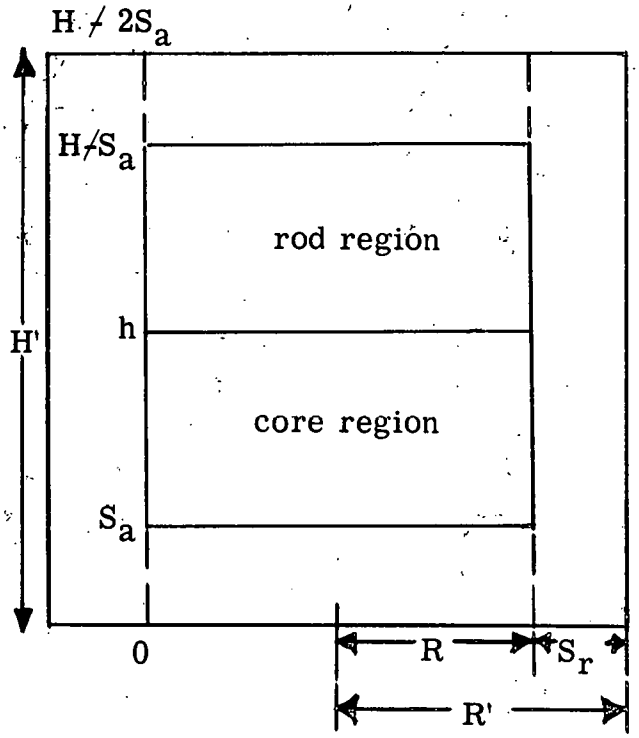

Fig. A.16 Core Model

Figure A.1. Physical Arrangement of Core and Core Model

The differential equations of modified two-group theory serve as the starting point for the solution

$$D_1 \nabla^2 \phi_1 - \phi_1 \Sigma_1 + \phi_2 \Sigma_2 \eta f + \phi_1 \Sigma_1 (1-p) \eta_r f_r = 0$$

$$D_2 \nabla^2 \phi_2 - \phi_2 \Sigma_2 + p \phi_1 \Sigma_1 = 0$$

where the thermal and resonance fission sources appear in the fast group equation. Since the two-group two-region problem is unduly complicated for a situation in which rod motion and burnup take place, a simpler group model is proposed. It is well known that the thermal leakage for a heavily loaded light water

moderated reactor is small compared with fast leakage. Thus we may neglect the term $D_2 \nabla^2 \phi_2$ with little error, giving

$$p\phi_1 \Sigma_1 = \phi_2 \Sigma_2$$

Substitution in the first equation yields

$$D_1 \nabla^2 \phi_2 - \Sigma_1 \left[1 - (1-p)\, \eta_r f_r \right] \phi_2 + \eta f \Sigma_2 \phi_2 p \Sigma_1 = 0$$

Letting

$$\frac{D_1}{\Sigma_1} = \tau \text{ and } K = \eta f p + (1-p)\, \eta_r f_r$$

$$\nabla^2 \phi_2 + \left(\frac{K - 1}{\tau} \right) \phi_2 = 0$$

This new one group model contains the necessary fast and thermal multiplication factors. The only assumption made is that neutrons diffuse very short distances after thermalization.

By virtue of the assumed radial distribution, the axial fluxes in the two regions involve a modified buckling and inverse diffusion length. Let $B^2 = (K - 1)/\tau$ and $B_r^2 = (K_r - 1)/\tau$. Use of the method of separation of variables with $\nabla^2 = \partial^2/\partial r^2 + 1/r \ \partial/\partial r + \partial^2/\partial z^2$ yields core and rod equations in what is now the axial distribution.

$$\frac{d^2 \phi_2}{dz^2} + \overline{B}^2 \phi_2 = 0$$

and

$$\frac{d^2 \phi_{2r}}{dz^2} - \overline{K}^2 \phi_{2r} = 0$$

where

$$\overline{B}^2 = B^2 + (j_o/R')^2$$

$$\overline{K}^2 = (j_o/R')^2 - B_r^2$$

The regions are distinguished by the fact that the subtraction of radial buckling in the rod region places the differential equation in the non-multiplying category.

The solutions of the equations for the two media that satisfy the boundary condition $\phi_2(0) = 0$ and $\phi_{2r}(H') = 0$ are readily seen to be

$$\phi(z) = A \sin Bz$$

$$\phi_r(z) = C \sinh \kappa (H' - z)$$

where the subscript 2 for thermal group has been suppressed, as have the bars over B and κ.

Continuity of flux and current at z = h with an assumed common thermal diffusion coefficient is invoked, leading to

$$A \sin Bh = C \sinh \kappa (H' - h)$$

$$BA \cos Bh = -C \kappa \cosh (H'-h)$$

from which the critical equation is derived

$$\tan Bh = - \frac{B}{\kappa} \tanh (H' - h)$$

and the constant C is

$$C = A \frac{\sin Bh}{\sinh \kappa (H' - h)}$$

A. 1. 3 Perturbation Theory

Consistent adaptation of one group perturbation theory is made. Consider the critical core equation in the form

$$\nabla^2 \phi + B_o^2 \phi = o$$

or compactly

$$M\phi = B_o^2 \phi$$

where

$$M = - \nabla^2 \text{ and } B_o^2 = \frac{K - 1}{\tau}$$

Assume that changes in fuel or absorption occur to cause a distributed change in buckling

$$\Delta B^2 = \Delta \left(\frac{K - 1}{\tau} \right) = \frac{\Delta K}{\tau}$$

There must be made a corresponding uniform buckling change δB^2 to accommodate this perturbation, giving a new critical equation

$$M'\phi' = B^2 \phi'$$

where $M' = -\nabla^2 + \Delta B^2$

Multiplying the differential equation through by the original flux ϕ and integrating over the core,

$$B^2 = \frac{\int \phi M' \phi' \, dV}{\int \phi \phi' \, dV}$$

The perturbation approximation $\phi' \simeq \phi$ is made, and

$$B^2 = B_o^2 + \frac{\int \phi \, \Delta B^2 \phi dV}{\int \phi^2 dV}$$

or

$$\delta B^2 = \frac{\int \Delta B^2 \phi^2 dV}{\int \phi^2 dV}$$

The correlation between δB^2 and reactivity ρ can be made through the neutron economy formula

$$k_e = K \mathcal{L}$$

where $\mathcal{L}$ is the constant non-leakage probability

$$\mathcal{L} = \frac{1}{1 + B^2_g \tau}$$

Now $\rho = \frac{\delta k_e}{k_e} = \frac{\delta K}{K}$

However $\delta B^2 = \frac{\delta K}{\tau}$ and $\rho = \frac{\tau \delta B^2}{K}$

Thus $\rho = \frac{\int \Delta K \phi^2 dV}{\int K \phi^2 dV}$

The relation between $\Delta K/K$ and microscopic changes can be deduced. Let $K_t = \eta f p$ and $K_f = (1-p) \eta_r f_r$. Then

$$\frac{\Delta K}{K} = \frac{\Delta K_t}{K} + \frac{\Delta K_f}{K}$$

Assuming negligible change in p, and going to the differential notation, we find for either themal or fast neutrons

$$\frac{dK_i}{K_i} = \frac{d\Sigma_{fi}}{\Sigma_{fi}} - \frac{d\Sigma_{ai}}{\Sigma_{ai}}$$

Further, since the principal absorbers are uranium (U) and boron (B),

$$\frac{d\Sigma_a}{\Sigma_a} = \frac{d\Sigma_{aU} + d\Sigma_{aB}}{\Sigma_a} = \frac{\Sigma_{aU}}{\Sigma_a}\frac{d\Sigma_{aU}}{\Sigma_{aU}} + \frac{\Sigma_{aB}}{\Sigma_a}\frac{d\Sigma_{aB}}{\Sigma_{aB}} = f_U \frac{dN_U}{N_U} + f_B \frac{dN_B}{N_B}$$

with f_U and f_B as the "utilizations" of the two elements. For either region then

$$\frac{\Delta K}{K} = \alpha \frac{\Delta N_U}{N_U} - \beta \frac{\Delta N_B}{N_B}$$

where

$$\alpha = 1 - \left(\frac{K_t f_{Ut} + K_r f_{Ur}}{K} \right)$$

$$\beta = \frac{K_t f_{Bt} + K_r f_{Br}}{K}$$

The "windowshade" method of treating the control bank is employed, in which the rod region is assumed to have a uniform thermal poison Σ_p. As the bank is moved, there is a local change in absorption $\Delta \Sigma_a = - \Sigma_p$, giving rise to

$$\left(\frac{\Delta K}{K} \right)_p = + \frac{K_t}{K} \cdot \frac{\delta \Sigma_p}{\Sigma_a}$$

Integration over the volume that rod motion affects is to be made.

A. 1. 4 Burnup Theory

The rate of consumption of fuel is governed by

$$\frac{dN_U}{dt} = -A_t - A_r$$

where the absorption rate of thermals is

$$A_t = \phi_2 N_U \sigma_{aUg}$$

where g is a self-shielding factor for the fuel plate and that in the resonance region is

$$A_r = \phi_1 \Sigma_1 (1-p) f_r$$

The two absorptions can be expressed entirely in terms of the thermal flux, if we invoke the following relations:

$$f_r = \frac{N_U \sigma_{aU_r}}{\Sigma_{ar}}$$

$$p\phi_1 \Sigma_1 \simeq \phi_2 \Sigma_2$$

Then

$$A_r = \phi_2 N_U \left[\frac{\Sigma_2 (1-p) \sigma_{aUr}}{p \Sigma_{ar}} \right]$$

Combining terms, and using an effective uranium absorption cross section

$$\sigma_{aU}^e = \sigma_{aU} + \frac{\Sigma_2 (1-p) \sigma_{aUr}}{p \Sigma_{ar}}$$

the fuel burnup equation becomes

$$\frac{dN_U}{dt} = -\phi N_U \sigma_{aU}^e$$

The flux is assumed to be separable in space and time

$$\phi(r, z, t) = c(t)\phi(\bar{r})$$

and letting $u = \int_0^t c(t)dt$

$$N_U(\bar{r}, t) = N_U^o \, e^{-\phi(\bar{r}) \sigma_{aU}^e u}$$

Similarly the boron atom density is

$$N_B(\bar{r}, t) = N_B^o \, e^{-\phi(r) \sigma_{aB}^e u}$$

with an analogous effective boron cross section,

$$\sigma_{aB}^e = \sigma_{aB} + \frac{\Sigma_2 (1-p) \sigma_{aBr}}{p \Sigma_{ar}}$$

The condition on constant fission rate or core power is invoked to obtain a relation between u and time. Reference is made to standard burnup theory* which carries over to yield the expression

$$t = \frac{1 - B_o(x_U)}{c_o \sigma^e_{aU} \phi(\bar{r})}$$

where c_o is the initial amplitude of the flux, $\overline{\phi(\bar{r})}$ is the spatial average over the core and rod region, $x_U = \sigma^e_{aU} u$, and the zero order burnup function is

$$B_o(x) = \int_V e^{-\phi(\bar{r})x} \, dV$$

a series expansion of which is

$$B_o(x) = 1 - \bar{\phi}x + \frac{\overline{\phi^2}x^2}{2!} - \frac{\overline{\phi^3}x^3}{3!} + \ldots.$$

A.1.5 Reactvity Due to Rod Motion

The position dependent reactivity effect or rod motion through a differential distance dz when the bank position is z is

$$d\rho = \frac{\int \frac{\Delta K}{K} \phi^2 dV}{\int \phi^2 \, dV}$$

If one assumes in first approximation that the flux is separable in space and time, the time variation cancels out in the above expression, thus

$$d\rho = \frac{\frac{K_t}{K} \Sigma_p dz \, \phi^2(z)}{\Sigma_{2_{c+r}} \int \phi^2(z) dz} = \frac{K_t \Sigma_p \phi^2(z) dz}{\Sigma_2 KH \, \overline{\phi^2}}$$

The total reactivity due to removal from initial z = h to any level z is

$$\rho(x) = \frac{K_t \frac{\Sigma_p}{\Sigma_a} \int_h^z \phi^2(z) \, dz}{K \left[k\overline{\phi^2_c} + m\overline{\phi^2_r} \right]}$$

where $k = h = S_a$ and $m = H + 2S_a - h$ are the core and bank lengths, and the average square fluxes are over the two regions. The reactivity associated with fuel and boron consumption is computed from

---

* Murray, et al, ibid.

$$\rho = \frac{\int \frac{\Delta K}{K} \phi^2 dV}{\int \phi^2 dV} = \frac{\int \left[\alpha \frac{\Delta N_U}{N_U} - \beta \frac{\Delta N_B}{N_B} \right] \phi^2 \, dV}{\int \phi^2 \, dV}$$

Now for a given point of the system

$$\frac{\Delta N_U}{N_U} \cong \frac{N_U - N_U^o}{N_U^o} = - \left[1 - e^{-\phi(\bar{r}) \sigma_{aU}^e u} \right]$$

$$\frac{\Delta N_B}{N_B} \cong \frac{N_B - N_B^o}{N_B^o} = - \left[1 - e^{-\phi(\bar{r}) \sigma_{aB}^e u} \right]$$

In this relation for ρ, the time amplitude cancels, and integration over the regions of length $k = h - S_a$ and $m = H + 2S_a - h$

$$\rho = - \left\{ \alpha_c \overline{\phi_c^2} k \left[1 - \frac{B_2(X_{Uc})}{\overline{\phi_c^2}} \right] + \alpha_r \overline{\phi_r^2} m \left[1 - \frac{B_2(X_{Ur})}{\overline{\phi_r^2}} \right] \right\}$$
$$+ \left\{ \beta_c \overline{\phi_c^2} k \left[1 - \frac{B_2(X_{Bc})}{\overline{\phi_c^2}} \right] - \beta_r \overline{\phi_r^2} m \left[1 - \frac{B_2(X_{Br})}{\overline{\phi_r^2}} \right] \right\}$$

where

$$B_2(x) = \frac{1}{V} \int_V \phi^2 (\bar{r}) \; e^{-\phi (\bar{r}) \, x} \, dV$$

depends on the region (c, r) over which the integration is taken and on the nature of the material being consumed (U, B).

A series expansion is

$$B_2(x) = \overline{\phi^2} - \overline{\phi^3} x + \frac{\overline{\phi^4} x^2}{2!} - \frac{\overline{\phi^5} x^3}{3!} + \ldots$$

As the formula for ρ is written, the negative sign in front of α correlates with fuel removal and the positive sign with boron removal to increase multiplication.

A. 1. 6 Calculation of System Group Constants

The basic constants chosen were those regularly employed by Alco Products in its nuclear analysis. * They are tabulated here for reference.

Atoms/cm^3 of core at 440°F

	Fixed Element	Control Fuel Element
Hydrogen (x 10^{22})	4. 4398	4. 2767
Steel (x 10^{22})	1. 4819	1. 7793
U^{235} (x 10^{20})	4. 2863	3. 4796
U^{238} (x 10^{20})	0. 3151	0. 2558
B^{10} (x 10^{20})	0. 07049	0. 05722

Microscopic Cross Sections (barns) for 0. 0549 ev Distribution

	Thermal	Epithermal
Boron	2398	84. 68
U^{235} absorption	385. 5	18. 98
U^{235} fission	326. 7	13. 34
Xe^{135}	1. 98 x 10^6	-----
H	0. 1998	-----

Thermal $1 + \alpha = 1.18$, epithermal $1 + \alpha = 1.42$

Buckling	radial	0. 004465
	axial	0. 002129
	total	0. 006594

Core dimensions Height 55. 88 cm, extrapolated 68. 08 cm
Radius 28. 19 cm, extrapolated 35. 99 cm

"Windowshade" cross section Σ_p = 0. 07756 cm^{-1}

Self-shielding factors - fixed 0. 9443, control 0. 9061

* Williamson, T. G., Leibson, M. J., and Byrne, B. J., "Reactor Analysis APPR-1 Core II," APAE No. 32, July 15, 1958, and separate communications from Paul E. Bobe.

Group Constants at 440°F

	Fixed	Control
Age, τ	43.02	43.05
Fast Diffusion Coefficient, D_1	1.490	1.440
Thermal Diffusion Coefficient, D_2	0.2571	0.2551
Thermal Multiplication, ηf	1.5705	1.4486
Fast Multiplication, $\eta_r f_r$	1.3014	1.1820
Resonance Escape Probability, p	0.7297	0.7464
Fast Product $\nu_r \Sigma_{fr}$	0.01219	0.01003
Thermal Product $\nu \Sigma_f$	0.3242	0.2523
Thermal absorption Σ_a	0.2065	0.1742

(no Xe or control poison)

A.1.7 Region Group Constants

Composite constants for the core and rod bank region were formed by use of importance (ϕ^2) weighting. The two regions have the fuel element arrangement sketched in Fig. 2. The designation C refers to a control fuel element, R to a control rod, the remainder are fixed fuel elements.

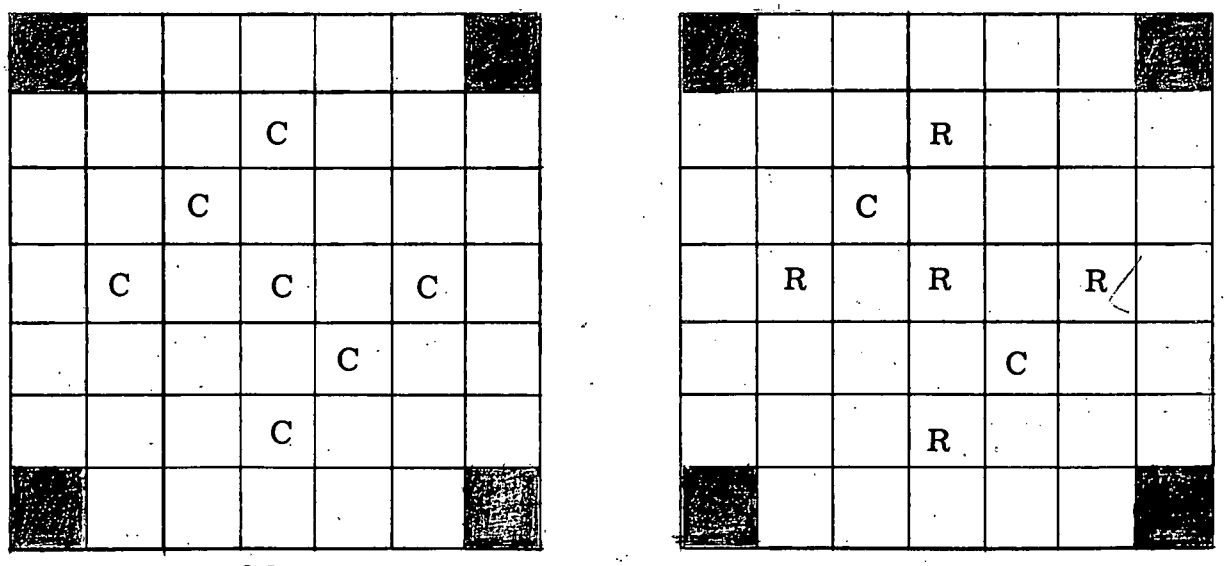

Figure 2. Fuel, Control Elements, Bank and Rods

Weighting of the composite multiplication factor

$$K = \eta f p + (1 - p)\eta_r f_r$$

was performed with the use of the recipe

$$\overline{K} = \frac{\sum_i N_i (J_o^2)_i K_i}{\sum_i N_i (J_o^2)_i}$$

where there appears the appropriate square of the radial Bessel function J_o $(j_o r/R')$, the number of elements at a characteristic distance from the origin r, and the value of K_{fixed} or $K_{control}$ for those elements. The treatment of the bank region with reference to substitution of uniform control poison of 0.7756 cm^{-1} in place of rod effects is somewhat ambiguous. The procedure adopted was to perform the above weighting ignoring rods completely, followed by a thermal multiplication correction due to insertion of control poison in the rod region. The results of all these computations are summarized below.

	Core	Rod Region
K thermal	1.1294	0.7811
K epithermal	0.3385	0.3467
K total	1.4679	1.1278
Fractional absorption		
U^{235}, thermal	0.7409	0.5428
B^{10}, thermal	0.0758	0.0555
U^{235}, epithermal	0.8454	0.8597
B^{10}, epithermal	0.0620	0.0631

Effective cross sections for U^{235} (fission and absorption) and B^{10} for core and rod region were obtained by the relation

$$\sigma_{ai}^{e} = (\sigma_{ai})_t + \frac{\Sigma_2 (1 = p) (\sigma_{ai})_r}{p\Sigma_{ar}}$$

where subscripts i refer to either element, t to thermal and r to resonance. Weightings according flux and volume were then applied to form the composite cross sections for fuel and control elements of the core and bank regions. The results are:

	Fixed	Control	Core	Bank
$\sigma_f^e (U^{235})$	417.4	389.0	411.5	415.3
$\sigma_a^e (U^{235})$	518.9	481.7	511.1	516.1
$\sigma_a^e (B^{10})$	2941	2764	2904	2928

For purposes of establishing average flux from the fixed 10 Mw power level, fission rate F = 3.24 x 10^{17} fissions/sec, atom densities of uranium were computed, using flux and volume weightings. The results are:

	Fixed	Control	Core	Bank
N^o (U^{235}) (units of 10^{20})	4.826	3.480	4.118	3.611

Then, the amplitude of the flux c_o, is obtained from

$$F = \left[K\overline{\phi_{2C}(z)}N^o_{UC}\ \sigma^e_{fUC} + m\overline{\phi_{2r}(z)}N^o_{Ur}\ \sigma^e_{fUr} \right] \bar{J}_o \pi R^2 c_o$$

where k and m are the heights of the core and bank regions, 17.02 cm and 38.86 cm, respectively. The core radius is R = 28.19 cm, and averages over initial axial fluxes are: core 0.9057, bank 0.3964. The radial average flux $\bar{J}_o$ is 0.6174 for both regions. The amplitude was found to be 4.276 x 10^{13}/cm^2-sec.

A.1.8 Initial Criticality and Flux Calculations

The basic relations employed were

$$\tan \bar{B}h = -\frac{\bar{B}}{\bar{K}} \tanh (H' - h)\ \bar{K}$$

$$Z_C(z) = \sin \bar{B}z$$

$$Z_r(z) = \frac{\sin \bar{B}h \sinh \bar{K}(H' - z)}{\sinh \bar{K}(H' - h)} = \frac{C}{A} \sinh \bar{K}(H' - z)$$

With τ = 43.03 cm^2 taken as common for both regions, and $(j_o/R')^2$ = 0.004465, one finds

$$\bar{B} = 0.008006, \quad \bar{\eta} = 0.003867$$

The known critical bank position without Xe^{135} poisoning was 6.70 in. (17.02 cm) out. In order to reproduce this result for the beginning of core life, different deflector savings were chosen S_a = 8.60 cm, at the bottom and S_a' = 3.60 cm at the top. These are qualitatively different since the addition of reflector at the top has relatively little effect on criticality.

A.1.9 Summary

A geometrical model for the representation of SM-1 Core I has been adapted to account for reactivity changes due to material burnup and rod motion. Realizing the smallness of the term $D_2\nabla^2\phi_2$ the two group modified theory equations reduce to a one group. Use of perturbation techniques and series burnup method lead to the calculation of critical bank position vs energy release.

A. 2 FLUX DISTRIBUTION AND ROD BANK CALIBRATION

A. 2. 1 Rod Bank Position

The general behavior of the reactor system with time is complex in that rod motion is accompanied by variable local flux changes and accumulated fuel consumption, which in turn affects the necessary rate of rod withdrawal to maintain criticality. In order to estimate these effects, a series of reactor states corresponding to different bank positions was chosen, and criticality and flux calculations performed for each. In lieu of inclusion of fuel pattern changes, a uniform variation in the number of neutrons per fission, ν, was made. By trail and error methods the ratio ν / ν_o was determined for each selected bank position. The basic criticality equations were solved, using

$$B_C^2 = \frac{\frac{\nu}{\nu_o} K_C^o - 1}{\tau} \quad \text{and} \quad B_r^2 = \frac{\frac{\nu}{\nu_o} K_r^o - 1}{\tau}$$

and the previously stated equations. The important results are listed blow.

h (cm)	Bank Position(In.)	Critical ν/ν_o	$\bar{B}$	$\bar{K}$	C/A
25. 62	6. 70	1. 000	0. 0801	0. 0387	0. 3568
30	8. 43	0. 966	0. 0726	0. 0481	0. 2700
36	10. 79	0. 934	0. 0645	0. 0568	0. 2427
42	13. 15	0. 910	0. 0579	0. 0620	0. 2693
48	15. 51	0. 894	0. 0527	0. 0653	0. 3339
54	17. 87	0. 883	0. 0491	0. 0679	0. 4248
60	20. 24	0. 876	0. 0469	0. 0690	0. 5484
64. 48	22. 00	0. 874	0. 0462	0. 0694	0. 6169

According to perturbation theory the reactivity ρ is related to changes in ν by

$$\rho = \frac{\Delta \nu}{\nu} = \frac{\nu_o - \nu}{\nu_o} = 1 - \frac{\nu}{\nu_o}$$

A plot of system reactivity as a function of rod bank position is shown in Fig. A. 3.

The detailed axial flux distributions for these states were obtained, using

$$Z_c(z) = \sin \bar{B} z$$

$$Z_r(z) = \frac{C}{A} \sin \bar{K} (H' - z)$$

and the constants listed above. Figure A. 4 shows a plot of these results. The shift is in accord with physical expectations.

With these savings, the critical value of $h = 17.02 + S_2 = 25.62$ cm was obtained, thence the flux distribution, as shown in Fig. A. 5. The peaking in the core region and the depression in the bank region are evident.

Flux averages for the two regions are readily obtained by integration. Now the core averages may be translated into a form where the tables of $\overline{\phi^n}$* are useful.

$$\overline{Z_c^n} = \frac{1}{h - S_a} \int_{S_a}^{h} (\sin \overline{B}z)^n dz = \frac{1}{h - S_a} \left[\int_{S_a}^{Z_{max}} (\sin \overline{B}z)^n dz + \int_{Z_{max}}^{h} (\sin \overline{B}z)^n dz \right]$$

This may be rewritten

$$\overline{\phi_c^n} = \frac{\delta_1}{\delta_1 + \delta_2} \overline{\phi_1^n} + \frac{\delta_2}{\delta_1 + \delta_2} \overline{\phi_2^n}$$

where $\delta_1 = z_{max} / (h - S_a)$, $\delta_2 = (h - z_{max}) / (h - S_a)$ and $\overline{\phi_1^n}$ and $\overline{\phi_2^n}$ are the tabulated averages corresponding to the given δ_1 and δ_2, for slabs. The rod region average must be performed in detail

$$\overline{Z_r^n} = \frac{\left(\frac{C}{A}\right)^n \int_h^{H' - S'_a} \left[\sinh \overline{K} (H' - z)\right]^n dz}{H' - S'_a - h}$$

By a change in variables, this becomes

$$\overline{Z_r^n} = B_n \int_b^a \sinh^n x \, dx$$

where

$$B_n = (C/A)^n \frac{1}{(a - b)}$$

$$a = \overline{K} (S'_a) = 1.6419$$

$$b = \overline{K} (H' - h) = 0.1392$$

The recursion integration relation is used

$$I_n = \int \sinh^n x \, dx = \frac{1}{n} \sinh^{n-1} x \cosh x - \frac{n-1}{n} \int \sinh^{n-2} x \, dx$$

---

* Raymond L. Murray and Lawrance A. Mink, Tables of $\overline{\phi^n}$ for Reactor Slabs, Cylinders and Spheres n = 1 to n = 20.

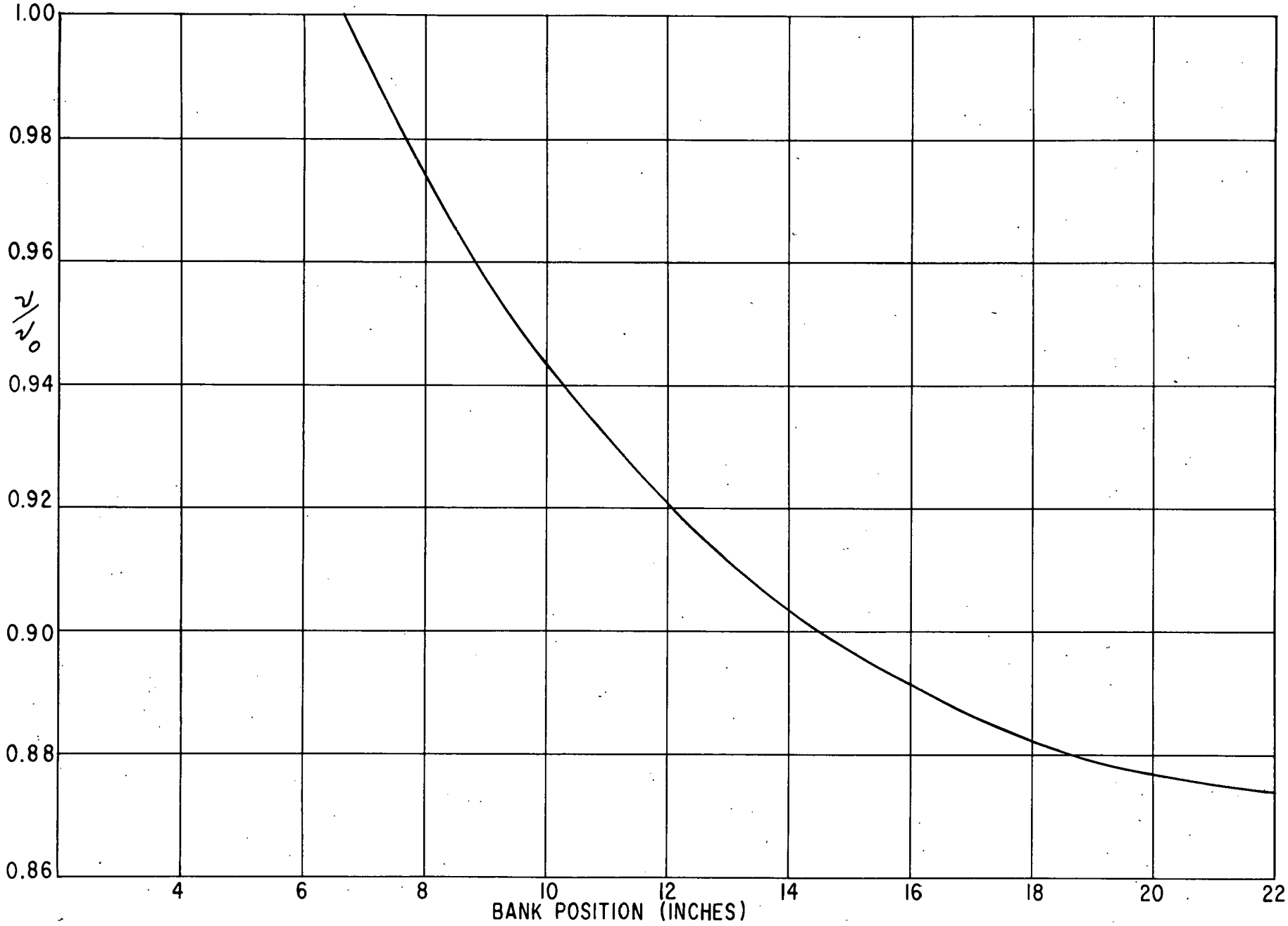

Figure A.3 Critical ν / ν_0 vs. Bank Position

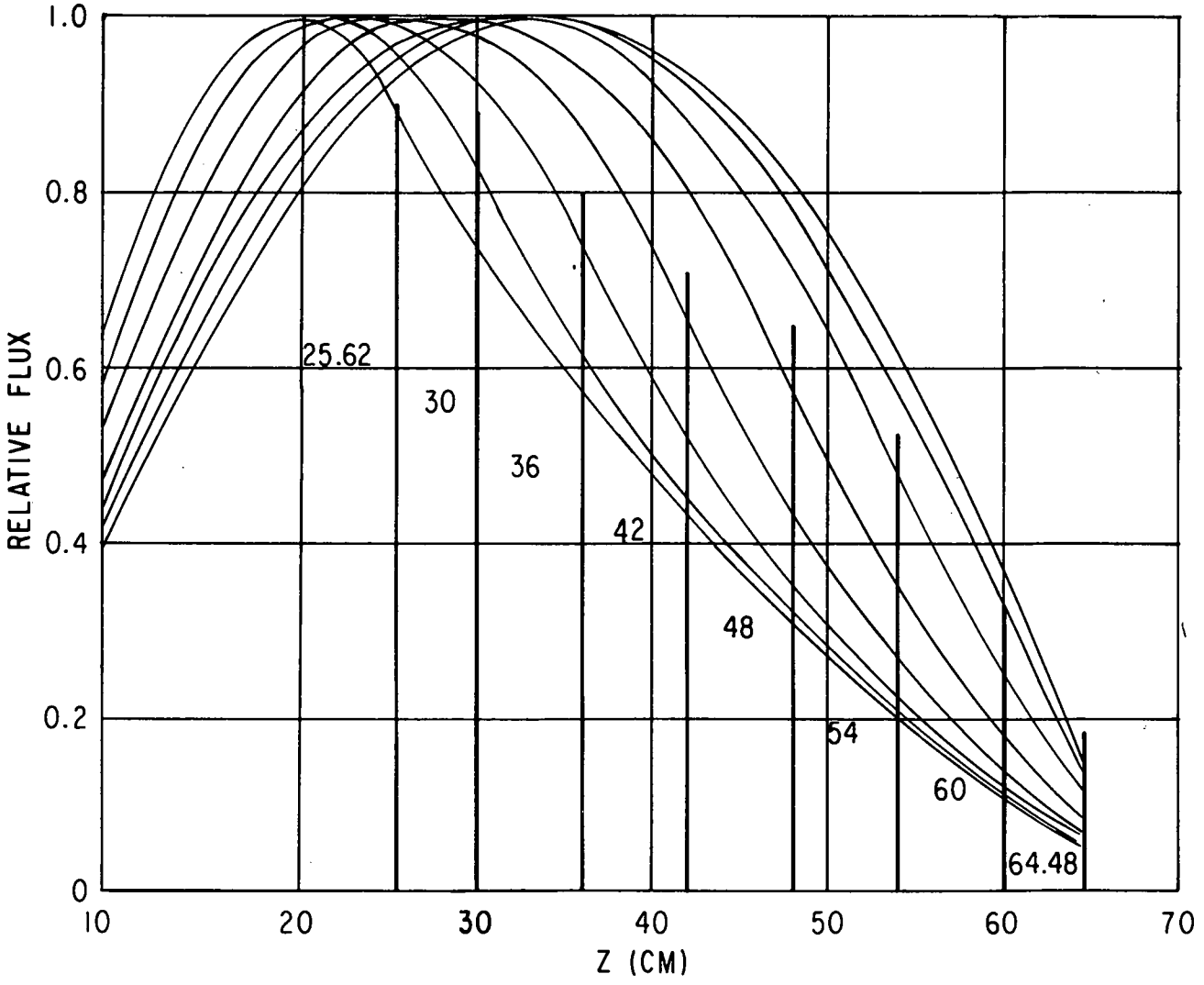

Figure A.4 Flux Distribution as a Function of ν / ν_o

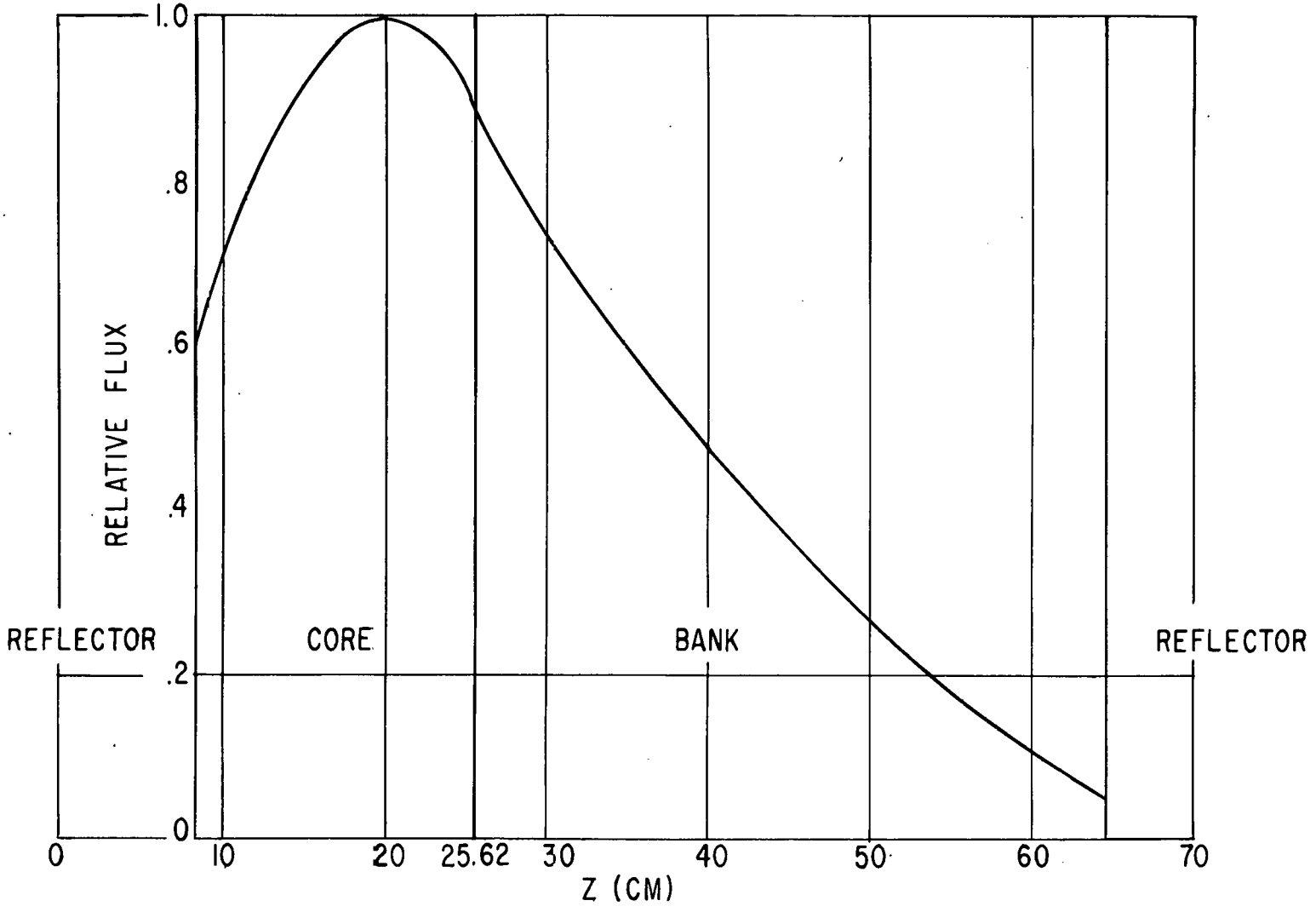

Figure A. 5 Initial Flux Distribution

with starting expressions

$$I_1 = \cosh x$$

$$I_2 = \frac{1}{2}(\sinh x \cosh x - x)$$

The average values for various n, for the axial flux and for the complete flux are tabulated below.

n	$\overline{Z_c^n(z)}$	$\overline{Z_r^n(z)}$	$\overline{\phi_c^n(r, z)}$	$\overline{\phi_r^n(r, z)}$
1	0.9057	0.3964	0.5592	0.2447
2	0.8302	0.2126	0.3512	0.08993
3	0.7665	0.1329	0.2408	0.04176
4	0.7152	0.0906	0.1771	0.02243
5	0.6754	0.0652	0.1375	0.01327
6	0.6391	0.0485	0.1104	0.00838
7	0.6078	0.0371	------	-------
8	0.5805	0.0289	------	-------

A.2.2 Variation of Core Reactivity with Fuel Consumption

The burnup theory described in an earlier section was applied to compute the core reactivity as a function of operating time. In the evaluation of the burnup functions for boron, it was necessary to force a series expansion of the form

$$B_2(x) = \frac{\overline{\phi^3}}{\overline{\phi^2}} x \left[e^{-\frac{\overline{\phi^4} x}{2\overline{\phi^3}}} + ax^2 e^{-\frac{b}{a}x} \right]$$

where

$$a = \frac{\overline{\phi^5}}{3!\,\overline{\phi^3}} - \frac{1}{2!}\left(\frac{\overline{\phi^4}}{2\overline{\phi^3}}\right)^2, \quad b = \frac{\overline{\phi^6}}{4\overline{\phi^3}} - \frac{1}{3!}\left(\frac{\overline{\phi^4}}{2\overline{\phi^3}}\right)^3$$

The effect of fission product poisons other than xenon-135 was incorporated by inserting a correction of the form

$$1 - \frac{\sigma_{aFP}}{\sigma_{aU}}$$

as a multiplier of f_U in the coefficient α. The relation between the reduced flux-time variable u and the number of megawatt years was computed. The results are listed on the following page.

u	MWYR	$-\rho$
0.0	0	0
0.25	2.235	0.0004
0.50	4.322	0.0076
0.75	6.278	0.0186
1.00	8.106	0.0316
1.25	9.813	0.0453
1.50	11.31	0.0598
1.75	12.88	0.0707
2.00	14.26	0.0820
2.25	15.54	0.0923
2.50	16.73	0.1011

A plot is given in Fig. A. 6.

In the performance of the perturbation theory estimate of rod reactivity, proper cognizance should be taken of flux changes during operation. For rod motion near the start of the cycle, the end of the bank moves in the initial highly distorted flux pattern, while at the end, it moves in a more symmetric flux. Evaluations of $\rho(z)$ were performed using the expression

$$\rho(z) = \frac{Kt}{K} \frac{\Sigma_p}{\Sigma_a} \left[\int_h^z \phi^2(z)\, dz \Big/ \int_{core} \phi^2(z)\, dz \right]$$

but with the two types of fluxes. The use of this relation both at the end of the cycle and at the beginning is valid in that the reduced factor ν / ν_o is common to numerator and denominator. In terms of rod calibration, using the initial flux gives correct ρ at early times but underestimates the worth toward the end of the cycle. The converse is true for the use of the final flux. To give an approximate realistic value, the average of the two calculations was taken as listed on Page A-24.

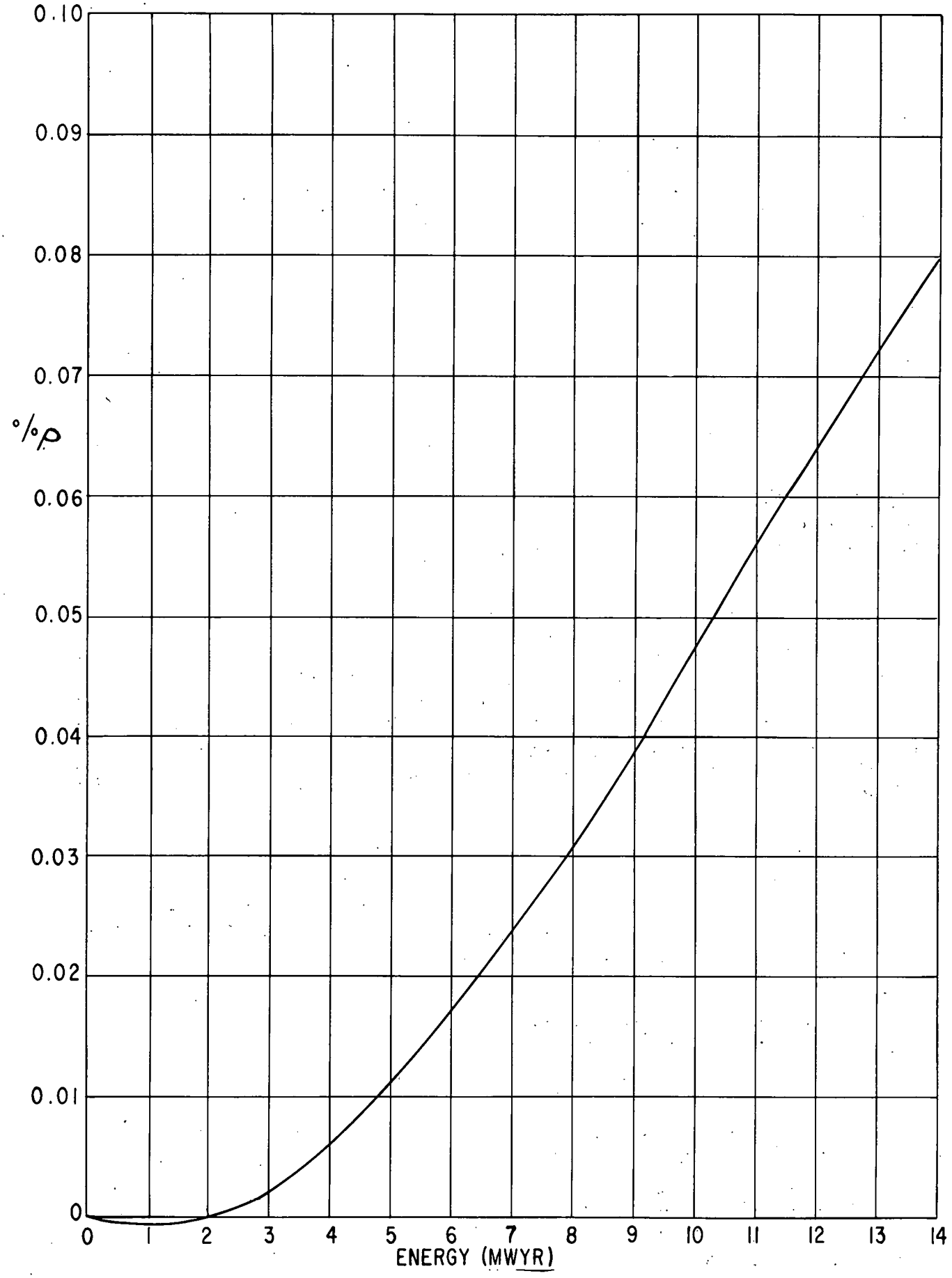

Figure A. 6 Burnout Reactivity of U-235, B-10 Fission Products

z (in.)	$\overline{\rho}$ (z)
6.70	0
7.64	0.0133
9.21	0.0336
10.79	0.0515
12.36	0.0671
13.94	0.0795
15.51	0.0903
17.09	0.0979
18.66	0.1027
20.24	0.1055
21.81	0.1064
22.00	0.1064

Figure A.7 shows the trend with rod position. For comparison, the integrated rod worth as measured in the SM-1 is shown. Considering the simplicity of the theory employed, the agreement is suprisingly good.

A.2.3 Combined Bank and Burnout Reactivities

The predicted rod bank removal pattern may be deduced by combining the data on ρ (z) for the bank and ρ for the fuel burnout as a function of megawatt years of operation. Two plots are predicted in Fig. A.8, one for each of the two methods or rod calibration calculation, for the case of no xenon poisoning. The experimentally measured bank position as a function of energy release for the SM-1 core is also shown for comparison. The agreement is seen to be reasonable.

A.2.4 Summary

Application of perturbation techniques in a stepwise control rod motion, combined with series burnup calculation gave good agreement between measured and calculated control rod position vs lifetime.

A.3 TEMPERATURE COEFFICIENT ANALYSIS

A.3.1 Introduction

A simplified theory of the temperature coefficient of reactivity α was developed and applied in order to determine the variation of α with control rod bank position during reactor life. The principal innovation is the specific account for the two reative regions. Since the dominant effect is due to fast leakage, the modified one-group approach employed in the basic burnup calculations is again applicable.

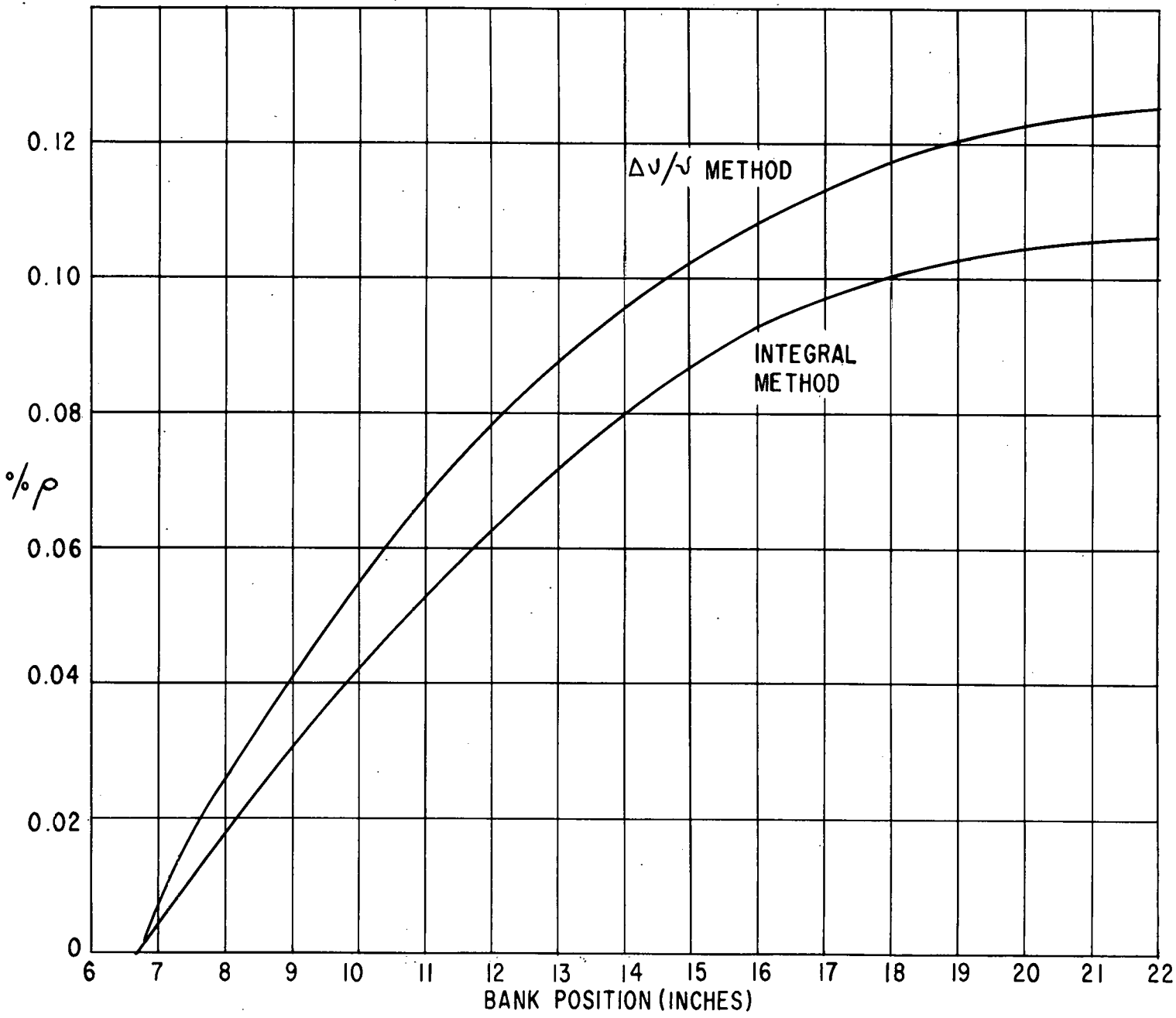

Figure A.7 Bank Reactivity vs. Position

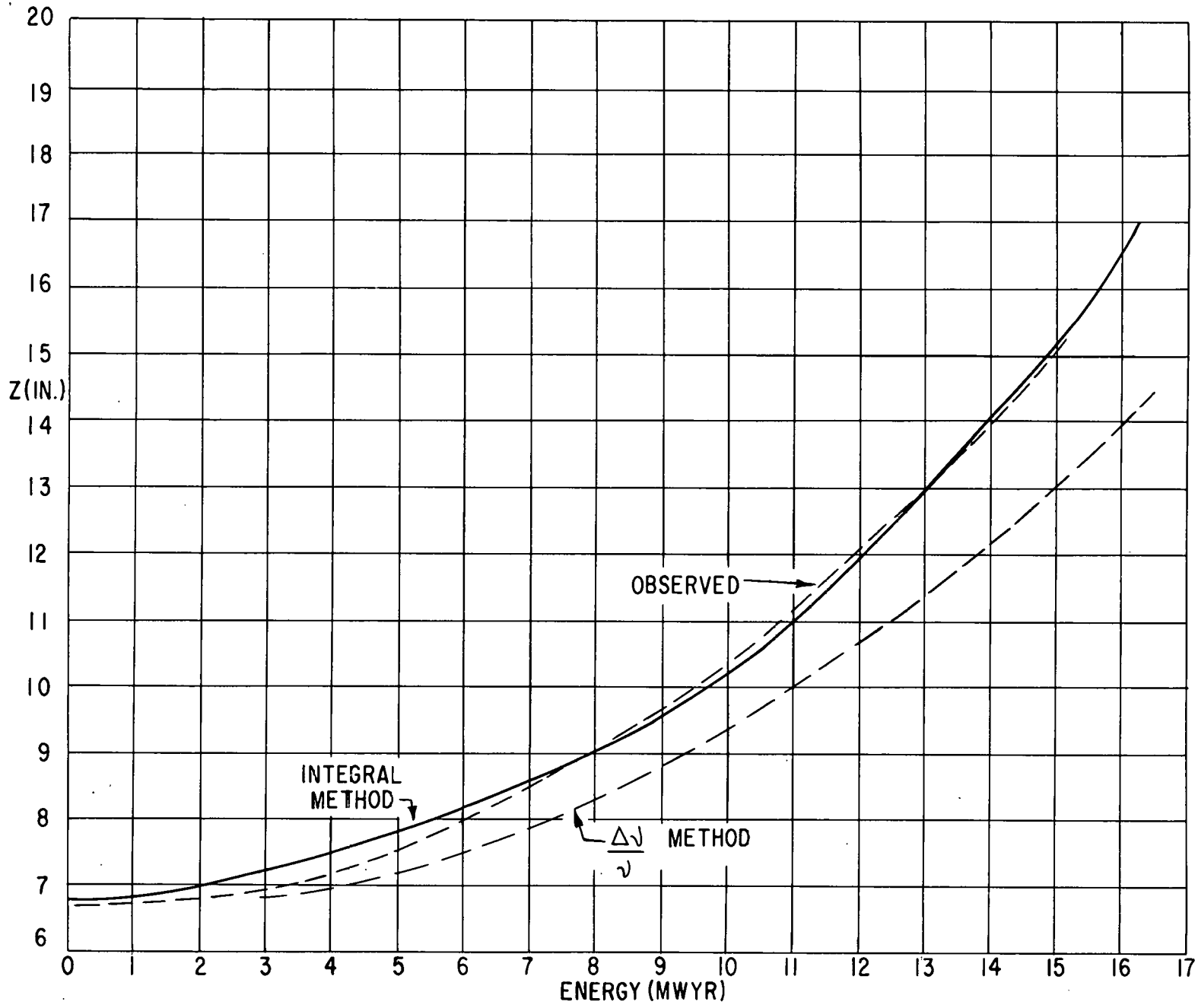

Figure A. 8 Critical Bank Position During Core Life, No Xenon

A.3.2 Theory

During the course of operation, the system remains essentially critical with rod bank motion balancing the fuel-boron consumption. The series of criticality states characterized by reduced numbers of neutrons per fission ν can serve as points of departure for finding the temperature coefficient. A change in temperature causes a change in moderator-coolant density with negligible effect on metal structure. Define the temperature coefficient as

$$\alpha = \frac{1}{\nu} \frac{d\nu}{dT}$$

where the change in ν is that required to balance the effect of change in moderator density, retaining a critical state. The latter is given by

$$\tan \bar{B}h = - \frac{\bar{B}}{\bar{K}} \tanh \bar{K} (H' - h)$$

where

$$\bar{B}^2 = \frac{\frac{\nu}{\nu_o} K_C^o - 1}{\tau} - \left(\frac{j_o}{R'} \right)^2$$

$$\bar{K}^2 = \left(\frac{j_o}{R'} \right)^2 \left[\frac{\frac{\nu}{\nu_o} K_r^o - 1}{\tau} \right]$$

Differentiating the criticality condition and rearranging gives

$$d\bar{B} \; F = -d\bar{K} \; G$$

where

$$F = \bar{K} h (1 + \tan^2 \bar{B}h) + \tanh \bar{K}\lambda$$

$$G = \bar{B}\lambda (1 - \tanh^2 \bar{K}\lambda) + \tan \bar{B}h$$

with $H' - h = \lambda$

Now

$$d\bar{B} = \frac{1}{2\bar{B}\tau} \left[K_C \left(\frac{d\nu}{\nu} + \frac{dK_C^o}{K_C^o} \right) - (K_C - 1) \frac{d\tau}{\tau} \right]$$

and

$$d\bar{K} = - \frac{1}{2\bar{K}\tau} \left[K_r \left(\frac{d\nu}{\nu} + \frac{dK_r^o}{K_r^o} \right) - (K_r - 1) \frac{d\tau}{\tau} \right]$$

Inserting,

$$\frac{d\nu}{\nu} = \frac{d\tau}{\tau}\left[\overline{K}\,F\,(K_C - 1) - \overline{B}G\,(K_r - 1)\right] - \left[\overline{K}FK_C\frac{dK_C^o}{K_C^o} - \overline{B}GK_r\frac{dK_r^o}{K_r^o}\right]$$

There remains the evaluation of the effects on τ, K_C^o and K_r^o. By invoking the assumption that the composite age of a heterogeneous medium may be written

$$\frac{1}{\sqrt{\tau}} \simeq \frac{v_w}{\sqrt{\tau_w}} + \frac{v_m}{\sqrt{\tau_m}}$$

where subscripts refer to water and metal, and v's are volume fractions. One deduces that

$$\frac{d\tau}{\tau} = -2v_w\frac{dN_w}{N_w}\sqrt{\frac{\tau}{\tau_w}}$$

with water molecule number density N_w. The quantity

$$\frac{1}{N_w}\frac{dN_w}{dT}$$

is the temperature coefficient of expansion of water, labeled α_T. It has the same absolute value as $\frac{1}{\rho}\frac{d\rho}{dT}$. Also, using

$$K = K_t + K_r$$

with $K_t = \eta\, fp$ and $K_r = (1 - p)\eta_r f_r$, the fractional change in K for a process that is predominantly thermal is

$$\frac{dK}{K} = \frac{K_t}{K}\frac{df}{f} = -\frac{K_t}{K}\frac{d\Sigma_a}{\Sigma a} = -\frac{K_t}{K}\,f_w\,\frac{dN_w}{N_w}$$

Here f_w is the "utilization" of water. Combining we find

$$\frac{\alpha}{\alpha_T} = \frac{-2v_w\sqrt{\frac{\tau}{\tau_w}}\left[(K_C - 1) - \frac{\overline{B}}{\overline{K}}\frac{G}{F}(K_r - 1)\right] + \frac{\nu}{\nu_o}\left[K_{tC}^o f_{wC} - \frac{\overline{B}G}{\overline{K}F}K_{tr}^o f_{wr}\right]}{K_C - \frac{\overline{B}}{\overline{K}}\frac{G}{F}K_r}$$

This is the working formula.

A. 3. 3 Calculations

The variation of specific volume and density of saturated water in the vicinity of the operating temperature was obtained from the Nuclear Engineering Handbook, pages 9-10 as follows:

T(°F)	ft^3/lb	cm^3/gm	gm/cm^3
430	0.01910	1.1924	0.8386
440	0.01926	1.2024	0.8317
450	0.01940	1.2111	0.8257

The quantity $|\alpha_T| = \frac{1}{\rho}\frac{d\rho}{dT}$ was found to be $7.78 \times 10^{-4}/^{o}F$. Other data needed are:

f_w(core) = 0.04452

f_w(bank) = 0.03149

τ = 43.03 cm^2

τ_w = 47.50 cm^2

v_w = 0.792, v_m = 0.198

The value of α/α_T was determined for four states, corresponding to the bank at its initial position, full out, and two intermediate locations. Tabulated results are as follows:

h(cm)	ν/ν_o	K_C	K_r	G/F	α/α_T	$\alpha/^{o}F$	¢/°F
25.62	1.000	1.4679	1.1278	-0.2596	0.3491	2.72×10^{-4}	3.49
36	0.934	1.3710	1.0534	-0.1621	0.3232	2.51×10^{-4}	3.22
54	0.883	1.2962	0.9958	-0.0410	0.2916	2.27×10^{-4}	2.91
64.48	0.874	1.2829	0.9857	+0.0016	0.2872	2.23×10^{-4}	2.86

The last column is based on the assumption of an effective delayed neutron fraction of (1.20) (0.0065) = 0.0078. It is notable that there is only a slight variation of temperature coefficient with core life, being a downward trend. The theoretical results are compared with the experimental observations on SM-1 in Fig. A. 9. Within the accuracy of measurement and the limitations of the theory, the agreement is good.

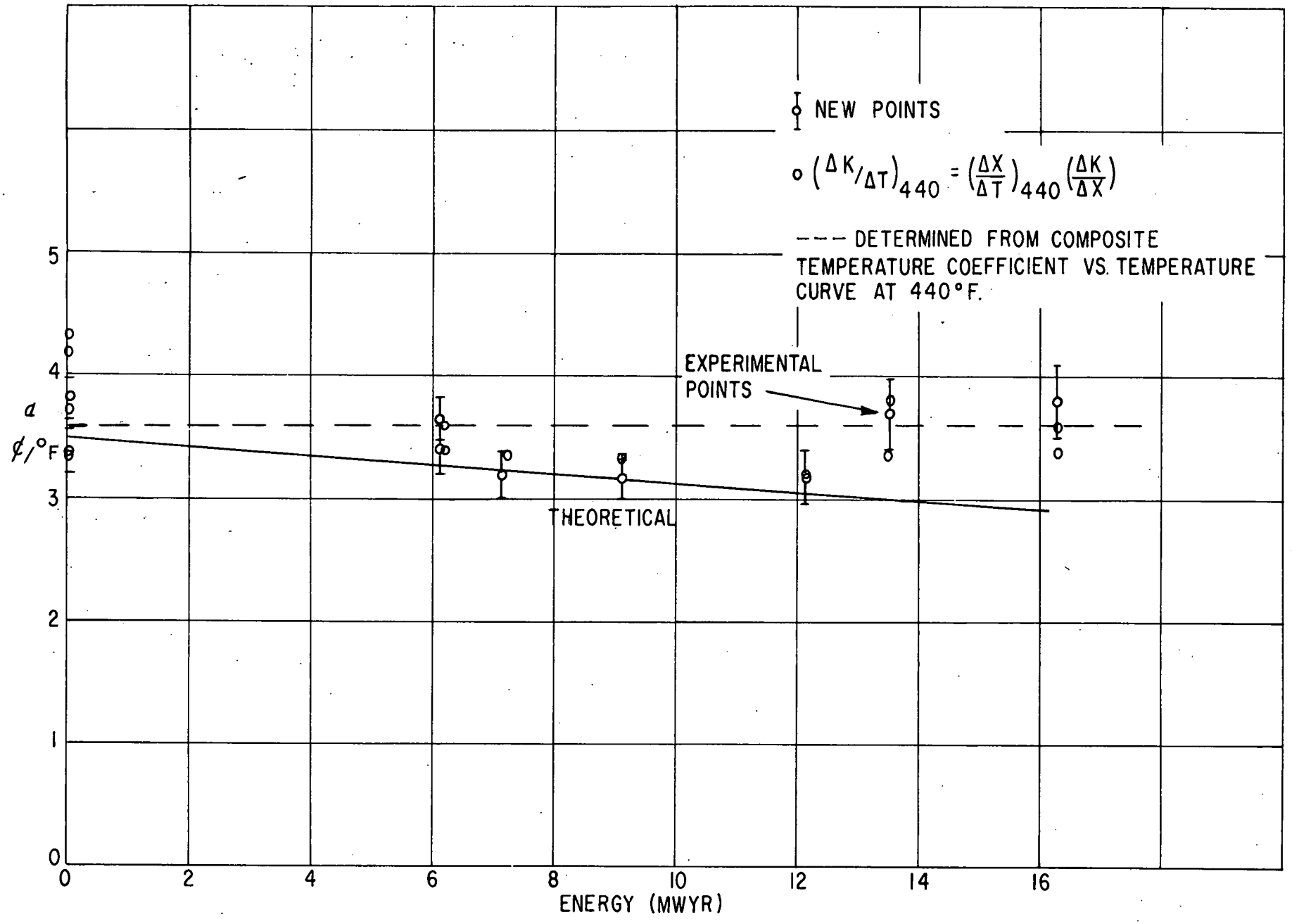

Figure A.9 Temperature Coefficient at 440°F

A. 3. 4 Summary

While it is very difficult to account explicitly for all parameters contributing to the change of the temperature coefficient vs energy release, it is possible to considerably simplify the calculations by disregarding thermal leakage.

Use of the one group modified theory gave a temperature coefficient slightly decreasing with energy release.

The difference of the results of Sec. A. 3 with Sec. 6. 0 is attributed to the approximations made.

A. 4 STEADY STATE XENON POISONING

A. 4. 1 Introduction

An adaptation of the burnup theory is made to account for the reactivity due to xenon poisoning. It can be assumed that the cycle life of the reactor is far greater than the half-life of the isotopes I^{135} and Xe^{135}, such that essential equilibrium is maintained even though fuel is being consumed.

A. 4. 2 Analysis

The steady state local poisoning due to Xe^{135} is readily written

$$\Sigma_{ax}(\bar{r}, t) = \frac{y\Sigma_f (r, t)}{\frac{\lambda_{xe}}{\sigma_{xe}\phi (r, t)} + 1}$$

The reactivity of the system is of the form

$$\rho = \frac{\int \frac{\delta K}{K} \phi^2 (\bar{r}, t)}{\int \phi^2(\bar{r}, t)dV}$$

where

$$K = \eta f p + (1 - p)\eta_r f_r$$

Now for a thermal poison

$$\frac{\delta K_t}{K_t} = - \frac{\overline{\delta\Sigma_a}}{\Sigma_a} \text{ or } \delta K_t = - \frac{\delta\Sigma_a}{\Sigma_a} K_t$$

Substituting

$$\rho = \frac{-\int \frac{\delta\Sigma_a}{\Sigma_a} \frac{K_t}{K} \phi^2 \, dV}{\int \phi^2 \, dV}$$

or

$$\rho = \frac{-y \int \frac{\frac{\Sigma_f}{\Sigma_a} \frac{K_t}{K} \phi^2(\bar{r},t) \, dV}{1 + \frac{\lambda_{xe}}{\sigma_{xe}\phi(\bar{r},t)}}}{\int \phi^2(\bar{r},t) \, dV}$$

Letting the quotient λ_{xe}/σ_{xe} be defined by ϕ_1, a polynomial expansion can be made

$$\frac{1}{1 + \frac{\phi_1}{\phi}} = \sum_{n=o}^{m} (-1)^n (\phi_1/\phi)^n + \text{remainder}$$

To three terms, this is

$$1 - \frac{\phi_1}{\phi} + \left(\frac{\phi_1}{\phi}\right)^2$$

with a remainder of

$$\frac{-\left(\frac{\phi_1}{\phi}\right)^3}{1 + \frac{\phi_1}{\phi}}$$

Now let $\phi(\bar{r},t) = C(t)\,\phi(\bar{r})$, where C(t) is the time dependent amplitude, with initial value $C_o = \phi_C$ the central initial flux. Then invoking the burnup function

$$B\lambda = \frac{1}{V} \int \phi\lambda(\bar{r}) \, e^{-\phi(\bar{r})x} \, dV$$

the reactivity becomes

$$\rho = \frac{-y\sum_f^o K_t}{\phi^2 \sum_a^o K} \left[B_2(x) - \left(\frac{\phi_1}{C}\right) B_1(x) + \left(\frac{\phi_1}{C}\right)^2 \cdot B_o(x) + \ldots . \right]$$

where

$$x = \sigma_{aU} u.$$

Noting that

$$\frac{1}{C} = \frac{B_1(x)}{\phi_C \overline{\phi(\bar{r})}}$$

the final working formula to three terms for a given region is

$$\rho = \frac{-y\sum_f^o K_t}{\overline{\phi^2}\sum_a^o K} \left[B_2(x) - \left(\frac{\phi_1}{\phi_C \overline{\phi}}\right) B_1^2(x) + \left(\frac{\phi_1}{\phi_C \overline{\phi}}\right)^2 B_1^2(x)\, B_o(x) - \ldots . \right]$$

Exponential approximations to the burnup functions may be used.

$$B_0 = e^{-\phi_{e0} x} \qquad \phi_{e0} = \overline{\phi}$$

$$B_1 = \overline{\phi} e^{-\phi_{e1} x} \qquad \phi_{e1} = \overline{\phi^2}/\overline{\phi}$$

$$B_2 = \overline{\phi^2} e^{-\phi_{e2} x} \qquad \phi_{e2} = \overline{\phi^3}/\overline{\phi^2}$$

Some of the functions are available from previous calculations of the burnup.

An investigation of the contribution of the correction due to all other terms in the series was made. Rigorously, the <u>remainder</u> is of the form

$$\frac{1}{V} \int \frac{\phi^2(\bar{r}) \left[\frac{\phi_1}{\phi_C \phi(\bar{r})}\right]^3}{1 + \frac{\phi_1}{\phi_C \phi(\bar{r})}} = \left(\frac{\phi_1}{\phi_c}\right)^3 \frac{1}{V} \int \frac{\frac{1}{\phi(\bar{r})}\, dV}{1 + \frac{\phi_1}{\phi_C \phi(\bar{r})}}$$

$$= \left(\frac{\phi_1}{\phi_C} \right)^3 \quad \frac{1}{V} \int \frac{\phi(\bar{r})\, dV}{\phi(\bar{r}) + (\phi_1/\phi_C)}$$

The coefficient of $(\phi_1/\phi_C)^3$ lies between 0 and 1, and hence the remainder lies between p and $(\phi_1/\phi_C)^3$, which will be negligible if ϕ_1/ϕ_C is considerably less than 1, as it is (0.249) for the reactor considered.

The composite reactivity for a two region core is

$$\rho = \frac{\int_C \frac{\delta K}{K} \phi^2\, dV + \int_r \frac{\delta K}{K} \phi^2\, dV}{\int_C \phi^2 dV + \int_r \phi^2\, dV}$$

which may be rearranged to

$$\rho = \frac{\rho_C \overline{\phi^2}_C k + \rho_r \overline{\phi^2}_r m}{\overline{\phi^2}_C k + \overline{\phi^2} m}$$

The values for ρ for each region i are weighted by the average square of the flux and the volume of that region

$$\rho_i = \int_i \frac{\delta K}{K} \phi^2 dV / \int \phi^2 dV$$

A.4.3 Constants for Xe^{135} Calculations

Basic data used are listed:

Absorption cross section of Xe, $(\sigma_a)_{xe} = 1.98 \times 10^6$ barns

Yield of Xe + I, y = 0.064

Decay Constant $\lambda_{xe} = 2.11 \times 10^{-5}\ sec^{-1}$

$\phi_1 = \lambda_{xe}/(\sigma_a)_{xe} = 1.066 \times 10^{13}/cm^2\text{-sec}$

Fission cross section of U^{235} = 411.5 barns (core), 415.3 (bank)

Initial central flux, $C_o = \phi_C = 4.276 \times 10^{13}/cm^2\text{-sec}$

K_t = 1.1294 (core), 0.7811 (bank)

K = 1.4679 (core), 1.1278 (bank)

$\sum_a$ = 0.2758 (core), 0.2809 (bank)

Region lengths k = 17.02 cm, m = 38.86 cm

Average flux squares $\overline{\phi_C^2}$ = 0.3512, $\overline{\phi_r^2}$ = 0.08993

Flux averages from earlier calculations were employed to determine the following variation of equilibrium xenon reactivity with operating time.

u	W(MWYR)	ρ
0	0	0.0242
0.25	2.235	0.0222
0.50	4.322	0.0205
0.75	6.278	0.0189
1.00	8.106	0.0174
1.25	9.813	0.0162
1.50	11.31	0.0150
1.75	12.88	0.0140
2.00	14.26	0.0131
2.25	15.54	0.0123
2.50	16.73	0.0115

A.4.4 Combined Burnup, Fission Product and Xe Reactivity

The total negative reactivity due to U^{235} consumption, boron burnup, fission product poison, and Xe^{135} poison was obtained by addition. The results are listed in the table below, and plotted in terms of rod bank position in Fig. A.10. The trends developed by theory agree rather well with the experimentally observed results on SM-1.

W (MWYR)	ρ Total	W (MWYR)	ρ Total
0	0.024	8	0.048
1	0.022	9	0.055
2	0.022	10	0.062
3	0.024	11	0.070
4	0.026	12	0.078
5	0.030	13	0.081
6	0.035	14	0.093
7	0.041	15	0.100
		16	0.108

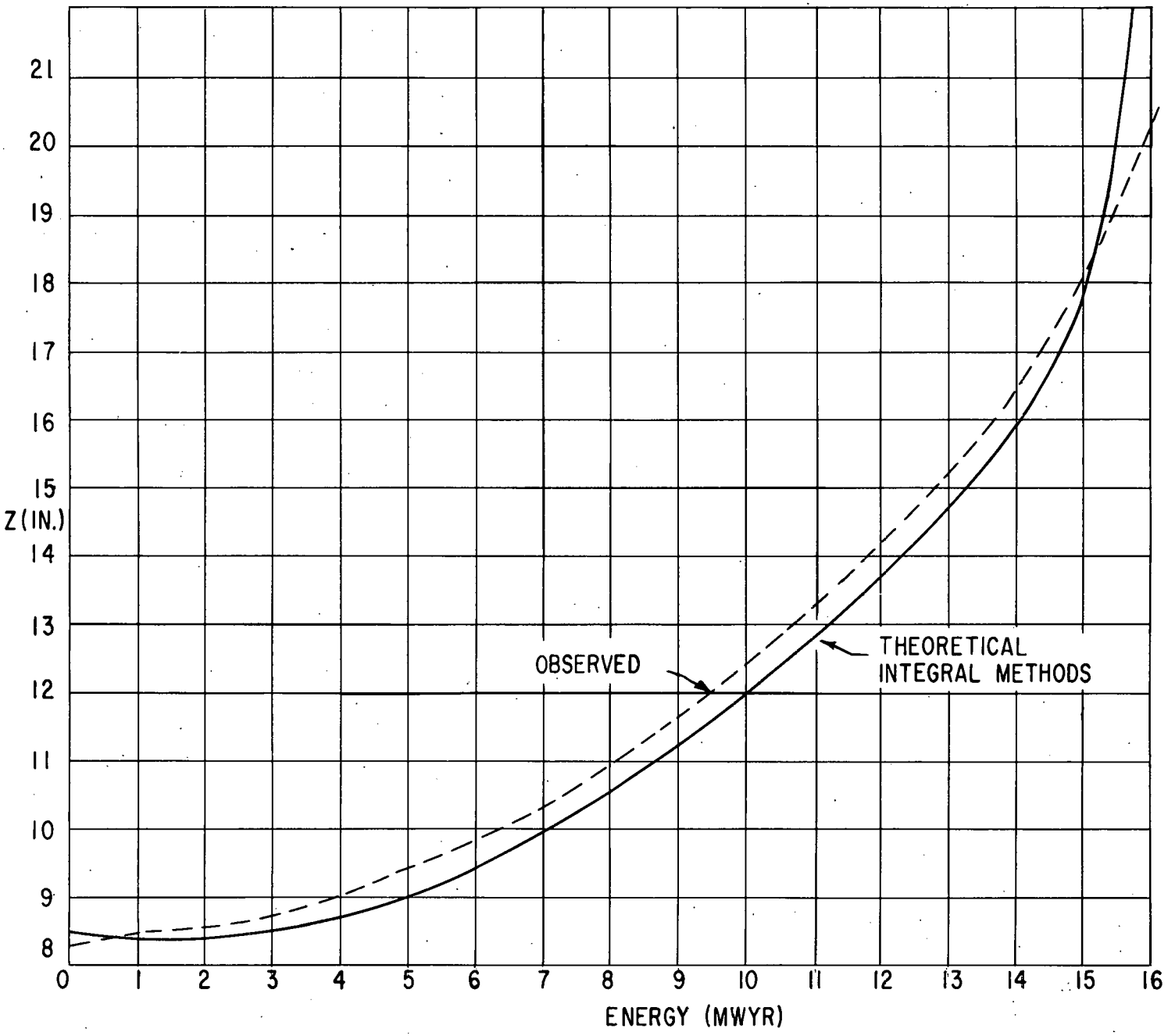

Figure A.10 Critical Bank Position During Core Life Equilibrium Xenon

A. 4. 5 Summary

Using perturbation techniques in conjunction with the series burnup, the reactivity due to equilibrium xenon has been evaluated vs energy release of the core.

This combined with the results of Sec. A. 2 gives an estimate of the control rod bank position vs energy release and therefore lifetime. It can be seen that the lifetime is 15. 8 MWYR vs 16. 05 experimental for the unperturbed core.

A. 5 EFFECTIVE DELAYED NEUTRON FRACTION AS A FUNCTION OF BANK POSITION

A. 5. 1 Introduction

Calculations of the effective delayed neutron fraction β_e by two group analytic methods are very laborious, even for simple geometrical shapes such as the reflected sphere or a two-region bare cylinder. A simple method is developed and applied to the SM-1, under conditions of operation with banked control rods. A modified one-group approach is employed, in which advantage is taken of the short thermal diffusion length.

A. 5. 2 Critical Conditions

The reactor core is taken to be a cylinder with side reflector replaced by a radial savings $R' = R + S_r$, and end reflector replaced by bottom savings S_a and top savings S'_a. With origin at the bottom, the core extends from $z = S_a$ to $z = h$, at which point the bank begins, extending to $z = H' - S'_a$ where $H' = H + S_a + S'_a$. The two regions are similar except for the differences in rod follower fuel elements and the equivalent control poison in the rod region. The critical conditions and axial flux distributions are

$$\tan \bar{B}h = -\frac{\bar{B}}{\bar{K}} \tanh \bar{K}(H' - h)$$

$$Z_{2C}(z) = A \sin \bar{B}z$$

$$Z_{2r}(z) = C \sinh \bar{K}(H' - z)$$

where

$$C/A = \frac{\sin \bar{B}h}{\sinh \bar{K}(H' - h)}$$

and $$\overline{B}^2 = \frac{(K_C - 1) + (j_o/R')^2}{\tau}$$

$$\overline{K}^2 = (j_o/R')^2 - \frac{(K_r - 1)}{\tau}$$

$$K = \eta f p + (1 - p)\eta_r f_r$$

A. 5. 3 Effective β Analysis

The general two-group equations for delayed neutron fluxes in a given region are

$$D_{1d}\nabla^2 \phi_{1d} - \phi_{1d}\Sigma_{1d} + \left[\phi_2 \Sigma_2 \eta f + \phi_1 \Sigma_1 (1-p)\eta_r f_r \right] \beta = 0$$

$$D_2 \nabla^2 \phi_{2d} - \phi_{2d}\Sigma_{2d} + P_d \phi_{1d} \Sigma_{1d} = 0$$

where one composite group of neutrons of fraction β is assumed to have slowing properties D_{1d} and Σ_{1d}, related by $\tau = D_{1d}/\Sigma_{1d}$. Since the thermal diffusion length is short compared with the age, we may write $\phi_1 \Sigma_{1p} \cong \phi_2 \Sigma_2$ and $\phi_{1d} \Sigma_{1d} p_d \cong \phi_2 \Sigma_2$. Insertion and simplification yields the inhomogeneous equation

$$\tau_o \nabla^2 \phi_{2d} - \phi_{2d} = - \phi_2 K \beta$$

where the termal flux ϕ_2 is known functionally. Extraction of the radial buckling yields

$$\frac{d^2 Z_{2d}}{dz^2} - \overline{K}_{1d}^2 Z_{2d} = - \frac{K \beta Z_2}{\tau_d}$$

where

$$\overline{K}_{1d}^2 = \frac{1}{\tau_d} + (j_o/R')^2$$

The complementary functions are $\sinh \overline{K}_{1d} z$ and $\sinh \overline{K}_{1d} (H'-z)$ for the two regions, and the particular integrals readily obtained by operator methods. The result is

$$Z_{2dc} = E \sinh \overline{K}_{1d} z + GA \sin \overline{B} z$$

$$Z_{2dr} = F \sinh \overline{K}_{1d} (H' - z) + HC \sinh \overline{K} (H'-z)$$

where

$$G = \frac{K_c \beta}{\tau_d (\overline{K}_{1d}^2 + \overline{B}^2)} = \frac{K_c \beta}{1 + B^2 \tau_d}$$

$$H = \frac{K_r \beta}{d (\overline{K}_{1d}^2 - \overline{K}^2)} = \frac{K_r \beta}{1 - \overline{K}^2 \tau_d}$$

with E and F as arbitrary constants.

Abbreviating,

$$V = \sinh \overline{K}_{1d} z$$

$$W = \sinh \overline{K}_{1d} (H' - z)$$

$$T = \sin \overline{B} z$$

$$U = \sinh \overline{K} (H' - z)$$

$$Z_{2dc} = EV + GAT$$

$$Z_{2dr} = FW + HCU$$

The effective β is defined as

$$\beta_{eff} = \frac{\int \phi_{2d} dV}{\int \phi_2 dV} = \frac{\int_c Z_{2dc} dV + \int_r Z_{2dr} dV}{\int_c Z_{2c} dV + \int_r Z_{2r} dV}$$

Letting $\int T dV = \tilde{T}$ and similarly for other terms,

$$\beta_{eff} = \frac{E\tilde{V} + F\tilde{W} + GA\tilde{T} + HC\tilde{U}}{A\tilde{T} + C\tilde{U}}$$

The necessary integrals are

$$\tilde{T} = \int_{Sa}^{h} \sin \overline{B} z dz = \frac{\cos \overline{B} S_a - \cos \overline{B} h}{\overline{B}}$$

$$\tilde{U} = \int_{h}^{H'-S'_a} \sinh \bar{K}\,(H' - z)\,dz = \frac{\cosh \bar{K}(H'-h) - \cosh \bar{K} S'_a}{\bar{K}}$$

$$\tilde{V} = \int_{Sa}^{h} \sinh \bar{K}_{1d} z dz = \frac{\cosh \bar{K}_{1d} h - \cosh \bar{K}_{1d} S_a}{\bar{K}_{1d}}$$

$$\tilde{W} = \int_{h}^{H'-S'_a} \sinh \bar{K}_{1d}(H'-z)dz = \frac{\cosh \bar{K}_{1d}\,(H'-h) - \cosh \bar{K}_{1d} S'_a}{\bar{K}_{1d}}$$

The arbitrary constants are obtained by equating flux and current at z = h. The results are listed without proof.

$$E = \frac{HC\,(\,[U]_w - U'\,) - GA\,[T]_w - [T']\,)}{[V]\,(w - v)}$$

$$F = \frac{HC([U]_v - [U']) - GA\,[T]_v - [T'])}{[W]\,(w - v)}$$

where all quantities are evaluated at h, and

$$w = \frac{[W']}{[W]} = -\frac{\bar{K}_{1d} \cosh \bar{K}_{1d}\,(H'-h)}{\sinh \bar{K}_{1d}\,(H'-h)} = \bar{K}_{1d} \coth \bar{K}_{1d}(H'-h) \simeq = \bar{K}_{1d}$$

$$v = \frac{[V']}{[V]} = \bar{K}_{1d}\,\frac{\cosh \bar{K}_{1d} h}{\sinh \bar{K}_{1d} h} = \bar{K}_{1d} \coth \bar{K}_{1d} h \simeq \bar{K}_{1d}$$

For rod bank positions over most of the range, $\tilde{V} \simeq \frac{\cosh \bar{K}_{1d} h}{\bar{K}_{1d}} = \frac{[V]}{\bar{K}_{1d}}$

$\tilde{W} \simeq \frac{\cosh \bar{K}_{1d}\,(H'-h)}{\bar{K}_{1d}} = \frac{W}{\bar{K}_{1d}}$. Also, $w - v = -2\bar{K}_{1d}$ and $w + v = 0$.

Thus

$$E\tilde{V} + F\tilde{W} \simeq \frac{HC\,[U'] - GA\,[T']}{\bar{K}^2_{1d}}$$

where $\left[U'\right] = -\overline{K}\cosh \overline{K}(H'-h)$

$\left[T\right] = \overline{B}\cos \overline{B}h$

A. 5. 4 Calculations

A set of critical states for the core hot, with no xenon, at various rod bank positions was achieved by varying the effective number of neutrons per fission ν, and applying the basic critical conditions. A summary of the pertinent values follows:

Bank Position* (cm)	$\overline{B}$	$\overline{K}$	K_c	K_r	ν/ν_o
25. 62	0. 0801	0. 0387	1. 4679	1. 1278	1. 000
30	0. 0726	0. 0481	1. 4180	1. 0895	0. 966
36	0. 0665	0. 0568	1. 3710	1. 0534	0. 934
42	0. 0579	0. 0620	1. 3358	1. 0263	0. 910
48	0. 0527	0. 0653	1. 3123	1. 0083	0. 894
54	0. 0491	0. 0679	1. 2962	0. 9958	0. 883
60	0. 0469	0. 0690	1. 2859	0. 9880	0. 876
64. 48 (out)	0. 0462	0. 0694	1. 2829	0. 9857	0. 874

* With full in position at 8. 60 cm.

Application of the effective β formulas was then made using these group constants:

$\tau_d = 10.52\ cm^2$

$\overline{K}_{1d} = 0.3155\ cm^{-1}$

The results are listed on the following page, and plotted in Fig. A. 11 on an expanded scale in terms of $(\beta_{eff}/\beta) - 1$. The β_{eff} values have been obtained for delayed neutron fraction $\beta = .0065$*.

---

* See Keepin, G. R., Wimett, T. F., and Ziegler R. K., "Delayed Neutrons from Fissionable Isotopes of Uranium, Plutonium and Thorium," Nm. Energy G., No. 1/2, 1, (1957).

Bank Position (In.)	β_{eff}/β	β_{eff}
6.70	1.208	.007852
8.43	1.203	.007820
10.79	1.199	.007794
13.15	1.195	.007768
15.51	1.194	.007761
17.87	1.196	.007774
20.24	1.199	.007794
22.00	1.202	.007813

It will be noted that the variation is regular, but small over the large range of rod motion. The minimum appears to be quite real. The average value of β_{eff}/β has been taken as 1.200 elsewhere in this report yielding a β_{eff} = .0078. Detailed examination of the calculations reveals that the first two terms in the numerator of β_{eff} are very small, and that a good approximation is

$$\beta_{eff} = \frac{GA\tilde{T} + HC\tilde{U}}{A\tilde{T} + C\tilde{U}}$$

or

$$\beta_{eff}/\beta = \frac{\frac{k_c}{1 + B^2 \tau_d} \tilde{\phi}_c + \frac{k_r}{1 - K^2 \tau_d} \tilde{\phi}_r}{\tilde{\phi}_c + \tilde{\phi}_r}$$

where $\tilde{\phi}_c$ and $\tilde{\phi}_r$ are the integrals of the flux over the core and rod region respectively. Qualitatively, the approximate relation is a total-flux-weighted effective multiplication factor for delayed neutrons. Beyond this, no detailed physical explanation of the formula has been attempted.

A.5.5 Summary

A simplified theory is used to account for the preferential neutron leakage and therefore the effective delayed neutron fraction. Advantage is also taken of the short thermal diffusion length to simplify the two group modified equations.

Using the results of the previous sections of this Appendix, β_{eff} has been found to vary between 0.00783 to 0.00776, the minimum occurring at about 13.5 MWYR.

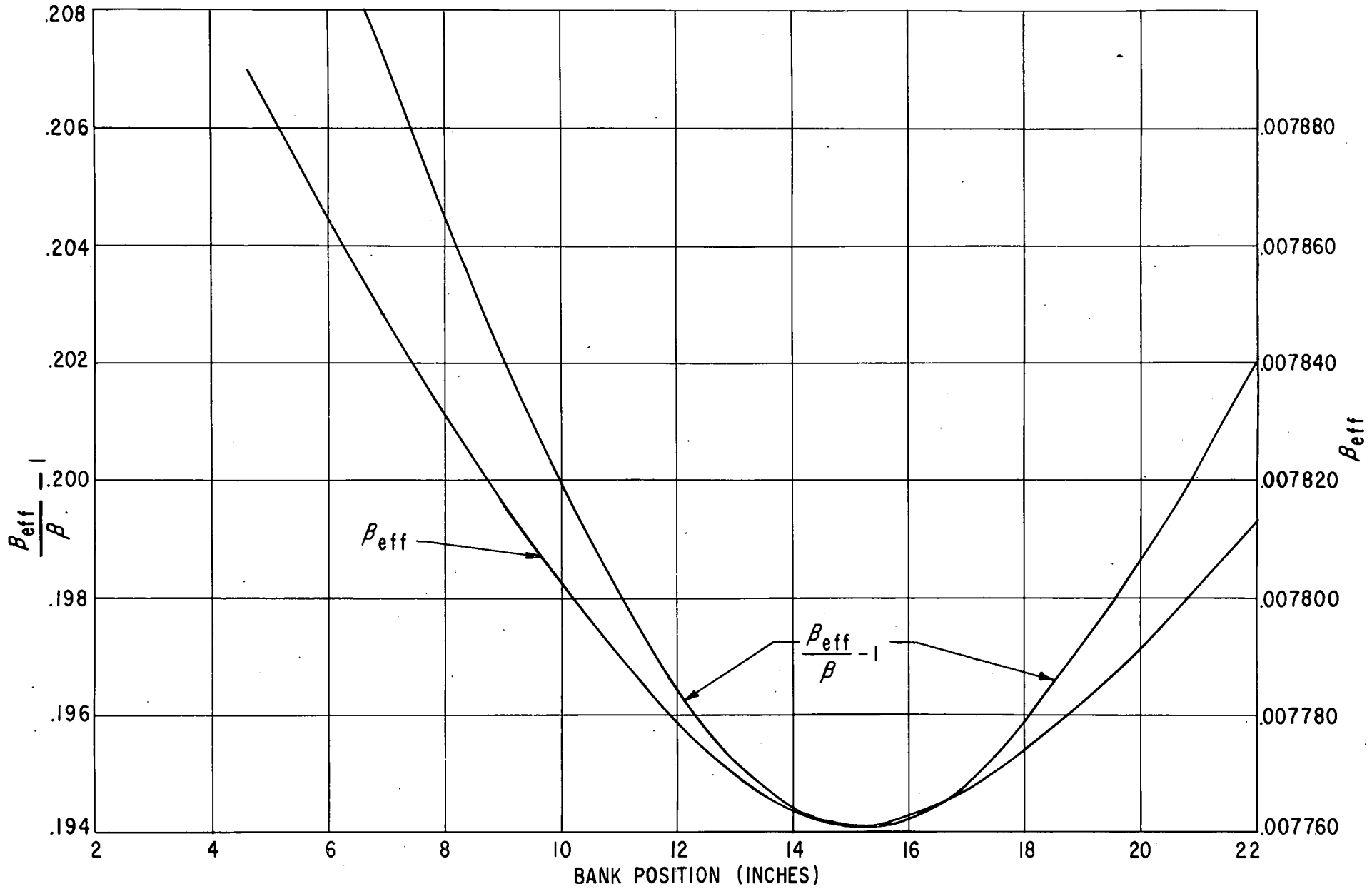

Figure A.11 Variation of $(\beta_e/\beta) - 1$ and β_{eff} with Bank Position

APPENDIX B

APPENDIX B

CANDLE-2 INPUT FOR AXIAL SM-1 CORE I-440°F

To understand the following CANDLE-2 input listing, it is necessary to obtain copies of WAPD-TM-53[1] and WAPD-TM-53 Add. 1.[2] AP Note 268[3] will also be of assistance.

Table B.1 shows the numbering system for the elements as used at Alco.

TABLE B.1
ALCO ELEMENT NUMBERS FOR THE CANDLE-2 IBM-704 CODE

Element	Number	Element	Number
Unit (1)	0	Mn_{55}	15
H	1	Li	16
0-16	2	In	17
Zr	3	U-235	18
C	4	U-236	19
$\sum_{a_{th}}$ / $\sum_{a_{fp}}$	5	U-238	20
S.S.	6	Pu-239	21
Ni	7	Pu-240	22
Nb	8	Pu-241	23
Al	9	Pm-149	24
Sn	10	I-135	25
Cr	11	Sm-149	26
Co	12	Xe-135	27
Cd	13	Fission Products	28
H_f	14	B-10	29
			30

REFERENCES

1. O. J. Marlowe, P. A. Ombrellaro, "Candle-A One Dimensional Few-Group Depletion Code for the IBM-704," WAPD-TM-53, May, 1957.

2. O. J. Marlowe, P. A. Ombrellaro, "Candle-A One Dimensional Few-Group Depletion Code for the IBM-704, Addendum 1, Candle-2," WAPD-TM-53 Add. 1, October, 1957.

3. H. N. Lerman, "Candle Input and Output Instructions for the Depletion Code - Candle-2," AP Note 268, Alco Products, Inc., June 10, 1960.

```
1&099&04&000-1-1&1-1&47500&00000&2&1&1-1&003-1&08&05&12&00000534&00
2&54250536866&0000000 0 &          &          &          &
3&52206500006&51364200006&0000     &          &          &5211579000
4&00000 -   &          &          &          &
5&00000     &          &          &                     5339451200
6&00000     &          &          &          &
7&0000      &          &          &          &542281118966&0000000000
8&501973530006&000000   &          &          &511000000006&5117628140
9&00000 0   &          &          &          &
10&00000    &          &          &                     5338553843
11&514000000006&0       &          &          &          &
12&0000     &          &572600000006&521100000006&542277012366&0000000000
13&538010345006&0000000  &          &          &          &
14&533256236866&0000000 0 &          &          &          &
15&495990000006&00000    &          &          &          &
16&00000&55252&1&0&1&1&1&1&1&1&1&1&1&1&1&1&1&00000000000
17&28&44&72&98&0000000000
18&2&30&70&42&000000000
19&00000000  &          &          &          &
20&51125556806&51125556806&51125556806&51125556806&00000000006&
21&00000 0000&503000000006&504000000006&00       &          &
22&57459900006&57459900006&57459900006&57459900006&57459900006&5745990000
23&57459900006&57459900006&57459900006&57459900006&57459900006&5745990000
24&581000000006&581000000006&581000000006&581000000006&581000000006&5810000000
25&581000000006&581000000006&581000000006&581000000006&581000000006&5810000000
26&49775600006&49775600006&49775600006&000000    &          &
27&48446500006&00000      &          &          &          &
28&48659300006&48659300006&48659300006&48659300006&000000    &
29&51100000006&51100000006&51100000006&51100000006&00        &
30&511000000006&0         &          &          &          &
31&1&06&0000000
32&49558066676&49443984296&49443984296&49558066676&00000000006&
33&2&06&00000000
34&49279033336&49231195006&49231195006&49279033336&00000000006&
35&5&2&3&00000000
36&48857300006&48857300006&0000      &          &          &
37&6&2&3&0000000000
38&49148187706&49148187706&000000000 &          &          &
39&18&2&3&000000000
40&47428631606&47428631606&000000000 &          &          &
41&26&2&3&000000000
42&43435887706&43435887706&000000000 &          &          &
```

```
43&27&2&3&000000000
44&00000     &          &          &          &
45&29&2&3&000000000
46&4570492000&4570492000&0000000    &          &          &
47&18&2&3&000000000
48&5094000000&5094000000&000        &          &          &
49&27&2&3&000000000
50&5095730100&5095730100&0000000    &          &          &
51&29&2&3&000000000
52&5094000000&5094000000&000        &          &          &
53&32&2&3&000000000
54&5094000000&5094000000&000        &          &          &
55&34&2&3&000000000
56&5094000000&5094000000&000        &          &          &
```

```
5340000000000000 SIGMA LAMDA*POWER*FLUXS*INMOD*NODEN GSELF
5340000001000001 SIGMA LAMDA*POWER*FLUXS*INMOD*NODEN GSELF
5340000004000004 SIGMA LAMDA*POWER*FLUXS*INMOD*NODEN GSELF
5340000007000007 SIGMA LAMDA*POWER*FLUXS*INMOD*NODEN GSELF
5340000010000010 SIGMA LAMDA*POWER*FLUXS*INMOD*NODEN GSELF
5340000012000012 SIGMA LAMDA*POWER*FLUXS*INMOD*NODEN GSELF
```

APPENDIX C

APPENDIX C.

REFERENCE PARAMETERS FOR SM-1 CORE I

During the course of the analysis performed under Subtask 2.3 of the PWR Support Program, slightly revised estimates of material contents and geometrical parameters became available; in addition, with the completion of the BOBCAT, IBM-650 code,[1] a more detailed analysis of the core composition and nuclear properties was feasible. Accordingly, the BOBCAT code was utilized to compute the atomic composition and nuclear parameters for the SM-1 Core I elements at start of life. The fast parameters were calculated by the MUFT-III code, using the cross sectional files listed in Appendix F, for both the P-1 and P1-SG slowing down approximations. For the cold ($68^{o}F$) and hot ($440^{o}F$) operating cores, with a system pressure of 1200 psia, 59 and 58 energy groups were used, respectively. The thermal parameters were computed by the P_3 theory codes [2],[3] presently used for the stationary and control rod fuel elements. The microscopic cross sections needed as input to the P_3 theory codes have been averaged over a hardened Maxwell-Boltzmann neutron distribution. The effective hardened neutron energies for the cold ($68^{o}F$) and hot ($440^{o}F$) SM-1 Core I at 0 MWYR are 0.0331 ev and 0.0549 ev, respectively.

The reference modified two group nuclear parameters, as calculated by the methods described above, are listed in the tables on the following pages; also included are the best estimates of geometrical and material data. Comparison of these parameters to various others reported earlier in this report will reveal minor deviations; however, checks were made to verify that the effects of the revised parameters are negligible upon the analysis reported in the preceding chapters. To be even more accurate, it is recommended that the parameters listed in this appendix be utilized for future calculations.

TABLE C.1
MATERIAL AND GEOMETRICAL DATA FOR SM-1 CORE ELEMENTS

Geometrical - Core	
Core configuration	7 x 7 (Corners Missing)
Cell size, in.	2.9375 x 2.9375
Active core height, in.	21.75
Equivalent diameter, in.	22.2
Number of cells	45
Control rod cells	7
Stationary element cells	38
Material Composition - Core	
Fuel	Highly enriched UO_2
Burnable Poison	Natural boron in B_4C
Stainless Steel	
Cladding and Side Plates	304 L
Fuel Matric	302 B
Absorber Material	Originally B_4C, later changed to Eu_2O_3
Approximate Densities of Pure Materials	
UO_2, gms/cm^3	10.9
B_4C, gms/cm^3	2.535
Stainless Steel	
304 L	7.90
302 B	7.56

Geometrical - Elements

	Fixed Element	Control Fuel Element
Number in core	38	7
Number of fuel plates	18	16
Fuel Plates		
Active length, in.	21.75	21.75
Dead edge, in.	0.117	0.117
Active width, in.	2.54	2.318
Clad thickness, in.	0.005	0.005
Active thickness, in.	0.0195	0.0195
Side Plates		
Thickness, in.	0.05	0.05
Width, in.	2.863	2.619
Groove depth, in.	0.025	0.025
Control Rod Basket		
Outer width, in.	------	2.781
Thickness, in.	------	0.05

Material Composition

UO_2 per fuel plate, gm	35.092	32.014
U per fuel plate, gm	30.751	28.054
U-235 per fuel plate, gm	28.62	26.11
B_4C per fuel plate, gm	0.1439	0.1313
B per fuel plate, gm	0.1092	0.0997
B-10 per fuel plate, gm	0.0200	0.0183
w/o UO_2 in fuel matrix, %	25.9601	25.9522
w/o B_4C in fuel matrix, %	0.1065	0.1065
w/o SS in fuel matrix, %	73.9334	73.9413
w/o B in fuel matrix, %	0.0808	0.0808

w/o B-10 in fuel matrix, %	0.0148	0.0148
w/o U in fuel matrix, %	22.7488	22.7419
w/o U-235 in fuel matrix, %	21.1723	21.1659
a/o U-235 in fuel matrix, %	5.6181	5.6162
a/o B in fuel matrix, %	0.4662	0.4662
a/o B-10 in fuel matrix, %	0.0923	0.0923
U-235 per fuel element, gm	515.16	417.76
B-10 per fuel element, gm	0.36054	0.29248
Stainless Steel per fuel element, gm	4200.36	5024.79
Mass of H_2O per fuel element, gm		
68°F, 1200 psia	2456.77	2369.33
440°F, 1200 psia	2051.93	1978.90
Total U-235 in the core, kg	22.5	
Total B-10 in the core, gm	15.748	

Volumes - Elements

Total element volume, $in.^3$	187.6787	187.6787
Dead region, in^3	25.3965	56.0356
Active region, $in.^3$	162.2822	131.6431
Water in active region, $in.^3$	132.9471	107.8465
SS in active region, $in.^3$	23.8400	19.3400
Water in dead region, $in.^3$	16.7793	36.5513
SS in dead region, $in.^3$	8.6172	19.4843
Metal to water volume ratio	0.253	0.300

TABLE C-2
ATOMIC NUMBER DENSITIES * FOR SM-1 CORE I ELEMENTS

(0 MWYR, 1200 psia)

Number Densities (atoms/cm^3)*

		Stationary Element		Control Rod Fuel Element	
		T = 68°F	T = 440°F	T = 68°F	T = 440°F
H	(x 10^{-24})	0.053408	0.044609	0.051508	0.043021
0	(x 10^{-24})	0.027625	0.023226	0.026501	0.022258
U-235/	(x 10^{-22})	0.042908	0.042908	0.034796	0.034796
U-238/	(x 10^{-22})	0.003155	0.003155	0.003155	0.002558
B-10//	(x 10^{-20})	0.070494	0.070494	0.057187	0.057187
B natural //	(x 10^{-20})	0.356030	0.356030	0.288823	0.288823
SS///	(x 10^{-24})	0.014594	0.014594	0.017503	0.017503
Fe	(x 10^{-24})	0.010154	0.010154	0.012142	0.012142
Ni	(x 10^{-24})	0.001277	0.001277	0.001525	0.001525
Cr	(x 10^{-24})	0.002929	0.002929	0.003531	0.003531
Mn	(x 10^{-24})	0.000234	0.000234	0.000305	0.000305

---

* Atomic number densities are given as atoms per cm^3 of fuel element.

/ Based upon 87.63 w/o U in UO_2 and 93.07 w/o U-235 in U.

// Based upon 75.9 w/o B in B_4C and 19.8 a/o B-10 in B.

The boron densities listed reflect a 22.4% average fabrication loss.

/// Stainless steel assumed to be composed only of Fe, Ni, Cr and Mn.

TABLE C-3

THERMAL PARAMETERS * FOR SM-1 CORE I ELEMENTS

(0 MWYR, 1200 psia)

Parameter	Units	Stationary Element		Control Rod Fuel Element	
		T = 68°F (En=0.0331 ev)	T = 440°F (En=0.0549 ev)	T = 68°F (En=0.0331 ev)	T = 440°F (En=0.0549 ev)
Σ_a**	cm^{-1}	0.266078	0.205902	0.221898	0.173456
Σ_s	cm^{-1}	2.100701	1.540316	2.048670	1.516377
Σ_{tr}	cm^{-1}	1.961792	1.351166	1.884407	1.308841
$\nu\Sigma_f$	cm^{-1}	0.415949	0.323948	0.317678	0.251908
K_t	----	1.563258	1.573311	1.431640	1.452290
D	cm	0.169913	0.246700	0.176890	0.254678
L^2	cm^2	0.638581	1.198146	0.797170	1.468261
Σ_a^{xe} /	cm^{-1}	-------	.006975	--------	--------
g' //	---	0.910110	0.942506	--------	--------

---

* Caculated by the P_3 theory codes [2], [3] using microscopic cross section averaged over a hardened Maxwell-Boltzmann energy distribution (E_n).

** Does not include Σ_a^{xe}

/ Calculated using parameters given in this report and methods described in APAE No. 65, [4] at a power level of 10 Mwt for the entire core.

// Average flux in fuel plate divided by average flux in fuel element.

TABLE C-4

FAST PARAMETERS* OF COLD CLEAN SM-1 CORE I ELEMENTS

(o MWYR, T= 68°F, 1200 psia)

(B = 0.0845 cm^{-1})

Parameter	Units	Stationary Element		Control Rod Fuel Element	
		P-1 Model /	P-1 SG Model //	P-1 Model /	P-1SG Model //
τ	cm^2	30.310198	34.247459	30.912692	34.672212
$\Sigma_t = D/\tau$	cm^{-1}	0.040765	0.041181	0.039466	0.039837
D	cm	1.235593	1.410353	1.220002	1.381242
Σ_a	cm^{-1}	0.010168	0.010238	0.009182	0.009237
$\nu\Sigma_f$	cm^{-1}	0.013213	0.013340	0.010882	0.010979
K_f	----	1.299538	1.302989	1.185177	1.188564
p	----	0.750579	0.751386	0.767350	0.768125

* Computed by the MUFT-III code, using files listed in Appendix F, for cold clean core (59 energy groups).

/ Computed by use of P-1 slowing down approximation.

// Computed by use of P-1 SG slowing down approximation.

TABLE C-5

FAST PARAMETERS* OF HOT CLEAN SM-1 CORE I ELEMENTS

(0 MWYR, T = 440°F, 1200 psia)

(B^2 = .006594 cm^{-2})

Parameter	Units	Stationary Element		Control Rod Fuel Element	
		P-1 Model /	P1-SG Model //	P-1 Model /	P1-SG Model //
τ	cm^2	41.190926	46.021892	41.728927	46.295430
$\Sigma_T = D/\tau$	cm^{-1}	0.034501	0.034901	0.033428	0.033781
D	cm	1.421115	1.606221	1.393915	1.563902
Σ_a	cm^{-1}	0.009285	0.009360	0.008413	0.008471
$\nu\Sigma_f$	cm^{-1}	0.012012	0.012142	0.009902	0.010000
K_f	----	1.293656	1.297238	1.177021	1.180550
p	----	0.730866	0.731819	0.748323	0.749236

* Computed by the MUFT-III, using files listed in Appendix F for hot clean core (58 energy groups)

/ Computed by use of P-1 slowing down approximation.

// Computed by use of P-1 SG slowing down approximation

TABLE C.6
XENON PARAMETERS FOR SM-1 CORE I*, 0 MWYR

($T = 440^{o}F$, $E_n = 0.0549$ ev)

Parameter	Units	Description	Value
λ_I	sec^{-1}	Decay constant of iodine	2.89×10^{-5}
λ_{xe}	sec^{-1}	Decay constant of xenon	2.09×10^{-5}
γ_I	------	Fractional fission yield of iodine	0.060
γ_{xe}	------	Fractional fission yield of xenon	0.0029
δ	fission/watt	Fissions per watt per second	3.2175×10^{10}
α	------	Non-uniform distribution factor	1.13
g'	------	Self-shielding factor	.942506
P	watts	Thermal power	1×10^{7}
V	cm^3	Active core volume	1.3999×10^{5}
$\sum_a^{xe}$	cm^2	Xenon thermal absorption cross section	2.5×10^{-18}
$\sum_f$	cm^{-1}	Macroscopic fission cross section of core	.13169
β	------	Fraction of thermal fissions	.82439

* Refer to APAE No. 65, Appendix A.[4]

REFERENCES (APPENDIX C)

1. Bobe, P. E. and Caton, R. L., "BOBCAT (Program #56) Code Preparation Analysis on the IBM-650," APAE Memo No. 289, August 9, 1961.

2. Byrne, B. J., and Caton, R. L., "Two-Dimensional P_3 Calculation for APPR Type Fixed Fuel Elements," AP Note No. 96, Alco Products, Inc. February 14, 1958.

3. Caton, R. L. et al. "P-3 Approximation on the IBM-650," AP Note No. 85, Alco Products, Inc., November 13, 1957.

4. Bobe P. E. editor, "Interim Report of Nuclear Analysis Performed on SM-2 Core and Vessel, September 1, 1958 - December 31, 1959," APAE No. 65, May 27, 1960.

APPENDIX D

APPENDIX D
DISCUSSION OF Xe CROSS-SECTION AND NON-UNIFORM Xe FACTOR

Since the calculations in Section 5.0 were performed, there has been evidence that the Xe cross-section used is rather low. Following Westcott's formulation[1] i.e.

$$\bar{\sigma} = \frac{\sqrt{\pi}}{2}\sqrt{\frac{T_o}{T}}\,\hat{\sigma}$$

where $\hat{\sigma} = \sigma_o (g + rs)$ and $\sigma_o = \sigma(.0253\ ev)$

g is the non 1/v factor and rs accounts for the epithermal region. Values of $\hat{\sigma}$ have been measured by crystal spectrometer (Bernstein) and fast chopper (Smith) and given as function of T^{o} K Fig. 1. For the SM-1 core at 440°F we get:

$$T_n/T_o = 1 + A\,\frac{\sum a_{th}}{\xi \sum s} = 1.284^{(2)}$$

Hence:

$$\bar{\sigma} = 2.99\,\frac{10^6}{1.128}\sqrt{\frac{1}{1.284}} = 2.34 \times 10^6 \text{ barns (Bernstein)}$$

$$\bar{\sigma} = 3.23\,\frac{10^6}{1.128}\sqrt{\frac{1}{1.284}} = 2.60 \times 10^6 \text{ barns (Smith)}$$

The strong dependence of $\hat{\sigma}$ on T implies that the energy distribution of the neutron flux in the neighborhood of Xe must be accurately known for an accurate estimate of the Xe cross-section. Calculated Wigner-Wilkins spectra*[3] show a strong decrease of $\bar{\sigma}$ upon U-235 content in a homogeneous mixture, as can be seen in Fig. D.2 for 440°F. It is therefore necessary to assign an "effective" U-235 atom content as well as geometry. This problem however, cannot successfully be solved by diffusion techniques.

The effect of the non-uniform distribution of Xe poison on reactivity can be expressed in terms of the non-uniform factor α defined in such a way that $\alpha\delta\sum_a^{Xe}$ would give the amount of change in uniform absorption that will result in the same change in reactivity.

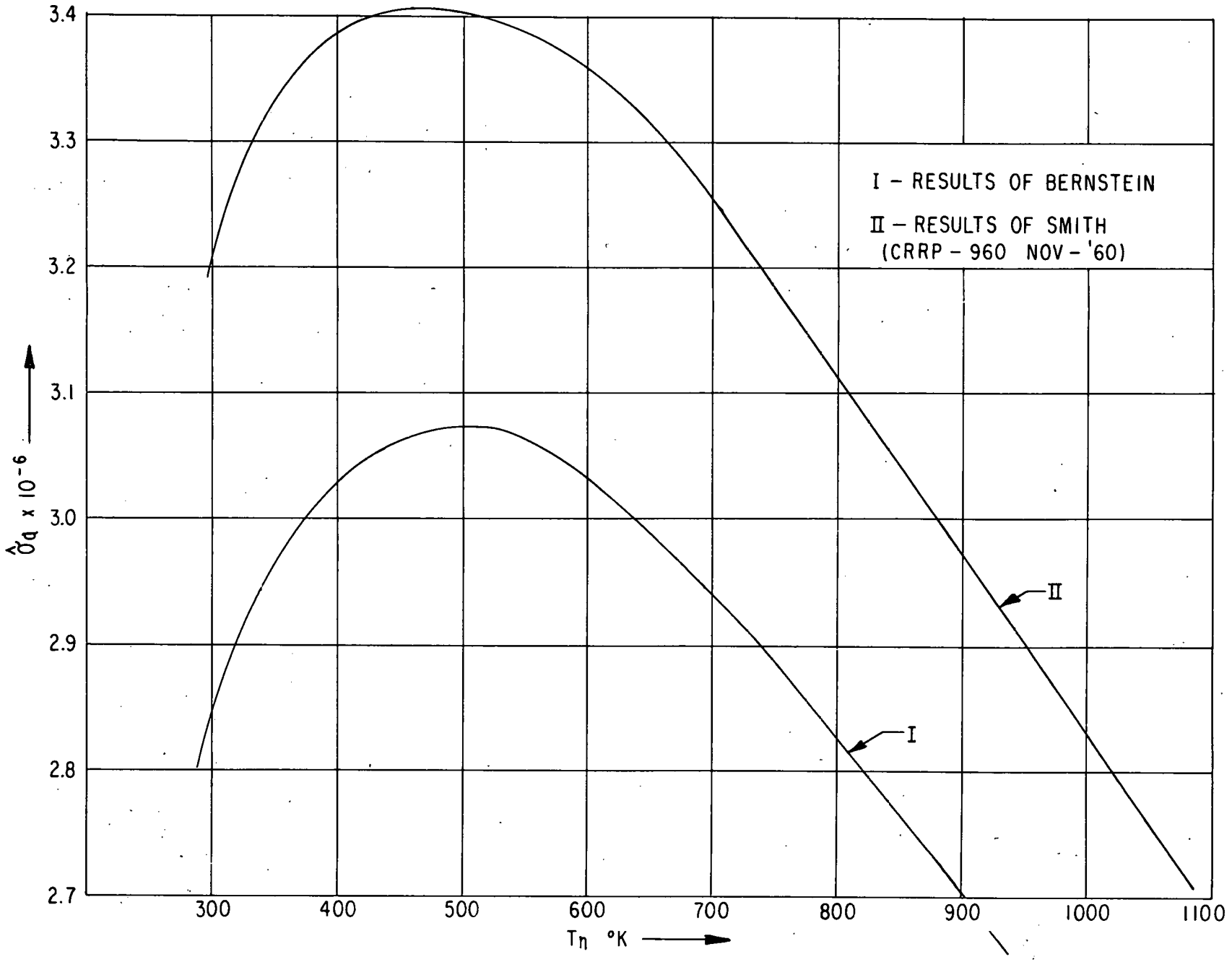

Figure D.1 Effective Xe-135 Cross Section $\hat{\sigma}_a$ vs. Effective Neutron Temperature T_n °K

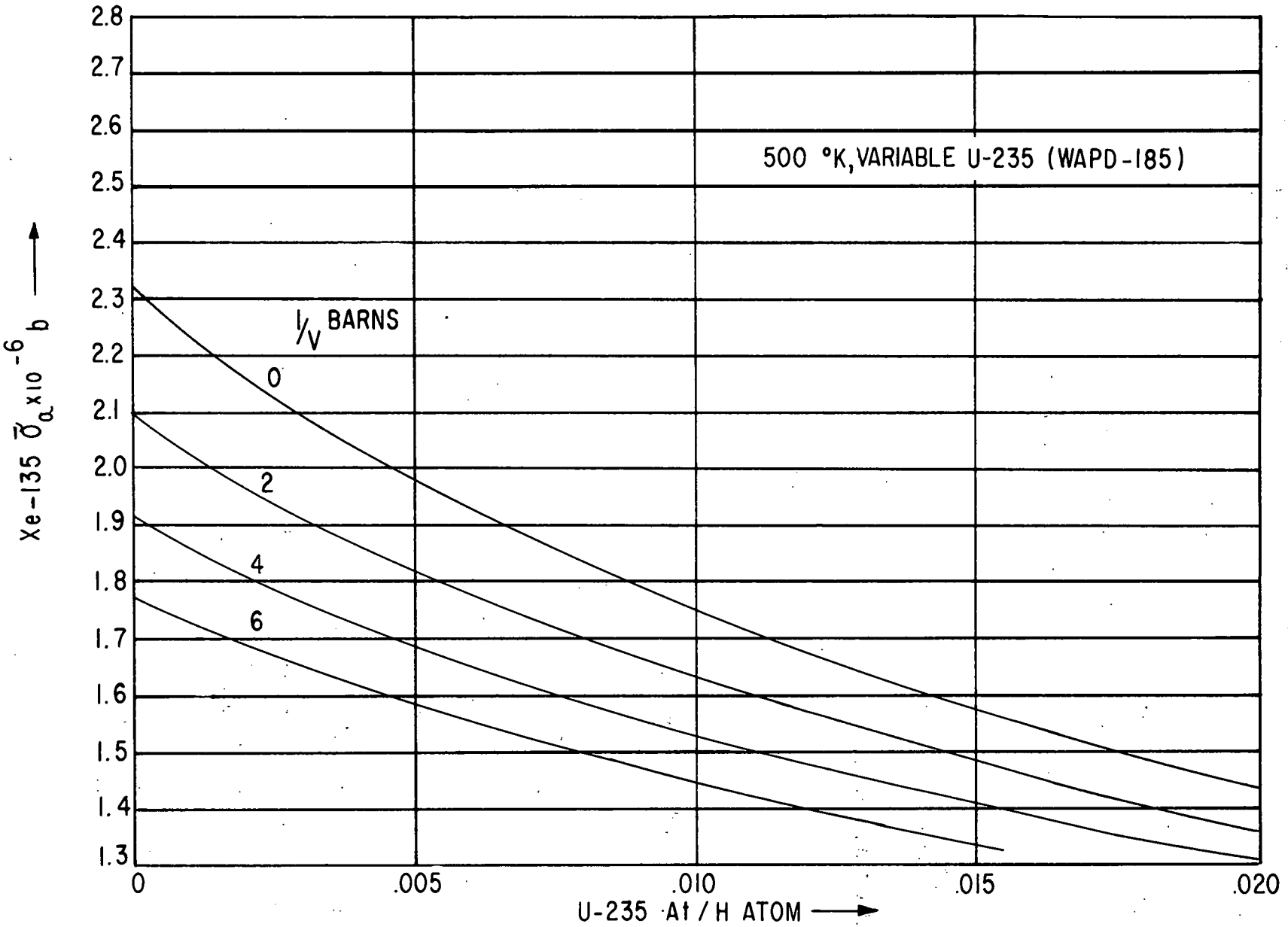

Figure D. 2 Average Xe-135 Absorption vs. U-235/H Atom Ratio

If we employ again perturbation techniques for a bare equivalent system:

$$\delta K = - \frac{1}{1 + L^2 B^2} \frac{\int \frac{\delta \sum a_{th}(x)}{\sum a_{th}(x)} d^2(x)\, dV}{\int \phi^2(x)\, dV}$$

where ϕ is the thermal flux and the local poison is:

$$\delta \sum a_{th}(x) = N_{xe} \cdot \delta \bar{x}e = \frac{Y \phi(x) \sum f_{th}}{\phi_1 + \phi(x)}$$

Substituting above we obtain:

$$\delta K = - \frac{1}{1 + L^2 B^2} \frac{\frac{\phi^3(x)}{\phi_1 + \phi(x)} \frac{\sum f_{th}}{\sum a_{th}} dV}{\int \phi^2(x)\, dV}$$

In the case of the uniform flux $\bar{\phi} = \frac{cp}{V \sum f_{th}}$

and $\delta \sum_a^{xe}{}_{eq} = \frac{\alpha Y \bar{\phi} \sum f_{th}}{\phi + \bar{\phi}}$ and

$$\delta K_{eq} = - \frac{1}{\sum a_{th} (1 + L^2 B^2)} \frac{\alpha Y \bar{\phi} \sum f_{th}}{\phi_1 + \bar{\phi}}$$

where $c = 3.121 \times 10^{10}$ fission/sec watt

P, V, $\sum_f$, core power, volume and fission cross-section respectively.
If we set $\delta K = \delta K_{eq}$ we obtain:

$$\alpha = \frac{\phi_1 + \bar{\phi}}{\bar{\phi}} \frac{\sum a_{th}}{\sum f_{th}} \frac{\int \frac{\sum f_{th}(x)}{\sum a_{th}(x)} \frac{\phi^3(x)}{\phi_1 + \phi(x)} dV}{\int \phi^2(x)\, dV}$$

In the case of no burnup

$$\Sigma_{f_{th}}(x) \cdot \Sigma_{a_{th}}(x) = \text{const}$$

therefore:

$$\alpha = \frac{\phi_1 + \bar{\phi}}{\bar{\phi}} \qquad \frac{\int \frac{\phi^3(x)}{\phi_1 + \phi(x)}\, dV}{\int \phi^2(x)\, dV}$$

Numerical integration over the thermal flux distribution at 0 MWYR (obtained from multiregion calculation and close to the experimental) leads to the values of $\alpha_{rad} = 1.0421$ and $\alpha_{ax} = 1.088$ then the overall $\alpha = \alpha_{rad}\ \alpha_{ax} = 1.134$.

At an appreciable burnup where $\Sigma_{f_{th}}(x)$ and $\Sigma_{a_{th}}(x)$ can no longer be considered as constants the former expression for α must be used where $\Sigma_{a_{th}}$ and $\Sigma_{f_{th}}$ must be flux and volume weighted.

Let us now use one group flux distribution to evaluate α i.e., if

$$\phi(r) = J_o\left(\frac{j_o\, r}{R'}\right) \quad \text{and}$$

$\phi(z) = A \sin B z$ for the core region and

$\phi_r(z) = C \sinh K(H'-z)$

Then we obtain $\alpha = 1.477$

This indicates the dependence of reactivity due to xenon poisoning upon the flux distribution. At high burnup however the representation of the flux as it has been done in Section A.1 is obviously on approximation, then the disagreement between calculated and experimental values should not be surprising.

SUMMARY

Perturbation techniques were employed to evaluate the non-uniform distribution factor for xenon in SM-1 Core I at 0 MWYR.

It has been found that the xenon concentration due to an average power must be multiplied by 1.134 to give the reactivity effect due to the non-uniform distribution of xenon. An evaluation of the xenon microscopic absorption cross section based on the latest data leads to the value of $\bar{\sigma}_a^{Xe} = 2.34 - 2.60 \times 10^6$ barns.

REFERENCES

1. Westcott, C. H., "Effective Cross Section Values for Well Moderated Thermal Reactor Spectra," CRRP-960, November 1960.

2. Bobe, P. E., editor, "Interim Report of Nuclear Analysis Performed on SM-2 Core and Vessel, September 1, 1959 - December 31, 1959," APAE No. 65, May 29, 1960.

3. Amster, H. T., "A Compendium of Thermal Neutron Cross Sections Averaged Over the Spectra of Wigner and Wilkins," WAPD-185, January 1958.

APPENDIX E

APPENDIX E. NOMENCLATURE

Symbol		Definition	Units
T_n	=	Effective neutron temperature	^oK
T, T_o	=	Temperature of the assembly	^oK
C	=	A constant = .91	
Σ_a	=	Macroscopic absorption cross-section at $\Sigma_o = KT$	cm^{-1}
$\xi\Sigma_s$	=	$\sum_{i=1}^{i=n} \xi^i \Sigma_s^i$	cm^{-1}
η	=	Number of elements present	
Σ_s	=	Macroscopic scattering cross-section	cm^{-1}
ξ^i	=	Average logarithmic energy decrement for element;	
H	=	Height of the active core	cm
R	=	Equivalent radius of the active core	cm
δ_z	=	Axial reflector savings, including extrapolation distance	cm
δ_r	=	Radial reflector savings including extrapolation distance	cm
S_f	=	Fast neutron source	N/cm^3-sec
S_t	=	Thermal neutron source	N/cm^3-sec
ψ	=	Fraction of thermal fissions	
p	=	Resonance escape probability	
τ	=	Age of fission neutrons to thermal energy	cm^2
τ_w	=	Age of fission neutrons to thermal energy in water	cm^2

Symbol		Definition	Units
L	=	Thermal diffusion length	cm
B^2	=	Core buckling	cm^{-2}
D_f	=	Fast neutron group diffusion coefficient	cm
Σ_{Tf}	=	Total macroscopic cross-section for the fast neutron group	cm^{-1}
Σ_{a_f}	=	Macroscopic absorption cross-section for the fast neutron group	cm^{-1}
ν	=	Number of neutrons per fission	
Σ_{sl}	=	Slowing down cross-section	cm^{-1}
Σ_{f_f}	=	Macroscopic fission cross-section for the fast neutron group	cm^{-1}
K_f	=	Fast neutron group multiplication	
D_{th}	=	Thermal neutron group diffusion coefficient	cm
$\Sigma_{a_{th}}$	=	Macroscopic absorption cross-section for the thermal neuttron group	cm^{-1}
$\Sigma_{f_{th}}$	=	Macroscopic fission cross-section for the thermal neutron group	cm^{-1}
K_{th}	=	Thermal neutron group multiplication factor	
$\Sigma_{a_{fp}}$	=	Macroscopic absorption cross-section of the fission products	cm^{-1}
ρ	=	Core reactivity	
N_{xe}	=	Xenon number density	$atoms/cm^3$
N_I	=	Iodine number density	$atoms/cm^3$
λ_I	=	Decay constant of I-135	sec^{-1}
λ_{xe}	=	Decay constant of Xe-135	sec^{-1}

Symbol		Definition	Units
Y_I	=	Fission fractional yield of I-135	
Y_{xe}	=	Fission fraction yield of Xe-135	
ϕ		Thermal neutron flux	N/cm^2-sec
β	=	Ratio of thermal fissions to total fissions	
ϕ_f	=	Fast neutron flux	N/cm^2-sec
L_f	=	Fast neutron leakage	
L_{th}	=	Thermal neutron leakage	
K_{eff}	=	Effective neutron multiplication	
α_T	=	Temperature coefficient	$^oF^{-1}$
B	=	Fuel burnup fraction (B = 0 at start of life)	
V		Core volume	cm^3
$\bar{\sigma}_a^{xe}$	=	Average xenon thermal absorption cross-section	barns
δ	=	Fissions /watt-sec	
α	=	Xenon non-uniform distribution factor	
P_{Mw}	=	Reactor power in megawatts	
g' (B)	=	Average flux in fuel plate divided by the average flux in the entire fuel element	

APPENDIX F

APPENDIX F

THE MUFT-III CROSS SECTION FILES

An evaluation of the agreement between calculated and experimental nuclear quantities using MUFF-III cross section files was made in Section 3.0.

The inelastic scattering matrix in iron has been determined by using known cross sections for the (n, n', γ) reaction to various levels from the threshold at 0.85 Mev to about 4 Mev. At higher incident neutron energies the slowing down distributions have been determined by using more recent values of the "Nuclear temperature."(1)

The behavior of neutrons scattered elastically is described by means of μ_0 the average cosine of the angle between the direction of the incident and scattered neutron and ξ, the average loss in the logarithmic energy decrement. In order to account for anisotropic scattering events in the center of mass system, the elastic slowing down distributions of scattered neutrons have been determined by using known angular distributions.

The total cross section curve for iron indicates that there are unresolved resonances between 0.008 to 10 Mev. These are mainly scattering, since there are no sharp peaks. However, the measured resonance integral for iron, 2.1 barns, is higher than the value 1.26 barns to be expected if the iron cross section followed a 1/2 behavior.

The MUFT-III energy-lethargy group structure is given in references (2) and (3).

REFERENCES

1. Rosen, L., and Stewart, L., "The Determination of Nuclear Temperatures by Means of the Evaporation Model," LA-1560, August 18, 1953.

2. Bobe, P.E., editor, "Interim Report of Nuclear Analysis Performed on SM-2 Core and Vessel, September 1, 1958, December 31, 1959," APAE No. 65, May 27, 1960.

3. Byrne, B. J., and Oby, P. V., "Analysis of Extended Zero Power Experiments on the Army Package Power Reactor - ZPE-2," APAE No. 27, May 7, 1958.

FILE NO 01 HYDROGEN

GROUP	$\bar{\mu}$	$\bar{\xi}$	$\bar{\sigma}_{s0} \times 10^{-1}$	$\bar{\sigma}_c^s$	$\bar{\sigma}_{in}$	$\bar{\sigma}_F$	ν	Δu
1	.666666	0.000000	.102500	.0000	.000	.00000	.0000	.25000
2	.666666	0.000000	.126250	.0000	.000	.00000	.0000	.25000
3	.666666	0.000000	.154250	.0000	.000	.00000	.0000	.25000
4	.666666	0.000000	.183250	.0000	.000	.00000	.0000	.25000
5	.666666	0.000000	.216500	.0000	.000	.00000	.0000	.25000
6	.666666	0.000000	.253500	.0000	.000	.00000	.0000	.25000
7	.666666	0.000000	.293250	.0000	.000	.00000	.0000	.25000
8	.666666	0.000000	.337250	.0000	.000	.00000	.0000	.25000
9	.666666	0.000000	.387000	.0000	.000	.00000	.0000	.25000
10	.666666	0.000000	.443500	.0000	.000	.00000	.0000	.25000
11	.666666	0.000000	.506500	.0000	.000	.00000	.0000	.25000
12	.666666	0.000000	.575000	.0000	.000	.00000	.0000	.25000
13	.666666	0.000000	.652500	.0000	.000	.00000	.0000	.25000
14	.666666	0.000000	.737500	.0000	.000	.00000	.0000	.25000
15	.666666	0.000000	.827500	.0000	.000	.00000	.0000	.25000
16	.666666	0.000000	.928000	.0000	.000	.00000	.0000	.25000
17	.666666	0.000000	1.040500	.0000	.000	.00000	.0000	.25000
18	.666666	0.000000	1.155000	.0000	.000	.00000	.0000	.25000
19	.666666	0.000000	1.275000	.0000	.000	.00000	.0000	.25000
20	.666666	0.000000	1.395000	.0000	.000	.00000	.0000	.25000
21	.666666	0.000000	1.537500	.0000	.000	.00000	.0000	.50000
22	.666666	0.000000	1.725000	.0000	.000	.00000	.0000	.50000
23	.666666	0.000000	1.900000	.0000	.000	.00000	.0000	.50000
24	.666666	0.000000	1.987500	.0000	.000	.00000	.0000	.50000
25	.666666	0.000000	2.000000	.0000	.000	.00000	.0000	.50000
26	.666666	0.000000	2.005000	.0000	.000	.00000	.0000	.50000
27	.666666	0.000000	2.015000	.0000	.000	.00000	.0000	.50000
28	.666666	0.000000	2.035000	.0000	.000	.00000	.0000	.50000
29	.666666	0.000000	2.050000	.0000	.000	.00000	.0000	.50000
30	.666666	0.000000	2.050000	.0000	.000	.00000	.0000	.50000
31	.666666	0.000000	2.050000	.0000	.000	.00000	.0000	.50000
32	.666666	0.000000	2.050000	.0000	.000	.00000	.0000	.50000
33	.666666	0.000000	2.050000	.0000	.000	.00000	.0000	.25000
34	.666666	0.000000	2.050000	.0000	.000	.00000	.0000	.25000
35	.666666	0.000000	2.050000	.0000	.000	.00000	.0000	.25000
36	.666666	0.000000	2.050000	.0000	.000	.00000	.0000	.25000
37	.666666	0.000000	2.050000	.0000	.000	.00000	.0000	.25000
38	.666666	0.000000	2.050000	.0000	.000	.00000	.0000	.25000
39	.666666	0.000000	2.050000	.0000	.000	.00000	.0000	.25000
40	.666666	0.000000	2.050000	.0000	.000	.00000	.0000	.25000

FILE NO 01 HYDROGEN

GROUP	$\bar{\mu}$	$\bar{\xi}$	$\bar{\sigma}_{s0} \times 10^{-1}$	$\bar{\sigma}_{c}^{s}$	$\bar{\sigma}_{in}$	$\bar{\sigma}_{f}$	ν	Δu
41	.666666	0.000000	2.050000	.0000	.000	.00000	.0000	.25000
42	.666666	0.000000	2.050000	.0000	.000	.00000	.0000	.25000
43	.666666	0.000000	2.050000	.0000	.000	.00000	.0000	.25000
44	.666666	0.000000	2.050000	.0000	.000	.00000	.0000	.25000
45	.666666	0.000000	2.050000	.0000	.000	.00000	.0000	.25000
46	.666666	0.000000	2.050000	.0000	.000	.00000	.0000	.25000
47	.666666	0.000000	2.050000	.0000	.000	.00000	.0000	.25000
48	.666666	0.000000	2.050000	.0000	.000	.00000	.0000	.25000
49	.666666	0.000000	2.050000	.0000	.000	.00000	.0000	.25000
50	.666666	0.000000	2.055000	.0000	.000	.00000	.0000	.25000
51	.666666	0.000000	2.065000	.0000	.000	.00000	.0000	.25380
52	.666666	0.000000	2.072500	.0000	.000	.00000	.0000	.24620
53	.666666	0.000000	2.087500	.0000	.000	.00000	.0000	.30000
54	.666666	0.000000	2.130000	.0000	.000	.00000	.0000	.28840
55	.666666	0.000000	2.180000	.0698	.000	.00000	.0000	.22300
56	.666666	0.000000	2.220000	.0781	.000	.00000	.0000	.22360
57	.666666	0.000000	2.260000	.0876	.000	.00000	.0000	.23800
58	.666666	0.000000	2.310000	.0899	.000	.00000	.0000	.23800
59	.666666	0.000000	2.370000	.1112	.000	.00000	.0000	.23900
60	.000000	0.000000	.000000	.0000	.000	.0000A	.0000	.0000A

FILE NO 02 OXYGEN

GROUP	$\bar{\mu}$	$\bar{N}$	$\bar{\sigma}_{so} \times 10^{-1}$	$\bar{\sigma}_c^s$	$\bar{\sigma}_{in}$	$\bar{\sigma}_f$	ν	Δu
1	.718000	0.040100	.051500	.2750	.000	.00000	.0000	.25000
2	.668000	0.040100	.086500	.2200	.000	.00000	.0000	.25000
3	.618000	0.046450	.071500	.1800	.000	.00000	.0000	.25000
4	.569250	0.053100	.159500	.1450	.000	.00000	.0000	.25000
5	.479250	0.064550	.203500	.0600	.000	.00000	.0000	.25000
6	.362500	0.081250	.139500	.0000	.000	.00000	.0000	.25000
7	.275750	0.092100	.162500	.0000	.000	.00000	.0000	.25000
8	.228000	0.096550	.308000	.0000	.000	.00000	.0000	.25000
9	.201000	0.099650	.443000	.0000	.000	.00000	.0000	.25000
10	.176250	0.102750	.389000	.0000	.000	.00000	.0000	.25000
11	.154000	0.105750	.322000	.0000	.000	.00000	.0000	.25000
12	.133950	0.108550	.520500	.0000	.000	.00000	.0000	.25000
13	.115700	0.110800	.626500	.0000	.000	.00000	.0000	.25000
14	.100800	0.112350	.458500	.0000	.000	.00000	.0000	.25000
15	.088800	0.113800	.381000	.0000	.000	.00000	.0000	.25000
16	.073750	0.115350	.365500	.0000	.000	.00000	.0000	.25000
17	.060000	0.116400	.357000	.0000	.000	.00000	.0000	.25000
18	.047500	0.117000	.351500	.0000	.000	.00000	.0000	.25000
19	.032500	0.117700	.350000	.0000	.000	.00000	.0000	.25000
20	.017500	0.118300	.350000	.0000	.000	.00000	.0000	.25000
21	.007500	0.118650	.350000	.0000	.000	.00000	.0000	.50000
22	.002500	0.118950	.350000	.0000	.000	.00000	.0000	.50000
23	.000000	0.119250	.360000	.0000	.000	.00000	.0000	.50000
24	.000000	0.119700	.372500	.0000	.000	.00000	.0000	.50000
25	.000000	0.120000	.377500	.0000	.000	.00000	.0000	.50000
26	.000000	0.120000	.380000	.0000	.000	.00000	.0000	.50000
27	.000000	0.120000	.380000	.0000	.000	.00000	.0000	.50000
28	.000000	0.120000	.380000	.0000	.000	.00000	.0000	.50000
29	.000000	0.120000	.380000	.0000	.000	.00000	.0000	.50000
30	.000000	0.120000	.380000	.0000	.000	.00000	.0000	.50000
31	.000000	0.120000	.380000	.0000	.000	.00000	.0000	.50000
32	.000000	0.120000	.380000	.0000	.000	.00000	.0000	.50000
33	.000000	0.120000	.380000	.0000	.000	.00000	.0000	.25000
34	.000000	0.120000	.380000	.0000	.000	.00000	.0000	.25000
35	.000000	0.120000	.380000	.0000	.000	.00000	.0000	.25000
36	.000000	0.120000	.380000	.0000	.000	.00000	.0000	.25000
37	.000000	0.120000	.380000	.0000	.000	.00000	.0000	.25000
38	.000000	0.120000	.380000	.0000	.000	.00000	.0000	.25000
39	.000000	0.120000	.380000	.0000	.000	.00000	.0000	.25000
40	.000000	0.120000	.380000	.0000	.000	.00000	.0000	.25000

FILE NO 02 OXYGEN

GROUP	$\bar{\mu}$	$\bar{\xi}$	$\bar{\sigma}_{s0} \times 10^{-1}$	$\bar{\sigma}_c^s$	$\bar{\sigma}_{in}$	$\bar{\sigma}_f$	ν	Δu
41	.000000	0.120000	.380000	.0000	.000	.00000	.0000	.25000
42	.000000	0.120000	.380000	.0000	.000	.00000	.0000	.25000
43	.000000	0.120000	.380000	.0000	.000	.00000	.0000	.25000
44	.000000	0.120000	.380000	.0000	.000	.00000	.0000	.25000
45	.000000	0.120000	.380000	.0000	.000	.00000	.0000	.25000
46	.000000	0.120000	.380000	.0000	.000	.00000	.0000	.25000
47	.000000	0.120000	.380000	.0000	.000	.00000	.0000	.25000
48	.000000	0.120000	.380000	.0000	.000	.00000	.0000	.25000
49	.000000	0.120000	.380000	.0000	.000	.00000	.0000	.25000
50	.000000	0.120000	.380000	.0000	.000	.00000	.0000	.25000
51	.000000	0.120000	.380000	.0000	.000	.00000	.0000	.25380
52	.000000	0.120000	.380000	.0000	.000	.00000	.0000	.24620
53	.000000	0.120000	.380000	.0000	.000	.00000	.0000	.30000
54	.000000	0.120000	.380000	.0000	.000	.00000	.0000	.28840
55	.000000	0.120000	.380000	.0000	.000	.00000	.0000	.22300
56	.000000	0.120000	.380000	.0000	.000	.00000	.0000	.22360
57	.000000	0.120000	.380000	.0000	.000	.00000	.0000	.23800
58	.000000	0.120000	.380000	.0000	.000	.00000	.0000	.23800
59	.000000	0.120000	.380000	.0000	.000	.00000	.0000	.23900
60	.000000	0.000000	.000000	.0000	.000	.0000A	.0000	.0000A

FILE NO 04 NATURAL BORON

GROUP	$\bar{\mu}$	$\bar{\xi}$	$\bar{\sigma}_{s0}$	$\bar{\sigma}_c^s \times 10^{-1}$	$\bar{\sigma}_{in}$	$\bar{\sigma}_f$	ν	Δu
1	.000000	0.000000	.000000	.0000	.000	.00000	.0000	.25000
2	.000000	0.000000	.000000	.0045	.000	.00000	.0000	.25000
3	.000000	0.000000	.000000	.0051	.000	.00000	.0000	.25000
4	.000000	0.000000	.000000	.0058	.000	.00000	.0000	.25000
5	.000000	0.000000	.000000	.0066	.000	.00000	.0000	.25000
6	.000000	0.000000	.000000	.0074	.000	.00000	.0000	.25000
7	.000000	0.000000	.000000	.0084	.000	.00000	.0000	.25000
8	.000000	0.000000	.000000	.0096	.000	.00000	.0000	.25000
9	.000000	0.000000	.000000	.0109	.000	.00000	.0000	.25000
10	.000000	0.000000	.000000	.0123	.000	.00000	.0000	.25000
11	.000000	0.000000	.000000	.0139	.000	.00000	.0000	.25000
12	.000000	0.000000	.000000	.0158	.000	.00000	.0000	.25000
13	.000000	0.000000	.000000	.0179	.000	.00000	.0000	.25000
14	.000000	0.000000	.000000	.0203	.000	.00000	.0000	.25000
15	.000000	0.000000	.000000	.0230	.000	.00000	.0000	.25000
16	.000000	0.000000	.000000	.0261	.000	.00000	.0000	.25000
17	.000000	0.000000	.000000	.0296	.000	.00000	.0000	.25000
18	.000000	0.000000	.000000	.0335	.000	.00000	.0000	.25000
19	.000000	0.000000	.000000	.0382	.000	.00000	.0000	.25000
20	.000000	.000000	.000000	.0431	.000	.00000	.0000	.25000
21	.000000	0.000000	.000000	.0516	.000	.00000	.0000	.50000
22	.000000	0.000000	.000000	.0663	.000	.00000	.0000	.50000
23	.000000	0.000000	.000000	.0852	.000	.00000	.0000	.50000
24	.000000	0.000000	.000000	.1095	.000	.00000	.0000	.50000
25	.000000	0.000000	.000000	.1405	.000	.00000	.0000	.50000
26	.000000	0.000000	.000000	.1816	.000	.00000	.0000	.50000
27	.000000	0.000000	.000000	.2333	.000	.00000	.0000	.50000
28	.000000	0.000000	.000000	.2979	.000	.00000	.0000	.50000
29	.000000	0.000000	.000000	.3822	.000	.00000	.0000	.50000
30	.000000	0.000000	.000000	.4902	.000	.00000	.0000	.50000
31	.000000	0.000000	.000000	.6300	.000	.00000	.0000	.50000
32	.000000	0.000000	.000000	.8090	.000	.00000	.0000	.50000
33	.000000	0.000000	.000000	.9813	.000	.00000	.0000	.25000
34	.000000	0.000000	.000000	1.1128	.000	.00000	.0000	.25000
35	.000000	0.000000	.000000	1.2616	.000	.00000	.0000	.25000
36	.000000	0.000000	.000000	1.4294	.000	.00000	.0000	.25000
37	.000000	0.000000	.000000	1.6190	.000	.00000	.0000	.25000
38	.000000	0.000000	.000000	1.8345	.000	.00000	.0000	.25000
39	.000000	0.000000	.000000	2.0786	.000	.00000	.0000	.25000
40	.000000	0.000000	.000000	2.3547	.000	.00000	.0000	.25000

FILE NO 04 NATURAL BORON

GROUP	$\bar{\mu}$	$\bar{w}$	$\bar{\sigma}_{s_0}$	$\sigma_c^s \times 10^{-1}$	$\bar{\sigma}_{in}$	$\bar{\sigma}_t$	ν	Δu
41	.000000	0.000000	.000000	2.6674	.000	.00000	.0000	.25000
42	.000000	0.000000	.000000	3.0226	.000	.00000	.0000	.25000
43	.000000	0.000000	.000000	3.4239	.000	.00000	.0000	.25000
44	.000000	0.000000	.000000	3.8787	.000	.00000	.0000	.25000
45	.000000	0.000000	.000000	4.3926	.000	.00000	.0000	.25000
46	.000000	0.000000	.000000	4.9650	.000	.00000	.0000	.25000
47	.000000	0.000000	.000000	5.6160	.000	.00000	.0000	.25000
48	.000000	0.000000	.000000	6.3800	.000	.00000	.0000	.25000
49	.000000	0.000000	.000000	7.2520	.000	.00000	.0000	.25000
50	.000000	0.000000	.000000	8.2180	.000	.00000	.0000	.25000
51	.000000	0.000000	.000000	9.3170	.000	.00000	.0000	.25380
52	.000000	0.000000	.000000	10.5600	.000	.00000	.0000	.24620
53	.000000	0.000000	.000000	12.0910	.000	.00000	.0000	.30000
54	.000000	0.000000	.000000	14.0060	.000	.00000	.0000	.28840
55	.000000	0.000000	.000000	15.9700	.000	.00000	.0000	.22300
56	.000000	0.000000	.000000	17.8600	.000	.00000	.0000	.22360
57	.000000	0.000000	.000000	20.0470	.000	.00000	.0000	.23800
58	.000000	0.000000	.000000	22.5920	.000	.00000	.0000	.23800
59	.000000	0.000000	.000000	25.4370	.000	.00000	.0000	.23900
60	.000000	0.000000	.000000	0.0000	.000	.00000	.0000	.00000

FILE NO 05 BORON 10

GROUP	$\bar{\mu}$	$\bar{\xi}$	$\bar{\sigma}_{s0}$	$\bar{\sigma}_c s \times 10^{-2}$	$\bar{\sigma}_{in}$	$\bar{\sigma}_t$	ν	Δu
1	.000000	0.000000	.000000	.0000	.000	.00000	.0000	.25000
2	.000000	0.000000	.000000	.0022	.000	.00000	.0000	.25000
3	.000000	0.000000	.000000	.0026	.000	.00000	.0000	.25000
4	.000000	0.000000	.000000	.0029	.000	.00000	.0000	.25000
5	.000000	0.000000	.000000	.0033	.000	.00000	.0000	.25000
6	.000000	0.000000	.000000	.0037	.000	.00000	.0000	.25000
7	.000000	0.000000	.000000	.0042	.000	.00000	.0000	.25000
8	.000000	0.000000	.000000	.0048	.000	.00000	.0000	.25000
9	.000000	0.000000	.000000	.0055	.000	.00000	.0000	.25000
10	.000000	0.000000	.000000	.0062	.000	.00000	.0000	.25000
11	.000000	0.000000	.000000	.0070	.000	.00000	.0000	.25000
12	.000000	0.000000	.000000	.0080	.000	.00000	.0000	.25000
13	.000000	0.000000	.000000	.0090	.000	.00000	.0000	.25000
14	.000000	0.000000	.000000	.0102	.000	.00000	.0000	.25000
15	.000000	0.000000	.000000	.0116	.000	.00000	.0000	.25000
16	.000000	0.000000	.000000	.0132	.000	.00000	.0000	.25000
17	.000000	0.000000	.000000	.0149	.000	.00000	.0000	.25000
18	.000000	0.000000	.000000	.0169	.000	.00000	.0000	.25000
19	.000000	0.000000	.000000	.0193	.000	.00000	.0000	.25000
20	.000000	0.000000	.000000	.0217	.000	.00000	.0000	.25000
21	.000000	0.000000	.000000	.0261	.000	.00000	.0000	.50000
22	.000000	0.000000	.000000	.0335	.000	.00000	.0000	.50000
23	.000000	0.000000	.000000	.0430	.000	.00000	.0000	.50000
24	.000000	0.000000	.000000	.0553	.000	.00000	.0000	.50000
25	.000000	0.000000	.000000	.0709	.000	.00000	.0000	.50000
26	.000000	0.000000	.000000	.0917	.000	.00000	.0000	.50000
27	.000000	0.000000	.000000	.1178	.000	.00000	.0000	.50000
28	.000000	0.000000	.000000	.1504	.000	.00000	.0000	.50000
29	.000000	0.000000	.000000	.1930	.000	.00000	.0000	.50000
30	.000000	0.000000	.000000	.2475	.000	.00000	.0000	.50000
31	.000000	0.000000	.000000	.3181	.000	.00000	.0000	.50000
32	.000000	0.000000	.000000	.4086	.000	.00000	.0000	.50000
33	.000000	0.000000	.000000	.4956	.000	.00000	.0000	.25000
34	.000000	0.000000	.000000	.5620	.000	.00000	.0000	.25000
35	.000000	0.000000	.000000	.6372	.000	.00000	.0000	.25000
36	.000000	0.000000	.000000	.7219	.000	.00000	.0000	.25000
37	.000000	0.000000	.000000	.8177	.000	.00000	.0000	.25000
38	.000000	0.000000	.000000	.9265	.000	.00000	.0000	.25000
39	.000000	0.000000	.000000	1.0498	.000	.00000	.0000	.25000
40	.000000	0.000000	.000000	1.1892	.000	.00000	.0000	.25000

FILE NO 05 BORON 10

GROUP	$\bar{\mu}$	$\bar{\xi}$	$\bar{\sigma}_{s0}$	$\bar{\sigma}_c^s \times 10^{-2}$	$\bar{\sigma}_{in}$	$\bar{\sigma}_f$	ν	Δu
41	.000000	0.000000	.000000	1.3472	.000	.00000	.0000	.25000
42	.000000	0.000000	.000000	1.5266	.000	.00000	.0000	.25000
43	.000000	0.000000	.000000	1.7292	.000	.00000	.0000	.25000
44	.000000	0.000000	.000000	1.9589	.000	.00000	.0000	.25000
45	.000000	0.000000	.000000	2.2185	.000	.00000	.0000	.25000
46	.000000	0.000000	.000000	2.5075	.000	.00000	.0000	.25000
47	.000000	0.000000	.000000	2.8363	.000	.00000	.0000	.25000
48	.000000	0.000000	.000000	3.2222	.000	.00000	.0000	.25000
49	.000000	0.000000	.000000	3.6626	.000	.00000	.0000	.25000
50	.000000	0.000000	.000000	4.1505	.000	.00000	.0000	.25000
51	.000000	0.000000	.000000	4.7055	.000	.00000	.0000	.25380
52	.000000	0.000000	.000000	5.3333	.000	.00000	.0000	.24620
53	.000000	0.000000	.000000	6.1065	.000	.00000	.0000	.30000
54	.000000	0.000000	.000000	7.0737	.000	.00000	.0000	.28840
55	.000000	0.000000	.000000	8.0656	.000	.00000	.0000	.22300
56	.000000	0.000000	.000000	9.0202	.000	.00000	.0000	.22360
57	.000000	0.000000	.000000	10.1247	.000	.00000	.0000	.23800
58	.000000	0.000000	.000000	11.4101	.000	.00000	.0000	.23800
59	.000000	0.000000	.000000	12.8469	.000	.00000	.0000	.23900

FILE NO 21 IRON

GROUP	$\bar{\mu}$	$\bar{\xi}$	$\bar{\sigma}_{so} \times 10^{-1}$	$\bar{\sigma}_{\epsilon}^{s}$	$\bar{\sigma}_{in}$	σ_t	ν	Δu
1	.850000	0.005400	.172000	.0820	1.380	.00000	.0000	.25000
2	.822000	0.006400	.203000	.0820	1.370	.00000	.0000	.25000
3	.751000	0.008900	.225000	.0820	1.350	.00000	.0000	.25000
4	.651000	0.016000	.229000	.0820	1.310	.00000	.0000	.25000
5	.542000	0.016000	.212000	.0820	1.180	.00000	.0000	.25000
6	.456000	0.020000	.220000	.0820	1.000	.00000	.0000	.25000
7	.380000	0.022000	.220000	.0820	.800	.00000	.0000	.25000
8	.220000	0.028000	.218000	.0820	.620	.00000	.0000	.25000
9	.220000	0.028000	.203000	.0820	.470	.00000	.0000	.25000
10	.230000	0.028000	.259700	.0820	.200	.00000	.0000	.25000
11	.150000	0.032000	.239600	.0820	.000	.00000	.0000	.25000
12	.210000	0.028000	.309600	.0820	.000	.00000	.0000	.25000
13	.150000	0.030000	.404400	.0820	.000	.00000	.0000	.25000
14	.094000	0.032000	.304500	.0820	.000	.00000	.0000	.25000
15	.089000	0.033000	.309600	.0820	.000	.00000	.0000	.25000
16	.068000	0.033000	.354500	.0820	.000	.00000	.0000	.25000
17	.054000	0.034000	.339500	.0820	.000	.00000	.0000	.25000
18	.045000	0.034000	.344600	.0820	.000	.00000	.0000	.25000
19	.040000	0.034000	.439400	.0820	.000	.00000	.0000	.25000
20	.034000	0.035000	.324500	.0820	.000	.00000	.0000	.25000
21	.021000	0.035000	.529300	.0820	.000	.00000	.0000	.50000
22	.017000	0.035000	.464300	.0820	.000	.00000	.0000	.50000
23	.014000	0.035000	.484300	.0820	.000	.00000	.0000	.50000
24	.013000	0.035000	.696500	.0820	.000	.00000	.0000	.50000
25	.012000	0.035000	.699000	.0820	.000	.00000	.0000	.50000
26	.012000	0.035000	.609100	.0820	.000	.00000	.0000	.50000
27	.012000	0.035000	.589100	.0820	.000	.00000	.0000	.50000
28	.012000	0.035000	.634100	.0820	.000	.00000	.0000	.50000
29	.012000	0.035000	.714000	.0820	.000	.00000	.0000	.50000
30	.012000	0.035000	.828800	.0820	.000	.00000	.0000	.50000
31	.012000	0.035000	.907700	.0820	.000	.00000	.0000	.50000
32	.012000	0.035000	1.044400	.0820	.000	.00000	.0000	.50000
33	.012000	0.035000	1.085200	.0820	.000	.00000	.0000	.25000
34	.012000	0.035000	1.083500	.0820	.000	.00000	.0000	.25000
35	.012000	0.035000	1.093600	.0820	.000	.00000	.0000	.25000
36	.012000	0.035000	1.100300	.0820	.000	.00000	.0000	.25000
37	.012000	0.035000	1.108400	.0820	.000	.00000	.0000	.25000
38	.012000	0.035000	1.101000	.0820	.000	.00000	.0000	.25000
39	.012000	0.035000	1.101700	.0820	.000	.00000	.0000	.25000
40	.012000	0.035000	1.122200	.0820	.000	.00000	.0000	.25000

FILE NO 21 IRON

GROUP	$\bar{\mu}$	$\bar{w}$	$\bar{\sigma}_{so} \times 10^{-1}$	$\bar{\sigma}_c^s$	$\bar{\sigma}_{in}$	$\bar{\sigma}_f$	ν	Δu
41	.012000	0.035000	1.139400	.0896	.000	.00000	.0000	.25000
42	.012000	0.035000	1.127300	.1016	.000	.00000	.0000	.25000
43	.012000	0.035000	1.104000	.1150	.000	.00000	.0000	.25000
44	.012000	0.035000	1.088700	.1303	.000	.00000	.0000	.25000
45	.012000	0.035000	1.083800	.1476	.000	.00000	.0000	.25000
46	.012000	0.035000	1.139700	.1668	.000	.00000	.0000	.25000
47	.012000	0.035000	1.166200	.1887	.000	.00000	.0000	.25000
48	.012000	0.035000	1.153600	.2144	.000	.00000	.0000	.25000
49	.012000	0.035000	1.107600	.2437	.000	.00000	.0000	.25000
50	.012000	0.035000	1.124400	.2761	.000	.00000	.0000	.25000
51	.012000	0.035000	1.118600	.3131	.000	.00000	.0000	.25380
52	.012000	0.035000	1.164600	.3548	.000	.00000	.0000	.24620
53	.012000	0.035000	1.139000	.4067	.000	.00000	.0000	.30000
54	.012000	0.035000	1.087500	.4711	.000	.00000	.0000	.28840
55	.012000	0.035000	1.087500	.5353	.000	.00000	.0000	.22300
56	.012000	0.035000	1.092600	.5985	.000	.00000	.0000	.22360
57	.012000	0.035000	1.091200	.6718	.000	.00000	.0000	.23800
58	.012000	0.035000	1.089500	.7571	.000	.00000	.0000	.23800
59	.012000	0.035000	1.087500	.8524	.000	.00000	.0000	.23900

FILE NO 25 STAINLESS STEEL

GROUP	Σ_t	Σ_w	$\Sigma_{s0} \times 10^{-1}$	Σ_{s2}	Σ_{s1}	Σ_f	ν	Δu
1	.850000	0.005400	.156200	.0955	1.380	.00000	.0000	.25000
2	.822000	0.006400	.184300	.0955	1.370	.00000	.0000	.25000
3	.751000	0.008900	.204300	.0955	1.350	.00000	.0000	.25000
4	.651000	0.016000	.207900	.0955	1.310	.00000	.0000	.25000
5	.542000	0.016000	.192500	.0955	1.180	.00000	.0000	.25000
6	.456000	0.020000	.199800	.0955	1.000	.00000	.0000	.25000
7	.380000	0.022000	.199800	.0955	.800	.00000	.0000	.25000
8	.220000	0.028000	.197900	.0955	.620	.00000	.0000	.25000
9	.220000	0.028000	.184300	.0955	.470	.00000	.0000	.25000
10	.230000	0.028000	.235800	.0955	.200	.00000	.0000	.25000
11	.150000	0.032000	.217600	.0955	.000	.00000	.0000	.25000
12	.210000	0.028000	.281100	.0955	.000	.00000	.0000	.25000
13	.150000	0.030000	.367200	.0955	.000	.00000	.0000	.25000
14	.094000	0.032000	.276500	.0955	.000	.00000	.0000	.25000
15	.089000	0.033000	.281100	.0955	.000	.00000	.0000	.25000
16	.068000	0.033000	.321900	.0955	.000	.00000	.0000	.25000
17	.054000	0.034000	.308300	.0955	.000	.00000	.0000	.25000
18	.045000	0.034000	.312900	.0955	.000	.00000	.0000	.25000
19	.040000	0.034000	.399000	.0955	.000	.00000	.0000	.25000
20	.034000	0.035000	.294600	.0955	.000	.00000	.0000	.25000
21	.021000	0.035000	.480600	.0955	.000	.00000	.0000	.50000
22	.017000	0.035000	.421600	.0955	.000	.00000	.0000	.50000
23	.014000	0.035000	.439700	.0955	.000	.00000	.0000	.50000
24	.013000	0.035000	.632400	.0955	.000	.00000	.0000	.50000
25	.012000	0.035000	.634700	.0955	.000	.00000	.0000	.50000
26	.012000	0.035000	.553100	.0955	.000	.00000	.0000	.50000
27	.012000	0.035000	.534900	.0955	.000	.00000	.0000	.50000
28	.012000	0.035000	.575800	.0955	.000	.00000	.0000	.50000
29	.012000	0.035000	.648300	.0955	.000	.00000	.0000	.50000
30	.012000	0.035000	.752500	.0955	.000	.00000	.0000	.50000
31	.012000	0.035000	.824200	.0955	.000	.00000	.0000	.50000
32	.012000	0.035000	.948300	.0955	.000	.00000	.0000	.50000
33	.012000	0.035000	.985300	.0955	.000	.00000	.0000	.25000
34	.012000	0.035000	.983800	.0955	.000	.00000	.0000	.25000
35	.012000	0.035000	.993000	.0955	.000	.00000	.0000	.25000
36	.012000	0.035000	.999100	.0955	.000	.00000	.0000	.25000
37	.012000	0.035000	1.006400	.0955	.000	.00000	.0000	.25000
38	.012000	0.035000	.999700	.0955	.000	.00000	.0000	.25000
39	.012000	0.035000	1.000300	.0955	.000	.00000	.0000	.25000
40	.012000	0.035000	1.018900	.0955	.000	.00000	.0000	.25000

FILE NO 25 STAINLESS STEEL

GROUP	$\bar{\mu}$	$\bar{W}$	$\bar{\sigma}_{so} \times 10^{-1}$	$\bar{\sigma}_c^s$	$\bar{\sigma}_{in}$	$\bar{\sigma}_f$	ν	Δu
41	.012000	0.035000	1.034600	.1044	.000	.00000	.0000	.25000
42	.012000	0.035000	1.023600	.1184	.000	.00000	.0000	.25000
43	.012000	0.035000	1.002400	.1340	.000	.00000	.0000	.25000
44	.012000	0.035000	.988500	.1518	.000	.00000	.0000	.25000
45	.012000	0.035000	.984100	.1720	.000	.00000	.0000	.25000
46	.012000	0.035000	1.034800	.1943	.000	.00000	.0000	.25000
47	.012000	0.035000	1.058900	.2199	.000	.00000	.0000	.25000
48	.012000	0.035000	1.047400	.2498	.000	.00000	.0000	.25000
49	.012000	0.035000	1.005700	.2839	.000	.00000	.0000	.25000
50	.012000	0.035000	1.020900	.3217	.000	.00000	.0000	.25000
51	.012000	0.035000	1.015700	.3648	.000	.00000	.0000	.25380
52	.012000	0.035000	1.057400	.4134	.000	.00000	.0000	.24620
53	.012000	0.035000	1.034200	.4738	.000	.00000	.0000	.30000
54	.012000	0.035000	.987400	.5489	.000	.00000	.0000	.28840
55	.012000	0.035000	.987400	.6237	.000	.00000	.0000	.22300
56	.012000	0.035000	.992100	.6973	.000	.00000	.0000	.22360
57	.012000	0.035000	.990800	.7827	.000	.00000	.0000	.23800
58	.012000	0.035000	.987400	.8821	.000	.00000	.0000	.23800
59	.012000	0.035000	.987400	.9931	.000	.00000	.0000	.23900
60	.000000	0.000000	.000000	.0000	.000	.00000	.0000	.00000

FILE NO 25 MATERIAL U-235

GROUP	$\bar{\chi}$	$\bar{\nu}$	$\bar{\sigma}_{s0} \times 10^{-2}$	$\bar{\sigma}_{s}^{s} \times 10^{-2}$	$\bar{\sigma}_{in} \times 10^{-1}$	$\bar{\sigma}_{f} \times 10^{-3}$	$\nu \times 10^{-1}$	Δu
1	.002830	.008486	.025950	.003100	.200	.0021999	.3572	.25000
2	.002830	.008486	.033400	.005000	.200	.0016750	.3327	.25000
3	.002830	.008486	.040600	.006000	.200	.0012574	.3133	.25000
4	.002830	.008486	.044199	.008000	.200	.0012724	.2983	.25000
5	.002830	.008486	.044699	.010300	.198	.0012825	.2867	.25000
6	.002830	.008486	.042699	.013400	.193	.0012899	.2777	.25000
7	.002830	.008486	.042599	.014100	.184	.0012924	.2707	.25000
8	.002830	.008486	.045050	.015600	.161	.0012874	.2650	.25000
9	.002830	.008486	.048599	.017300	.123	.0012825	.2607	.25000
10	.002830	.008486	.054099	.019200	.103	.0012774	.2575	.25000
11	.002830	.008486	.061300	.020900	.092	.0012825	.2549	.25000
12	.002830	.008486	.069600	.022400	.081	.0012950	.2529	.25000
13	.002830	.008486	.078899	.024800	.067	.0013150	.2510	.25000
14	.002830	.008486	.087199	.027100	.050	.0013549	.2498	.25000
15	.002830	.008486	.093700	.030000	.032	.0014149	.2490	.25000
16	.002830	.008486	.100099	.035500	.015	.0014899	.2482	.25000
17	.002830	.008486	.106300	.037700	.000	.0015775	.2476	.25000
18	.002830	.008486	.112050	.041800	.000	.0016725	.2470	.25000
19	.002830	.008486	.117050	.046800	.000	.0017850	.2467	.25000
20	.002830	.008486	.121799	.052290	.000	.0019100	.2464	.25000
21	.002830	.008486	.128600	.062090	.000	.0021199	.2461	.50000
22	.002830	.008486	.134249	.078800	.000	.0024700	.2459	.50000
23	.002830	.008486	.133800	.098890	.000	.0029100	.2458	.50000
24	.002830	.008486	.128550	.125000	.000	.0034700	.2458	.50000
25	.002830	.008486	.123350	.159000	.000	.0041699	.2458	.50000
26	.002830	.008486	.119600	.203000	.000	.0050499	.2458	.50000
27	.002830	.008486	.113750	.259000	.000	.0061750	.2458	.50000
28	.002830	.008486	.102500	.325990	.000	.0075749	.2458	.50000
29	.002830	.008486	.081499	.413990	.000	.0093999	.2458	.50000
30	.002830	.008486	.075249	.525990	.000	.0116749	.2458	.50000
31	.002830	.008486	.082249	.665990	.000	.0145000	.2458	.50000
32	.002830	.008486	.080999	.840990	.000	.0180499	.2458	.50000
33	.002830	.008486	.079250	1.010000	.000	.0215000	.2458	.25000
34	.002830	.008486	.078249	1.150000	.000	.0243750	.2458	.25000
35	.002830	.008486	.077400	1.300000	.000	.0273750	.2458	.25000
36	.002830	.008486	.076399	1.460000	.000	.0307000	.2458	.25000
37	.002830	.008486	.075899	1.659990	.000	.0346999	.2458	.25000
38	.002830	.008486	.075650	1.879990	.000	.0392500	.2458	.25000
39	.002830	.008486	.075399	2.120000	.000	.0440000	.2458	.25000
40	.002830	.008486	.075149	2.320000	.000	.0482500	.2458	.25000
41	.002830	.008486	.074749	2.479990	.000	.0514499	.2458	.25000
42	.002830	.008486	.074250	2.559990	.000	.0529499	.2458	.25000

FILE NO 25 MATERIAL U-235

GROUP	$\bar{\mu}$	$\bar{w}$	$\bar{\sigma}_{so} \times 10^{-2}$	$\bar{\sigma}_s^s \times 10^{-1}$	$\bar{\sigma}_{in} \times 10^{-1}$	$\bar{\sigma}_f \times 10^{-3}$	$\nu \times 10^{-1}$	DU
43	.002830	.008486	.073899	2.520000	.000	.0520000	.2458	.25000
44	.002830	.008486	.073600	2.329900	.000	.0480000	.2458	.25000
45	.002830	.008486	.073199	1.820000	.000	.0375000	.2458	.25000
46	.002830	.008486	.072749	1.200000	.000	.0247500	.2458	.25000
47	.002830	.008486	.072249	.863990	.000	.0177500	.2458	.25000
48	.002830	.008486	.071499	.741990	.000	.0154500	.2458	.25000
49	.002830	.008486	.070999	.939990	.000	.0152500	.2458	.25000
50	.002830	.008486	.070999	.879990	.000	.0167999	.2458	.25000
51	.002830	.008486	.070500	.839990	.000	.0207500	.2458	.25380
52	.002830	.008486	.070500	1.450000	.000	.0302500	.2458	.24620
53	.002830	.008486	.073499	1.069990	.000	.0500000	.2458	.30000
54	.002830	.008486	.076999	.269990	.000	.0735000	.2458	.28840
55	.002830	.008486	.080000	1.100000	.000	.0740000	.2458	.22300
56	.002830	.008486	.080000	1.800000	.000	.1000000	.2458	.22360
57	.002830	.008486	.080000	3.000000	.000	.1540000	.2458	.23800
58	.002830	.008486	.080000	5.900000	.000	.1890000	.2458	.23800
59	.002830	.008486	.080000	5.100000	.000	.1780000	.2458	.23900

INELASTIC FILE U-235

GROUP								
3	.001800	.000000	.00000	.00000	.000	.00000	.0000	.00000
4	.022600	.000100	.00000	.00000	.000	.00000	.0000	.00000
5	.086800	.009600	.00000	.00000	.000	.00000	.0000	.00000
6	.175101	.061100	.10000	.00000	.000	.00000	.0000	.00000
7	.247402	.151300	3.08000	.00000	.000	.00000	.0000	.00000
8	.284102	.240001	11.95005	.54000	.000	.00000	.0000	.00000
9	.268502	.277802	21.41015	6.83001	.000	.00000	.0000	.00000
10	.224102	.264702	26.03022	16.22008	1.200	.00000	.0000	.00000
11	.179402	.232102	26.57026	22.92016	7.510	.00000	.0000	.00000
12	.131701	.182002	23.06024	23.95020	13.210	2.14000	.0000	.00000
13	.099601	.144401	19.64022	22.91021	16.240	8.10003	.0000	.00000
14	.075500	.113401	16.21019	20.39020	16.620	12.14009	.0326	.00000
15	.057400	.088501	13.11015	17.37018	15.430	13.49012	.0833	.00334
16	.042100	.066200	10.07012	13.85014	13.020	12.60012	.1031	.00705
17	.030200	.048200	7.47009	10.55011	10.310	10.61011	.0989	.00791
18	.022200	.035900	5.64007	8.13009	8.160	8.75009	.0878	.00752
19	.015500	.025200	4.02005	5.87006	6.020	6.63007	.0695	.00617
20	.010900	.017900	2.88004	4.25005	4.420	4.97005	.0536	.00486
21	.013000	.021500	3.48004	5.21006	5.490	6.29007	.0696	.00642
22	.006300	.010500	1.71002	2.59003	2.770	3.22004	.0364	.00340
23	.003000	.005100	.83001	1.26001	1.360	1.60002	.0183	.00172
24	.001400	.002400	.39000	.60001	.650	.77001	.0088	.00083
25	.000700	.001200	.19000	.29000	.310	.37000	.0043	.00041
26	.000300	.000500	.09000	.14000	.150	.18000	.0021	.00019
27	.000200	.000300	.04000	.07000	.070	.08000	.0010	.00009
28	.000100	.000100	.02000	.03000	.030	.04000	.0005	.00004
29	.000000	.000100	.01000	.01000	.020	.02000	.0002	.00002
30	.000000	.000000	.01000	.01000	.010	.01000	.0001	.00001
31	.000000	.000000	.00000	.00000	.000	.00000	.0001	.00001

INELASTIC FILE-FE AND S.S.

GROUP								
2	.001000	.000000	.00000	.00000	.000	.00000	.0000	.00000
3	.005000	.001000	.00000	.00000	.000	.00000	.0000	.00000
4	.018000	.006000	.00000	.00000	.000	.00000	.0000	.00000
5	.044000	.018003	.00000	.00000	.000	.00000	.0000	.00000
6	.078000	.045000	4.63000	.00000	.000	.00000	.0000	.00000
7	.110000	.079001	1.97003	.00000	.000	.00000	.0000	.00000
8	.134001	.114001	.37005	.63000	.000	.00000	.0000	.00000
9	.134001	.133001	.60000	.63000	.000	.00000	.0000	.00000
10	.120001	.131000	.76000	.33001	.000	.00000	.0000	.00000
11	.101001	.121000	.44000	.00004	.000	.00000	.0000	.00000
12	.078000	.100000	.34000	.00003	1.840	.00000	.0000	.00000
13	.068000	.092000	.35000	.00000	1.820	.00000	.0000	.00000
14	.030000	.042000	.20000	.00000	1.820	.00000	.0000	.00000
15	.028000	.041000	.16000	.00000	1.910	.00000	.0000	.00000
16	.019000	.027000	.10000	.00000	.860	.00000	.0000	.00000
17	.011000	.018000	.07000	.00000	.000	.00000	.0000	.00000
18	.008000	.012000	.01000	.07000	.000	.00000	.0000	.00000
19	.005000	.007000	.00000	.10000	.000	.00000	.0000	.00000
20	.003000	.005000	.00000	.09000	.000	.00000	.0000	.00000
21	.003000	.005000	.00000	.10000	.000	.00000	.0000	.00000
22	.001000	.002000	.00000	.05000	.000	.00000	.0000	.00000
23	.001000	.001000	.00000	.00000	.000	.00000	.0000	.00000
24	.000000	.000000	.00000	.00000	.000	.00000	.0000	.00000